2011

Micropile response to combined loading

Kyle Allen Kershaw

Department: Civil, Architectural and Environmental Engineering

MICROPILE RESPONSE TO COMBINED LOADING

by

KYLE ALLEN KERSHAW

A DISSERTATION

Presented to the Faculty of the Graduate School of the

MISSOURI UNIVERSITY OF SCIENCE AND TECHNOLOGY

In Partial Fulfillment of the Requirements for the Degree

DOCTOR OF PHILOSOPHY

in

CIVIL ENGINEERING

2011

Approved
Ronaldo Luna, Advisor
Richard Stephenson
Louis Ge
Ian Prowell
Erik Loehr

ABSTRACT

The familiarity and acceptance of micropiles by engineers, contractors, and owners has greatly expanded in recent years such that they are routinely considered on many projects. However, research regarding the behavior of micropiles has lagged behind. The goal of this research project was to address some of the fundamental gaps that were not addressed in engineering practice and require further study and testing. Specifically, this research studied the behavior of micropile foundations subjected to simultaneous axial and lateral (combined) loading, including an assessment of the impact of axial load on lateral behavior of micropiles. This research project consisted of three experimental tasks to evaluate the effect of combined loading on micropiles. Task 1 consisted of laboratory testing of scale model micropiles installed in prepared sand. Task 2 consisted of installation and testing of six (6) full-scale micropiles at a clay site to assess the impact of combined loading on the lateral capacity of micropiles. Task 3 consisted of instrumentation of production micropiles used to support a bridge in the Smoky Mountains in eastern Tennessee. The results indicated that, for micropiles in clay, the presence of an axial load resulted in small decreases in both lateral deflection and bending moment compared to the lateral load tests. For micropiles in sand, the lateral deflection was not significantly affected by introduction of a constant axial load, but bending moments in the micropiles were significantly increased for combined load conditions. In addition, p-y analysis accurately predicted load-deflection behavior of micropiles in clay, but over-predicted the maximum bending moments.

ACKNOWLEDGMENTS

I would like to express my appreciation and gratitude to the many individuals and organizations that have provided guidance and support. Completion of the work that culminated in this dissertation would not have been possible without them. I would like to thank my advisor, Dr. Ronaldo Luna, who has provided valuable input and advice throughout the process, has pushed me to produce quality research, and has always been an advocate for me. I am also grateful to my advisory committee, including Dr. Richard Stephenson, Dr. Erik Loehr, Dr. Louis Ge, and Dr. Ian Prowell for their advice, particularly during formulation of my research ideas. Several staff members in the Department of Civil Engineering at Missouri S&T were instrumental in this research project, including Brian Swift, John Bullock, Steve Gabel, and Gary Abbott. Several undergraduate students, including Sarah Bey, Alex Albandoz, and Skylar Knickerbocker, also contributed significantly to the research project. I would also like to thank the organizations that provided financial funding and in-kind donations. My main source of funding was through the US Department of Education GAANN Fellowship. ADSC-IAFD and Dan Brown & Associates also provided financial support. In-kind donations of labor and materials were invaluable to the project, including those from the MoDOT, Hayward Baker, Inc., DSI America, Williams Form Engineering, LB Pipe & Coupling, and Buzzi Unicem. Finally, I would like to thank my family for their constant support and encouragement, particularly my wife, Valeri, and son, Ethan. They have made many sacrifices throughout this process with nothing but extreme patience and love, and successful completion of this dissertation would not have been possible without them.

TABLE OF CONTENTS

Page

LIST OF ILLUSTRATIONS

Page

LIST OF TABLES

Page

1. INTRODUCTION

Micropiles were first developed in the early 1950s by Dr. Fernando Lizzi in Naples, Italy. Since their inception, the design, construction, and uses of micropiles have changed significantly. In addition to the common use of micropiles as vertical foundation elements, micropiles have been used in new innovative ways in the last 10 to 15 years, such as for slope stabilization, earth retention, seismic remediation, and to support both axial and lateral loads (combined loading) beneath structures. Because the use of micropiles in many of these situations is relatively new, research has not been conducted to evaluate the mechanisms responsible for adequate performance. Each of these new applications requires the micropiles to resist lateral loads. However, because of the slenderness of micropiles, the lateral load capacity is often small compared to traditional piles and drilled shafts. Micropiles were previously assumed to be inadequate to take typical lateral loads and lateral capacity was often ignored for design purposes. Furthermore, because lateral loads are rarely applied to micropiles in the absence of axial loads, combined loading research is needed to increase confidence in micropiles subjected to these loads.

For the purposes of the research described herein, micropiles are defined as deep foundation elements with diameter less than 12 inches. In addition, micropiles are constructed by drilling and then casting in-place using Portland cement grout. The grout is typically, but not always, installed under pressure. Micropiles may also include a single, steel, central reinforcing bar and/or permanent steel casing within a portion of the micropile length.

1.1. BACKGROUND AND MOTIVATION

The familiarity and acceptance of micropiles by engineers, contractors, and owners has greatly expanded in recent years such that they are routinely considered on many projects. This rise in popularity has also prompted engineers and contractors to use micropiles in innovative ways. However, research regarding the behavior of micropiles used in new, non-traditional applications has lagged behind. One such area that suffers from a lack of research is micropiles subjected to simultaneous axial and lateral loads, or combined loading. The results of this research will be valuable to the engineering community, the construction industry, and the general public. First, it will increase the confidence and knowledge base for micropile designers regarding the complex soil-structure interaction. Second, it may increase safety and/or reduce construction costs. If the combination of loads is found to decrease the axial or lateral capacity of micropiles, current design methods do not account for this reduction and the design is unconservative. If the combination of loads is found to increase the axial or lateral capacity of micropiles, the current design method is overconservative and application of the new design recommendations resulting from this research could reduce construction costs. A reduction in construction costs may also increase the popularity of micropiles by allowing designers to use micropiles in situations where they may have been previously uneconomical.

To assess the sensitivity of micropiles to an axial load when the micropile is subjected to lateral load conditions, an initial parametric study was conducted. Commonly within engineering practice, p-y analysis [Reese et. al. 2004] is used to predict behavior of micropiles subjected to lateral or combined loads. The p-y method

utilizes nonlinear load-deflection curves to model soil behavior as nonlinear springs. The structural bending stiffness of the micropile is paired with the soil springs to result in a soil-structure interaction model that is used to predict the deflection, shear, and bending moment within the micropile. The LPILE computer program [Reese et. al. 2004] was used to analyze a micropile with 10-foot-long permanent casing and 20-foot-long bond zone. The casing consisted of 6 inch schedule 80 casing (OD = 6.63 inches and wall thickness = 0.43 inch), and the bond zone diameter was 6.63 inches (outside diameter of casing). For the parametric study, the vertical load was incrementally increased, and the lateral failure load was determined for each increment of vertical load. The analysis was repeated for four different soil types, including loose sand, dense sand, soft clay, and stiff clay. The results were normalized as shown in Equation 1 below:

$$\frac{P_{lat-i}}{P_{lat-0}} \tag{1}$$

where: $P_{lat-i} = Lateral\ failure\ load\ with\ a\ vertical\ load\ applied$

$P_{lat-0} = Lateral\ failure\ load\ with\ no\ vertical\ load\ applied$

This normalized failure load was plotted versus the ratio of vertical load to lateral load, as shown in Figure 1.1. For all cases, application of a vertical load reduced the lateral load capacity of the micropile. These results indicate that it is important to determine the behavior of micropiles subjected to combined loads because the presence of an axial load may decrease the lateral capacity of the micropile. Thus, the supported structure could be adversely affected if the response if not accurately predicted.

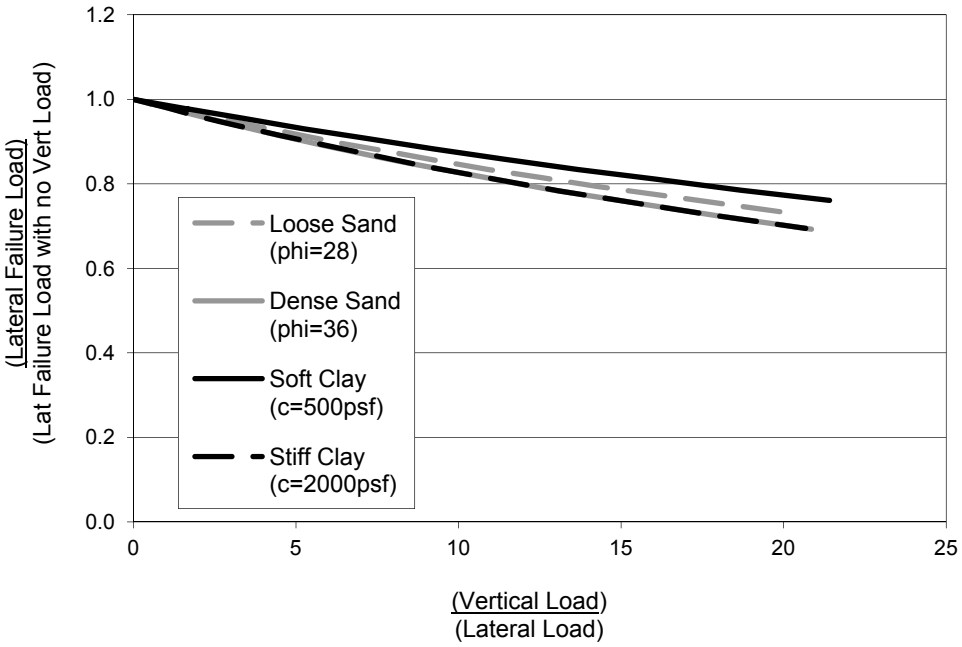

Figure 1.1. Results of LPILE Parameteric Study

1.2. RESEARCH OBJECTIVES

The goal of this research project was to address some of the fundamental gaps that were not addressed in engineering practice and that require further study and testing. Specifically, this research studied the behavior of micropile foundations subjected to combined loading. Combined loading was defined as simultaneous application of an axial load and a lateral load perpendicular to the axis of the micropile. The results of the study include an assessment of the impact of axial load on lateral behavior of micropiles.

1.3. APPROACH

The research consisted of three experimental tasks to evaluate the effect of combined loading on micropiles, including: 1) full-scale field testing, 2) scale-model laboratory testing, and 3) instrumentation of full-scale, production micropiles.

Task 1 (scale model laboratory testing) consisted of laboratory testing of scale model micropiles installed in prepared sand. The results of this task were used to gain additional understanding of the impact that combined loading has on the lateral capacity of micropiles installed in sand. In three different test set-ups, a total of 17 scale-model micropiles were tested. The testing included six (6) axial compression tests, six (6) lateral load tests, and six (6) combined load tests.

Task 2 (full-scale field testing) consisted of installation of six (6) micropiles at a clay site to assess the impact of combined loading on the lateral capacity of micropiles. Each of the micropiles were instrumented to determine load transfer with depth, as well as bending within the upper portion of the micropile. Testing consisted of two (2) axial compression tests, two (2) lateral load tests, and four (4) combined load tests.

Task 3 (in-service loading of micropiles) consisted of instrumentation of production micropiles used to support a bridge in the Smoky Mountains in eastern Tennessee. A total of eight (8) micropiles were instrumented at two bridge piers. The instruments will be monitored during and after construction to assess micropile response to combined loading, depth of load transfer, and residual loads resulting from cyclic or live loads.

1.4. DISSERTATION ORGANIZATION

This dissertation is organized in a traditional format with a total of eight sections. Section 2 presents the results of an in-depth literature review that primarily focuses on design of micropiles and behavior of deep foundations subjected to combined loading. Section 3 provides information regarding the design and development of experimental load testing capabilities at Missouri University of Science & Technology. Sections 4, 5,

and 6 present the development, execution, and results for the three main research tasks for this project, including Task 1 (scale model laboratory testing), Task 2 (full-scale field testing), and Task 3 (in-service loading of micropiles), respectively. The three research tasks were completed separate from each other but were inter-related in purpose and theoretical application. Therefore, Section 7 provides a synthesis of results, compares the results to previous research, and presents conclusions from the study. Finally, recommendations for future research are provided in Section 8.

2. LITERATURE REVIEW

Micropiles are a relatively new foundation technology that has seen rapid growth, particularly in the past 20 years. Because the advancement of micropile technology has largely been driven by innovative contractors, research regarding fundamental micropile behavior has often lagged behind use. This chapter provides a brief history of the development of micropile technologies, the current state-of-practice for micropile design, and a summary of previous research by others related to the behavior of micropiles and other deep foundation elements subjected to combined loading.

2.1. MICROPILE HISTORY

Micropiles were first developed in the early 1950s by Dr. Fernando Lizzi in Naples, Italy. Early micropiles, initially called pali radice (root piles), were used to underpin historic structures [Bruce and Juran 1997] as shown in Figure 2.1. The moderate capacity, small quantity of steel reinforcement, minimal vibration, and minimal ground disturbance resulted in an economical underpinning method for sensitive structures. As larger load capacities were required, Lizzi began using large groups of root piles battered at many different angles as shown in Figure 2.2 [Sabatini et. al. 2005, Bruce and Juran 1997]. The concept behind the design of these early reticulated micropile foundations was to create a large mass of soil tied together with micropiles that could act as a large diameter deep foundation element to transfer load to deeper, stronger soil layers [Lizzi 1983].

By 1962, micropile technology had spread to the United Kingdom, and micropiles were also used for the first time in West Germany in 1965 to underpin buildings adjacent to underground excavations [Bruce et. al. 1995]. Other proprietary micropile

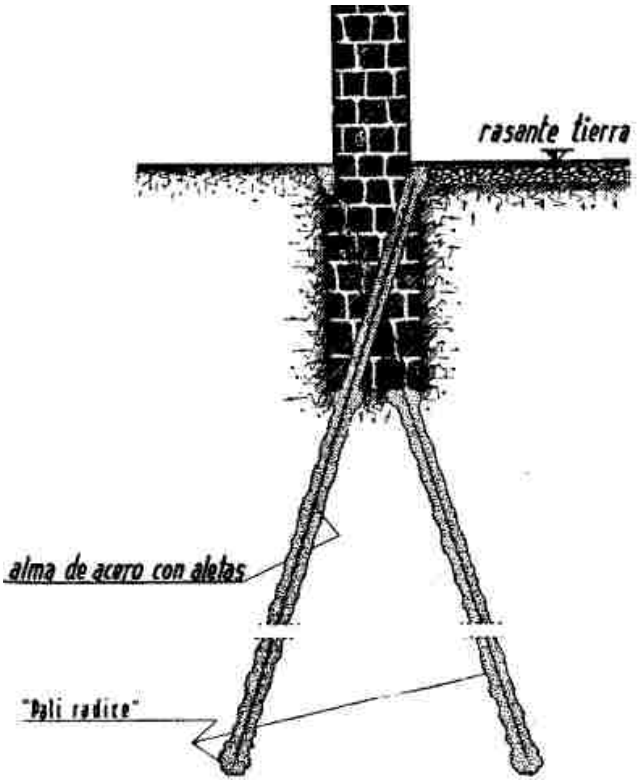

Figure 2.1. Schematic of Original Pali Radice (Root Piles) [Bruce and Juran 1997]

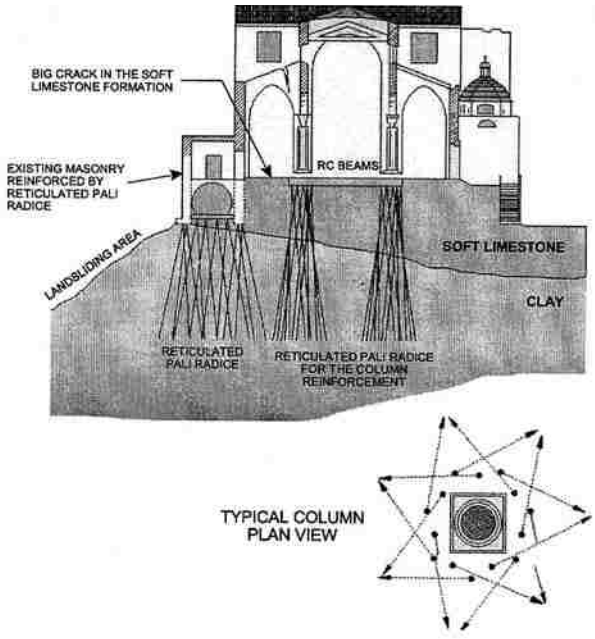

Figure 2.2. Schematic of Early Reticulated Micropile System [Sabatini et. al. 2005]

construction methods were developed in Europe in response to their growing popularity. The first micropiles were installed in North America in 1973, but failed to gain a foothold because of the low cost of steel and the popularity of pile driving in the United States [Bruce and Juran 1997]. It was not until the mid to late 1980s that the popularity of micropiles began to take hold in the United States because of the increase in urban redevelopment. As the use of micropiles increased, contractors began to modify drilling and grouting operations to greatly increase the axial capacity of the micropiles.

In response to the increased popularity of micropiles, the Federal Highway Administration (FHWA) commissioned a comprehensive study of the micropile state of the practice that culminated in a four volume review [Bruce and Juran 1997]. The International Society for Micropiles (ISM, originally termed the International Workshop on Micropiles) was established in 1994 to provide oversight for the project. Starting in 1999, ISM began holding annual workshops that have been steadily growing each year. Coincident with the FHWA study, the French government commissioned a study to gather existing micropile research and conduct new research in areas of need regarding the behavior of micropiles. The project, entitled Foundations Reinforced Vertically (FOREVER), resulted in a synthesis report that was recently translated into English [Cyna 2008]. Shortly after publication of the FHWA state of the practice review document, FHWA also published Micropile Design and Construction Guidelines [Armour et. al. 2000] in an attempt to standardize design of the micropiles for use in transportation projects. The document was updated as part of a National Highway Institute course in 2005 [Sabatini et. al. 2005]. In part due to the publication of these documents that have standardized the industry, the familiarity and acceptance of

micropiles by engineers, contractors, and owners has greatly expanded in recent years such that they are routinely considered on many projects.

2.2. STATE OF THE PRACTICE FOR MICROPILE DESIGN

The current state of the practice for micropile design in the U.S. is primarily based on the current FHWA Micropile Design and Construction Guidelines [Sabatini et. al. 2005], particularly for transportation projects. The American Association of State Highway Transportation Officials (AASHTO) Bridge Design Specifications [AASHTO 2007] also provides guidance on load and resistance factor (LRFD) design of micropiles for transportation projects. For vertical construction projects (such as buildings and towers), the International Building Code [ICC 2009] is also commonly referenced. LRFD is mandated by AASHTO for use on federal transportation projects, but allowable stress design (ASD) is also still commonly used for micropile design on other projects. The FHWA Guidelines define two different basic types of micropiles, including Case 1 piles that are non-reticulated and installed as individual piles or small groups and Case 2 piles that are reticulated and act as an integrated pile-soil mass. Bruce and Juran [1997] estimated that 90 percent of micropiles installed in the U.S. are Case 1 micropiles. Because this research project focuses on the behavior of single micropiles, the information provided herein for state of the practice and previous research by others is for Case 1 micropiles only.

2.2.1. Axial Analysis. Analysis of the axial capacity of micropiles includes design for both geotechnical and structural components of the micropile [Sabatini et. al. 2005]. Because the structural deflection is typically small and the deflection required to reach full side resistance is relatively small, settlement of properly designed micropiles is

typically not a concern except for extremely sensitive structures. The geotechnical capacity is calculated by reducing the ultimate bond strength by a factor of safety (ASD) or a resistance factor (LRFD) and multiplying by the surface area of the bond zone. Typical values of resistance factors are provided in Table 2.1.

Table 2.1. Typical Resistance Factors for LRFD Design [AASHTO 2007]

Limit State	**Method / Ground Condition**	**Resistance Factor**
Compression Resistance of Single Micropile	Side Resistance: Presumptive Values	0.55
	Tip Resistance on Rock O'Neill and Reese (1999)	0.50
	Side and Tip Resistance: From Load Test	< 0.70
Block Failure of Micropile Group	Clay	0.60
Uplift Resistance of Single Micropile	Presumptive Values	0.55
	Tension Load Test	<0.7
Group Uplift Resistance	Sand & Clay	0.50

Noticeably absent from the geotechnical capacity analysis is the contribution from the toe bearing of the micropile. All of the accepted design methods ignore the toe bearing because it is typically small compared to the side resistance due to the small toe area. In addition, research regarding toe bearing capacity is limited. The ultimate bond strength used to calculate side resistance is dependent on the soil/rock type within the bond zone and the type of installation. The four grouting methods in the FHWA Guidelines [Sabatini et. al. 2005] include Type A (gravity grouting), Type B (pressure grouting during casing withdrawal), Type C (gravity grouting with one phase of secondary grouting prior to grout set), and Type D (gravity grouting with one or more phase of

secondary grouting after initial grout set). Types A and B are the most common grouting methods, and pressure grouting methods (Types B, C, and D) are typically used to attempt to increase the bond strength.

For structural analysis of micropiles, the cased zone and bond zone must be analyzed separately because of the change in cross-section. However, the analysis method is the same. For micropiles subjected to tension loads, the structural capacity is derived from the micropile steel only (reinforcing bar and/or casing). The area of steel is multiplied by 55 percent of the minimum yield strength of the steel (F_y) [Sabatini et. al. 2005]. The structural capacity of a micropile subjected to compression loads is derived from both the steel and the grout. The area of grout is multiplied by 40 percent of the unconfined compression strength of the grout (f'_c), and the area of steel (reinforcing bar and/or casing) is multiplied by 47 percent of the minimum yield strength of the steel (F_y) [Sabatini et. al. 2005]. Because the strength of both the grout and steel contribute to the structural capacity of the micropile, strain compatibility must be considered which typically means that the F_y of the steel may be limited to a maximum value. The method to calculate structural capacity in the IBC is essentially identical to the FHWA method except that 40 percent of F_y is used in the analysis [ICC 2009].

2.2.2. Lateral Analysis. The analysis of micropiles subjected to lateral loads is typically completed using p-y analysis [Sabatini et. al. 2005]. This type of analysis models the lateral load-deflection response of the soil using non-linear springs [Reese et. al. 2004]. As a lateral load is applied to the micropile, the p-y analysis considers both the soil springs and the flexural resistance of the structural elements. The resulting output from the analysis includes lateral deflection with depth, as well as shear and moment with

depth in the micropile. Because micropiles are slender elements that typically have light steel reinforcement, the lateral capacity is relatively small. This is particularly true for the bond zone where casing is not present. Generally, lateral deflection is the controlling factor in lateral micropile design, but the estimated shear and moment are also compared to the calculated allowable shear and moment to ensure that structural failure does not occur when the micropile is subjected to the anticipated lateral loads. LPILE is a common software program for p-y analysis, but other commercial software options are available.

To assess the validity of the conventional p-y method and to further understand the behavior of micropiles subjected to lateral loads, Long et. al. [2002, 2004] conducted 10 full-scale lateral load test. The lateral load-deflection response of the micropiles installed at the clay and sand site matched the LPILE prediction with a maximum deviation of 10 percent. However, LPILE generally underestimated the bending moment. Richards and Rothbauer [2004] also reported results from eight lateral load tests on micropiles at eight different sites and compared them to several different prediction methods. The measured lateral deflections were generally greater than the lateral displacement predicted by LPILE, but the p-y analysis provided the best fit of the predictive methods.

2.2.3. Combined Load Analysis. The FHWA Guidelines [Sabatini et. al. 2005] and IBC [ICC 2009] do not address analysis of micropiles subjected to combined axial and lateral loads. Therefore, a standard analysis method does not exist and practitioners use several different techniques to address micropile foundations subjected to combined loading, including: 1) analyzing the pile for two separate loads using accepted design

methods such as FHWA or IBC for axial analysis and LPILE or another predictive method for lateral analysis, 2) battering micropiles to resist the combined loads, and 3) using p-y analysis (such as LPILE) and including an axial load in the analysis. The first method (separate analysis) obviously has limitations because it does not account for synergistic effects between the two loads. The second method (battered micropiles) includes an assumption that the combined loads are transferred to the battered micropile as an axial load. While this assumption may be true for stiffer pile or drilled shaft cross-sections, it is unlikely that the slender micropiles are capable of transferring the combined loads into an axial load in the micropile. Thus, the micropile also experiences bending that is not considered in most battered pile analyses. The third method of analysis (p-y) is common in engineering practice. However, because the p-y curves used in LPILE analysis were based on lateral load tests in the absence of an axial load and because research has been minimal (see Section 2.3.1), it is unclear if the p-y analysis using the common software is applicable for combined load situations.

2.3. PREVIOUS RESEARCH

2.3.1. Combined Load Response of Micropiles. The most comprehensive, coordinated micropile research project to date consisted of a multi-year effort sponsored by the French government and many other public and private partners to gather existing micropile research results and complete new research. The results of this project were published in the FOREVER book [Cyna 2008]. This synthesis report has a short section regarding combined loading on vertical micropiles and references two studies that used three-dimensional finite element models. The results of one of the studies [Shahrour and Meimon 1991] indicated that lateral stiffness of micropiles within the working load range

is independent of the vertical load, but application of a lateral load increases the stiffness of a micropile in the vertical direction. In addition, the study concluded that inclination of the applied load decreases the ultimate capacity in both the axial and lateral directions. The second study [Boulon 2001] was primarily concerned with structural behavior of the micropile, and the results indicated that combined loading generally increased confinement on the micropile, thus decreasing the maximum bending moment. A third study reported in the FOREVER book reported on the effect of micropile batter using plane strain finite element analysis [Sharour and Ata 1994]. Pile batter may be roughly analogous to combined loading. The study concluded that behavior in the axial and lateral directions are independent and can be evaluated separately.

Further literature searches on the subject of combined loading on micropiles yielded few results. A paper by You et. al. [2003] presented the results of scale-model laboratory testing of groups of micropiles in very dense, fine silica sand subjected to inclined loads. The results indicated that the vertical stiffness of the micropiles decreased slightly as the axial load was increased. The results also indicated that lateral stiffness does not change significantly as a result of different load inclinations. As expected, the research also showed that lateral movement predominates for all but subvertical loadings because of the slenderness of the micropiles. Based on the literature search, it appears that there have not been any full-scale field tests to study the response of micropiles to combined loading.

2.3.2. Combined Load Response of Other Deep Foundation Types. Because publications regarding the response of micropiles to combined loads were sparse, the literature search was expanded to include other deep foundation types subjected to

combined loading. The studies reported in the papers can be divided into three categories based on analysis method, including numerical modeling, scale model experimental testing, and full-scale experimental testing.

2.3.2.1 Numerical modeling. Karthigeyan et. al. [2006, 2007] completed three-dimensional finite element analysis to assess the influence of a vertical load on the lateral resistance of square concrete piles. The applied axial loads were from 0.2 to 0.8 times the ultimate axial capacity of the piles and analysis was completed in loose sand, dense sand, and clay. For loose sand, application of vertical loads minimally increased the lateral capacity of the piles (up to 2.5 percent) except for the largest vertical load (80 percent of ultimate) that decreased the lateral capacity by up to 8.6 percent. Application of a vertical load in dense sands significantly increased the lateral capacity of the piles by up to 39 percent. In addition, the authors found that the lateral capacity of piles in clay is somewhat decreased by application of a vertical load. The bending moments were increased by addition of a vertical load for all cases.

Similar to the work by Karthigeyan, Chik et. al. [2009] analyzed the effect of combined loading on a square concrete pile. However, the analysis was only for medium dense sand and the lateral load was applied first followed by a vertical load of 0.2 to 0.8 times the ultimate axial capacity of the pile. The results indicated that, as the axial load increased, the lateral resistance of the pile decreased.

Zhang et. al. [2011] developed an elasto-plastic analytical solution using a spring and slider model to estimate deflection and bending moment in piles subjected to combined lateral and axial loads. The solution was primarily developed to analyze offshore structures, and it ignored the effect of side friction and pile self-weight. The

results of the analytical solution indicated that application of a vertical load significantly increases lateral deflection and maximum bending moment in a pile. This effect was especially prevalent for axial loads that were applied after relatively large lateral loads.

Within a paper by Jain et. al. [1987], brief summaries of other analytical work on the subject of piles subjected to combined loading were provided. Davisson [1960] indicated that for a given lateral load, application of an axial load increased lateral deflection and maximum moment. Work by Ramasamy [1974] and Goryunov [1975] also found that an axial load significantly increases lateral displacement and maximum bending moment. Finally, Klein and Karavaev [1979] obtained different results that indicated an increase in lateral capacity (decrease in lateral deflection) when an axial load was applied to a concrete pile in dense sand.

2.3.2.2 Scale model testing. In response to conflicting results reported in literature regarding the response of piles in sand subjected to combined loading, Jain et. al. [1987] conducted scale model tests on single and groups of aluminum tube piles installed in a prepared sand subgrade. The sand was prepared with a relative density of 78 percent, and the axial load was varied from 20 to 50 percent of the ultimate axial capacity of the piles. Testing was conducted with a free-head condition, and the results indicated that lateral deflection increased with increasing vertical load for all cases.

To investigate the combined load response of aluminum tube piles installed in clay, Anagnostopoulos and Georgiadis [1993] conducted six (6) scale model tests. The results indicated that a lateral load significantly increases vertical settlement, but application of a vertical load only had a small effect on lateral behavior. The maximum

increase in lateral deflection was approximately 10 percent and the increase in maximum bending moment was about 4 percent due to application of an axial load.

A recent dissertation by Lee [2008] utilized scale model testing to assess the effect of combined loading on steel piles in sand. The fine sand used for testing was prepared at three different relative densities (40, 60, and 90 percent), and the piles were driven into the sand. For the 21 combined load tests, the axial load was varied from 25 to 75 percent of the ultimate axial capacity. For all cases, the lateral displacement and maximum bending moment of the piles were increased by the addition of a vertical load. This effect was more prominent as the axial load was increased and as the soil density was increased. The ultimate lateral capacity was decreased by the addition of an axial load by 40, 20, and 10 percent for the dense, medium dense, and loose sand conditions, respectively.

Jain et. al.'s publication [1987] also provided a brief summary of an additional set of scale model tests. Pise [1975], Majumdar [1980], and Saxena [1982] conducted scale model testing of aluminum tube piles in sand. The results indicated that application of a vertical load reduces lateral deflection.

2.3.2.3 Full-scale testing. Lehane et. al. [1999] discussed the results of instrumented driven piles in a mix of sand and clay that were subjected to combined vertical and lateral loads. This paper stated that it was the first field test that had explicitly studied combined loading. The square concrete piles were loaded using a free-head condition. The results indicated that the lateral stiffness of the soil- pile system subjected to combined axial and lateral loads was approximately 3 times greater than a

similar pile subjected to a lateral load only. The bending moments were also less in the combined load test piles compared to the lateral only load tests.

Zukhov and Balov [1978] conducted full-scale combined load tests on short, driven, concrete piles primarily used for agricultural buildings in the former USSR. Both of the sites were primarily clay with one being very stiff and the other being less stiff with saturated conditions. Axial loads were varied from 40 to 70 percent of the ultimate axial capacity. The results indicated that the lateral capacity of the piles was increased with addition of an axial load, particularly at high axial loads. For the saturated clays, the lateral capacity increase was 10 to 24 percent. For the very stiff clay, the lateral capacity was increased by about 57 to 93 percent.

The publication by Jain et. al. [1987] discussed above also provided brief summaries of several other full scale combined load tests on piles. Two of the studies included clay sites [Sarochan and Bykov 1976, Bartolomey 1977], one of the studies was conducted at a sand site [Karasev 1977], and two of the sites had a subgrade with mixed sand and clay [Evans 1953, McNulty 1956]. Despite the differences in subsurface conditions and pile types (pre-cast concrete, cast-in-place concrete, timber, and steel H-piles), the results all indicated that addition of an axial load reduces lateral deflection and increases the ultimate lateral capacity of piles. However, Jain et. al. [1987] argues that restraint of the pile head during loading may significantly skew the results of full scale combined load tests on piles.

2.3.3. Summary and Conclusions. As demonstrated in this section, research regarding the effects of combined loading of micropiles was sparse and provided conflicting results. Of the studies discussed above, two (2) indicated that application of a

vertical load had no effect on the lateral behavior of micropiles, one indicated a positive effect (decreased lateral deflection and/or bending moments), and one indicated a negative effect (increased lateral deflection and/or bending moment) on lateral behavior as a result of applying a vertical load.

For other types of deep foundations, more studies regarding the response to combined loading have been published. However, the results were also conflicting and seemed to depend more on the type of study than on the load pattern, soil conditions, or pile type. Table 2.2 summarizes the results of the combined load studies on other deep foundation types that were reported above. The two columns shown in the table indicate that the study either reported a positive effect (decreased lateral deflection and/or bending moments) or a negative effect (increased lateral deflection and/or bending moment) on lateral behavior as a result of applying a vertical load.

Table 2.2. Summary of Published Research on Combined Loading of Deep Foundations

Type of Study	**No. of Papers Showing a Positive Effect (reduced deflection and/or bending moment)**	**No. of Papers Showing a Negative Effect (increased deflection and/or bending moment)**
Numerical	3	3
Scale Model	1	3
Full-Scale	7	0
Total	***11***	***6***

3. DEVELOPMENT OF LOAD TEST CAPABILITIES

Prior to commencement of the field load testing, scale model testing, and production micropile instrumentation programs, the in-house load testing capabilities at Missouri University of Science & Technology (Missouri S&T) needed to be evaluated and updated. While foundation load tests have previously been completed in conjunction with Missouri S&T research projects, it had been several years since the previous load tests. Thus, instrumentation technology had advanced significantly and other existing equipment needed to be tested and updated, as necessary. This chapter presents details regarding an initial load test, a trial production micropile instrumentation program, and design of a new data acquisition system that were completed to fully develop the load testing capabilities at Missouri S&T.

3.1. BER JUAN TEST SITE

An axial, vertical load test (pull test) was completed on a Type A (gravity grouted) micropile on June 30, 2009 in Ber Juan Park in Rolla, Missouri. The micropile was instrumented with resistive strain gages, load cell, and DCDT. The load test was performed to assess the load transfer along the sides of the micropile, as well as to assess the effectiveness and applicability of the selected instrumentation for future load tests, and to troubleshoot the available load test equipment prior to testing additional research grade micropiles of varying sizes and lengths with alternate loading patterns. The results of the load tests were evaluated using the current standard of practice for micropiles, as well as using computer numerical modeling methods. The following sections describe the installation, testing details, and results for the load test.

3.1.1. Site Selection. The main criterion for site selection was proximity to the Missouri S&T campus, such that support staff would be available to assist during the preliminary micropile load test. However, several other important criteria were also considered during the site selection process. First, to reduce the cost associated with the load test, a locally available geotechnical drill rig was used to install the micropile rather than mobilizing a specialty micropile installation rig to the site. The drill rig was supplied by Ozark Testing/Anderson & Associates of Rolla, MO and consisted of a buggy-mounted CME 75 drill rig with auger drilling capabilities. The rig did not have the capability to drill a large diameter (greater than 6 inches) in rock. Therefore, it was important to find a site with at least 10 feet of soil overlying rock. Second, the site needed relatively easy tuck access to transport materials and equipment to the site. Third, because large equipment would be traversing the site, landscaped areas or other areas that would need significant restoration needed to be avoided. Fourth, the site needed to accommodate the micropile long-term below ground because it could not be determined if the micropile could be pulled completely out of the ground or how deep the micropile could be cut off. Finally, a cooperative site owner needed to grant access to the site and assist if problems occurred during the test.

Considering the criteria listed above, the search was narrowed to sites owned by Missouri S&T or the City of Rolla Parks Department. With input and cooperation from Ken Kwantes, Rolla Parks and Recreation Director, a site near the east edge of Ber Juan Park was selected (see Figure 3.1). The site consisted of a gravel parking lot that had been constructed using up to approximately 15 feet of fill material. The City of Rolla Parks and Recreation Department granted a special use permit for the site.

Figure 3.1. Ber Juan Load Test Vicinity Map

3.1.2. Subsurface Conditions. Subsurface investigation at the load test site consisted of one hand-augered boring and logging of the cuttings during drilling of the micropile. During drilling of the hand-augered boring, a cobble or boulder was encountered, resulting in auger refusal at about 4 feet below the ground surface. Based on the boring and the cuttings observed during micropile drilling, the generalized subsurface conditions at the site consisted of pulverized asphalt fill from the ground surface to a depth of 0.1 feet underlain by stiff, tan, slightly sandy, gravelly, low plasticity clay fill to a depth of 6 feet. These materials were underlain by stiff, gray, slightly gravelly, highly plastic clay fill to a depth of 9.5 feet. Moderately to highly weathered limestone (likely a boulder) was encountered below the fill where auger refusal was reached and the micropile was terminated at a depth of 10.25 feet.

3.1.3. Micropile Design. The test pile was designed as a single, vertical micropile with a full-length bond zone (no casing). In addition, the designed considered the planned method testing by vertically pulling the central reinforcing bar. Several aspects were necessary for design of the test pile, including geotechnical and structural design of the micropile itself, structural design of the load frame system, and specification of a proper size jack and load cell.

Geotechnical and structural design of the micropile was completed in general accordance with the Federal Highway Administration Micropile Design and Construction Reference Manual [Sabatini et. al. 2005]. Because the drill rig did not have the capability to pressure grout the micropile, gravity grouting techniques were planned, corresponding to a Type A micropile. For Type A micropiles, the typical ultimate grout-to-ground bond values range from 5 to 17.5 psi for soft to stiff silt and clay with some sand. Because the results of the geotechnical design of the micropile would be used to size the reinforcing bar that would be used in the micropile, design bond value of 15 psi (near the high end of the published range) was selected such that the reinforcement would not be under designed. The ultimate geotechnical capacity of the micropile was calculated to be 36 kips, assuming a 6.25-inch-diameter, 10.25-foot-long micropile with a bond value of 15 psi. Assuming a factor of safety of 2.0, the resulting design load for the test was 18 kips.

The structural capacity of the micropile was designed assuming a single, steel, central reinforcing bar in the micropile. The bar was used to transfer the tensile load from the jack to the micropile grout and ultimately to the soil surrounding the micropile. For ease of use and the compatibility of the bar with their standard nuts washers and plates, threadbar reinforcement from Dywidag-Systems International (DSI) was used as

the central reinforcing bar. DSI recommends that allowable load for temporary loading conditions be taken as 90 percent of the theoretical yield strength of the bar [DSI 2011]. Using the DSI recommendations, a #9 Grade 75 bar with a temporary allowable load of about 67 kips was selected.

The reaction beam used for the load test consisted of two C15x40 pieces of steel channel oriented back-to-back with a 2 inch clear space between the backs of the channels. Steel plates were used to connect the two channels and provide additional reinforcement at several points along the 11-foot-long beam. Using the American Institute of Steel Construction manual of Steel Construction for LRFD [AISC 1998], it was determined that the reaction beam could support a load of at least 67 kips (maximum allowable load for the central reinforcing bar). Based on the design loads for the micropile load test and availability at Missouri S&T, a hydraulic jack with a maximum capacity of 200 kips and a load cell with a maximum capacity of 100 kips were selected.

3.1.4. Micropile Installation. The test micropile was installed on June 25, 2009. Ozark Testing/Anderson & Associates of Rolla, MO provided personnel and equipment, including a buggy-mounted CME 75 drill rig, to install the micropile. They utilized a hollow stem auger with an outside diameter of 6.25 inches to advance the drill hole to a depth of 10.25 feet below the existing ground surface at the site. Because groundwater was not encountered and the soil had a relatively high clay content, the hole was left open after drilling without the use of temporary or permanent casing. Following drilling, the rig was demobilized from the site and grout was placed in the hole within approximately two hours of drilling. Visual inspection of the open hole indicated that significant collapse did not occur. The grout used to construct the micropile was a neat cement grout

(only cement and water) that utilized Type I/II Portland cement and had a water cement ratio of 0.45. The grout was batched and mixed on site using a portable mixer and placed using gravity feed through a tremie pipe. A positive head of grout was kept above the outlet of the tremie pipe in an attempt to push any loose soil material out of the top of the hole. A circular cardboard sono-tube concrete form was used to continue cast the head of the micropile approximately 6 inches above the ground surface. Because of the size of the mixer, the grout was mixed in three different batches to fill the drilled hole. However, it is our opinion that each batch was placed quickly enough (within about 30 minutes) that cold joints were not formed in the micropile. Following grout placement, 6-inch-diameter plastic centralizers were placed on the central reinforcing bar (see Figure 3.2), and it was lowered through the wet grout to the bottom of the micropile.

3.1.5. Instrumentation. Instrumentation for the micropile load test consisted of strain gages, load cell and DCDT displacement transducer. The strain gages were resistance-type gages manufactured by Micro-measurements [Vishay 2010]. Following preparation of the bar by grinding and sanding a relatively flat spot, the gages were attached to the center reinforcing bar using epoxy, consistent with Vishay installation recommendations. Because of the potential for gages to fail when bumped or exposed to water, two gages were installed at 180 degrees from each other at each measurement location. These pairs of strain gages were installed every 2 feet along the central reinforcing bar starting from approximately 3 inches above the lower end of the bar (10 feet below the ground surface) and terminating at the ground surface, resulting in a total of 12 strain gages. The DCDT displacement transducer was placed at the top of the micropile, just above the ground surface, to measure displacement of the pile head. The

load cell was placed between the jack and the lock-off plate. The locations of the DCDT and load cell are shown in Figure 3.2, and the instrumented central reinforcing bar is shown in Figure 3.3. The load test data was collected and recorded during the test using an existing data acquisition system built at Missouri S&T called the "orange box."

Figure 3.2. Ber Juan Load Test Instrumentation Location

Figure 3.3. Ber Juan Load Test Instrumented Center Bar

3.1.6. Load Test Setup and Procedure. After installation of the micropile, the grout was allowed to cure for 5 days before conducting the load test. As previously discussed, the micropile load test was designed to conduct an axial, vertical (uplift) test. Figure 3.4 shows the setup of the load test, including the micropile, instrumentation, reaction beam, support beams, and hydraulic jack.

Figure 3.4. Ber Juan Load Test Setup

Based on the pre-test design of the micropile, the estimated ultimate axial pullout resistance of the micropile was approximately 36 kips. Using this estimated capacity, a loading schedule was developed that included 4 loading cycles. In addition, a 10-minute-long creep test was planned during the third loading cycle at a load equal to 65 percent of the estimated ultimate capacity. Table 3.1 shows the loading procedure used for the load test. Each load was applied using a hand pump that increased the hydraulic pressure in

the jack. During the hold time for each load, the real-time output from the load cell could be monitored on the data acquisition box such that additional pressure could be applied to the jack as needed to maintain a relatively constant load on the micropile. Continuous data was recorded by the data acquisition box for the strain gages, DCDT, and load cell. A separate output file was recorded for each cycle of the load test and was post-processed as described below.

Table 3.1. Ber Juan Load Test Schedule

Load Cycle	Applied Load (kips)	Hold (min)
Alignment Load	AL	2.5
Cycle 1	2.7	2.5
	5.4	2.5
	8.1	2.5
	AL	1
Cycle 2	2.7	1
	5.4	1
	8.1	2.5
	10.8	2.5
	13.5	2.5
	16.2	2.5
	18	2.5
	AL	1
Cycle 3	2.7	1
	18	1
	20.7	2.5
	23.4	10
	26.1	2.5
	AL	1

Load Cycle	Applied Load (kips)	Hold (min)
Cycle 4	2.7	1
	26.1	1
	28.8	1
	31.5	2.5
	34.2	2.5
	36	5
	45	5
	54	5
	63	5
	54	5
	45	5
	36	5
	27	5
	18	5
	9	5
	AL	5

3.1.7. Results. The results of the load test are shown graphically in Figures 3.5 and 3.6. The load applied at the top of the micropile is the reading directly from the load cell. The deflection at the top of the pile was obtained from the DCDT and is the

difference in readings between the zero reading at the beginning of the test and the reading at the end of the hold time for each load increment. The load in the micropile at different depths was obtained from the strain gages. The direct strain gage output is in microstrain, but we were able to compute the load knowing the elastic modulus and cross-sectional area of the central reinforcing bar. Individual strain gages at two locations, 6 and 10 feet below the ground surface, were lost (no readings) at the time of the load test. Thus, the loads calculated at those two locations are based only on the one working gage that remained. In all other locations, the two strain gage readings were averaged to compute the resulting load.

Figure 3.5 shows the pile head load (from the load cell) versus pile head displacement (from DCDT). Based on this plot, there are several different methods of interpretation to determine the ultimate or failure load of the micropile. The maximum load that the micropile was able to withstand was approximately 26.6 kips (1.5 times design load). Using Davisson's method (not a universally accepted method of load test interpretation for micropiles), the ultimate micropile capacity was 19.8 kips. The FHWA Manual [Sabatini et. al. 2005] recommends interpreting the micropile failure load as the load where the slope of the load versus micropile head deflection plot first exceeds 0.025 in/kip. This interpretation results in a failure load of 17.8 kips. Also, the creep portion of the test failed according to the FHWA Manual criterion (greater than 0.04 inches of displacement between 1 and 10 minutes). Using these different interpretations of the ultimate or failure load and assuming that the grout-ground bond along the micropile is uniform at failure (see discussion below), the bond strength was calculated to be between

7.4 and 11.0 psi. These values are reasonable for the stiff gravelly clay encountered at the Ber Juan load test site [Sabatini et. al. 2005].

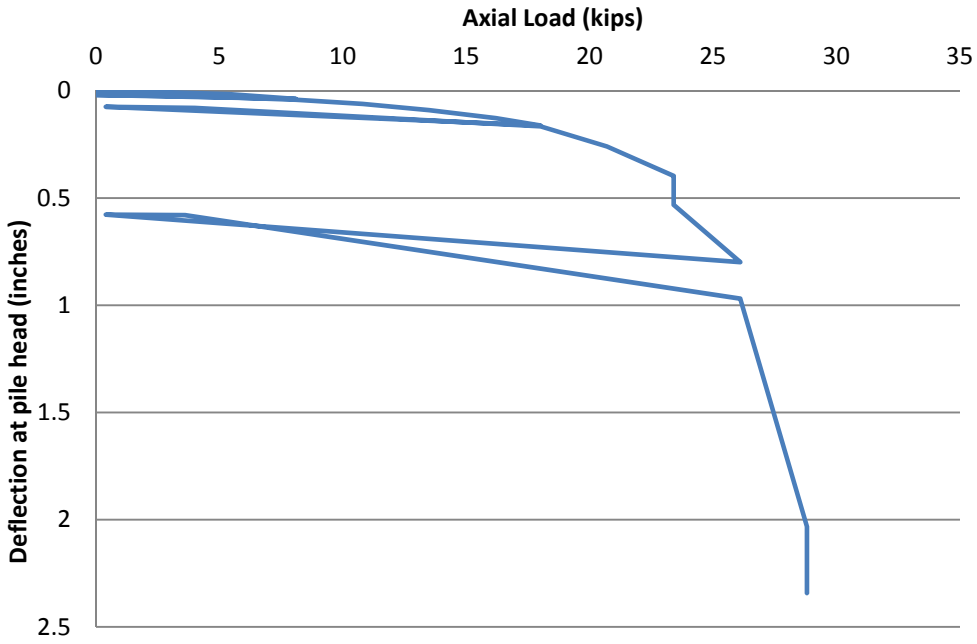

Figure 3.5. Ber Juan Load Test Results – Load vs. Deflection

Using reduced data from the strain gages, load transfer plots (load versus depth) were prepared, as shown in Figure 3.6 for several load increments during the test. The text box shown at the top of each line is the applied upward axial load determined from the load cell readings, and each data point along a single line coincides with a strain gage location within the micropile. This plot shows that, as the load increases, friction/ adhesion along the micropile is mobilized at greater depths. When the load is at the maximum or failure load of the pile, the full friction/adhesion is mobilized along the entire length of the micropile. Except for the portion of the micropile in the vicinity of two feet below the ground surface, the friction/adhesion appears to be relatively uniform

along the length of the micropile. This is shown as a relatively uniform slope of the curves along the entire depth of the micropile. For the two mid-range loads shown in the plot (13.5 and 18.0 kips), the friction/adhesion is likely different in the upper two feet because the ground bulged and cracked at the ground surface resulting in a loss of confinement, and therefore, a reduction in bond strength. This phenomenon was also occurring during the two largest loads (23.4 and 28.8 kips). However, rather than having a vertical load transfer plot that would represent zero bond strength, the measured load actually increases in the upper two feet. There are several possible explanations for this apparent load increase, including lack of precision of the strain gages and bending in the central reinforcing bar that resulted in a false measurement of axial load.

Figure 3.6 also shows a plot of the estimated load versus depth curve that was used to design the test (black dashed line) and a plot of load versus depth that was back-calculated from the applied failure load (grey dashed line). The estimated capacity curve very accurately predicts the behavior in the lower four feet of the micropile and is still fairly accurate in the zone between 2 and 6 feet below the ground surface. However, because the upper two feet of the micropile was also used for the estimation, the failure load is overpredicted.

3.1.8. Discussion and Conclusions. The successful completion of a simple, axial uplift test on an instrumented micropile was an indication that additional micropile tests were possible using the resources available at Missouri S&T. However, several experiences from the initial, simple test provided insight into changes that may need to be made to improve the quality of data and avoid possible complications during subsequent load tests. The most important discovery during the load test was related to the resistive

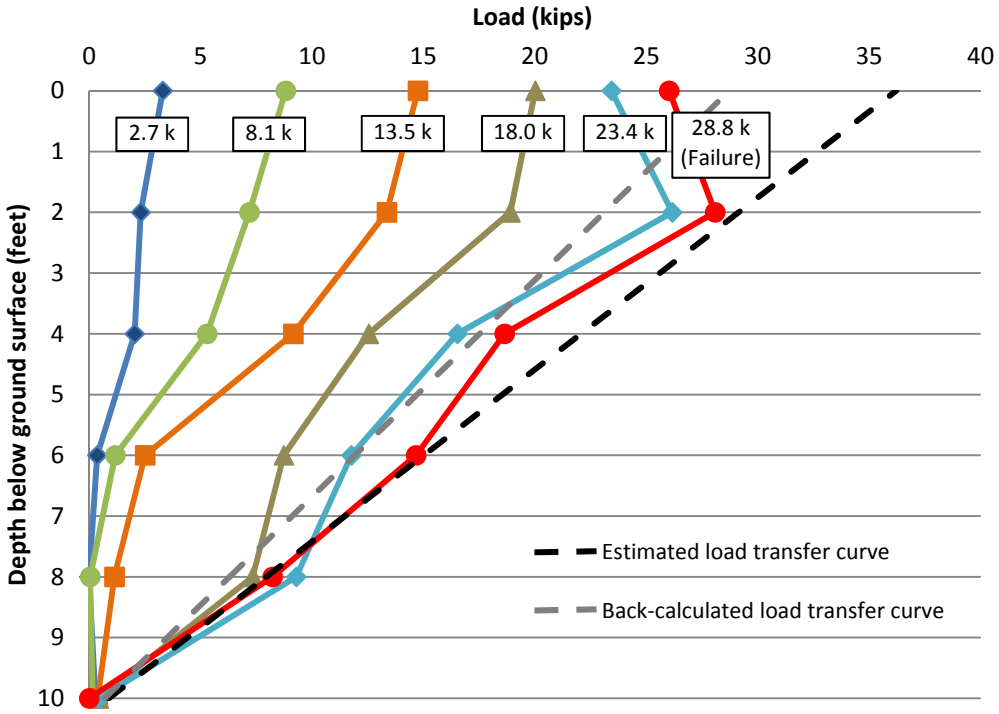

Figure 3.6. Ber Juan Load Test Results – Load vs. Depth

strain gages. While the resistive strain gages provided adequate data during the Ber Juan load test, the failing strain gages and the gage installation issues were concerning. As previously stated, 2 out of 12 gages (or about 17 percent) failed. For this test, the two failing gages were not located at the same level. However, even with redundant gages, important data could be lost because of gage failures. In addition, the resistive strain gages needed to be installed on a relatively flat metal surface for the best results. This results in time consuming installation, as well as complications when bending moment measurements are needed. Dual strain gages, as far from the center of the micropile as possible, are required to obtain reliable bending moment measurements. Thus, a reinforcing steel cage would need to be constructed rather than the single central reinforcing bar that is typically used in U.S. industry. Finally, additional loading

apparatus needed to be designed to accommodate different loading directions and combinations.

3.2. COLT RAILROAD MICROPILES

Two micropiles were instrumented at the south abutment of the new Colt Railroad Bridge and monitored during and after construction, including during a load test at the beginning of the project. The purpose of the instrumentation was to monitor micropile response to combined (vertical and lateral) loading, depth of load transfer, and residual loads resulting from cyclic or live loads. Research involving monitoring of in-service loading and behavior has been very limited to nonexistent for all foundation types, including micropiles.

3.2.1. Site and Project Description. The Colt Railroad project consisted of a new railroad bridge that spans U.S. Highway 63 approximately 2.5 miles north of the U.S. 63 intersection with Interstate 70 in Columbia, Missouri. The topography at the site is hilly and the roadway traverses a low area between two hills. Thus, the bridge supports a railway span between the two hills on opposite sides of the highway. The new bridge replaced an at-grade railroad crossing (located approximately ¼ mile to the north) with a 453-foot-long, 6 span steel structure supported by reinforced concrete piers and abutments. The piers and abutments were founded on groups of micropiles that were connected via reinforced concrete pile caps. The micropiles that were monitored for this preliminary project were located at End Bent No. 1, located at the south abutment of the bridge. The micropiles at End Bent No. 1 consisted of 16 battered and 13 vertical micropiles such that battered micropiles were designed to resist lateral loads from the bridge and the abutment walls and the vertical loads were resisted by a combination of

the vertical and battered micropiles. Four of the battered micropiles were designed as end bearing micropiles with permanent casing installed for the full length of the micropile and the axial resistance of the micropile was derived from a short rock socket. The remainder of the battered micropiles and all of the vertical micropiles at End Bent No. 1 were friction micropiles that had a permanent cased section and an uncased bond zone that were both entirely within the overburden soils.

3.2.2. Subsurface Conditions. Subsurface explorations at the site were completed by Terracon during the design phase of the project and provided to us by Hayward Baker, Inc. (HBI). Borings B-5 and B-5a were drilled at End Bent No. 1. These borings indicate that the subsurface profile generally consisted of alternating layers of very stiff to hard, sandy clay and dense to very dense, clayey, sandy, gravelly cobbles and boulders underlain by limestone that was encountered at a depth of approximately 94 feet. Within the upper 50 feet of the subsurface profile, where the micropiles discussed herein were founded, the subsurface conditions consisted of 36 feet of very stiff to hard sandy clay underlain by the cobble and boulder mix described above.

3.2.3. Micropile Installation. Instrumentation was installed in one battered micropile and one vertical micropile at End Bent No. 1, as shown in the plan view in Figure 3.7. Instrumented Micropiles 61-E (vertical) and 58-G (battered at 10 degrees from vertical) were installed by HBI on December 14 and 21, 2009, respectively. The vertical micropile had a cased length of 10 feet and a bond zone of 20 feet for a total length of 30 feet. The casing consisted of 7-inch outside diameter, 0.498-inch wall thickness pipe with a minimum yield strength of 80 ksi. The battered micropile had a cased length of 10 feet and an uncased length of 40 feet, and the casing consisted of

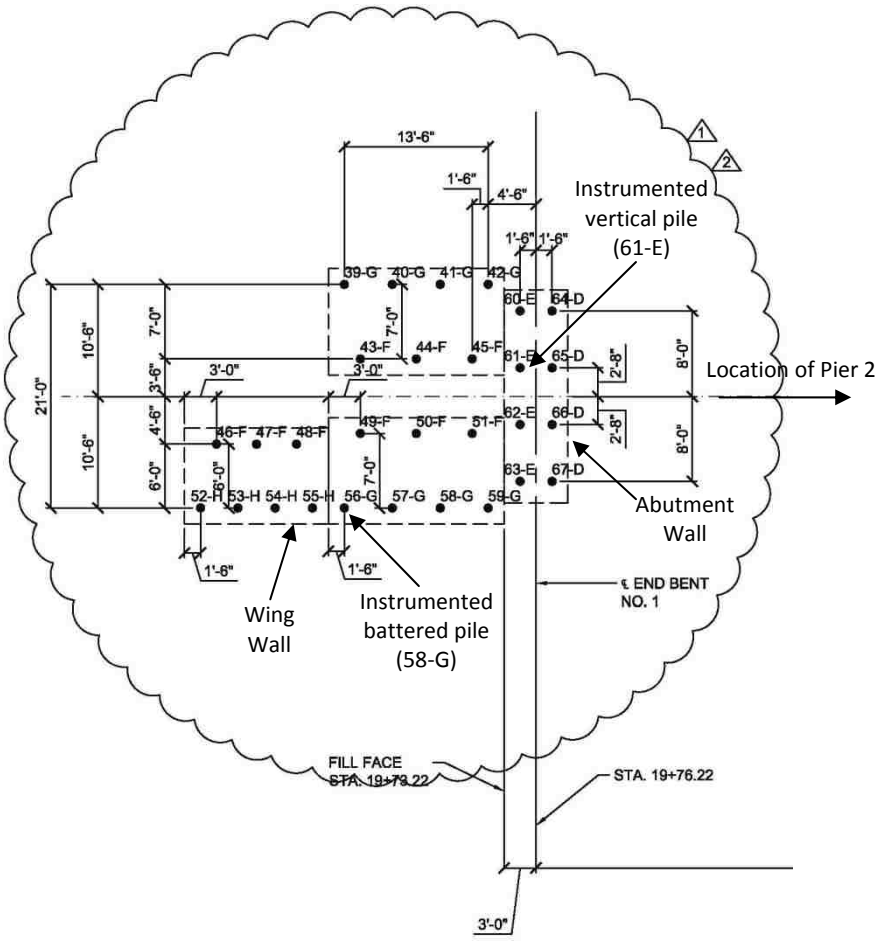

Figure 3.7. Plan View of End Bent No. 1

4.5-inch outside diameter, 0.430-inch wall thickness pipe with a minimum yield strength of 80 ksi. A single reinforcing bar, consisting of a #10 dywidag threadbar with a minimum yield strength of 150 ksi, was installed for the full length of each micropile. The grout used in each micropile had a minimum unconfined compressive strength of 5 ksi. Schematics of the two micropiles are provided in Figure 3.8.

The micropiles were installed as in general accordance with typical Type B micropiles. The casing and a center drill bit were advanced simultaneously to the minimum required depth. After removal of the center drill bit, the casing was filled with

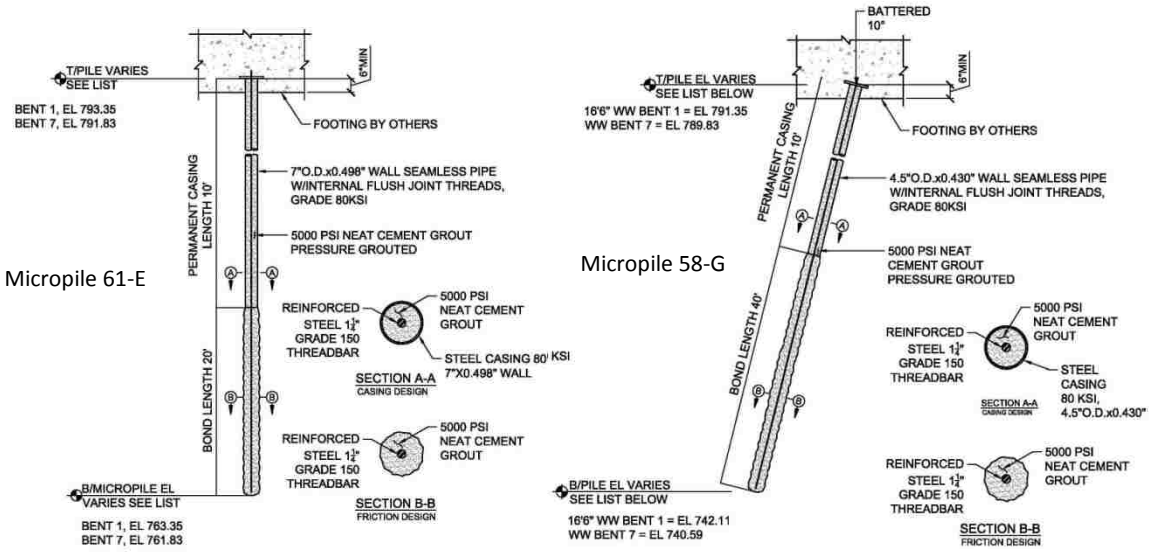

Figure 3.8. Schematic of Instrumented Micropiles

grout and raised out of the hole to the minimum required casing depth. The central reinforcing bar was then placed through the casing to the bottom of the hole and additional grout was placed to fill the casing. A pressure cap was then placed on the top of the casing and the grout was pressurized to increase the grout-to-ground contact within the bond zone. The completed Micropile 58-G with the central reinforcing bar and strain gage wires sticking out above the casing is shown in Figure 3.9.

3.2.4. Instrumentation. Instrumentation for the two micropiles (58-G and 61-E) at End Bent No. 1 consisted of resistance-type strain gages manufactured by Vishay Micro-measurements [Vishay 2010]. The strain gages were attached to the center reinforcing bar in the field. Specifically, the central reinforcing bar was ground down slightly to provide a relatively flat surface and the strain gage was attached to the prepared and cleaned area using epoxy. The lead wires were then soldered on to the strain gages and loosely attached to the central reinforcing bar. To waterproof and

protect the gages during installation, a waterproof coating and tar flashing tape were applied over the top of the gages. The central reinforcing bars with attached strain gages are shown in Figure 3.10.

Figure 3.9. Photographs of Completed Micropile 58-G

Figure 3.10. Photographs of Strain Gage Installation

Seven strain gages were installed on the central reinforcing bar of Micropile 61-E, a 30-foot-long vertical micropile. Strain gage spacing was approximately 5 feet, as shown in Table 3.2. A total of 7 strain gages were installed in Micropile 58-G, but the configuration was slightly different than the instrumentation for Micropile 61-E. Micropile 58-G was a 50-foot-long, battered micropile. Five strain gages at a spacing of approximately 10 feet were installed along the central reinforcing bar, and two strain gages were installed on the outside of the casing near the ground surface. Locations of the strain gages are shown in Table 3.2. Because of time constraints during construction, redundant pairs of strain gages were not installed in either micropile. The instrumentation data was gathered and recorded after construction and the during the load test using an existing data acquisition system built at Missouri S&T called the "orange box." A subsequent post-construction reading was taken using the newly constructed black box instrumentation system (see Section 3.3). Unfortunately, the majority of the strain gages did not work properly during the load test and monitoring. Further discussion of strain gage failure and the lessons learned are provided in Section 3.2.6.

3.2.5. Design Capacity. Micropile 61-E was designed to resist an allowable axial compression load of 20 kips and an allowable axial tension load of 51 kips. Micropile 58-G was designed to resist an allowable axial compression load of 106 kips. For both of the piles, the axial resistance was derived from the bond strength between the grout and the surrounding soil. The frictional resistance within the cased zone and the end bearing at the toe of the bond zone were ignored for the design.

Table 3.2. Colt RR Strain Gage Locations

Micropile	Gage Number	Gage Location – Depth Below Ground Surface (ft)
58-G	1	-0.5
	2	-0.5
	3	10
	4	20
	5	30
	6	40
	7	50
61-E	1	-1
	2	4
	3	9.5
	4	15
	5	19
	6	25
	7	29.5

3.2.6. Load Test. An axial, tension proof-load test of Micropile 61-E was completed by HBI on December 20, 2009. The purpose of the load test was to prove that the minimum bond strength requirements were met. Because it was planned as a tension test, reaction piles were not needed to support the load frame. The reaction beam, consisting of dual wide flange beams, was supported on timber blocking founded directly on the natural ground surface. The micropile central reinforcing bar traversed between the two beams and a hydraulic jack with a central hole was placed over the bar and supported by the beams. A hydraulic jack with a calibrated jack was used to apply the load at the top of the micropile, and a load cell was placed on top of the jack to monitor load. Deflection at the top of the micropile was measured using two dial gages. A photograph of the test setup is shown in Figure 3.11.

Figure 3.11. Photograph of Colt RR Proof Load Test Setup

The maximum load for the test was approximately three times the axial tension design load for the pile. Thus, because the pile did not reach failure during the load test, it has a factor of safety of at least 3.0. Figure 3.12 shows the load-deflection response of the tension load test. In addition to the load and deflection data measured during the load test, Figure 3.12 also shows the theoretical structural deflection of the micropile. As a load is applied to the top of the micropile, the load is transferred through the central reinforcing bar to the structural member and then to the surrounding soil. For small applied loads, resistance is derived from the upper portion of the soil profile and load is not transferred deeper into the pile. As progressively higher loads are applied, the bond capacity between the pile and soil is mobilized and the load is transferred deeper though the pile resulting in greater structural deflection. By comparing the measured deflection with the theoretical structural deflection, it is possible to estimate how deep the load was transferred. Three theoretical deflection curves were plotted in Figure 3.12,

corresponding to load transfer depths of 80 percent of the cased length, 100 percent of the cased length plus 25 percent of the bond length, and 100 percent of the cased length plus 50 percent of the bond length. Because the deflections are similar at the maximum load, it appears that the load was transferred through the entire cased section and approximately 25 percent (5 feet) of the bond zone.

Assuming an estimated mobilized bond length of 5 feet and that the casing provides negligible axial resistance, the ultimate bond strength can be calculated. The back-calculated bond strength of 115 psi is approximately two times larger than the recommended upper range values for Type B micropiles (grout installed under pressure through the casing) installed in very dense gravel noted in the FHWA micropile manual [Sabatini et. al. 2005]. The discrepancy is likely a result of increased bond strength from the mix of cobbles and boulders, as well as a small axial resistance contribution from the based section.

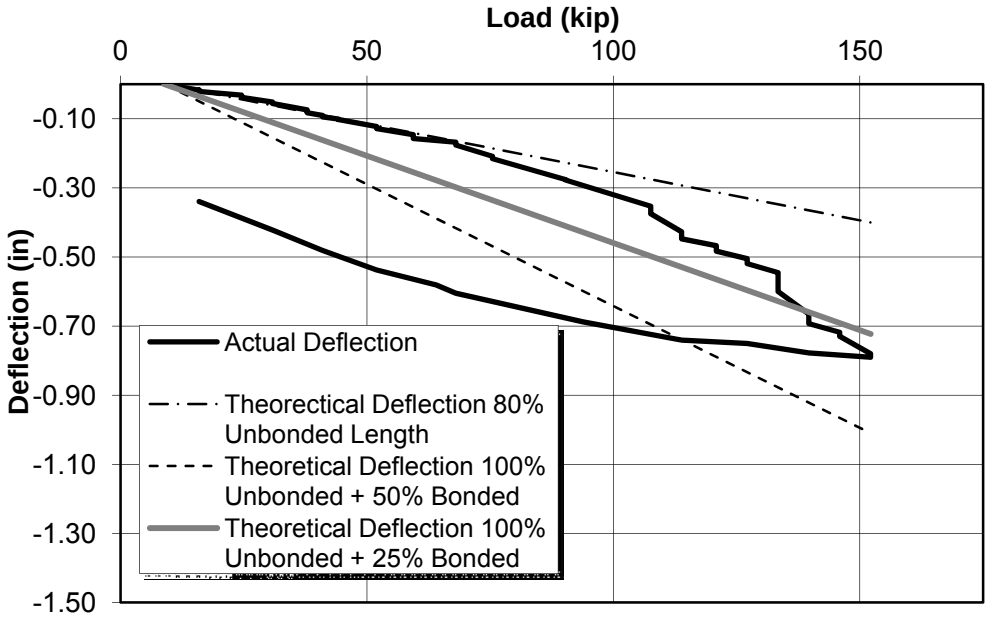

Figure 3.12. Results of Micropile 61-E Load Test – Load versus Deflection

3.2.7. Monitoring. Using the "orange box" and the newly designed black box data acquisition systems, strain gage readings were obtained to monitor Micropiles 58-G and 61-E. These readings were taken after installation, prior to construction of the pile cap, after construction of the pile cap, and upon completion of the bridge. Stain readings were also taken during a vertical tension load test of Micropile 61-E, as discussed in Section 3.2.4. Unfortunately, not enough of the strain gage readings resulted in meaningful data. Therefore, it was not possible to observe changes in load transfer depths, bending within the upper portion of the pile or the influence of cyclic loads on the micropiles.

3.2.8. Lessons Learned. As previously stated, monitoring of the micropiles using resistive strain gages was not successful. The failure of this test program can likely be attributed to three sources, including deficiencies in the type of strain gages used, environmental factors during gage installation, and damage of strain gages during construction. First, the resistive strain gages used to monitor the Colt RR micropiles were not ideally suited for this application. They are typically used in laboratory situations because they are relatively fragile, susceptible to moisture, and have a relatively short life. In addition, accuracy of the gages is reduced when long lead wires are used. We attempted to waterproof the gages and placed tar flashing tape over the gages to protect them, but it may not have been effective in the relatively harsh field construction conditions. Second, the temperatures were around or below freezing during strain gage installation. Because of time and logistical considerations, it was not possible to transport the long central reinforcing bars to a heated laboratory to install the gages. The effectiveness of the epoxy is greatly diminished in freezing temperatures and the

gages may not have been properly secured to the central reinforcing bars. Third, following installation of the micropiles, a portion of the casing above the ground surface was cut off. In this process, some of the lead wires were cut and some were slightly damaged. The cut and damaged wires were spliced by soldering new lead wires, but the field conditions for splicing were not ideal. Some of the wires were cut very close to the top of the casing, and access was difficult because of reinforcing cages, forms and other obstructions that had been constructed prior to splicing operations.

The results of the Colt RR project reinforced the idea that vibrating wire strain gages (VWSG) are better suited for field monitoring projects. They are much more robust and have a longer life than the resistive strain gages. The new black box (see Section 3.4) was designed to accommodate VWSG and they were used on subsequent projects.

3.3. DESIGN OF DATA ACQUISITION SYSTEM

A major component of any field research program is the ability to efficiently read and record data from specialized instruments during testing and/or monitoring operations. Because of the variety of instruments that may be used, it is advantageous to be able to use a single piece of equipment to record data from all devices. The existing data acquisition system (orange box) that was designated for field use could not accommodate the variety of instruments needed for micropile testing and monitoring. In particular, it was not equipped to read vibrating wire strain gages (VWSG). As discussed above, results of the preliminary research work indicated that vibrating wire strain gages (VWSG) would be well-suited for installation in full-scale micropiles and have distinct advantages over resistive strain gages for long-term monitoring applications. Thus, a

new data acquisition system was designed and implemented to work both as a load test and monitoring device.

For the purposes of this micropile research project, the data acquisition system was designed to read and record data during full-scale field load tests and scale-model laboratory load tests. In addition, the system was designed for the second purpose of monitoring instruments installed in full-scale production micropiles. Flexibility of the system was also important because of the potential for changes within the research program and such that the system could be used for subsequent field and laboratory projects.

3.3.1. System Requirements. In addition to the general requirements discussed above, there were several other requirements for performance and usability of the data acquisition system. First, the system needed to have the capability to read and record data from several different instruments simultaneously. There were six different types of instruments considered for design of the system. Specifically, the instruments planned for this project included VWSG, resistive strain gages, load cells, DCDT and string gage displacement transducers, and load cells. However, as previously stated, it was important that the system had the potential to be expanded for other devices, as well. Second, the system needed to be extremely portable. Particularly for long-term monitoring, the locations for readings may be difficult access sites, including bridge abutments or piers and building basements or crawl spaces. In these situations, it would be important for a single person to carry the data acquisition system over rough terrain or into tight spaces. Third, the data acquisition system needed to be self-contained. Again, this quality is particularly important for long-term monitoring where power may not be available and it

may be difficult to transport additional appurtenances necessary for system operation. Fourth, the data acquisition box needed to be weatherproof because the majority of the research planned for the system would be outdoors. Finally, the data acquisition system needed to be user-friendly. Over the life of the system, there will likely be many different users and a difficult learning curve for use of the equipment would be prohibitive. Further, because much of the research involving the system would likely be in off-campus where electronics support staff is not available, operation needed to be simple intuitive, and efficient.

3.3.2. Description of Completed System. Recent advances in technology have made data acquisition components much smaller without sacrificing speed and efficiency. These advances made it possible to build a small, lightweight, self-contained, efficient system. With the parameters and requirements of the data acquisition system established, Brian Swift, electrical engineer for the Missouri S&T Civil Engineering Department, completed the electronic and computer software aspects of the design. The first step in building the data acquisition box was to select the basic platform for the system. The CompactRIO platform, manufactured by National Instruments (NI), was chosen because its attributes closely matched the requirements discussed above. Once the basic platform was chosen, the individual components of the system were selected. The basic components of the system included the controller, chassis, device modules, software, housing, and peripherals.

The controller is the brains of the data acquisition system because it has a built-in computer that can run software, execute commands from the software such as turning devices on and off, log data received from the devices, and complete basic processing of

data. The selected controller was a cRIO-9022 that is part of the ultra rugged category of controllers from NI [National Instruments 2010]. A photograph of the controller is shown in Figure 3.13 and pertinent technical data is shown in Table 3.3. In addition to the connections to the chassis and power source, the cRIO-9022 contained two Ethernet ports, one serial port, and one USB port to connect to other devices.

Figure 3.13. cRIO-9022 Data Acquisition System Controller

Table 3.3. cRIO-9022 Controller Technical Specifications

Specification	**Value**
Processor	533 MHz Freescale MPC8347
RAM	256 MB
Storage Capacity	2 GB
Input Power	9 – 35 Volts
	35 Watt Maximum

The chassis is the component that simply connects the controller to the device modules. For the CompactRIO system, the device modules are cartridges that slide directly into the chassis. Therefore, the two main considerations for selecting a chassis are compatibility with the controller and the number of device module slots. The chassis used to build the data acquisition system was a cRIO-9114, 8 slot, Virtex-5 LX50 reconfigurable field-programmable gate array (FPGA) chassis. The 8 slot variety of chassis was the largest that NI produced at the time the box was designed in 2010.

As previously stated, the device modules for the CompactRIO system are cartridges that slide into the chassis. Therefore, the system is easy to reconfigure by simply switching out cartridges to allow for the use of different types or quantities of devices. Because of the importance of vibrating wire strain gages (VWSG) in the planned field load testing and monitoring programs, it was important to accommodate the maximum number of VWSG into the data acquisition box. Each VWSG cartridge can accommodate four vibrating wire devices. However, for every pair of VWSG cartridges (8 devices), another cartridge that provides the excitation signal for the gages is needed. An 8-slot chassis can, therefore, accommodate a maximum of 20 VWSG that would fill all eight slots. For the typical box setup, the capacity included 16 VWSG (6 slots), 4 resistive devices including strain gages or load cells (1 slot), and 31 linear displacement devices (1 slot). Table 3.4 summarizes the different types of device modules that are available to use with the data acquisition box, along with the capacity and purpose of each. The chassis and controller with modules installed are shown in Figure 3.14.

Table 3.4. CompactRIO Device Modules

Module Designation	Purpose of Device	Number of Devices Per Module	Number of Modules Available for Box
NI 9234	Vibrating Wire	4	5
NI 9474	Vibrating Wire Excitation	8	3
NI 9237	Resistive Gage (Strain Gage and Load Cell)	4	4
NI 9205	Displacement Transducer	31	1

Figure 3.14. CompactRIO Controller and Chassis with Four Modules Installed

The software used to control the data acquisition system was developed using the LabVIEW graphical programming tools by NI [National Instruments 2009]. Because the primary intended purpose of the system was twofold (gathering data during field load tests and intermittent field monitoring), development of the software needed to consider the user needs for each intended purpose. For load tests, the user needs to monitor several different devices simultaneously and in real time. In addition, the need may arise during a load test to modify certain devices. To satisfy these requirements, a laptop

computer needs to be connected to the device as a user interface. The user interface was designed for maximum flexibility such that devices can be turned on and off, data recording can be started and stopped, individual gage factors can be changed, devices can be calibrated, and real-time data can be viewed in either a numerical or graphical format. When using the laptop interface, the user may specify whether the data is saved within the controller hard drive, on the laptop hard drive, or on a USB device connected to the system controller. When the data acquisition system is used for intermittent field monitoring, it is advantageous for it to function as a stand-alone device without the need for a laptop computer and, thus, limited user inputs and commands. The software was developed such that, when an external computer is not connected, the controller automatically detects which devices are connected and immediately starts recording data from the devices. The data is stored on a USB device, if connected. Otherwise, data is recorded on the controller hard drive. The data acquisition box also has two toggle switches and a small LCD readout screen that can be used to start and stop data recording and monitor real-time numerical data, respectively. At the time of publication, the LCD feature had not yet been activated.

The data acquisition system is housed in hard-sided, lightweight, HPX resin plastic Storm Case iM2450 manufactured by Hardigg Cases. The case is waterproof when closed and has a handle for carrying. Because it is only approximately 19 inches long by 15 inches wide by 9 inches thick, it can easily be carried by a single person and can fit into relatively tight spaces. A photograph of the carrying case is shown in Figure 3.15.

Figure 3.15. Photograph of Data Acquisition System Carrying Case

The peripherals added to the data acquisition system were added primarily to ensure proper operation of the system and to make the system easier to use. First, an AC to DC power converter was added so that the system could use 120 to 240 Volt power supplies, including typical outlets and generators. The DC output provided by the converter is 24 Volts/5Amps. The power converter can easily be switched out and replaced with a DC battery for use in areas where power is not available and it is not practical to bring a generator to the site. Second, power conditioners were added to the system to produce a constant power flow to the controller. Third, a board was added to the lid of the carrying case that contains 10-pin connectors for the linear displacement devices. The 10-pin connectors are a standard connection for all linear displacement devices within the Missouri S&T department of civil engineering. Finally, connection boxes for the vibrating wire devices were constructed. These boxes connect to the vibrating wire modules and consist of screw-type post connectors that simplify connection of the wires from the gages.

Photographs of the completed data acquisition box are shown in Figures 3.16 and 3.17 at the end of this section. Where possible, the individual components of the system have been labeled. It should be noted that the configuration of modules shown in the photographs is the typical configuration described above. In addition, the AC to DC power converter is shown in the photographs rather than the battery power source.

3.4. CONCLUSIONS

Development of load testing capabilities early within the schedule of the research project was essential preparation to ensure that the project goals could be met and the quality of data obtained during the project was satisfactory. Specifically, the Ber Juan load test was used to develop full-scale field load testing capabilities, the Colt RR project was necessary to refine field monitoring capabilities, and design of the data acquisition system was necessary for each of the three phases of the project (field load testing, scale model laboratory testing, and field monitoring). Perhaps the most important lesson learned during this portion of the project was that VWSG are better suited for field load testing and monitoring projects. They are much more robust and have a longer life than the resistive strain gages, and these attributes far outweigh the associated additional cost.

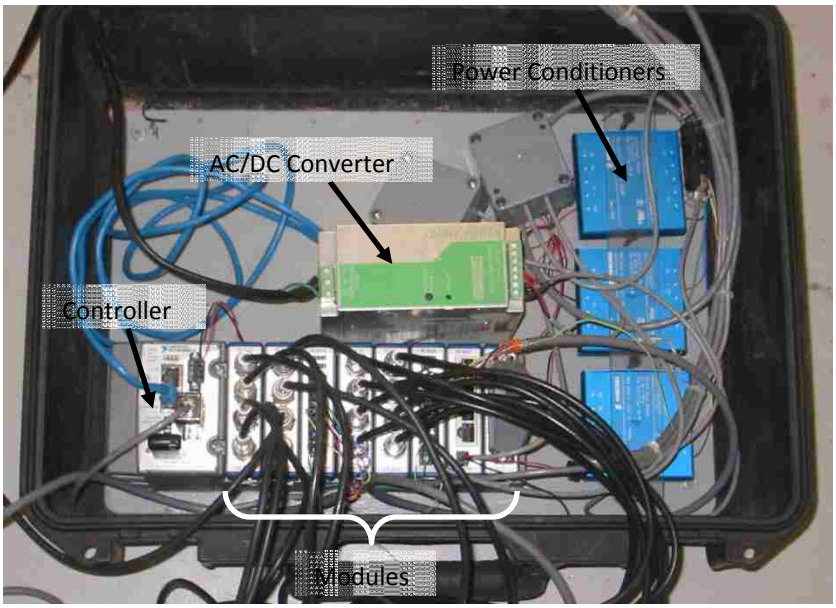

Figure 3.16. Photograph of Data Acquisition Box

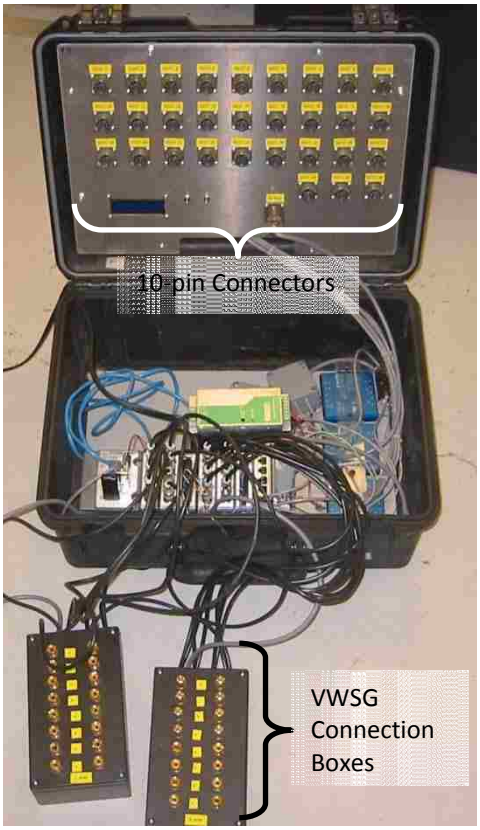

Figure 3.17. Photograph of Data Acquisition Box

4. SCALE MODEL TESTING

The scale-model testing portion of the research consisted of installation and testing of 17 model micropiles in fine sand. The purpose of the testing program was to assess the impact of combined loading (simultaneous axial and lateral loads) on the behavior of micropiles installed in a sand subgrade. Laboratory tests are beneficial because they are cost-effective compared to full-scale field testing. In addition, the parameters that influence behavior can be more controlled in the laboratory compared to field testing.

The 1/8th scale micropiles were installed in a prepared sand test pit, and each of the micropiles was instrumented to determine load transfer with depth and bending within the upper portion of the micropile. Testing consisted of three series of six tests (18 total with one pile being testing in both axial and lateral), including six axial compression tests, six lateral load tests, and six combined load tests. The following sections present details regarding testing materials, test design, soil conditions, instrumentation, installation, experimental program, and testing results.

4.1. EXPERIMENTAL EQUIPMENT

4.1.1. Design Philosophy. The purpose of the scale-model testing was to assess behavior of micropiles subjected to combined loading. To this end, the testing equipment and micropiles were designed to model, as closely as possible, the materials, ground conditions, installation, and load conditions that could be expected for production micropiles. Because preparations for the full-scale field load tests (see Section 5.0) were occurring simultaneously with design of the scale-model tests, it was possible to design the two test programs using similar micropiles and loading conditions. While the design

attempted to realistically model production micropiles, it was known that the scaling effects (discussed in further detail below) may prevent the results from being extrapolated directly for production micropiles. The most important benefit of this research task was comparison of the behavior of the lateral load test results with the combined load test results to better understand the impact of combined loading.

The first two steps necessary for designing the scale-model micropile test were selection of the test soil and selection of the scale to use for the micropiles. All other components of the test are dependent on these two parameters. First, fine, uniform, clean sand was selected for the test soil. The primary reason for choosing sand was that it is much easier and quicker to prepare an artificial granular subgrade compared to a clay subgrade. The uniformity and lack of fines in the sand were chosen to prevent segregation of the material during transport and placement and to reduce the potential for the soil to retain moisture and create a moisture gradient throughout the prepare soil mass. A fine sand was selected because the smaller diameter sand behaves similarly to a larger diameter sand when used in conjunction with the scale model micropile. These characteristics and details regarding the properties of the selected subgrade material are further discussed in Section 4.2 below. Second, a $1/8^{th}$ geometric scale was selected for the micropiles. This selection was based on considerations of required testing loads, size of the corresponding test pit, and availability of materials. In addition, the decision was also influenced by the scale-model micropile testing that had been completed at University of Missouri-Columbia (MU) [Textor 2007]. The micropile slope stabilization project used a $1/8^{th}$ geometric scale and the lessons learned from testing at that scale could be utilized for this research task. Details regarding the scaling effects for the

micropiles are discussed in Section 4.1.2, and the materials and characteristics of the model micropiles are provided in Section 4.1.5.

4.1.2. Scaling Effects. Design of scaled physical models must consider the equations that govern behavior of the soil and structure system, such as stress-strain relationships and equilibrium equations. Using these constitutive equations, dimensional analysis can be completed to determine scale factors that relate parameters in the model to parameters in the prototype. When the model is properly designed using the appropriate scale factors, the results of the model testing can be scaled up to predict behavior of the prototype. The relationship between the model and prototype is defined as similitude. For this research task, the similitude relationships were based on those developed by Iai [1989] for tests on models in a 1-g gravitational field. The general form of the similitude relationships is provided in below in Equation 2.

$$(X)_p = \lambda_X (X)_m \tag{2}$$

where: $(X)_p = Prototype\ parameter$

$(X)_m = Model\ parameter$

$\lambda_X = Scaling\ Factor\ (see\ Table\ 4.1)$

Based on the analysis of the governing equations by Iai [1989], three independent scale factors are typically needed for geotechnical and geo-structural models, including the geometric scaling factor, soil density scaling factor, and soil strain scaling factor. The geometric scaling factor simply relates lengths within the model to lengths within the prototype and it is what is commonly used to denote the "scale" of the model. For this

task, the geometric scale factor was selected as 8 to maximize the size of the model within the limitations of the space available for testing. The density scale factor for 1-g geotechnical applications is typically 1 because real soil is used and placed at densities typical for the soil. If the scale model is intended to model a specific prototype site, the soil strain scaling factor can be determined by completing shear wave velocity testing of the prototype site and the soil to be used for the model testing. Because the purpose of this task was to model a generic sand site, this method was not possible. In the absence of shear wave velocity testing, Iai [1989] recommends defining the soil strain scaling factor as the square root of the geometric scale factor for models in sand. Considering the assumptions regarding the soil density and soil strain scaling factors, the number of independent scaling factors is reduced to one (geometric scaling factor) and all other scaling factors can be determined in relation to the geometric scaling factor, as shown in Table 4.1

In an idealized situation, design of the model micropiles would satisfy all of the scaling relationships noted in Table 4.1, resulting in true similitude. However, due to limitations in the possible combinations of available material types and sizes, it is very difficult meet every criterion. Therefore, design of the micropiles required prioritizing which parameters were most critical to accurately model the assumed prototype. For the proposed testing program, including axial, lateral, and combined load testing, it was determined that correctly scaling the geometry and flexural rigidity were the most important scaling relationships because the lateral behavior of micropiles is dependent on the combination of soil stiffness and lateral structural stiffness. For axial load tests taken to failure, the displacement along the soil-pile interface is typically larger than the

structural deflection. Thus, the longitudinal stiffness of the micropile was a secondary consideration in the design of the model micropile. Further details of the model micropile design are provided in Section 4.1.3.

Table 4.1. Similitude Relationships for Scale Model Testing

Symbol	Item	Scaling Factor	Scaling Factor Used for This Project
x	Geometric Scale Factor	λ	8
ρ	Density	1	1
ε	Strain	$\lambda^{0.5}$	2.8
σ	Stress	λ	8
u	Displacement	$\lambda^{1.5}$	22.6
n	Porosity	1	1
EI	Flexural Rigidity	$\lambda^{3.5}$	1448
EA	Longitudinal Rigidity	$\lambda^{1.5}$	22.6
M	Bending Moment	λ^{3}	512
S	Shear Force	λ^{2}	64
F	Axial Force	λ^{2}	64

Even with consideration of similitude relations and proper design of a scale model test, there are still unresolved scaling effects for 1-g tests. First, the interaction of the scale model pile and the individual sand grains is not taken into account for the existing similitude relationships. In effect, the grain size used in the scale model tests represents a larger grain size within the prototype and behavior of the individual sand grains rather than the soil mass will predominate in the soil-structure interaction if the model sand is too coarse. This may result in overestimation of the lateral and axial capacity of

micropiles installed in sand [Lee 2008]. To reduce the potential for this overestimation, fine sand was chosen for this research task. The relationship is not directly related to the geometric scale factor, but experimental results have resulted in basic guidelines for selection of grain size for scale-model testing [Peterson 1988]. Peterson [1988] recommended that the ratio of pile diameter to soil particle diameter should be greater than 80 to reduce the potential for the behavior of individual grains to dictate the soil behavior. For this project, the ratio of pile diameter (0.875 inches) to median sand grain diameter (D_{50} = 0.0094 inches) is 93. Further discussion of sand properties is provided in Section 4.2. Second, as previously stated, it is difficult to scale the soil density in 1-g scale model tests and a scaling factor of one is typically used. This results in incorrect modeling of confining stresses within the soil mass. Because the interface friction of the bond zone and lateral soil stiffness are at least partially dependent on the confining stress of the soil, they are also likely not modeled adequately. In some cases, centrifuge testing is used to reduce these potential errors. The magnitude of error associated with incorrect modeling of confining stresses is not known, but by knowing the potential for error, it is acknowledged that increased understanding of the relative behavior of the lateral and combined load tests is the primary focus of this research task.

4.1.3. Model Micropiles. The model micropiles were designed using the general scaling relationships discussed above with the geometry and lateral stiffness being the primary parameters for model design. The model micropiles consisted of a cased section and a bond zone with a central bar that extended the entire length of the micropile. Two different model micropiles were used for testing. The first micropile type was designed to model the micropiles installed for the field load testing task, as discussed in Section

5.0. The second micropile type was designed to model a micropile with less lateral stiffness than the first micropile type. The properties of the two model micropiles alongside the properties of the prototype micropiles are shown in Table 4.2.

Table 4.2. Properties of Model and Prototype Micropiles

	Model 1	**Prototype 1**	**Model 2**	**Prototype 2**
Casing				
Outer Diameter (in)	0.875	7	0.875	7
Wall Thickness (in)	0.188	0.453	0.095	0.225
Length (ft)	2	16	2	16
Young's Modulus (ksi)	29,000	29,000	29,000	29,000
Yield Strength (ksi)	72	80	72	80
Center Bar				
Width (in)	0.3125	#11	0.3125	#11
Thickness (in)	0.125		0.25	
Length (ft)	3	24	3	24
Young's Modulus (ksi)	29,000	29,000	29,000	29,000
Yield Strength (ksi)	53.7	75	53.7	75
Bond Zone				
Diameter (in)	1	8	1	8
Length (ft)	1	8	1	8
Compressive Strength (ksi)	4	4	4	4

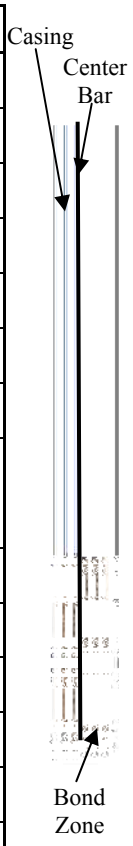

The primary purpose of a central reinforcing bar in micropiles subjected to axial compressive and lateral loads is to keep the bond zone from excessive cracking and to connect to the pile cap. The central bars contribute very little to the axial or lateral stiffness of the micropile. Thus, the central reinforcing bar in the model micropiles was

designed to accommodate the planned strain gages rather than to model the reinforcing bar in the prototype. For this reason, rectangular bars were chosen for the model micropile instead of round bars. As shown in Table 3.2, the strength of the materials in the models and prototypes do not exactly match. While the design attempted to match the strengths as closely as possible, the test results should not be affected by the differences because the geotechnical strength of the sand is much lower than the structural strength of the micropiles and therefore controls the behavior.

4.1.4. Soil Test Pit. The soil test pit was constructed using a wood frame with inside dimensions of 6 feet long by 3.25 feet wide by 4 feet deep as shown in Figure 4.1. It was designed to accommodate multiple model micropiles for each test pit setup while allowing sufficient space between adjacent micropiles and between each micropile and the sides of the test pit to prevent unwanted interaction. Previous research indicates that spacing between adjacent piles should be at least 3 diameters for axial loading [Bruce et. al. 2005] and up to 8 diameters for lateral loading [Rollins et. al. 2006] to prevent interaction between the piles. For the 7/8-inch-diameter piles used for this research, 8 diameter spacing would be equal to 7 inches. To allow for an additional assurance that the model micropiles would not influence one another, the minimum spacing in the direction of lateral loading was chosen as 12 inches and the minimum spacing perpendicular to lateral loading was 9 inches. Typical spacing for the model tests is shown on Figure 4.2.

In addition to concerns regarding interaction of adjacent micropiles, the sand test pit needed to be designed such that the boundary effects of the sides and base of the pit did not influence the behavior of the micropiles. Significant research has been completed

Figure 4.1. Photograph of Soil Test Pit

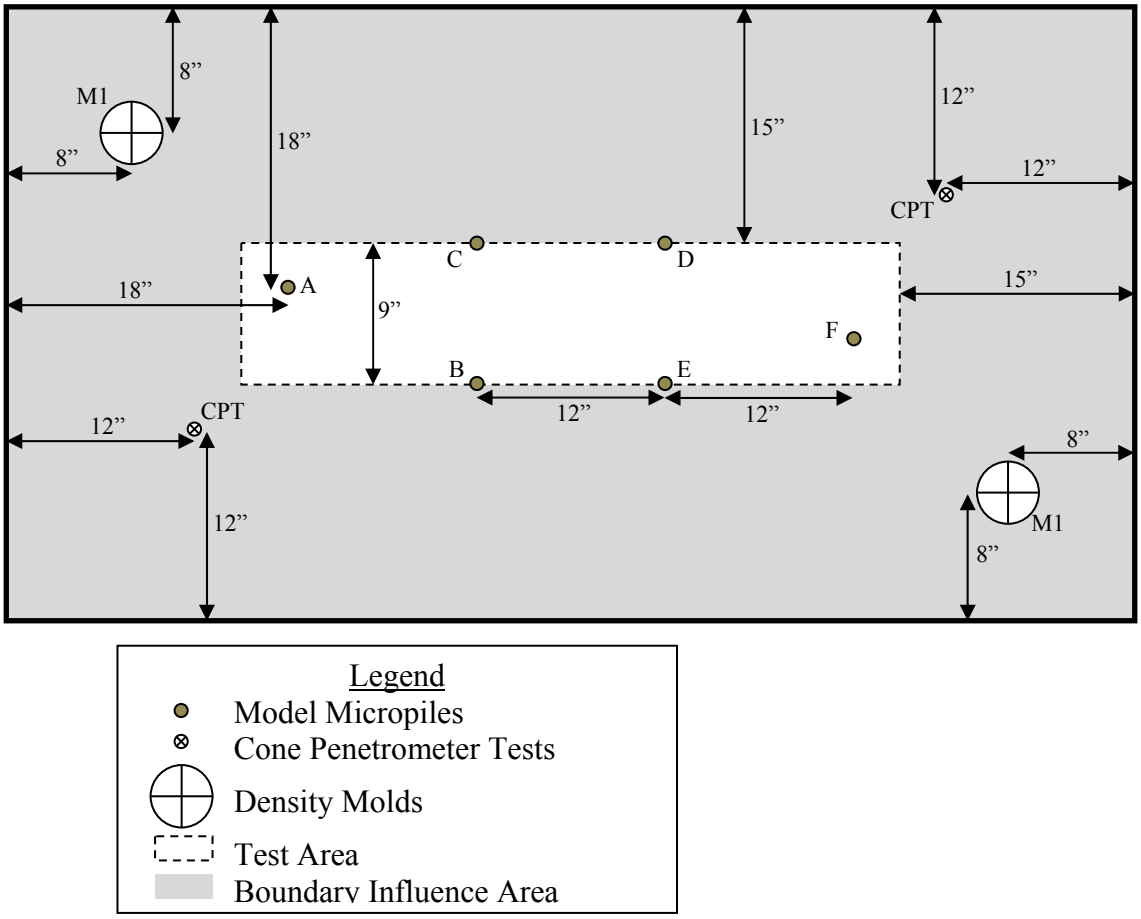

Figure 4.2. Plan View of Scale Model Test Pit

regarding the boundary effects of sand test chambers. The majority of the research has concentrated on the effects of the chamber diameter on the resistance of cone penetrometer tests (CPT). As summarized by Lee [2008], the results indicate that the diameter of the test chamber should be between 7.5 and 50 times the cone diameter to prevent any boundary effects during testing. The lower portion of the range generally corresponds to loose sands and the upper end of the range corresponds to dense sands. For the size of test piles used for this project (0.875 inches), the resulting minimum distance between the test pile and the edge of the test pit should be between about 3.3 and 22 inches, depending on the density of the sand. Because it was not anticipated that sand would be placed in the test pit in a very dense state and because of space constraints, the sand pit was designed such that test micropiles would not be installed within 15 inches of the edge of the pit, as shown in Figure 4.2. The figure also shows the locations of the CPT performed for each test at a distance of 12 inches from the edges of the test pit. The corresponding cone diameter to chamber diameter ratio for this distance is approximately 27. Thus, except for very dense sand, the edges of the pit likely did not influence the results of the CPT. In addition to the edge effects of the test pit, the base of the test pit can also influence test results. Sand test chamber research by Vipulanandan et. al. [1989] suggested that the tip of the test pile should terminate no closer than about 4 times the pile diameter from the base of the chamber. For the 0.875-inch-diameter model test piles, the resulting distance would be approximately 3.5 inches. The test pit was designed such that the test micropiles terminated approximately 12 inches above the base of the test pit. Finally, to further reduce the potential for boundary effects, steps were taken to reduce

the friction between the edges of the pit and the sand. Specifically, the wood on the inside of the pit was painted and then lined with 2 layers of plastic sheeting.

4.1.5. Sand Pluviator. Placing loose sand in a uniform, reproducible manner required the design of specialized equipment. Based on previous research, air pluviation was the preferred method of placement for loose sand. The main goal of the sand pluviator is for all of the sand particles to be distributed evenly and uniformly by "raining" the sand at a controlled rate into the test pit. The resulting density is a function of particle velocity of the sand particles as they are deposited. The two main types of sand pluviators are mass pluviators and moving pluviators. The size of a mass pluviator roughly corresponds to the size of the footprint of the test pit such that all areas within the pit are filled simultaneously and the lifts of sand rise uniformly. The traveling pluviators are smaller than the size of the test pit and are moved around the test pit such that each lift is placed incrementally within different sections of the test pit. While a mass pluviator would likely result in a more uniform deposition, it was not practical for this project because of the size of the test pit and the equipment available to aid in sand placement.

The general design of the sand pluviator was based on research completed by Lee [2008] and modified based on testing of the pluviation box after fabrication. It was constructed of wood and utilized a rectangular shape so that it could fit into the corners of the rectangular test pit. The three main components of the sand pluviator were the sand hopper, the shutter plate, and the sand diffusers, as shown in the photographs in Figure 4.3 and the schematic in Figure 4.4. The purpose of the sand hopper was to store sand prior to placement. It had internal dimensions of 26.5 inches long by 16.5 inches wide by

12 inches deep. The purpose of the shutter plate was to control the flow of sand out of the hopper and distribute the sand onto the diffuser sieves below. The shutter plate consisted of two independent plywood sheets with concentric holes. When the pluviator was being filled and moved, the bottom plate was offset (holes closed) such that the sand could not exit the bottom of the hopper. When the pluviator was in place and ready to deposit sand, the bottom plate was slid over such that the holes in both plates were aligned (holes open). The shutter plate holes were ½ inch in diameter and spaced at 2 inches center-to-center, resulting in a total of 77 holes (7 rows and 11 columns). The purpose of the diffuser sieves was to slow the velocity of the falling sand and to spread the sand to achieve an even deposition of sand below the pluviator.

Figure 4.3. Photographs of Sand Pluviator

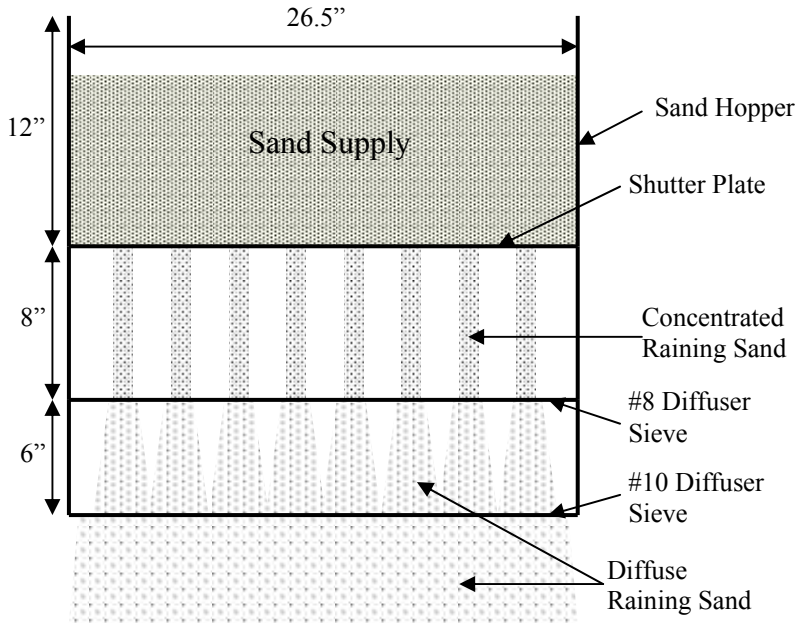

Figure 4.4. Schematic of Sand Pluviator

4.2. SAND PROPERTIES AND PLACEMENT TECHNIQUES

Soil used for scale model testing consisted of P-57 unground silica sand, manufactured by U.S. Silica Company. As discussed in Section 4.1.2, this sand was chosen because it is relatively fine and clean. In addition, the P-57 sand was relatively uniform such that the potential for segregation during placement was minimized. Manufactured sand was chosen to ensure a product with consistent properties.

4.2.1. Laboratory Testing. Laboratory testing was completed on the P-57 sand by Skylar Knickerbocker under the supervision of Kyle Kershaw and Dr. Ronaldo Luna as part of the Opportunities for Undergraduate Research Experiences (OURE) program. The complete testing report is provided in Appendix A, and a summary of the test results is provided below. Laboratory tests to classify the soil and determine strength properties included grain-size distribution, minimum and maximum density, direct shear, and

triaxial testing. Mechanical grain-size analysis was completed in accordance with ASTM D 422 and compared with the grain size distribution provided by U.S. Silica, as shown in Figure 4.5. The results indicate that the P-57 sand is fine (greater than 95% passing #40 sieve), clean (less than 0.3% fines), and uniform (poorly graded, $C_u = 1.6$, $C_c = 0.9$).

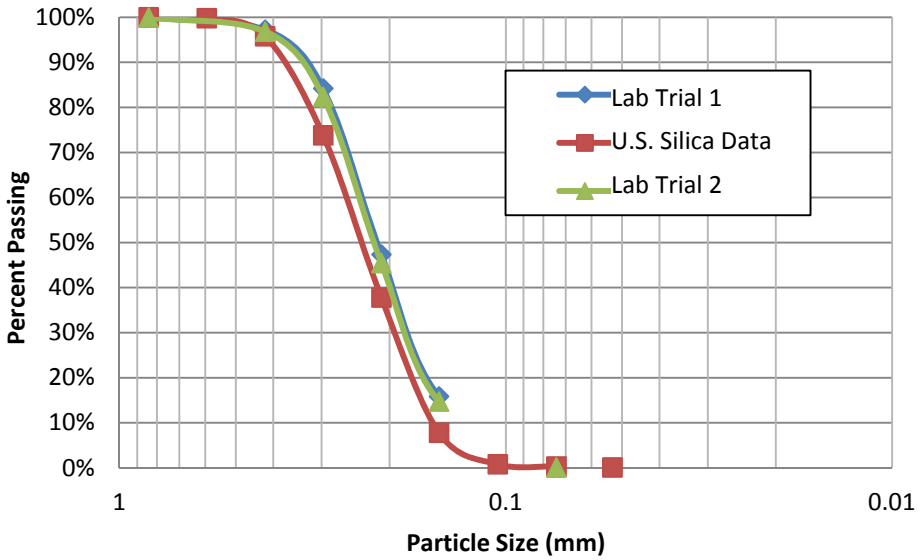

Figure 4.5. Grain-Size Distribution Results

Two trials were completed to determine the maximum dry density of the sand. One trial was conducted in accordance with ASTM D 4253 Method 2A using a vibratory table, and the other trial used manual compaction of the sand. The manual compaction method was used to determine the upper bound for density that could reasonably be prepared by hand for use in the direct shear and triaxial tests. To manually compact the sand, a cylinder with a known volume was filled using 1 inch lifts that were compacted using a dead weight and rodding. The minimum density of the sand was also determined using two different methods corresponding to ASTM D 4254 Method A and Method B.

Because method A used air pluviation to prepare the sample, it represented the minimum density that could reasonably be prepared by hand for use in the direct shear and triaxial tests. The results of the minimum and maximum density tests are provided in Table 4.3. As shown in the table, the range of densities that can be achieved using dry, manual methods is relatively small (6 pcf) as was expected for a clean, uniform sand.

Table 4.3. Results of Minimum and Maximum Dry Density Laboratory Tests

Maximum Density	(lb/ft^3)
ASTM 4254 Method 2A	115.5
Manual Compaction	106.1
Minimum Density	(lb/ft^3)
ASTM 4253 Method A	99.9
ASTM 4253 Method B	94.4

Direct shear testing was completed in accordance with ASTM D 3080 to determine the shear strength of the sand for both the loose and dense conditions. Using densities of approximately 100 pcf and 106 pcf, direct shear tests were performed using normal stresses of 200, 400, 600, and 1200 psf. In addition, a test with a normal stress of 900 pcf was completed on a loose sand sample to improve the fit of the failure envelope used to determine the friction angle. Plots of shear stress versus shear displacement from each test were used to determine the peak shear stress at failure. The peak failure stress at each normal load was used to plot the normal stress versus peak shear stress, as shown in Figures 4.6 and 4.7 for the loose and dense conditions, respectively. For each of the densities, a linear best fit line was plotted through the normal stress versus peak shear stress data. The R-squared values shown in the figures (greater than 0.98) indicate that

the line fits the experimental data well. The slope of the best fit line is equivalent to the friction angle of the sand, and the y-intercept of the best fit line is typically referred to as the cohesion of the soil. However, because the sand was clean and dry, it is unlikely that the cohesion derived from the best fit line is real. It is likely a result of non-linearity of sands at low confining stresses. The friction angles determined from the direct shear tests were 29.9 and 39.1 degrees for the 100 and 106 pcf densities, respectively.

Triaxial tests were also completed to further characterize the shear strength of the sand. Specifically, consolidated-drained (CD) triaxial tests were completed on dry sand. Similar to the direct shear tests, samples were prepared in a relatively loose (99.2 pcf) and relatively dense (105.1 pcf) condition. Confining stresses of 300, 600, and 1200 psf were used for the consolidation phase of the tests. Shearing of the samples was performed using a strain rate of 0.5 percent per minute up to a maximum strain of 20 percent. Because the specimens were dry and it was difficult to measure the volume of air coming out of the sample, the volume change of the sample was assumed to be equal to the volume change of the water in the cell. This volume was read every 30 seconds during the shearing phase of the tests.

Using data from each of the tests, the major and minor principal stresses at failure were determined and used to plot the Mohr circle for each confining stress, as shown in Figures 4.8 and 4.9 for the loose and dense sand conditions, respectively. From the Mohr circle plots, the peak friction angle for the loose and dense sand conditions were determined to be 35.1 and 39.4 degrees, respectively.

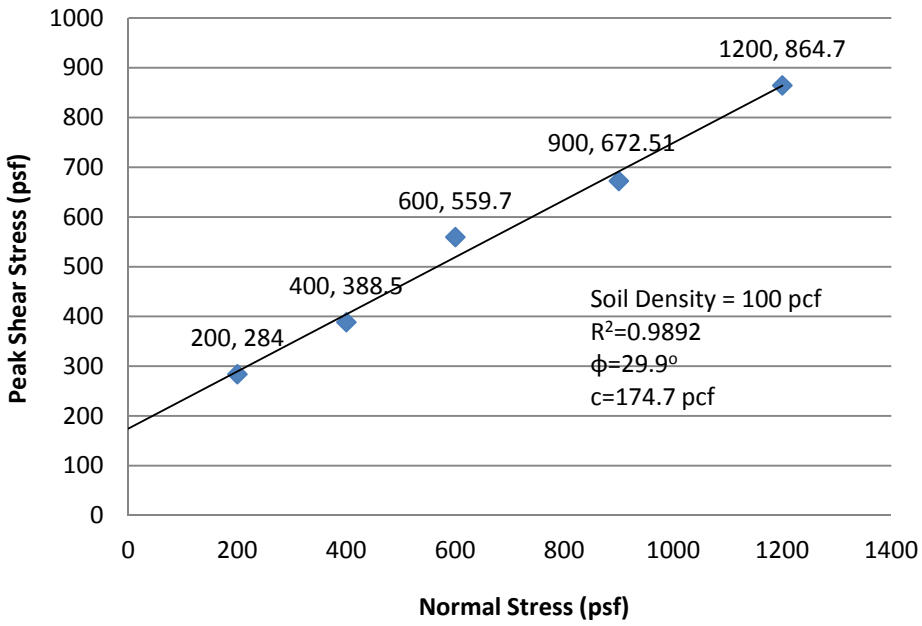

Figure 4.6. Peak Shear Stress vs. Normal Stress for Direct Shear Tests on Loose Sand

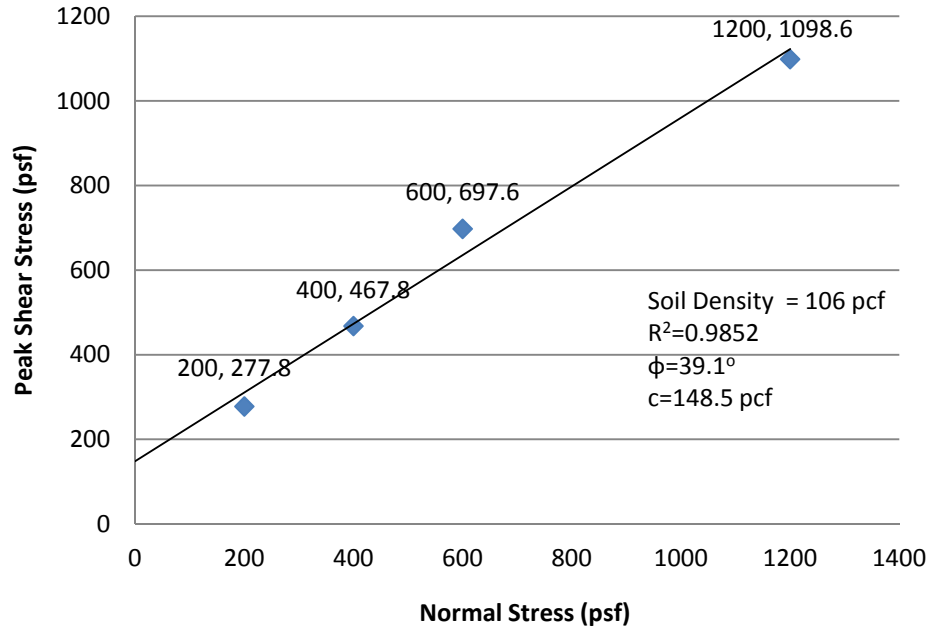

Figure 4.7. Peak Shear Stress vs. Normal Stress for Direct Shear Tests on Dense Sand

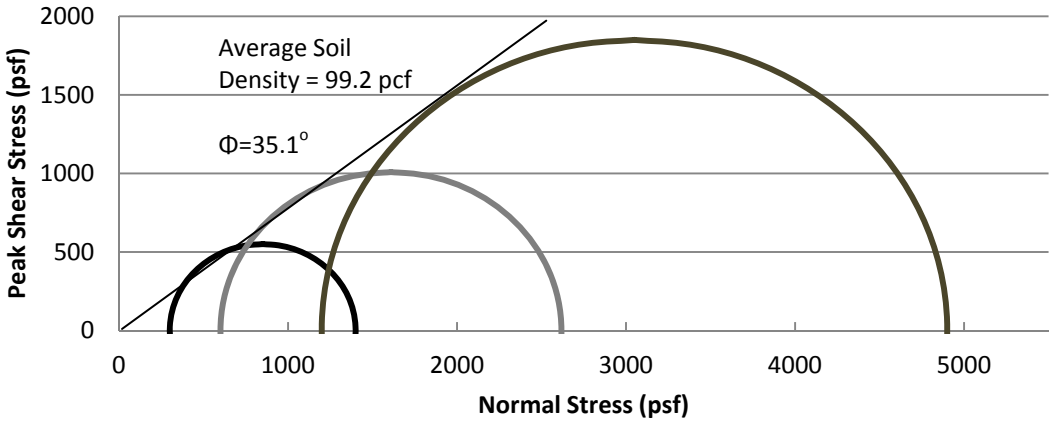

Figure 4.8. Failure Envelope for CD Triaxial Tests on Loose Sand

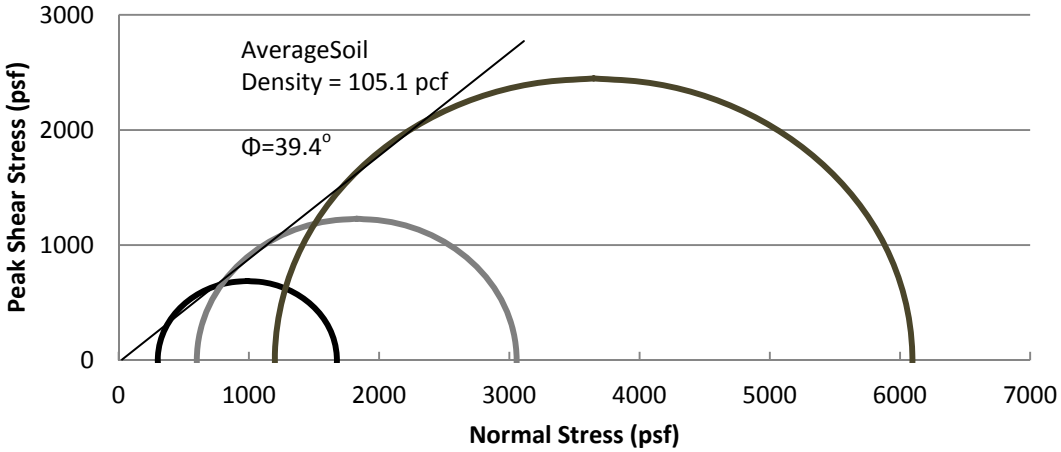

Figure 4.9. Failure Envelope for CD Triaxial Tests on Dense Sand

4.2.2. Sand Placement Techniques. The planned experimental program for the scale model micropiles included installing and testing micropiles using two different soil densities. Thus, two different techniques needed to be developed to place sand within the test pit described in Section 4.1.4. To place sand in a loose to medium dense condition, the sand pluviator described in Section 4.1.5 was developed. Based on research by Lee

[2008] using similar fine sand, the density is directly proportional to the sand drop height up to drop heights of approximately 2 feet. Thus, to achieve relatively low densities, a drop height of 12 inches measured from the bottom diffuser plate to the top of the previous sand lift, consistent with the shortest practicable drop height for the pluviator. Based on trial sand placement with the pluviator, a standard method was developed and followed for placement of loose to medium dense sand for the entire depth of the test pit. The general method consisted of filling the pluviator with approximately 90 pounds of sand with the shutter plate closed. The pluviator was then lifted into place using a gantry crane. After the pluviator was in place at a height of 12 inches above a specific location in the test pit, the shutter plate was opened and the sand allowed to rain into the pit. The pluviator was then moved systematically around the test pit such that the top level of the sand rose in a relatively uniform manner. This placement method resulted in sand lift heights of approximately 4 inches. After sand was placed to a level above the top of the pit, the excess sand was scraped off using a straightedge to create a smooth, level surface. To fill the pit with relatively loose sand using this process took approximately six hours. The photographs in Figures 4.10 through 4.12 show the sand pluviation process.

To place the sand in a relatively dense condition, an alternative placement technique was developed. The dense sand placement technique consisted of placing sand in loose lifts with a maximum thickness of 6 inches and compacting the sand using a small, hand-operated, vibratory plate compactor with a weight of 171 pounds and horsepower of 5.5. The compactor was systematically moved around the test pit using the gantry crane and left in-place at each location for approximately 15 seconds to uniformly compact the sand. The method was repeated for subsequent lifts until the sand

was slightly above the top of the pit when it was leveled and smoothed using a straightedge as shown in Figure 4.12. To fill the pit with relatively dense sand using this process took approximately four hours. A photograph of the sand compaction process is shown in Figure 4.13.

Figure 4.10. Photograph of Sand Placement Showing Pluviator and Gantry Crane

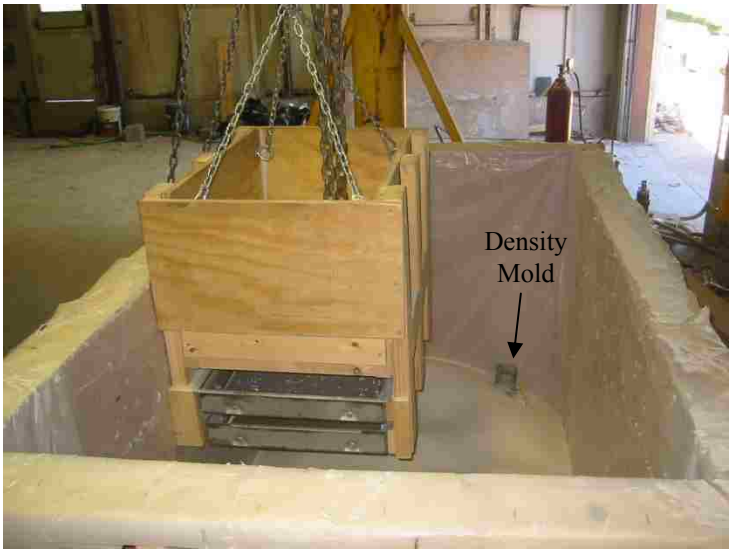

Figure 4.11. Photograph of Intermediate Lift During Sand Pluviation

Figure 4.12. Photograph of Final Surface of Filled Sand Test Pit

Figure 4.13. Photograph of Sand Placement using Vibratory Compactor

4.2.3. In-situ Testing. To assess the properties of the placed sand, in-situ tests were completed, including CPT and density molds. For each of the first two test pit set-ups, the sand was placed using air pluviation and molds were included within the sand

profile, as shown in Figure 4.11, to measure sand density. The density molds were placed at the plan locations shown in Figure 4.2 and at depths of approximately 1.5 and 2.75 feet below the top of the pit, resulting in a total of 4 density molds for each test set-up. After testing was complete, the molds were exhumed, and the density of the sand within each mold was determined. The resulting average densities for the first and second test pit set-ups were 111 and 108 pcf, respectively. Because the molds were exhumed by manually shoveling sand out of the test pit, the molds were likely slightly vibrated and the densities recorded are likely higher than the density of the soil mass. Because of the method used to place the dense sand, it was not possible to include density molds in the third test set-up.

CPTs were utilized to determine soil properties and to check the uniformity of the sand placed in the test pit. A total of seven CPTs were completed for the scale model testing program including two each for the first two loose to medium dense sand preparations and three for the dense sand condition in the third test set-up. Evaluation of the raw data from the CPTs indicates that tip stress increased with depth on all the tests and had a consistent shape. The sleeve stresses in all of the tests were low and relatively uniform with depth. Data within the first foot of the CPT was erratic because of lack of confinement around the cone. Reproducibility of the CPT raw data indicates that the sand was placed in a relatively uniform manner.

Using correlations published by Mayne [2006], the CPT data was used to estimate the friction angle of the sand. A summary of friction angle with depth for the three test set-ups is provided in Figure 4.14. The results from the CPTs from the first two set-ups (26 to 28 degrees) corresponds well to the friction angle for loose sand determined from

the direct shear test (30 degrees) and is slightly lower than the triaxial test results for loose sand (35 degrees). The friction angle determined from the CPTs from the third test set-up was 39 degrees which matches the friction angle determined in both the direct shear test and triaxial test.

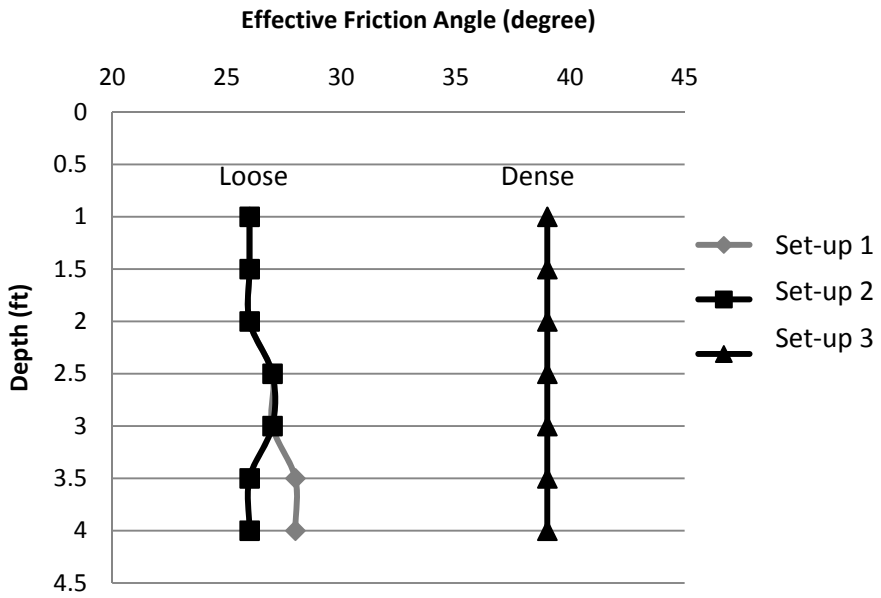

Figure 4.14. Sand Effective Friction Angle from CPT Correlations

Raw data from the CPTs was also used to estimate the relative density of the sand. Using correlations published by Jamiolkowski et. al. [2001], relative density from the first and second test set-ups were both negative which is not possible. This result is likely because of low confining pressure and may indicate that the relative density is relatively low. Using the same correlation for the third test set-up resulted in relatively uniform relative density below a depth of about one foot, as shown in Figure 4.15.

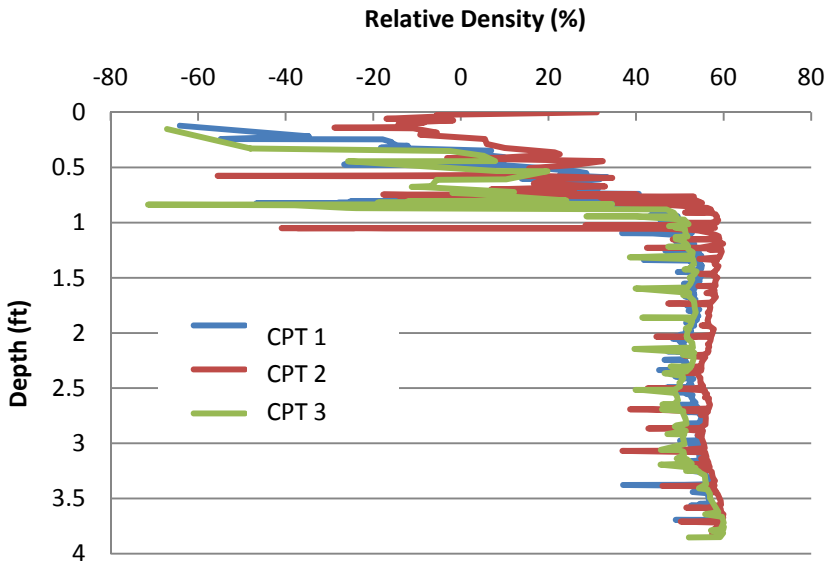

Figure 4.15. Sand Relative Density from CPT Correlations

4.3. INSTRUMENTATION AND CALIBRATION

Each micropile was instrumented with three to six resistive strain gages installed on the micropile casing and zero to four resistive strain gages installed on the central reinforcing bar within the bond zone of the micropile. The number of strain gages installed on each micropile, along with the type of test performed on each of the micropiles is provided in Table 4.4.

The resistive strain gages consisted of EA-06-250BG-120/LE and C2A-06-250LW-120 gages manufactured by Vishay Precision Group [2010a, 2010b]. The two types of strain gages differed slightly, but the pertinent specifications for the gages were identical and are shown in Table 4.5. Resistive strain gages were chosen for this project because of their economy and precision in a controlled laboratory condition. The purpose of the gages was to obtain strain measurements that could be converted into load and/or

bending moment readings. To obtain accurate bending moment readings, it is necessary to have a pair of strain gages oriented in the direction of lateral load. For the micropiles tested in lateral or combined loading, pairs were installed on opposite sides of the casing.

Table 4.4. Quantity of Strain Gages Installed in Model Micropiles

Micropile Name	Test Type	Number of Strain Gages	
		Casing	Bond Zone
1B	Lateral	6	2
1C	Combined	6	2
1D	Combined	6	2
1E	Lateral	6	0
1F	Axial	3	2
2A	Axial	5	1
2B	Lateral	6	4
2C	Combined	6	4
2D	Combined	6	4
2E	Lateral	6	4
2F	Axial	6	3
3A	Axial	6	4
3B	Lateral	6	4
3C	Combined	6	4
3D	Combined	6	4
3E	Lateral	6	4
3F	Axial	6	4

(See Figure 4.2 for Locations of Model Micropiles)

Table 4.5. Summary of Resistive Strain Gage Parameters

Parameter	Value	
Gage Designation	EA-06-250BG-120/LE	C2A-06-250LW-120
Gage Factor	2.085	2.085
Grid Resistance	120 Ω	120 Ω
Gage Length	0.25 in	0.25 in
Grid Width	0.125 in	0.100 in
Accuracy	± 0.15 %	± 0.6 %
Temperature Range	-100°C to +350°C	-60°C to +180°C

The strain gages were mounted to the steel casing and steel central bar after surface preparation using M-Bond adhesive, as recommended by Vishay Precision Group. Following mounting, lead wires were soldered to the gages and the gages were covered with a waterproof nitrile rubber coating and a combination of epoxy resin and tar coated flashing tape to protect the gages during micropile installation. Photographs of the installed strain gages and protective coatings are shown in Figure 4.16.

Figure 4.16. Photographs of Strain Gage Installation and Protection

Following installation of the strain gages, calibration was completed using a 3-point bending test. For this test, the model micropile casing was placed in a load frame that provided simple support, and the strain gages were oriented vertically with one set on top of the casing and one set on the bottom of the casing. Weights were then hung from the center point of the casing in several load increments. As the loads were placed, strain readings were using the black box data acquisition system (see Section 3.4). A photograph of the test is shown in Figure 4.17. The strain readings were converted to bending moment readings using the methods described in Section 4.6 and compared to

the theoretical bending moments for a simply supported pipe at the specific locations of the strain gages. For all seventeen 3-point bending tests, the measured bending moment was within 5 percent of the calculated theoretical bending moment. Despite the good results from the 3-point bending tests, the strain gages installed for the first test set-up (phase one testing) had significant problems during testing, including complete loss of gages, major scatter of readings, and major drift of readings. Of the 35 gages that were installed for phase one, 6 were completely lost and 20 had such large amounts of scatter or drift that the readings were unusable. The complete loss of gages was likely the result of damage to the gages and/or lead wires during installation. The faulty readings on other gages were probably due to delamination of the gages and problems with soldering of the lead wires. For the two subsequent phases of testing, greater care was taken in attachment of the gages, different gages with lead pre-attached wires were used to eliminate the need for soldering, and epoxy resin was used to coat and protect the gages during installation. For the 115 strain gages installed for the second two phases of testing, only seven did not provide usable data.

In addition to the strain gages, direct current displacement transducers (DCDTs) and a string pots (potentiometers) were used to monitor axial and lateral deflection at the head of the micropiles. To account for tilting during the axial load tests, twisting during the lateral load tests, and to provide redundancy, at least two displacement transducers were used on each micropile in the direction of movement for each test. Each displacement transducer was calibrated prior to the testing. Because dead weights were used to apply the vertical and lateral loads (via pulleys), load cells were not needed to monitor loads. The digital data during the test, including resistive gage strain data and

displacement transducer data was collected and stored using the black box data acquisition system described in Section 3.4. Each of the displacement transducers was calibrated to be used simultaneously with this specific data acquisition box.

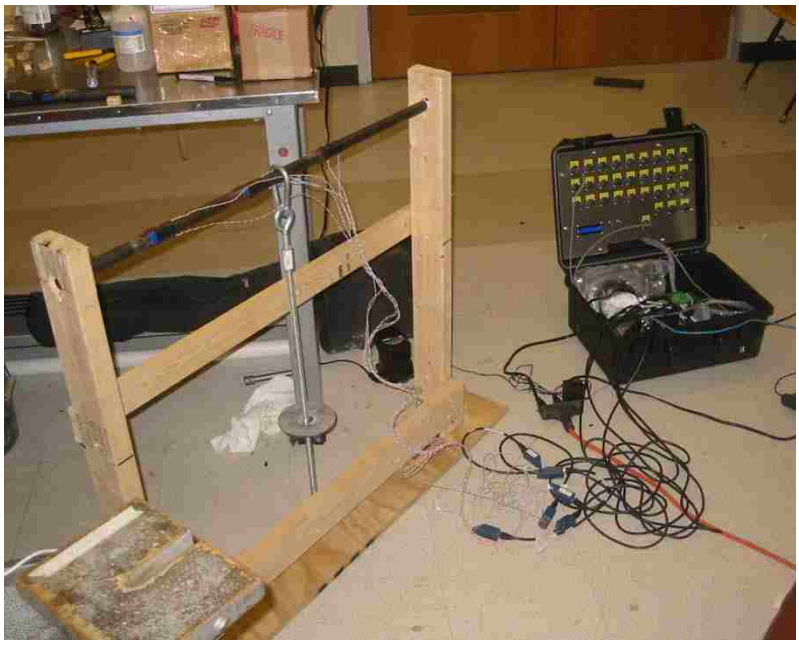

Figure 4.17. Photograph of 3-point Bending Test for Strain Gage Calibration

4.4. MICROPILE INSTALLATION

The micropile installation method was designed to model a typical installation of Type B micropiles in the United States, as shown in Figure 4.18. After completing several trial installations of model micropiles, a standard method was established as described in the steps below and shown in Figures 4.19 through 4.23. The steps listed below also indicate how the model micropile installation differed from the typical full-scale micropile installation described in Figure 4.18, where applicable.

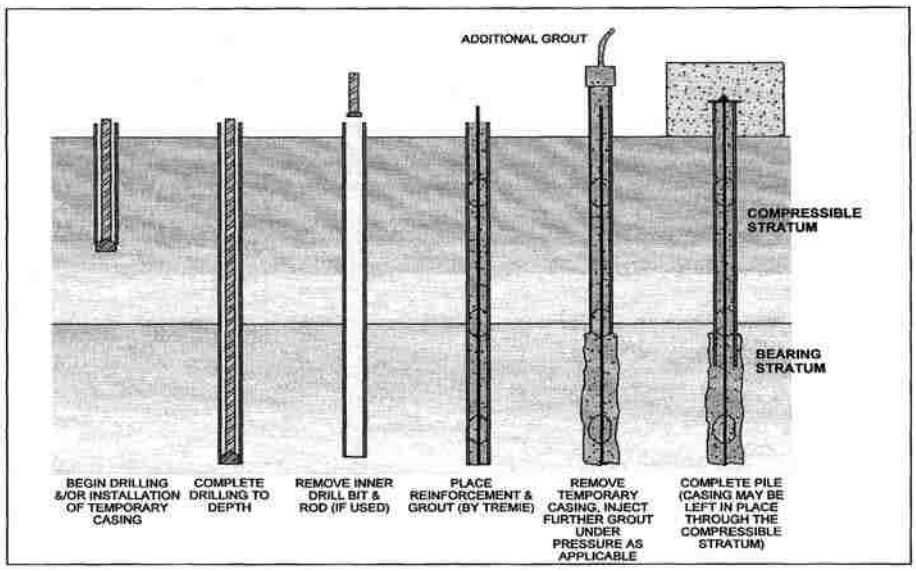

Figure 4.18. Typical Installation Method for Type B micropiles [Sabatini et. al. 2005]

1. Cover the end of the casing with aluminum foil and a metal disc to prevent sand infiltration (varies from full-scale installation where a central bit is used to drill out material and prevent sand infiltration).
2. Push casing into soil to maximum depth of micropile with strain gages aligned in planned direction of lateral loading (varies from full-scale installation where casing is rotated and drilled to maximum depth).
3. Insert rod through casing to dislodge end cap on casing (varies from full-scale installation where central bit is removed).
4. Mix grout and fill casing with grout.
5. Attach pressure cap to the top of the casing and slowly pull casing up to desired depth while keeping the pressure relatively constant. As necessary, stop pulling casing, release pressure, and refill casing with grout before continuing with pressurized removal of casing. For the loose to medium dense sand conditions, pressure varied from 15 to 20 psi. For the dense sand condition, pressure varied from 35 to 45 psi.

6. Place central reinforcing bar and fill casing with grout (Figure 4.18 shows central reinforcing bar placed prior to pressure grouting, but full-scale installation sometimes places bar after grouting).

Except for step two, the deviations from the typical field methods did not likely have an effect on the behavior of the model micropiles. By pushing the model micropile casing into the sand rather than drilling, the model micropile is a displacement pile instead of a replacement pile. Thus, for the loose sand condition, the sand within a zone equal to approximately two pile diameters would likely be densified from pushing the closed-end casing. The effect was likely not as significant for the dense sand condition.

Figure 4.19. Photograph of Micropile End Cap (Step 1)

Figure 4.20. Photograph of Casing Installation (Step 2)

Figure 4.21. Photograph of Grouting Process (Step 4)

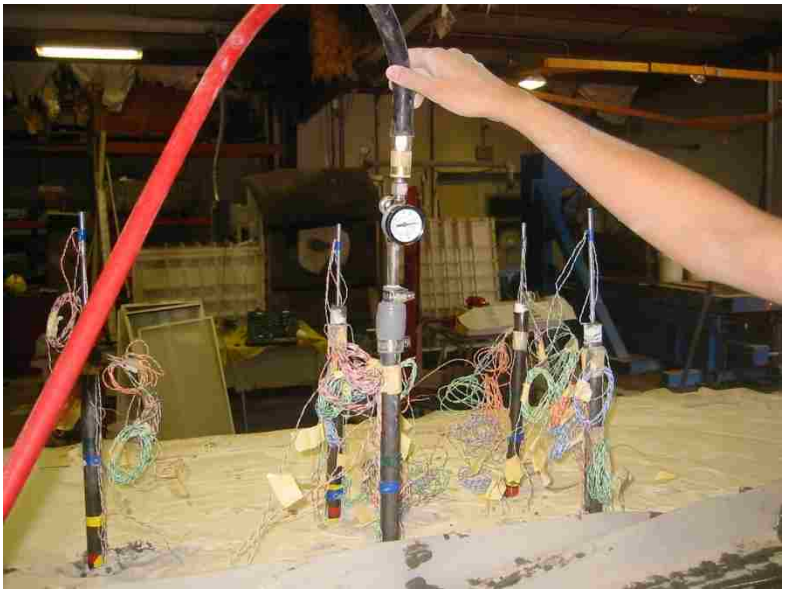

Figure 4.22. Photograph of Grout Pressurization and Casing Withdrawal (Step 5)

Figure 4.23. Photograph of Completed Model Micropiles with Central Bar (Step 6)

Because of the small size of the model micropiles, it was possible to use a single piece of casing for the installation, unlike typical field installation where casing sections of 5 to 10 feet in length are threaded together to form the cased section. Thus, after the casing was withdrawn to the final height, approximately 1 foot of casing was sticking up above the surface of the sand.

The grout used for micropile installation consisted of a neat (no aggregate) cement grout using Type I/II Portland cement with a water to cement ratio of 0.45. During installation of the trial micropiles and the three sets of tested micropiles, grout samples were taken using 2-inch cube molds. The samples were covered by damp rags and left at the testing laboratory for approximately 24 hours. After the initial grout set at the laboratory, the cubes were removed from the molds and kept in a moist room until they were tested in unconfined compression in general accordance with ASTM C 109. The results of unconfined compression tests are provided in Table 4.6.

Table 4.6. Results of Grout Cube Compression Tests

Sample	Pour Date	Test Date	Curing Days	f 'c (psi)
Trial A	28-Jun-10	26-Jul-10	28	4785
Trial B	28-Jun-10	26-Jul-10	28	4684
Trial C	28-Jun-10	26-Jul-10	28	6825
1A	10-Aug-10	14-Aug-10	4	4741
1B	10-Aug-10	14-Aug-10	4	3008
1C	10-Aug-10	17-Aug-10	7	5539
2A	26-Oct-10	3-Nov-10	8	4046
2B	26-Oct-10	3-Nov-10	8	4489
3A	17-Dec-10	27-Jan-11	41	3564
3B	17-Dec-10	27-Jan-11	41	3814

Following load testing, the micropiles were exhumed and examined, including taking photographs and measurements of bond zone length and diameter. For all model micropiles, the cased length beneath the ground was 2 feet. In an attempt to standardize the bond zone diameter measurements, they were taken at 2 inches from the toe of the micropile, 2 inches from the bond zone-casing interface, and at the midpoint of the bond zone. An additional diameter measurement was taken at the location of any anomalies within the bond zone. The measurements of the bond zone dimensions are provided in Table 4.7. Note that the bond length of the third set of micropiles is shorter than the other two sets because it was not possible to push the casing through the dense sand to the desired maximum depth, as described in Step 2 above. Example photographs of several exhumed piles are shown in Figures 4.24 through 4.29, and photographs of all exhumed piles are provided in Appendix B.

Table 4.7. Bond Zone Dimensions of Exhumed Micropiles

Micropile	Bond Length (in)	Bond Diameter (in)				Location of 4th diameter measurement (in from toe)
		2 in from toe	2 in from casing	Centerline	Other	
1B	11.25	1.41	1.55	1.28	2.41	10.25
1C	11.5	1.26	1.11	1.29	1.81	1.75
1D	11	Bond Zone Destroyed when Exhumed				
1E	11	Bond Zone Destroyed when Exhumed				
1F	11	1.2	1.26	1.29	1.52	3.75
2A	11.5	1.38	5.3	1.46	1.89	5.25
2B	10.75	3.86	1.65	1.5	1.97	8.25
2C	9.75	1.11	1.51	1.38	1.95	3.25
2D	11.75	1.38	3.26	1.47	1.2	5
2E	9.75	1.14	1.43	1.33	1.86	3.25
2F	11	2.24	1.39	1.57	2.09	4
3A	7.5	1.18	1.34	1.25	1	1
3B	7.75	1.18	1.28	1.26	1.03	1
3C	7.25	1.26	1.26	1.23	1.11	1
3D	7.5	1.18	1.36	1.2	1.34	1.5
3E	7	1.29	1.26	1.43	1.48	1.25
3F	8.25	1.18	1.34	1.3	1.6	7

Figure 4.24. Photograph of Exhumed Pile 1F Bond Zone

Figure 4.25. Photograph of Exhumed Pile 1B Bond Zone

Figure 4.26. Photograph of Exhumed Pile 2F Bond Zone

Figure 4.27. Photograph of Exhumed Pile 2B Bond Zone

Figure 4.28. Photograph of Exhumed Pile 3D Bond Zone

Figure 4.29. Photograph of Exhumed Pile 3B

As shown in Figures 4.24 and 4.25, the bond zone of the micropiles installed for the first test set-up were relatively uniform throughout the bond zone length. For the second test set-up, the bond zone was not as uniform with several bulges (Figures 4.26 and 4.27). These bulges may have been the result of non-uniform sand layers or momentary spikes in the pressure applied to the top of the casing. Similar to the first test set-up, the micropile bond zones for test set-up three were very uniform. It is likely that the dense sand in the third test set-up is not as susceptible to spikes in pressure, resulting in the most uniform bond zones of the three phases. This conclusion is also applicable for full-scale micropiles where pressure grouting results in larger benefits in axial load capacity in loose sand as compared to dense sand. For all three phases of micropile installation, there were no cases of necking of the micropile bond zone (bond zone diameter less than casing diameter), indicating that the grout pressure was always greater than the earth pressure of the surrounding soil.

4.5. EXPERIMENTAL TESTING PROGRAM

Testing of the scale model micropiles was completed in three different phases or test pit set-ups. The first test phase consisted of testing Model 1 micropiles (see Table 4.2 for micropile properties) in loose to medium dense sand placed using the air pluviation method. The second phase tests consisted of testing the thinner-walled Model 2 micropiles (see Table 4.2) in loose to medium dense sand placed using the air pluviation method. The third phase tests consisted of testing a combination of Model 1 and Model 2 micropiles in dense sand placed using the vibratory compaction method. For all three phases, the testing program consisted of applying vertical loads, lateral loads, and simultaneous vertical and lateral (combined) loads to the micropiles using dead weights. The loading schedule for the axial compression tests is shown in Table 4.8 and the loading schedule for the lateral and combined load tests is provided in Table 4.9. For all of the tests, deflection at the head of the micropile and strain within the micropile were recorded continuously throughout the test. The applied load was recorded manually for each load increment based on the dead weights placed on the micropile. A general description of the testing methods is provided in the following paragraphs.

A total of six (6) axial compression load tests were completed on the model micropiles, including two tests in phase one (1B and 1F), two tests in phase two (2A and 2F), and two in phase three (3B and 3F). To apply the axial load, a platform was attached near the top of the casing and steel plates with known weights were incrementally placed on the platform in general accordance with the load schedule shown in Table 4.8 until the failure load was reached. The failure load was defined as the load at which the micropile

plunged. Creep tests were conducted at an axial load of approximately 204 pounds. The axial compression test setup is shown in Figure 4.30.

Table 4.8. Axial Loading Sequence (planned)

Load Cycle	Axial Load (lbs)	Hold Time (min)
Alignment	9.6	2.5
Cycle 1	34.3	2.5
	56.6	2.5
	81.3	2.5
	9.6	1
Cycle 2	34.3	1
	81.3	1
	103.6	2.5
	128.3	2.5
	140.6	2.5
	152.9	2.5
	9.6	1

Load Cycle	Axial Load (lbs)	Hold Time (min)
Cycle 3	34.3	1
	150.6	1
	187.6	2.5
Begin Creep	204.3	10
End Creep	204.3	
	222.3	2.5
	244.6	2.5
	269.3	2.5
	291.6	2.5
	316.3	2.5
	341	2.5
	365.6	2.5
	244.6	1
	150.6	1
	99.6	1
	9.6	1

Table 4.9. Lateral/Combined Loading Sequence (planned)

Lateral Load (lbs)	Hold Time (min)
0	5
8.4	5
12.8	5
25.1	5
41	5
51	7.5
67.7	10
88	10
98	10

Lateral Load (lbs)	Hold Time (min)
110.3	10
122.7	10
135	10
147.3	10
110.3	5
75.6	5
41	5
0	5

Figure 4.30. Photographs of Axial Load Tests

A total of six (6) lateral load tests were completed on the model micropiles, including two tests in phase one (1B that was also tested in axial compression and 1E), two tests in phase two (2B and 2E), and two in phase three (3A and 3E). Lateral loads were applied using a cable pulled by dead weights on a pulley. Specifically, a cable was attached to the micropile casing and the cable traversed over a pulley on the side of the test pit and attached to a vertical load hanger. Steel plates with known weights were then placed on the load hanger in general accordance with the load sequence shown in Table 4.8 and the load was transferred to the micropile through tension in the cable. The tests were conducted until lateral failure that was defined as excessive tilt of the micropile such that additional weights could not be added to the load hanger. A schematic of the lateral load test set-up is provided in Figure 4.31 and a photograph of a lateral load test is shown in Figure 4.32.

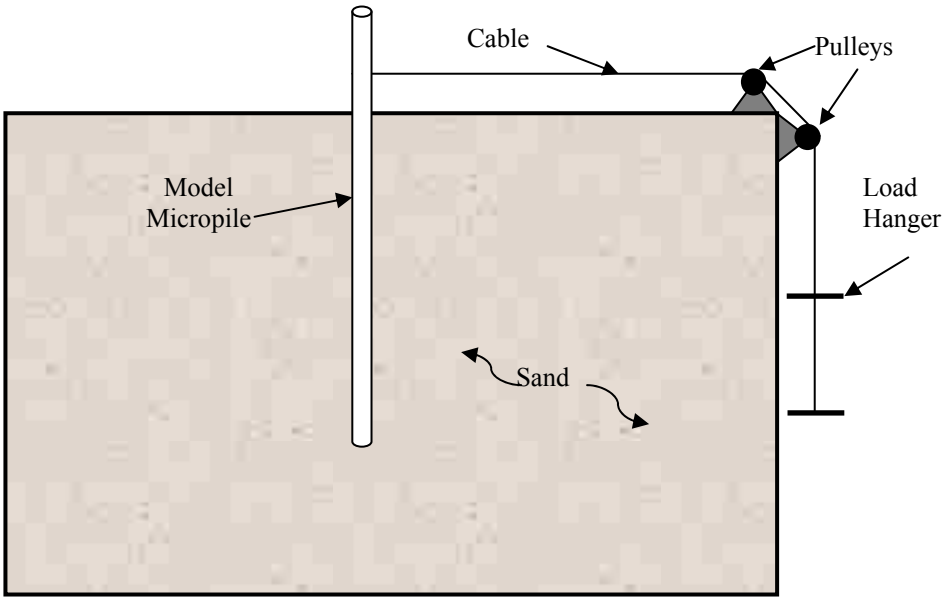

Figure 4.31. Schematic of Lateral Load Test Set-up

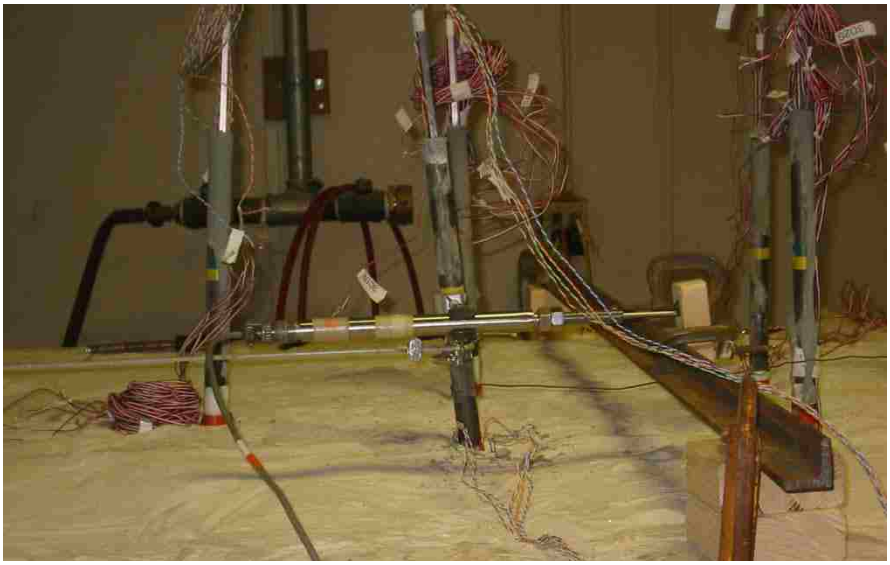

Figure 4.32. Photograph of Lateral Load Test

A total of six (6) combined load tests were completed on the model micropiles, including two tests in phase one (1C and 1D), two tests in phase two (2C and 2D), and

two in phase three (3C and 3D). The first step of the combined load tests was to incrementally apply an axial load using dead weight as described in the axial load test discussion above. The maximum axial load applied to the micropile during combined load testing was approximately one-half of the ultimate load determined during the axial load test. After the axial load was applied, lateral loads were incrementally applied as described in the lateral load testing discussion and in general accordance with Table 4.9. Similar to the lateral load tests, the combined load tests were taken to failure which was defined as excessive tilt of the micropile such that additional weights could not be added to the load hanger or the weights applying the axial load were beginning to slide off of the load platform. Photographs of the combined load tests are shown in Figure 4.33.

Figure 4.33. Photographs of Combined Load Tests

4.6. DATA REDUCTION

As previously discussed in Section 3.3, the data acquisition system recorded data from the displacement transducers and resistive strain gages. The displacement transducers were calibrated prior to testing such that the voltage that was read by the data acquisition system was automatically converted to a displacement reading and the output was recorded in inches.

Unlike the displacement transducers, the output from the resistive strain gages requires some post-processing to obtain the desired parameters from the gages, including load and bending moment. Resistive strain gages operate on the theory that the resistance of a wire will change as the tension in the wire is increased or decreased. A small current is run through the lead wires and the strain gage and the resistance in the loop is measured. The data acquisition box then converts the resistance to a strain reading via the gage factor that is listed in Table 4.5, and the recorded data is in the form of microstrain. The actual magnitude of microstrain is not of much use by itself. Rather, the changes in microstrain throughout the test are the desired data that can be used to obtain the load and bending moment at any point during each test. In locations where a single gage was present and bending was negligible, such as within the bond zone, the change in microstrain could be used to directly compute load (P) using Equation 3.

$$P = \Delta\mu\varepsilon * E * A \tag{3}$$

where: $\Delta\mu\varepsilon = Change\ in\ microstrain$

$E = Modulus\ of\ elasticity$

$A = Cross - sectional\ area\ of\ micropile$

To calculate bending moment, several assumptions need to be made. First, the calculations assume that the gages are located exactly within the plane where the bending occurs and are spaced equidistant from the center of the micropile. Second, the calculations assume that, because the grout is confined within the casing, significant cracking of the internal grout does not occur during bending and that any minor cracking that occurs is equal on the tension and compression sides of the grout. This assumption results in the neutral axis coinciding with the centerline of the micropile, as shown in Figure 4.34.

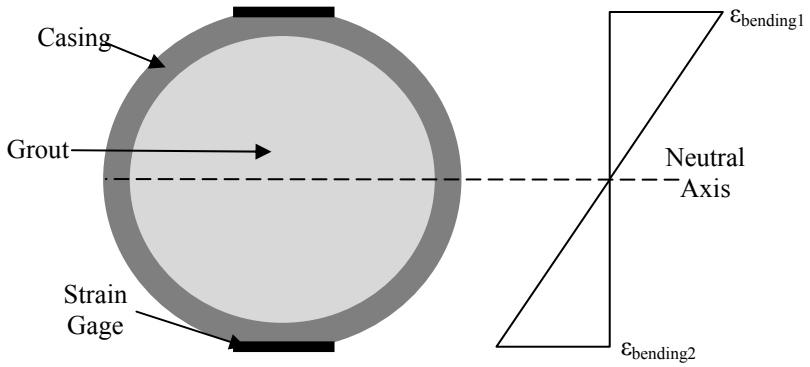

Figure 4.34. Strain Diagram for Micropile Subjected to Bending

Because bending does not occur at the neutral axis, the strain at the neutral axis is equal to the axial strain. In addition, because the strain gages are assumed to be equidistant from the centerline (distance x), the strain resulting from bending at the gage locations should be equal and opposite (see Figure 4.34). Therefore, the axial strain can be computed by averaging the two strain readings from the pair of strain gages (Equation 4) and the bending strain can be calculated by subtracting the axial strain from the

original strain reading, as shown in Equation 5. Axial load (P) and bending moment (M) can then be calculated from the resulting strains using Equations 6 and 7, respectively.

$$\varepsilon_{\text{axial}} = \frac{(\Delta\mu\varepsilon)_1+(\Delta\mu\varepsilon)_2}{2} \quad (4)$$

$$\varepsilon_{bending} = (\Delta\mu\varepsilon)_1 - \varepsilon_{axial} \quad (5)$$

$$P = \varepsilon_{axial} * E * A \quad (6)$$

$$M = \frac{I*E*\varepsilon_{bending}}{x} \quad (7)$$

Because the cross-section of the micropile consisted of grout and steel (central reinforcing bar and/or casing), transformed sections were used to calculate the moment of inertia (I) and the cross-sectional area (A). Specifically, the grout was transformed to an equivalent area of steel by multiplying the grout area by the ratio of steel modulus to grout modulus. The transformed area was then used to calculate an equivalent diameter and ultimately an equivalent moment of inertia. As previously discussed, some cracking of the grout may occur as higher lateral loads are applied. The standard of practice for design of micropiles subjected to lateral loads is to ignore the contribution of the grout to structural bending resistance. This approach is conservative, which is appropriate for design, but likely does not account for the actual behavior during lateral loading. Because this conservative approach is typically used, there is no consensus within the micropile design community on how to account for increased bending resistance from the grout. However, the American Concrete Institute (ACI) manual contains

recommendations for concrete-filled, steel pipe columns subjected to lateral or eccentric loads. The ACI manual recommends using 70 percent of the moment of inertia that is contributed from the concrete [ACI 1999]. By comparing the moments of inertia in the cased zone, it is apparent that inclusion of the grout in the moment of inertia calculation has little to no effect. Thus, assumptions regarding cracking within the casing do not have a large effect on the calculated bending moments, and does not need to be investigated further. If bending occurs within the bond zone, it is likely that the level of grout cracking will be greater than within the cased zone. Therefore, it was assumed that the transformed section moment of inertia for the bond zone included 50 percent of the moment of inertia that is contributed from the grout. The resulting transformed areas, moments of inertia, and modulus of elasticity used in the data reduction are shown in Table 4.10.

Table 4.10. Model Micropile Parameters Used for Data Reduction

Parameter	**Model 1**	**Model 2**
Modulus of Elasticity, E_{steel}	29,000 ksi	29,000 ksi
Cased Section		
Steel Area, A_{steel}	0.44 in^2	0.31 in^2
Steel Moment of Inertia, I_{steel}	0.026 in^4	0.018 in^4
Tranformed Area, A_{trans}	0.46 in^2	0.35 in^2
Tranformed Moment of Inertia, I_{trans} (Assumes 70% of I_{grout} to account for cracking)	0.026 in^4	0.020 in^4
Bond Zone		
Tranformed Area, A_{trans}	0.20 in^2	0.22 in^2
Tranformed Moment of Inertia, I_{trans} (Assumes 50% of I_{grout} to account for cracking)	0.0085 in^4	0.0081 in^4

4.7. INTERPRETATION OF RESULTS

This section presents the results of each type of test (axial, lateral, and combined), including interpretations and comparisons between the lateral and combined load tests.

4.7.1. Axial Load Test Results and Interpretation. Micropiles 1B, 1F, 2A, 2F, 3B and 3F were tested in axial compression to failure as previously discussed. Data from the displacement transducers was used to produce plots of applied axial load versus axial displacement at the micropile head, as shown in Figure 4.35.

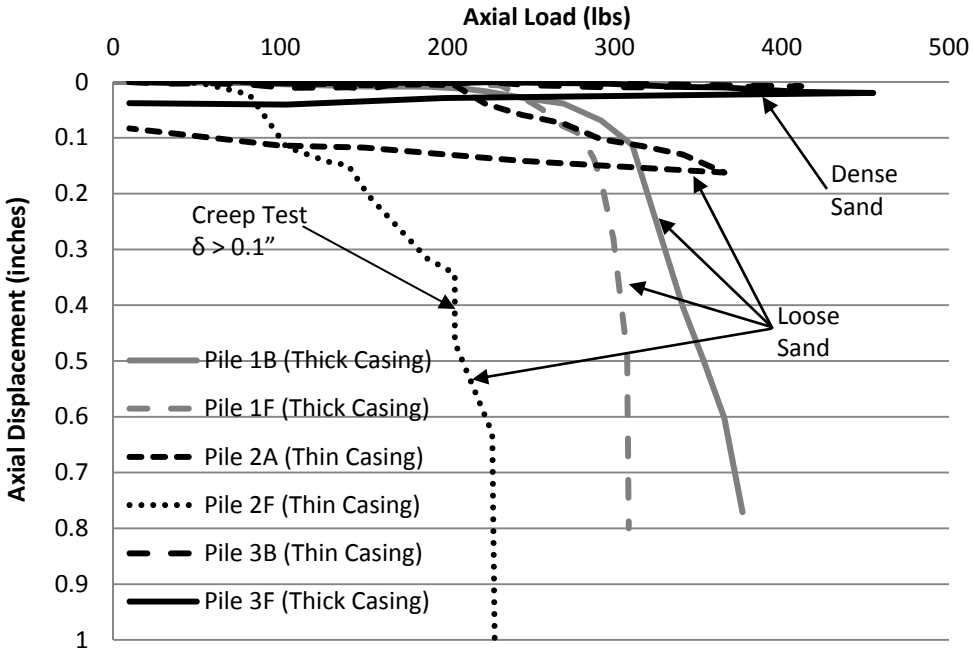

Figure 4.35. Axial Load Test Results – Load vs. Displacement

As previously discussed, the ultimate capacity of the micropiles tested in axial compression was defined as the load at which the pile plunged. Of the six micropiles tested, only three were plunged, including Micropiles 1B, 1F, and 2F. Micropile 2A was not plunged, but did experience excessive deflection of approximately 20 percent of the

micropile diameter. As shown in Figure 4.35, the plunge loads for Micropiles 1B, 1F and 2F were 308, 376, and 244 pounds, respectively.

A creep test was conducted at an axial load of approximately 200 pounds. The magnitude of deflection during the creep test was so small for all tests except Micropile 2F that it is difficult to see in Figure 4.35. The FHWA Micropile Manual [Sabatini et. al. 2005] states that the acceptance criterion for the creep test is that deflection should not exceed 0.04 inches between 1 minute and 10 minutes of hold time. For a displacement scale factor of 22.6, the resulting allowable deflection would be 0.002 inches. Because the magnitude is smaller than the precision of the displacement transducers, it is not possible to evaluate whether the majority of the creep tests passed the FHWA criterion. However, because the displacement of Micropile 2F was greater than 0.1 inches during the creep test, it is clear that it failed.

Using reduced data from the strain gages, load transfer plots (load versus depth) were prepared, as shown in Figures 4.36 and 4.37 for Micropiles 2A and 3F, respectively. A schematic showing the approximate locations of the casing, bond zone, and strain gages is provided on each figure. The text box shown at the top of each line is the applied axial load, and each data point along a single line represents the locations of strain gages within the micropile. As can be seen in the plots, the load is transferred deeper as the load increases. The reason for this phenomenon is that displacement must occur to mobilize the side friction resistance along the length of the pile. Thus, as a load is applied to the top of the micropile, the pile itself will elastically compress and begin to mobilize side friction in the upper portion of the micropile. When the full side friction is mobilized in the upper portion of the micropile, additional load is transferred deeper.

This iterative effect continues until load reaches the toe of the micropile where end bearing may then be mobilized. The micropile will fail when the applied load increases beyond the available side friction and end bearing resistance.

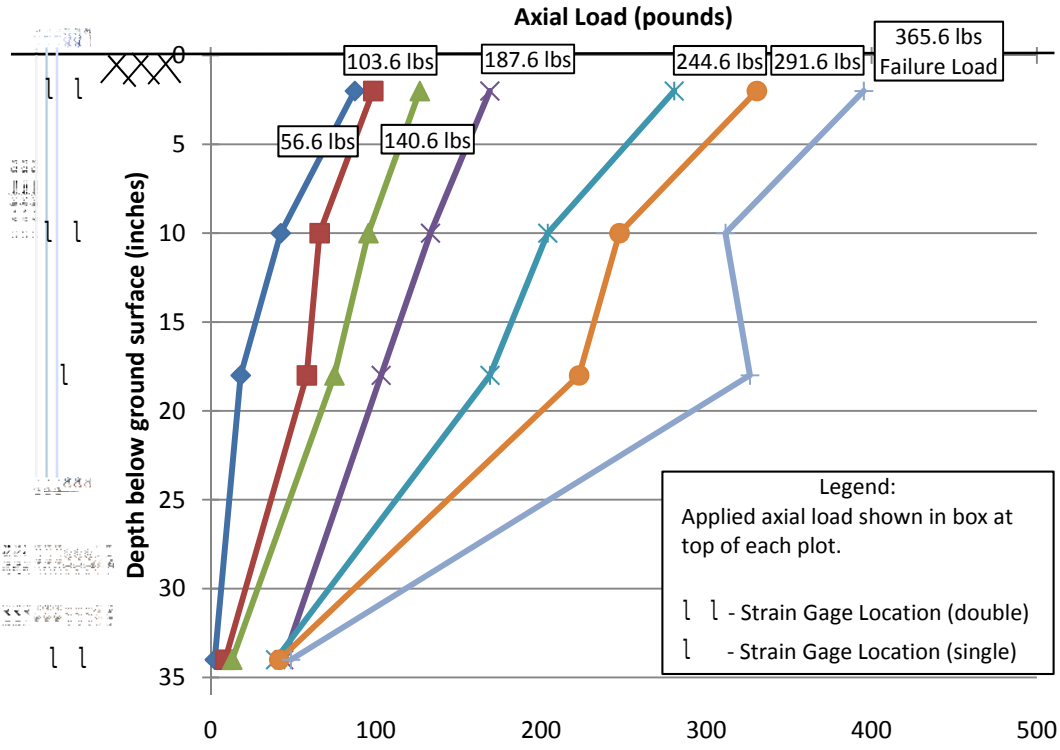

Figure 4.36. Micropile 2A Axial Load Test Results – Load vs. Depth

As expected, the micropiles installed in dense sand (3B and 3F) had much higher axial capacities and behaved much stiffer than the model micropiles installed in loose to medium dense sand. For Micropiles 3B and 3F, the majority of the displacement was a result of elastic compression of the structural member, as evidenced by the small about of residual deflection that resulted after the micropiles were unloaded (Figure 4.35). Because the bond zone diameters and lengths were similar for the phase one micropiles,

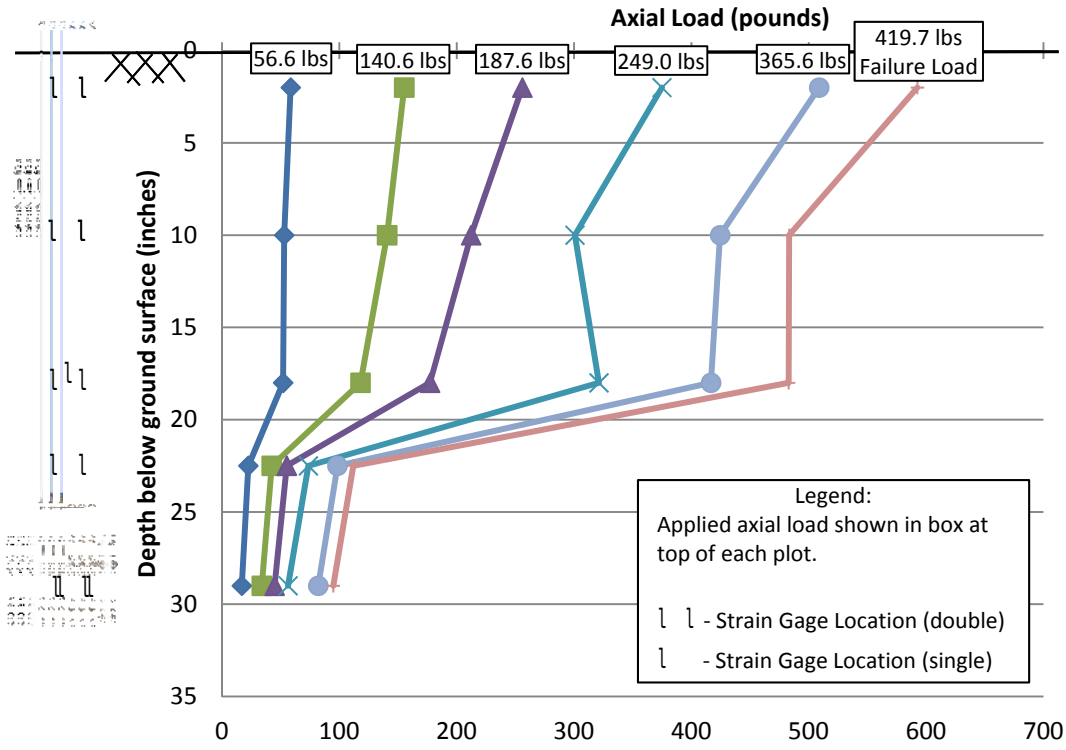

Figure 4.37. Micropile 3F Axial Load Test Results – Load vs. Depth

as shown in Figures 4.25 (1B) and 4.24 (1F) and Table 4.6, the load-deflection results were similar. Relatively small differences in axial capacity were likely the result of small differences in density throughout the sand pit. Conversely, for the phase two micropiles (2A and 2F; see Figure 4.26 and Table 4.6), the bond zone diameters were different, resulting in different load-deflection behavior. Specifically, the bond zone for Micropile 2A had a large bulge (5.3 inches) near the interface between the casing and the bond zone. The bulge increased the axial capacity such that Micropile 2A had a much larger capacity than Micropile 2F. Similar to the first phase of testing, the micropiles installed for the third phase had similar bond zone diameters and lengths, resulting in similar behavior when subjected to axial loads.

The slope of the load versus depth curves in Figures 4.36 and 4.37 give an indication of load transfer along the length of the micropile. Typcially, the load versus depth curves are flatter within the bond zone because the side resistance is much greater in the bond zone and more load is transferred from the micropile to the adjacent ground. This effect is especially apparent for Micropile 3F (Figure 4.37) where the load transfer curve is nearly vertical for the majority of the cased section. The near-vertical curves indicate that nearly all of the load is being transferred through the casing without shedding load to the adjacent ground. Below the vertical portion of the plot, the curve dramatically flattens, indicating that the bond strength is high and the majority of the applied load is being transferred to the surrounding soil within the bond zone. The differences in the steepness of the load versus depth curves are not as apparent in the results for Micropile 2A (Figure 4.36), except at the higher loads where the average steepness in the cased section is approaching vertical and the slope within the bond zone is flatter.

Visual comparison of the load transfer curves for the two axial load tests indicates that the micropile installed in dense sand (3F) has a higher bond strength than the micropile installed in loose sand (2A), as expected. To quantify these differences, the ultimate unit side resistance (α_{bond}) can be back-calculated using the loads calculated from the strain gages (P_{SG}) as shown in Equation 8. For micropiles loaded to failure, the failure condition was used to calculate the loads used in the equation. For the case of micropiles installed in dense sand that could not be taken to a failure condition, the plot for the maximum applied load was used. Because it was not taken to failure, the back-

calculated bond strength is likely less than the true ultimate bond strength that would be reached if a failure condition was achieved.

$$\alpha_{bond} = \frac{\Delta P}{\pi * D_{bond} * L_{SG}} \quad (8)$$

where: $D_{bond} = Diameter\ of\ bond\ zone$

$L_{SG} = Distance\ between\ two\ strain\ gages$

The resulting α_{bond} calculated from the load test data on Micropiles 2A and 3F were 2.2 psi and 19.3 psi, respectively. If these values are scaled up to the prototype using the stress scaling factor of 8 shown in Table 4.1, the resulting prototype α_{bond} for Micropiles 2A and 3F were 17.6 psi and 154.4 psi, respectively. The summary of typical α_{bond} values listed in the FHWA Micropile Manual [Sabatini et. al. 2005] indicates a range of 10 to 27.5 psi for Type B micropiles in loose to medium dense sand and 17.5 to 52 psi for Type B micropiles in medium dense to very dense sand. Thus, the back-calculated bond strength for Micropile 2A was within the expected range for loose to medium dense sand. However, the bond strength from the Micropile 3F axial load test was approximately 3 times higher than the upper end of the range provided in the FHWA Manual. The differences from published values may be a result of having a uniform manufactured sand, scaling effects, or differences in installation because the casing was pushed into place rather than drilled into place. Pushing the casing resulted in displacement of sand that may have increased lateral stress in the vicinity of the micropile

rather than stress relief that may result from drilling the casing and removing material from the micropile location.

Despite the generally accepted design premise that toe bearing of micropiles is minimal and should be ignored, some toe bearing was observed in the test results. If toe bearing was not occurring, the load calculated from the lowest level of strain gages would approach zero throughout the test. Rather, using the loads shown in the figures at the toe of the micropiles during the failure condition, values of toe bearing can be calculated. Because a failure condition was not reached for Micropile 3F, a very low percentage of the load reached the toe of the pile and the slope of the load transfer curve was nearly vertical above the toe. Thus, it is not valid to attempt to calculate a toe bearing value for the Micropile 3F test. For the axial load test on Micropile 2A, the toe bearing at failure was approximately 34 pounds which was approximately 9.4 percent of the ultimate failure load. This corresponded to a back-calculated ultimate net toe bearing of 22.9 psi which is equal to a value of 183.3 psi for the prototype micropile. Because toe bearing is typically ignored for micropiles, there is not a widely accepted analytical method for estimating toe bearing. Therefore, analytical methods that relate CPT tip resistance to toe bearing were used to compare a theoretical toe bearing to the observed toe bearing during the axial load test. Based on the method proposed by Eslami and Fellenius [Coduto 2001], the estimated ultimate unit toe bearing resistance was approximately 49.5 psi. The large discrepancy in the theoretical and measured values of toe bearing resistance were likely because the method was developed based on axial load tests of driven piles. While an adequate prediction method is not yet available, it is reasonable to expect that some toe bearing will be present during axial loading provided good construction techniques

are used during installation. If further research is conducted to assess the effect of different construction methods in different soil types, undue conservativism in certain micropile designs may be eliminated. Designers will also need to assess the amount of deflection that is required to mobilize toe bearing and compare it to the allowable settlement of the supported structure.

4.7.2. Lateral Load Test Results and Interpretation. Micropiles 1B, 1E, 2B, 2E, 3A, and 3E were tested by applying a lateral load near the head of the pile in the absence of an axial load, as previously discussed. Data from the displacement transducers were used to produce plots of lateral load versus lateral displacement near the micropile head, as shown in Figure 4.38.

The test results shown in Figure 4.38 indicate that the density of the sand has much more influence on the load-deflection behavior of the laterally loaded piles than the lateral stiffness (casing thickness) of the micropiles. The behavior of the two piles tested in dense sand behaved similarly, and the four piles tested in loose sand also behaved in a similar manner to each other. As expected, the micropiles installed in dense sand exhibited a much stiffer behavior than the micropiles installed in loose sand. The variation of behavior for the micropiles installed in loose sand does not appear to correlate to the lateral stiffness of the piles.

In addition to the lateral load versus lateral displacement curve, the data obtained from the strain gages was used to plot lateral load versus maximum bending moment. At each strain gage level and for each applied lateral load, bending moments were calculated as discussed in Section 4.7 and used to develop the plot shown in Figure 4.39.

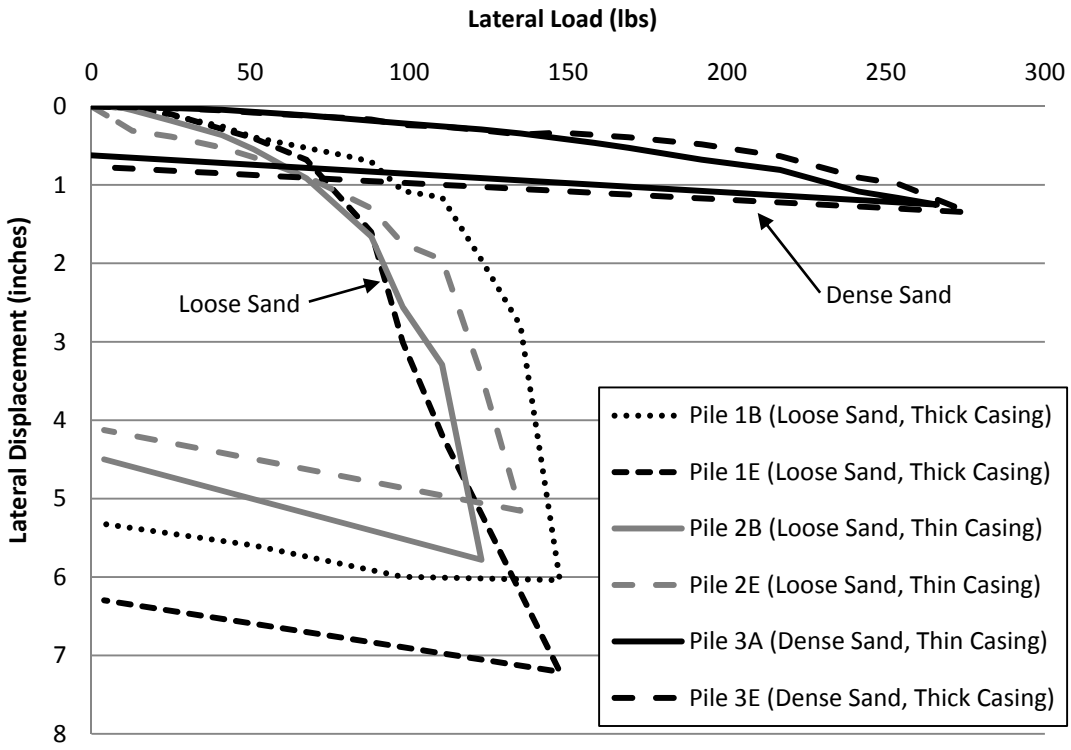

Figure 4.38. Lateral Load Test Results – Load vs. Displacement

Similar to the results in the load-deflection plots (Figure 4.38), the load versus maximum bending moment results shown in Figure 4.39 indicate that the lateral stiffness of the micropile has little effect on the bending moment. In addition, it appears that the maximum bending moment is very similar for the piles installed in loose and dense sands for loads less than approximately 100 pounds. Beyond lateral loads of about 100 pounds, the micropiles installed in loose sand began to experience larger maximum bending moments. This is likely because large deflections were occurring as the piles were reaching the maximum applied load.

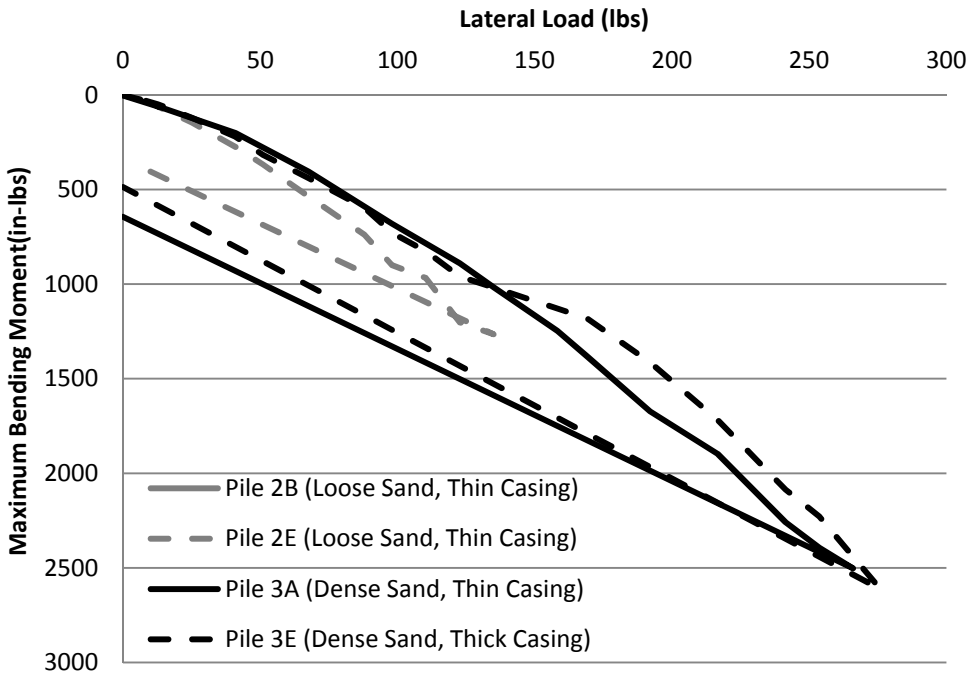

Figure 4.39. Lateral Load Test Results – Load vs. Maximum Bending Moment

Using the strain gage data, plots of bending moment versus depth were also prepared for several different magnitudes of lateral load, as shown in Figures 4.40, 4.41, 4.42 and 4.43 for Micropiles 2B, 2E, 3A, and 3E, respectively. Because of problems with the strain gages in trial one, the moment versus depth plots are not shown. Because the micropiles had a free head condition, the bending moment was assumed to be zero at the location where the lateral load was applied (approximately 4 inches above the ground surface). In addition, the bending moment was assumed to be zero at the toe of the micropiles. Sketches showing the approximate locations of the casing, bond zone, and strain gages are provided in each figure.

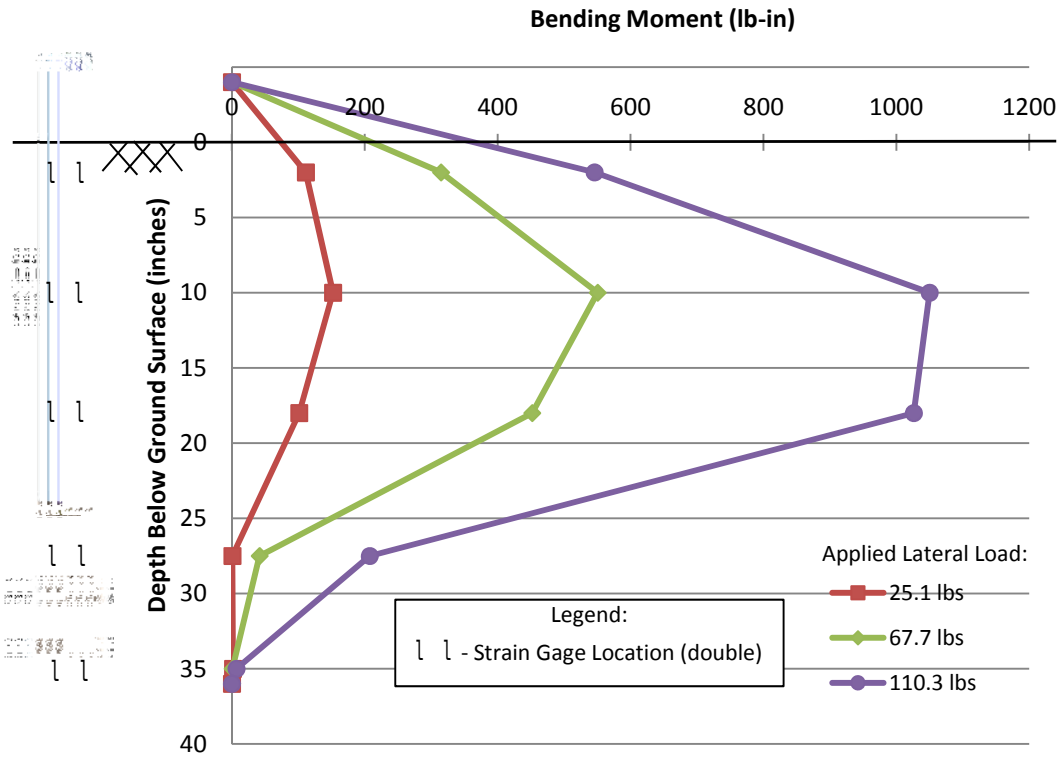

Figure 4.40. Micropile 2B (Loose Sand, Thin Casing) Lateral Load Test Results – Bending Moment vs. Depth

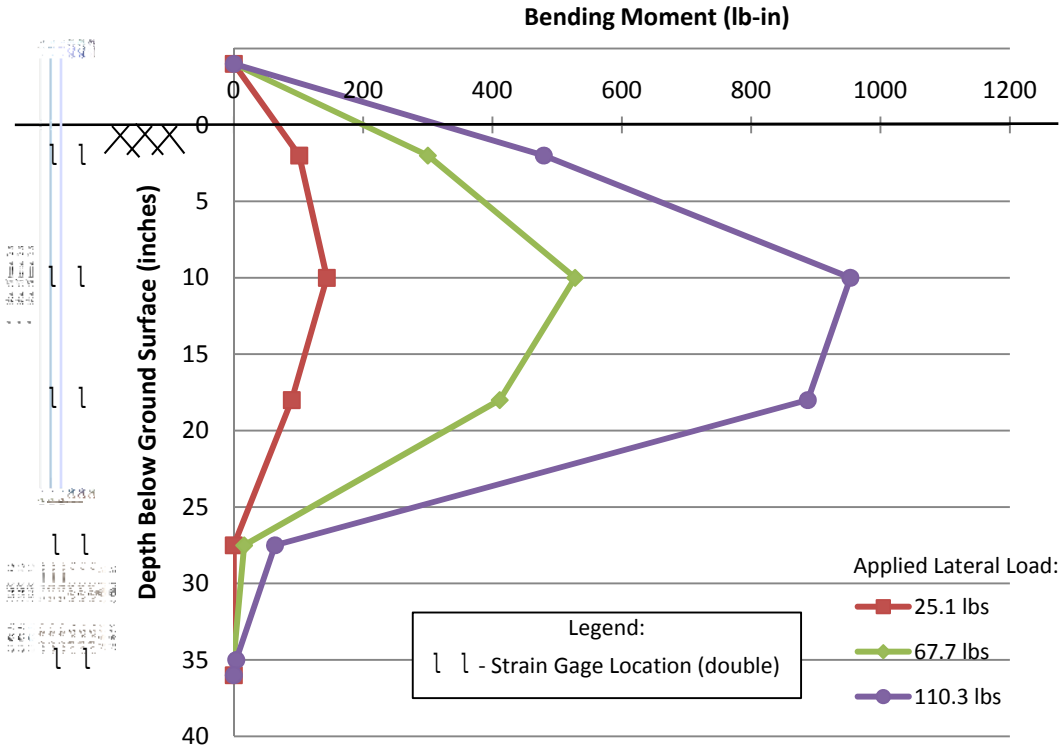

Figure 4.41. Micropile 2E (Loose Sand, Thin Casing) Lateral Load Test Results – Bending Moment vs. Depth

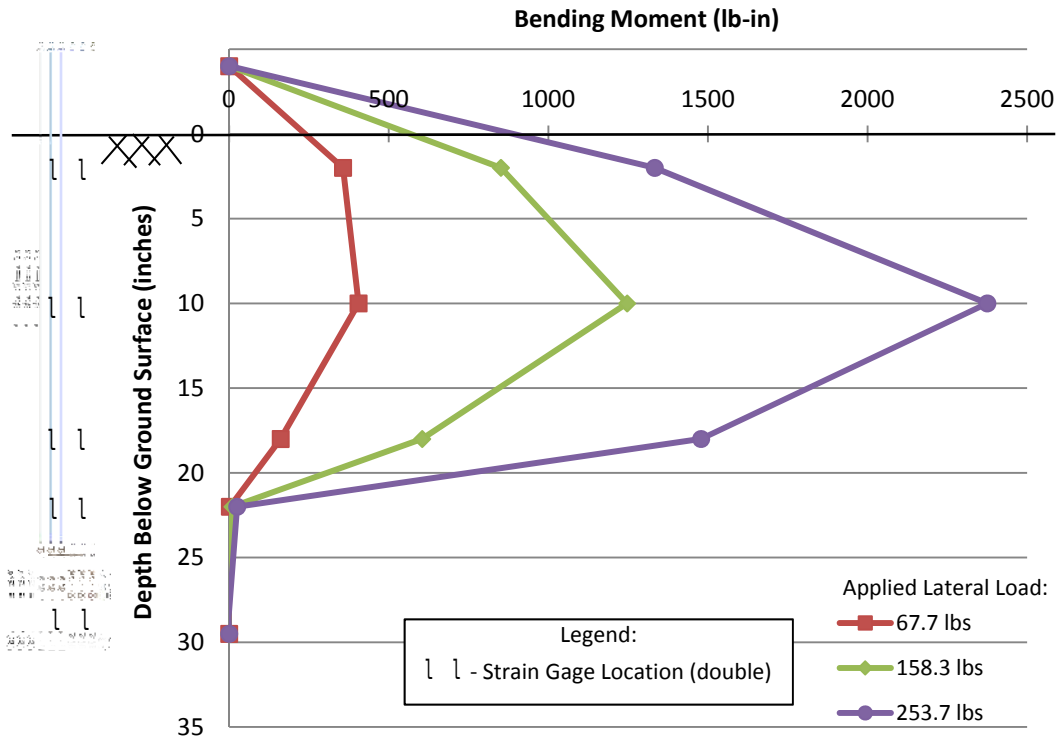

Figure 4.42. Micropile 3A (Dense Sand, Thin Casing) Lateral Load Test Results – Bending Moment vs. Depth

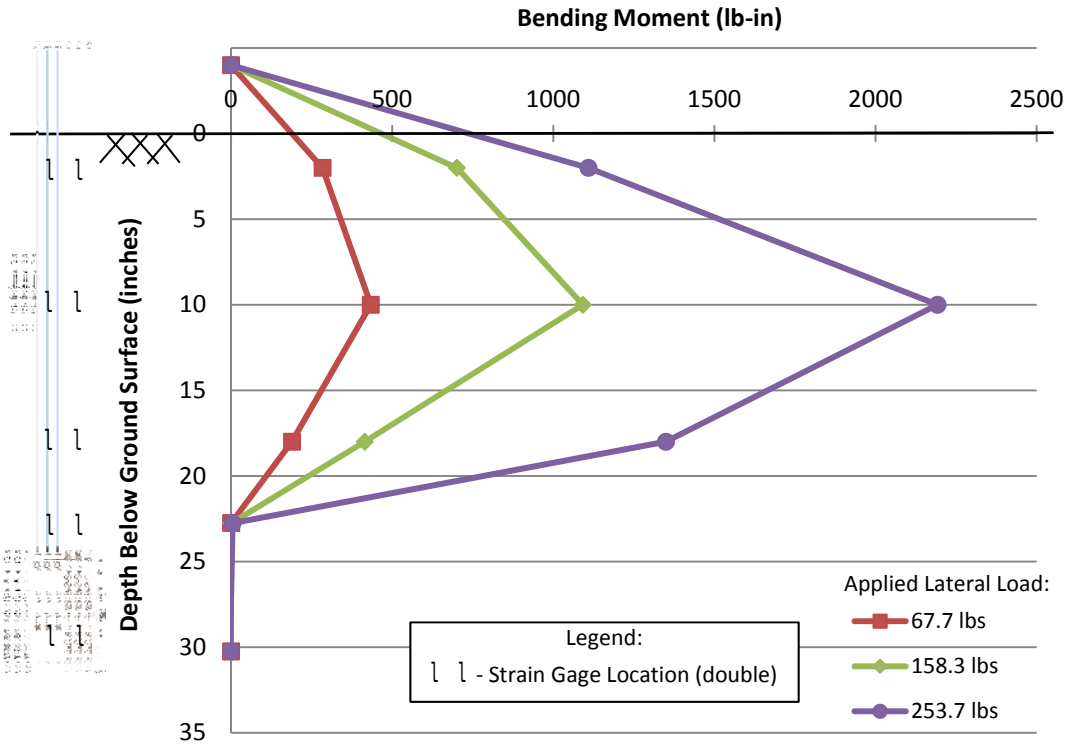

Figure 4.43. Micropile 3E (Dense Sand, Thick Casing) Lateral Load Test Results – Bending Moment vs. Depth

Comparison of the four bending moment versus depth plots indicates that the magnitude and location of the maximum bending moments, as well as the shape of the bending moment curves are very similar for similar soil densities (2B and 2E – loose; 3A and 3E – dense). Comparing the results of the tests in loose sand to the dense sand results, it appears that the shape of the curves is similar for the lower load increments. However, for the largest applied lateral loads, the shape of the bending moment curve for the loose sand condition appears to change as the bending moment is transferred deeper in the casing and even into the bond zone.

Finally, Figures 4.44 and 4.45 were prepared to further compare the results of four of the lateral load tests. Figure 4.44 compares the bending moment diagrams at similar applied lateral loads (approximately 98 lbs) for each test. However, lateral failure is typically defined in terms of a maximum allowable deflection. Therefore, Figure 4.45 was prepared to compare the bending moment diagrams at similar lateral displacement (approximately 0.2 inches). The 0.2-inch lateral displacement was chosen because it was difficult to get meaningful data from the strain gages below this deflection level for the loose sand cases since only small loads were required to get to 0.2 inch of lateral deflection. This lateral displacement is comparable to a deflection of about 4.5 inches in the prototype which is likely higher than would be allowed for design of production micropiles. The text on both plots indicates the lateral load and lateral displacement for each bending moment diagram. It appears that plotting the bending moment diagrams at similar applied lateral loads is the preferred method for plotting the results because the curves for micropiles installed in the same density sand (2B and 2E – loose; 3A and 3E – dense) are very close. The plots of data at similar lateral deflections do not work very

well for the loose sand condition because the assumed allowable deflection is reached at such a small load increment. A comparison of the bending moment diagrams for the four lateral tests shows that the maximum bending moments for the loose sand condition are slightly higher and slightly deeper than the dense sand condition. This result was expected because the micropiles in loose sand experienced greater later displacement and, thus, greater bending of the micropile.

The similarity of results for micropiles installed in similar soil conditions indicates that the lateral load tests were highly reproducible. Because of the reproducibility, the results can be used to develop basic conclusions regarding lateral behavior of micropiles.

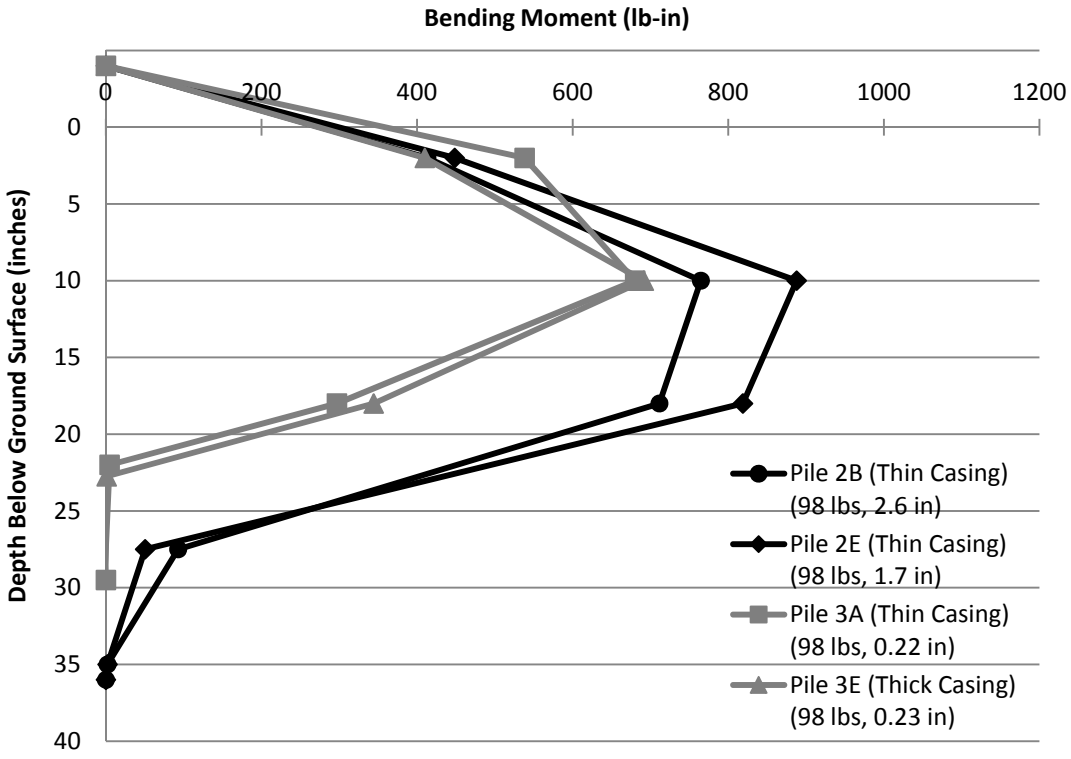

Figure 4.44. Bending Moment vs. Depth at Maximum Lateral Load (Approx. 98 lbs)

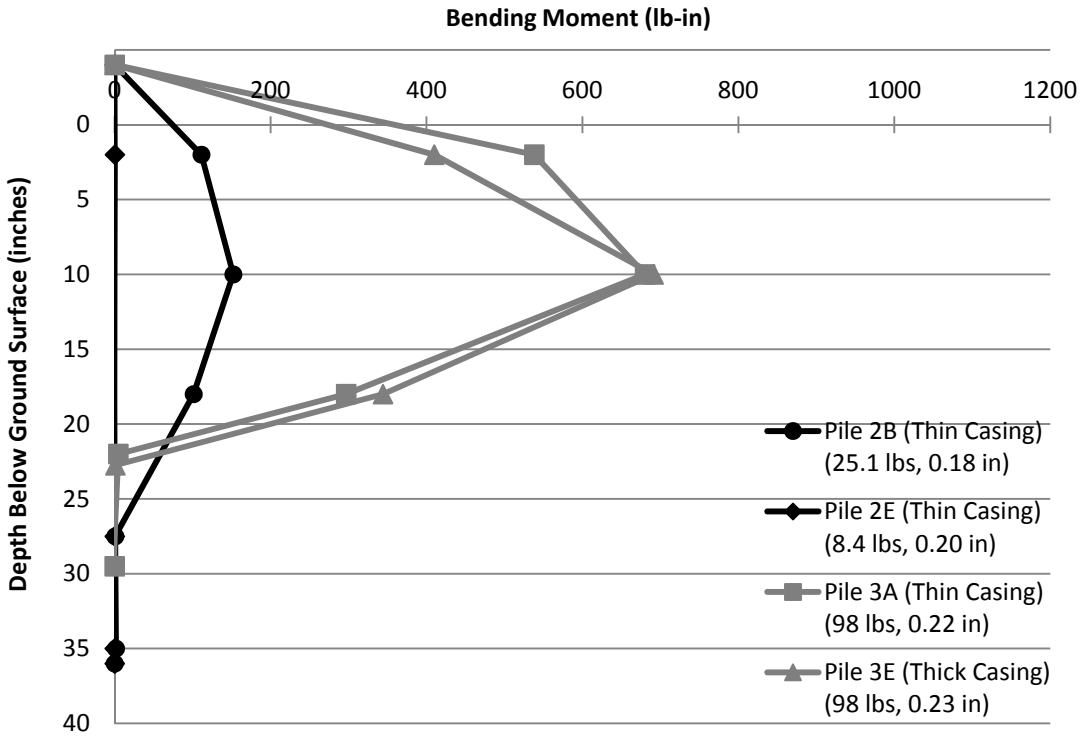

Figure 4.45. Bending Moment vs. Depth at Allowable Deflection (Approx. 0.2 in)

First, the density of the sand has a much greater effect on the lateral behavior of the micropiles than the structural stiffness of the micropiles. While it was expected that the soil density would have a large effect, it was surprising that the structural stiffness had no discernable effect on the lateral behavior, as shown in Figures 4.38, 4.39, 4.44, and 4.45. The practical considerations from this conclusion are that it is very important to properly characterize the subsurface conditions for a laterally loaded micropile. In addition, overdesign of the micropiles by increasing the casing thickness may not reduce the lateral deflection to acceptable levels.

Second, while the micropile installed in dense sand behaved somewhat differently than the micropile in loose and, there were some similarities between their behaviors. The most striking similarity was that the rate of increase of the maximum bending

moment was nearly identical for all of the tests. In other words, as the lateral load was increased, the maximum bending moment increased by approximately the same ratio for the micropiles, regardless of soil density, as shown by the general slope of the plots in Figure 4.38.

4.7.3. Combined Load Test Results and Interpretation. Micropiles 1C, 1D, 2C, 2D, 3C, and 3D were tested by applying a axial load and then incrementally applying lateral loads near the head of the pile as the axial load was held constant, as previously discussed. The applied axial load was approximately equal to one-half of the ultimate axial capacity or maximum applied load as determined from the axial load tests. Thus, micropiles in the first phase of testing (1C and 1D) were subjected to an axial load of 152.8 lbs, micropiles in the second phase of testing (2C and 2D) were subjected to an axial load of 130.5 lbs, and micropiles in the third phase of testing (3C and 3D) were subjected to an axial load of 188.6 lbs. Data from the displacement transducers were used to produce plots of lateral load versus lateral displacement near the micropile head, as shown in Figure 4.46. As expected, the results from the tests on micropiles installed in similar soil densities resulted in similar load-deflection behavior. The structural stiffness of the micropiles also appears to have a slight effect on the results.

Figure 4.47 presents lateral load versus maximum bending moment for four of the combined load tests. Because of problems with strain gages in the phase one testing (Micropiles 1C and 1D), the results are not presented. Similar to the load-deflection results, the results shown in Figure 4.47 indicate that micropiles installed in similar soil densities exhibit similar behavior, and the structural stiffness of the micropiles also appears to have a slight effect on the results.

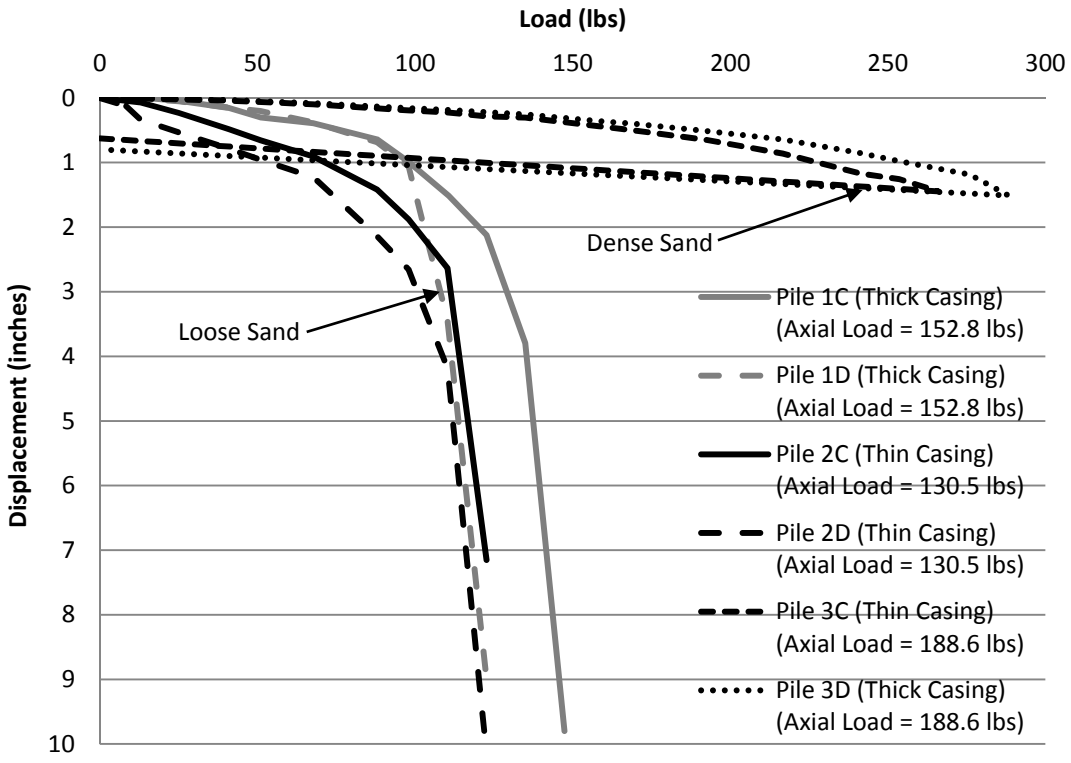

Figure 4.46. Combined Load Test Results – Load vs. Displacement

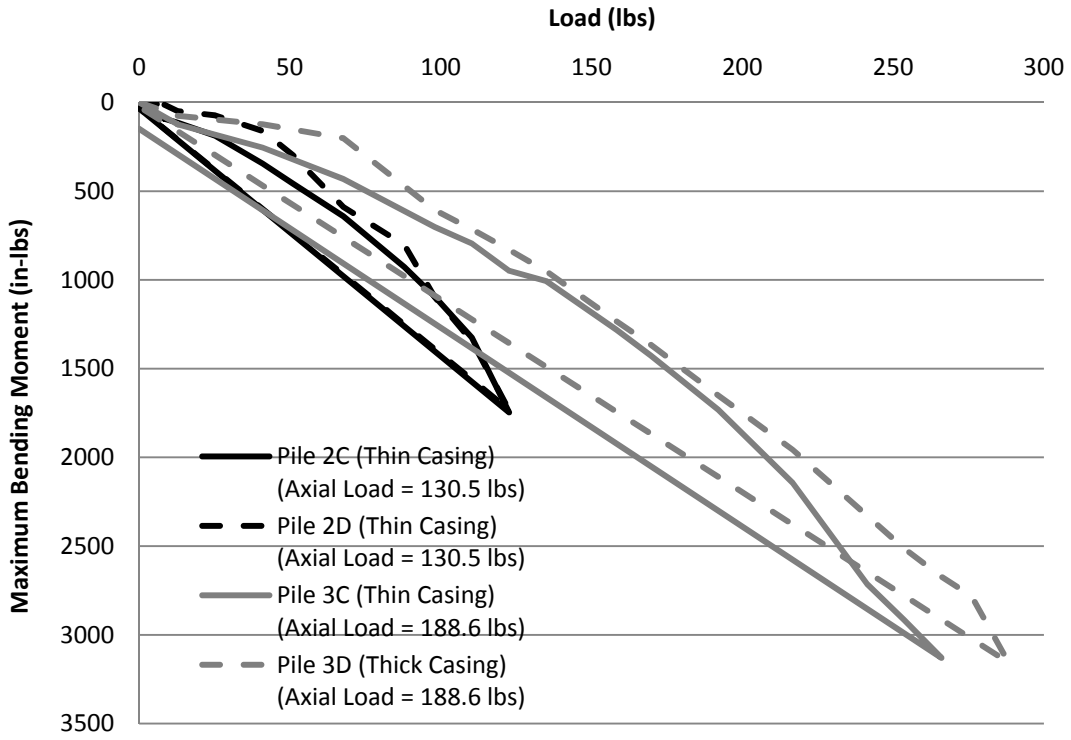

Figure 4.47. Combined Load Test Results – Load vs. Maximum Bending Moment

Using the strain gage data, plots of bending moment versus depth were also prepared for several different magnitudes of lateral load. The plots for combined load tests on Micropiles 2C, 2D, 3C, and 3D are shown in Figures 4.48, 4.49, 4.50, and 4.51, respectively. The testing apparatus was designed to model a free head condition by applying dead weights at the top of the pile such that it was able to rotate as lateral loads are applied and the micropile bends and rotates. Thus, the bending moment was assumed to be zero at the location where the lateral load was applied (approximately 4 inches above the ground surface). In addition, the bending moment was assumed to be zero at the toe of the micropile. Sketches showing the approximate locations of the casing, bond zone, and strain gages are provided in each figure.

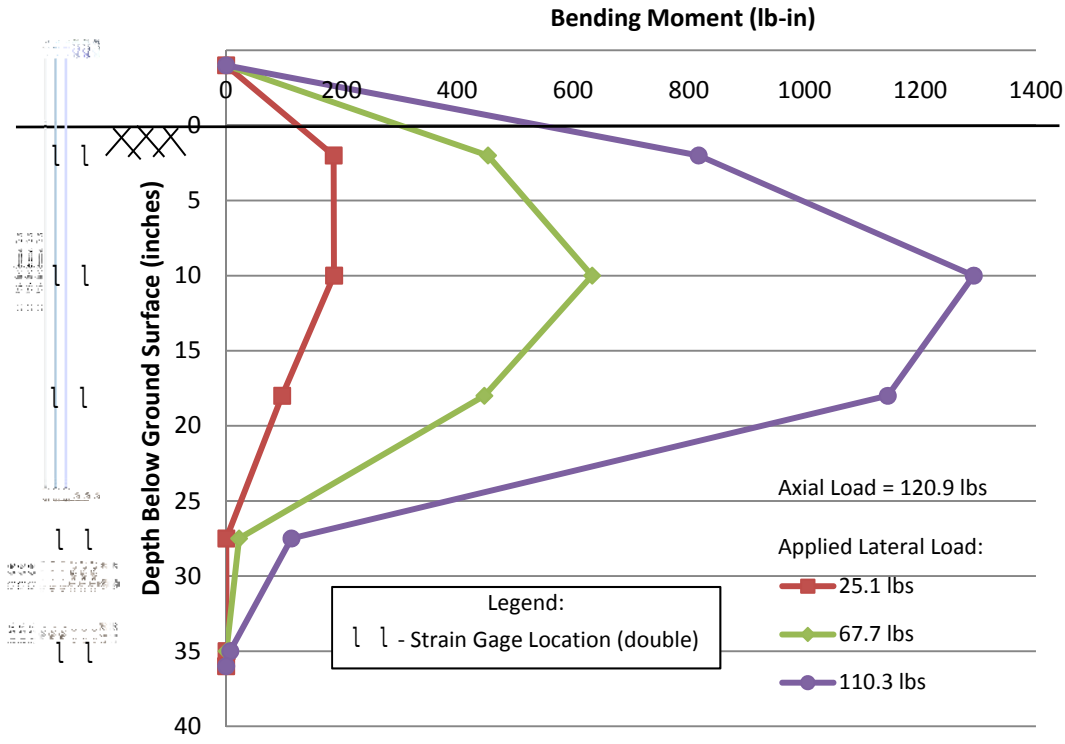

Figure 4.48. Micropile 2C Combined Load Test Results – Bending Moment vs. Depth

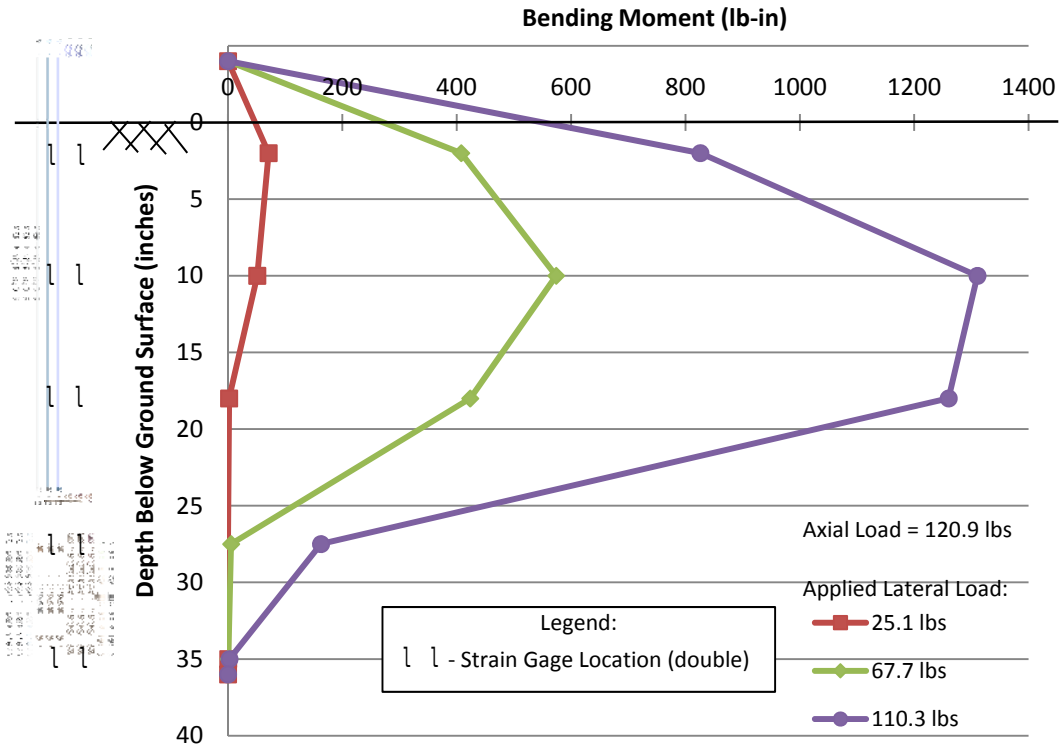

Figure 4.49. Micropile 2D Combined Load Test Results – Bending Moment vs. Depth

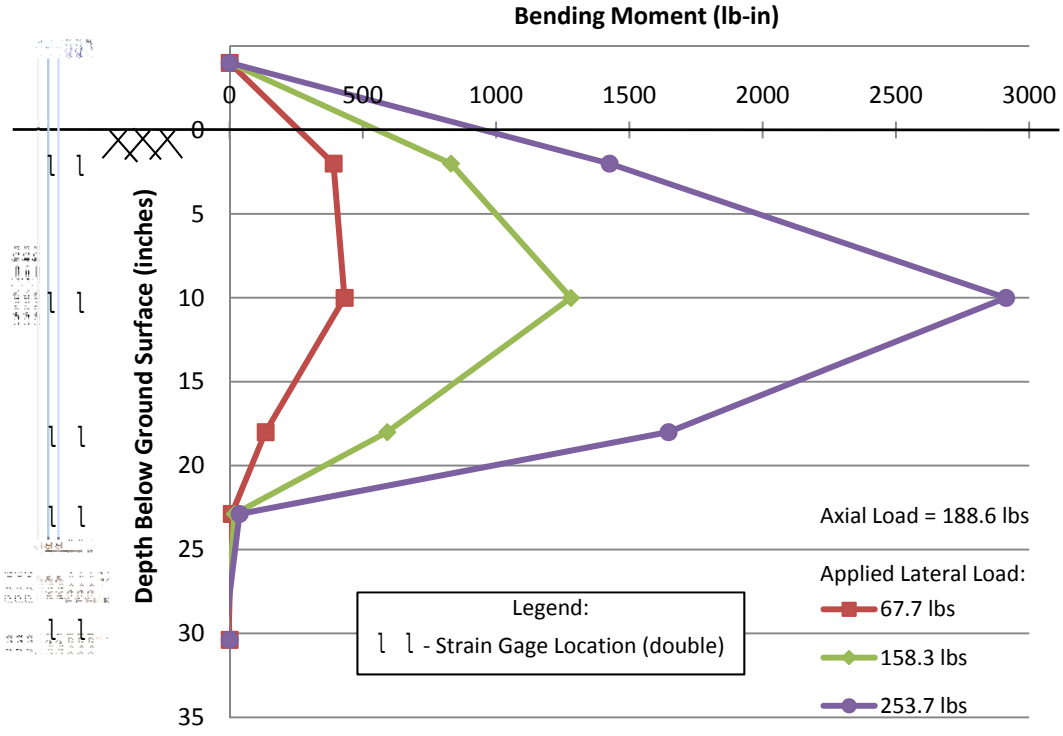

Figure 4.50. Micropile 3C Combined Load Test Results – Bending Moment vs. Depth

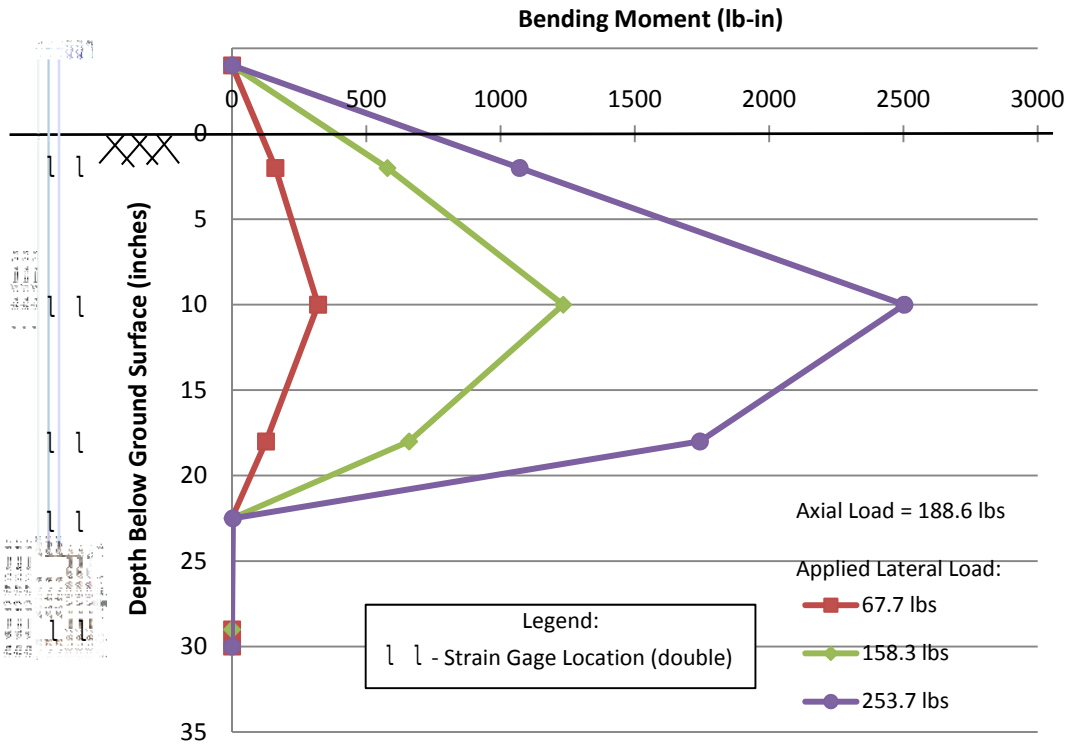

Figure 4.51. Micropile 3D Combined Load Test Results – Bending Moment vs. Depth

Comparison of the four bending moment versus depth plots indicates that the maximum being moment occurs in the vicinity of the midpoint of the cased section at a depth of approximately twelve inches below the ground surface. It appears that the maximum bending moment for the micropiles installed in loose sand (2C and 2D) is slightly deeper than the maximum bending moment for micropiles in dense sand (3C and 3D). The shape of the bending moment curves is similar for all four tests with the location of the maximum bending moment shifting deeper as larger lateral loads were applied.

Finally, Figures 4.52 and 4.53 were prepared to further compare the measured bending moments for each of the four tests. Figure 4.52 compares the bending moment diagrams at similar applied lateral loads (approximately 98 kips) for each test. However,

lateral failure is typically defined in terms of a maximum allowable deflection. Therefore, Figure 4.53 was prepared to compare the bending moment diagrams at similar head lateral displacement (approximately 0.2 inches). The 0.2-inch lateral displacement was chosen because it was difficult to get meaningful data from the strain gages below this deflection level for the loose sand cases since only small loads were required to get to 0.2 inch of lateral deflection. This lateral displacement is comparable to a deflection of about 4.5 inches in the prototype which is likely higher than would be allowed for design of production micropiles. The text on both plots indicates the lateral load and lateral displacement for each bending moment diagram.

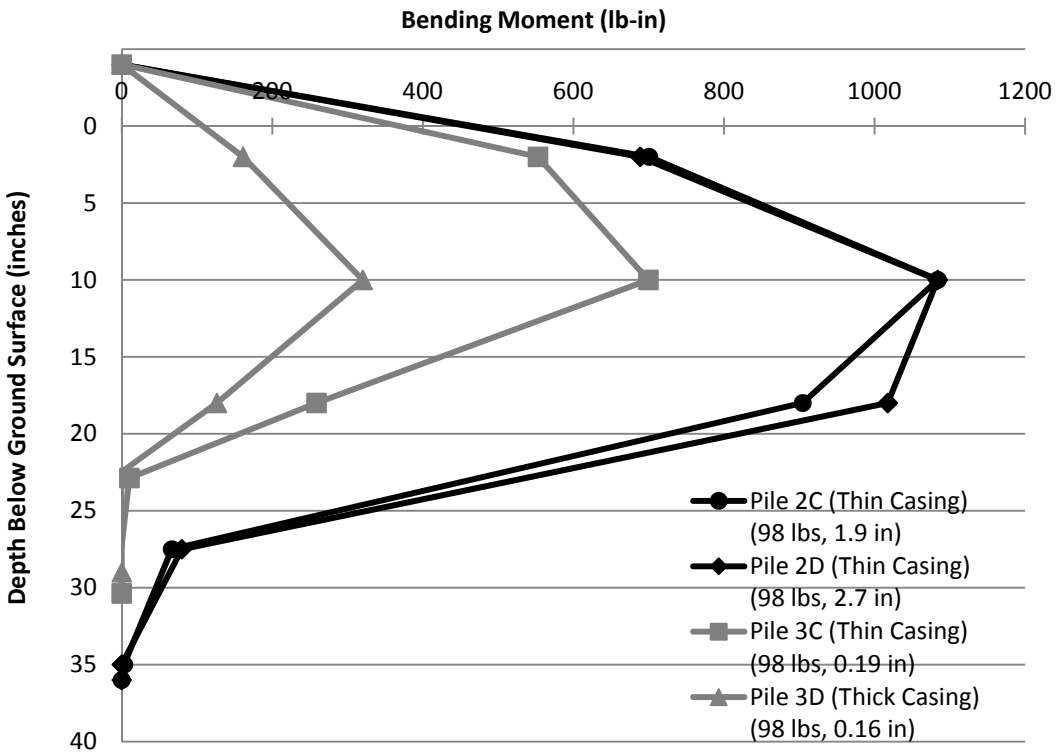

Figure 4.52. Bending Moment vs. Depth at Maximum Lateral Load (Approx. 98 lbs)

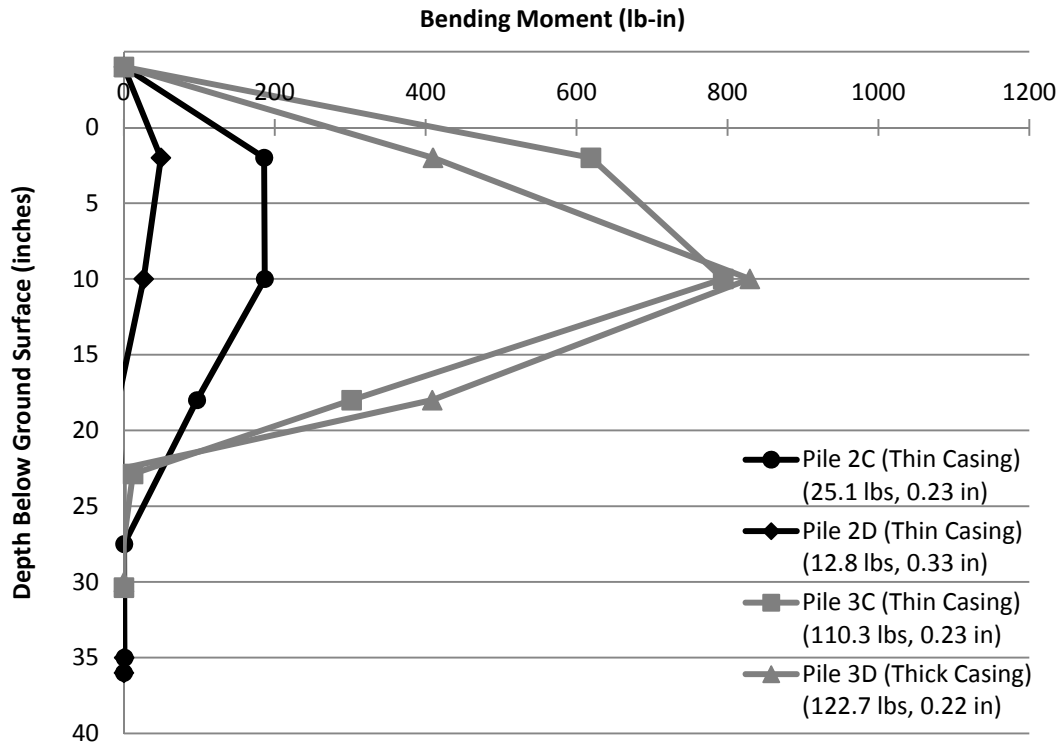

Figure 4.53. Bending Moment vs. Depth at Allowable Deflection (Approx. 0.2 in)

While the results of the combined load tests were not as reproducible as the lateral load test results, the results for micropiles installed in similar soil conditions were similar enough that they can be used to develop basic conclusions regarding behavior of micropiles subjected to combined loading conditions.

First, similar to the lateral load test results, the density of the sand has a much greater effect on the lateral behavior of the micropiles than the structural stiffness of the micropiles. However, based on results shown in Figure 4.46, the micropiles with thicker casing and higher structural stiffness behaved in a slightly stiffer manner than the micropiles with thinner casing installed in similar soil conditions. These results underscore the importance of proper soil characterization in micropile design, but also

indicate that the overall lateral deflection can be somewhat reduced by using thicker casing if an axial load is present during lateral loading. Further, for the dense sand conditions, the maximum bending moment was greater in the micropile with thinner casing for the same applied lateral load. However, when the results were plotted for similar lateral deflection, the differences in bending moments were negligible. These conclusions are important since the majority of structures supported by micropiles impart axial loads along with lateral loads. Except for cases of slope stabilization or retaining structures, it is rare for a lateral load to be applied to a micropile in the absence of an axial load.

Second, other than the obvious differences in load-deflection behavior between the dense sand and loose sand conditions, there are other differences and similarities that should be highlighted. As previously noted, the maximum bending moment for the micropiles installed in loose sand (2C and 2D) occurs slightly deeper than the maximum bending moment for micropiles in dense sand (3C and 3D), but the shape and progression of the bending moment curves is similar for all four tests. For similar applied lateral loads, the bending moments are higher for the loose sand condition. This phenomenon is expected because the bending moment is directly related to the deflection, and the lateral deflection was much higher in the loose sand cases. However, for combined loading conditions, the differences in bending moment may be exacerbated by the P-Δ effect in which the axial load becomes eccentric as the lateral deflection increases, thus imparting additional moment on the structural element and increasing bending.

4.7.4. Comparison of Lateral and Combined Load Test Results. Because the lateral load tests and combined load tests were performed in nearly identical ground

conditions in a controlled environment, the results of the tests can be compared to assess the effect of an axial load on the lateral behavior of micropiles (combined loading). Because the density of the sand had the largest effect on the behavior of the micropiles, as discussed above, the tests performed in different soil conditions were assessed separately in this section. The plots used to compare lateral and combined loading are shown below and include lateral load versus lateral displacement (Figures 4.54 and 4.55), lateral load versus maximum bending moment (Figures 4.56 and 4.57), and bending moment versus depth (Figures 4.58 and 5.49). For all of the plots, the lateral load results are represented by solid lines and the combined load results are represented by dashed lines.

A cursory visual comparison of the load-deflection results for loose sand shown in Figure 4.54 did not yield significant differences between the lateral and combined load tests. However, the behavior at the maximum applied load was somewhat different. For the combined load tests, the failure was dramatic and severe tilting of the pile precluded incremental unloading of the micropiles. This is observed in Figure 4.54 by the steepness of the combined load curves at the maximum loads and the absence of an unloading curve. In general, it also appears that the tests with thicker casing behaved in a slightly stiffer manner than the tests with thinner casing.

For the tests in dense sand (Figure 4.55), the combined and lateral load test results were indistinguishable for the majority of the lateral load increments. However, as the lateral load approached the maximum applied load, the micropiles tested using a combined load exhibited larger displacement than the lateral load tests for similar lateral load magnitudes. For the dense sand condition, the structural lateral stiffness of the

micropiles appeared to have a greater influence than in the loose sand condition. The micropiles with thinner casing behaved less stiff than those with thicker casing.

Comparison of the plots of applied lateral load versus maximum bending moment in Figures 4.56 and 4.57 indicates that the maximum bending moment in the combined load tests is larger than the maximum bending moment from the lateral load tests for the majority of applied lateral loads. While the effect appears to be larger for the loose sand tests, it is also present in the dense sand condition as evidenced by the steeper slope of the combined load test curves.

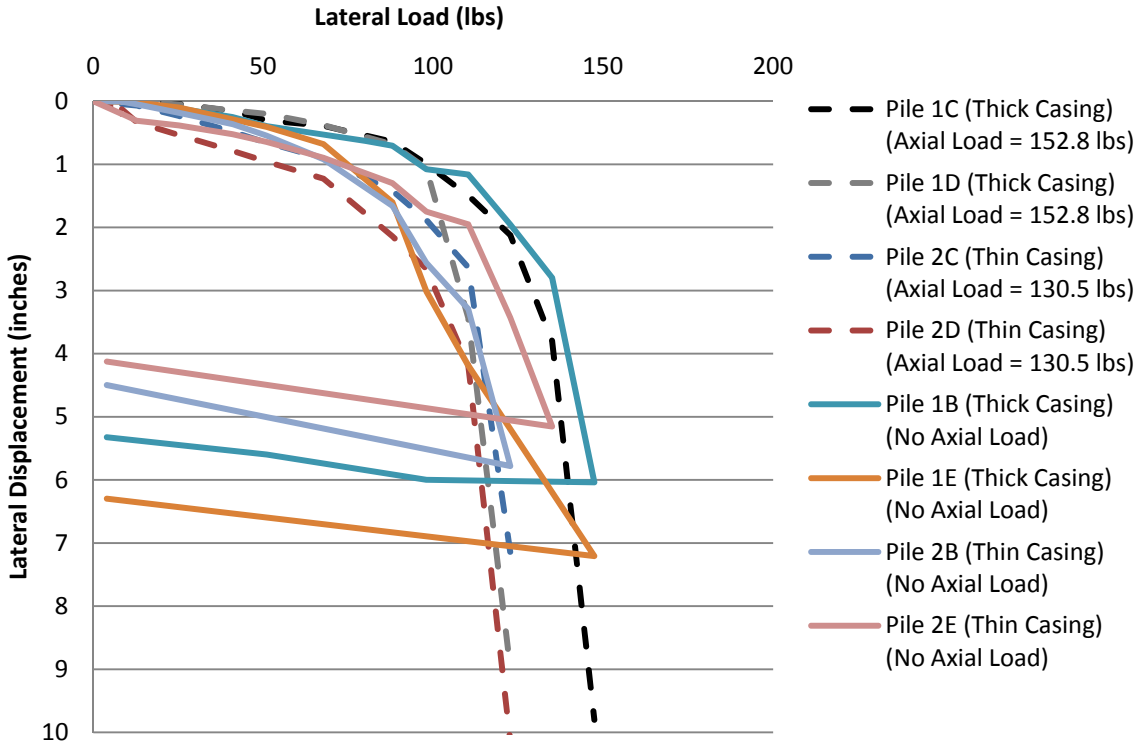

Figure 4.54. Comparison of Lateral and Combined Load Test Results for Loose Sand, Lateral Load vs. Lateral Displacement

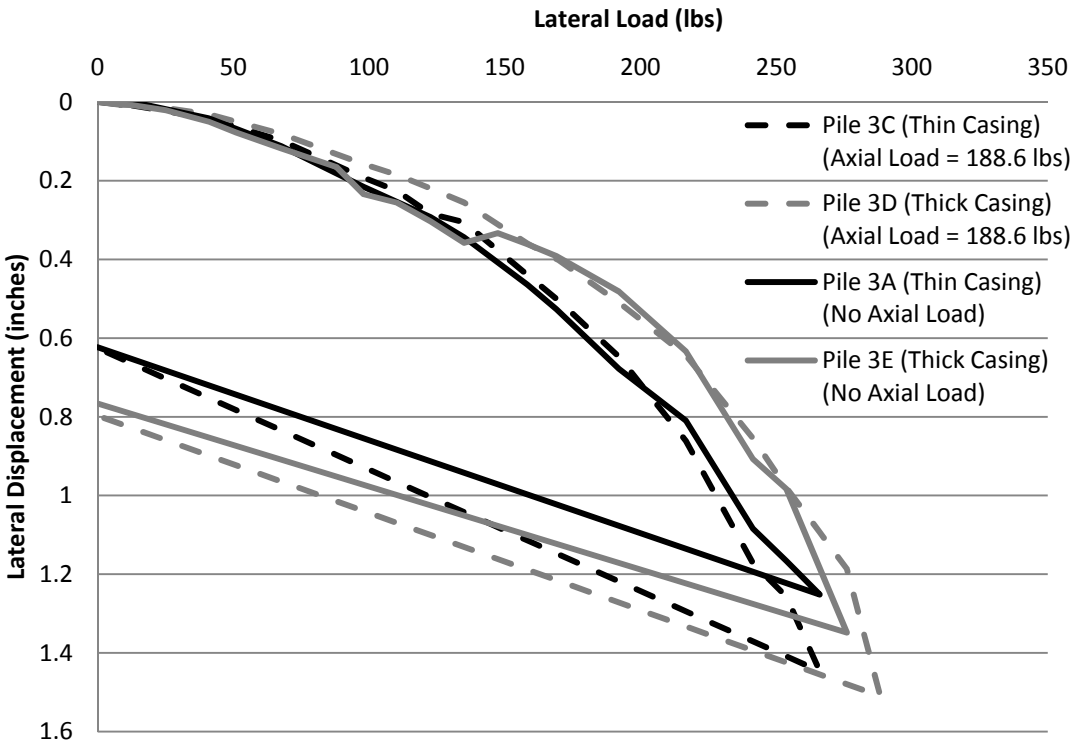

Figure 4.55. Comparison of Lateral and Combined Load Test Results for Dense Sand, Lateral Load vs. Lateral Displacement

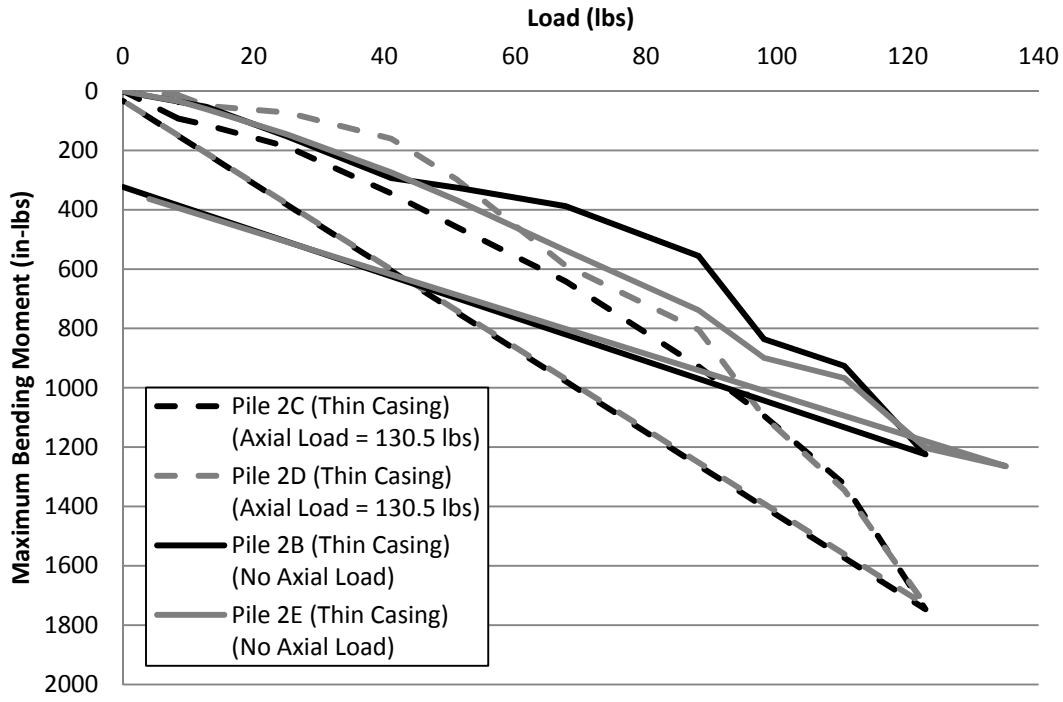

Figure 4.56. Comparison of Lateral and Combined Load Test Results for Loose Sand, Lateral Load vs. Maximum Bending Moment

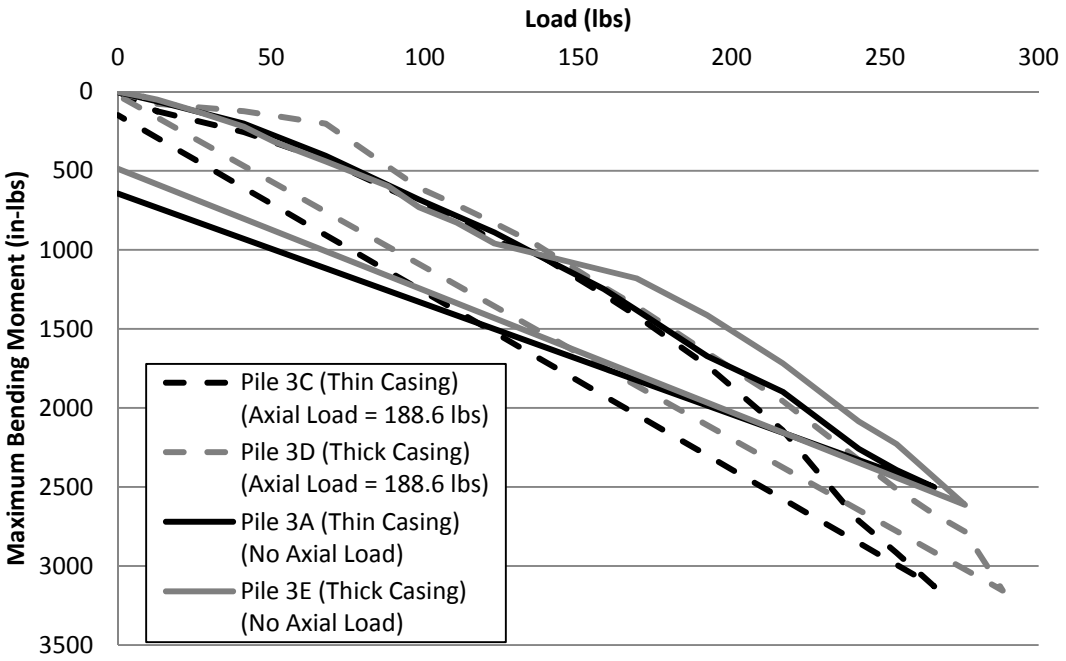

Figure 4.57. Comparison of Lateral and Combined Load Test Results for Dense Sand, Lateral Load vs. Maximum Bending Moment

The Figures 4.58 and 4.59 compare the bending moment diagrams at similar applied lateral loads (approximately 98 lbs) for loose sand and dense sand conditions, respectively. Because the bending moment is more closely related to the lateral deflection than the applied lateral load, Figures 4.60 and 4.61 were prepared to compare the bending moment diagrams at similar lateral displacement. The 0.2-inch lateral displacement was chosen because it was difficult to get meaningful data from the strain gages below this deflection level for the loose sand cases since only small loads were required to get to 0.2 inch of lateral deflection. This lateral displacement is comparable to a deflection of about 4.5 inches in the prototype which is likely higher than would be allowed for design of production micropiles. The text on the plots indicates the lateral load and lateral displacement for each bending moment diagram.

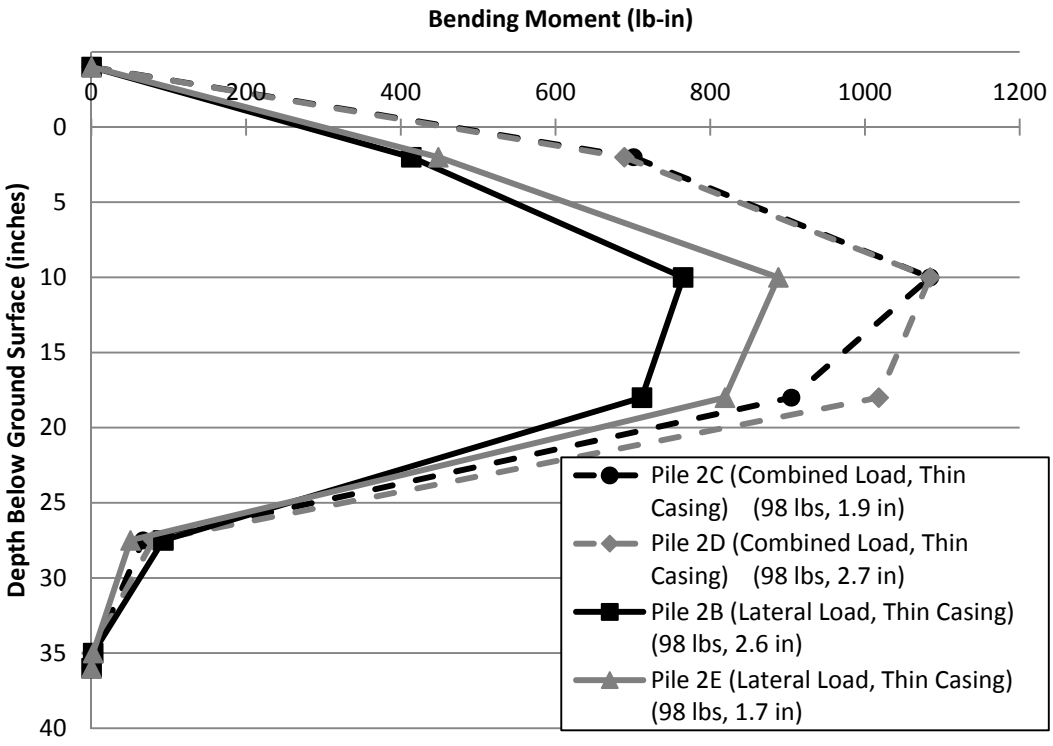

Figure 4.58. Comparison of Lateral and Combined Load Test Results for Loose Sand, Bending Moment vs. Depth at Maximum Lateral Load (Approx. 98 lbs)

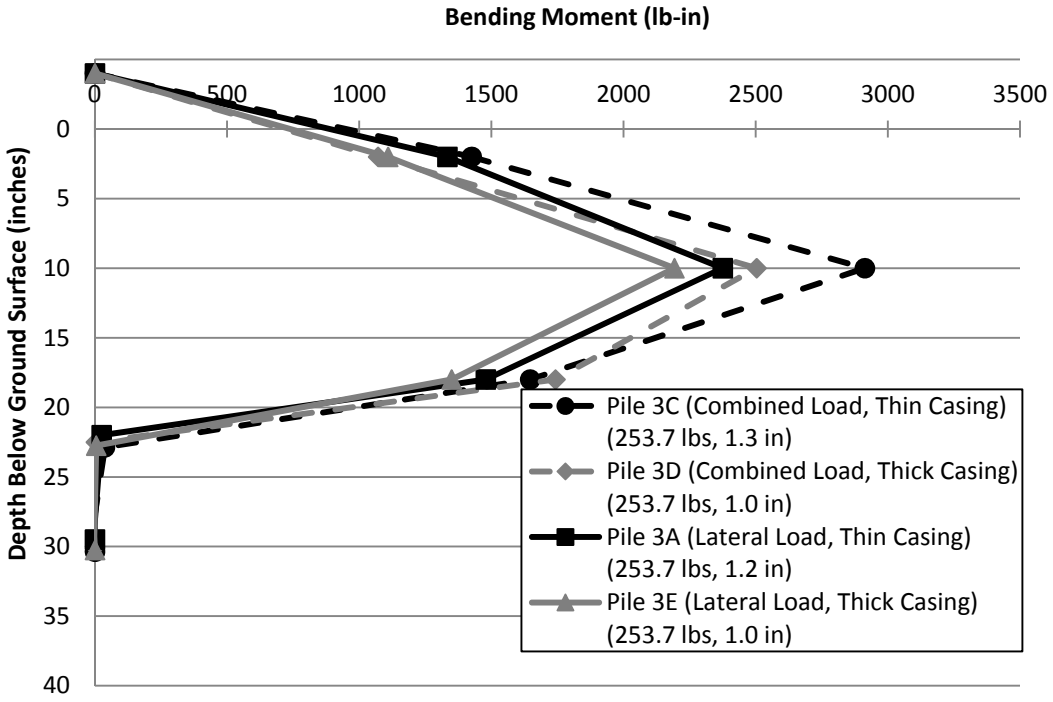

Figure 4.59. Comparison of Lateral and Combined Load Test Results for Dense Sand, Bending Moment vs. Depth at Maximum Lateral Load (Approx. 254 lbs)

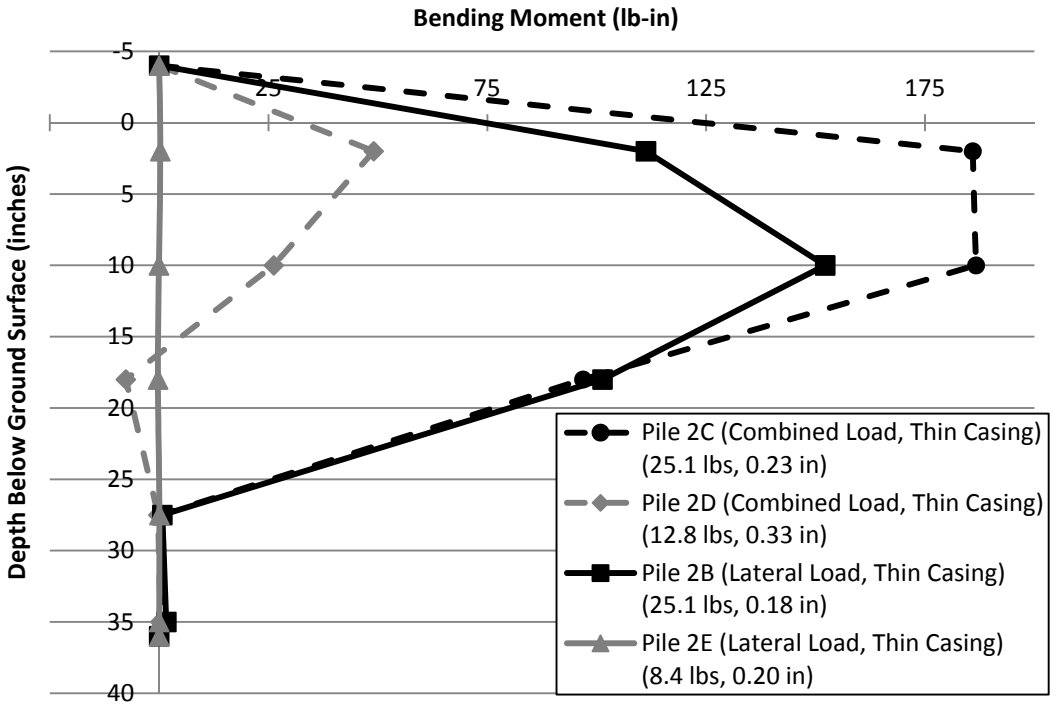

Figure 4.60. Comparison of Lateral and Combined Load Test Results for Loose Sand, Bending Moment vs. Depth at Allowable Deflection (Approx. 0.2 in)

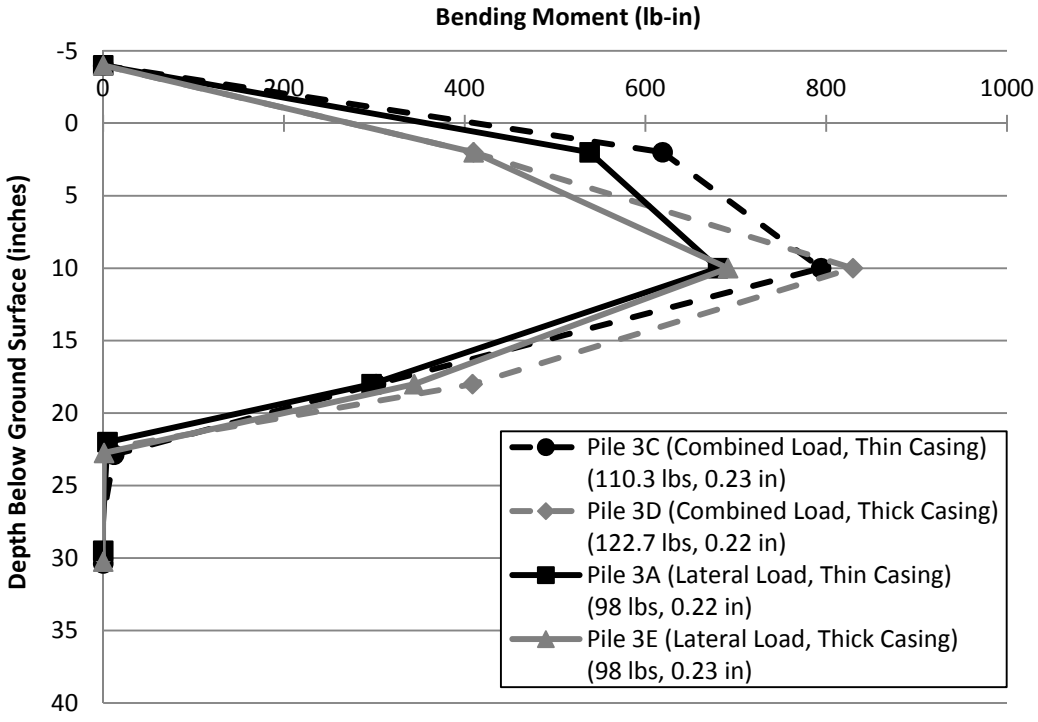

Figure 4.61. Comparison of Lateral and Combined Load Test Results for Dense Sand, Bending Moment vs. Depth at Allowable Deflection (Approx. 0.2 in)

Results from the six combined load tests and six lateral load tests were analyzed and the four plots shown above were developed to compare the results of the tests. Based on examination of the eight plots discussed above, there are several differences between the results of the lateral load tests and the combined load tests as noted below.

- For small lateral loads, the differences in behavior between lateral and combined load tests are minimal.
- As larger lateral loads are applied, differences in behavior become more distinct, especially for micropiles installed in loose sand. For example, the lateral deflection (see Figure 4.54 and 4.55) is larger in the combined load tests than the lateral load tests as the loads get larger and approach the failure load or maximum applied load used in the test.
- Lateral failure of the combined load tests was more sudden. In a practical sense, this characteristic may not have an effect on the behavior of the micropiles because the pile cap is typically restrained and the micropile will not be allowed to tilt to that extent. However, this characteristic of micropiles subjected to combined loading could result in more dramatic and sudden cracking of the superstructure.
- The combined loading condition resulted in higher bending moments than the lateral load condition. Again, this effect was more pronounced for the loose sand condition as shown in Figures 4.56 and 4.58 where the maximum bending moment was approximately 22 to 40 percent higher for the combined load tests at

a lateral load of 98 lbs. For the dense sand condition, Figure 4.57 shows a steeper curve and larger bending moments for the combined load tests at relatively large applied lateral load increments. As shown in Figure 4.59, for an applied lateral load of 253.7 lbs, the bending moment from the combined load tests ranges from 5 to 30 percent larger than the maximum bending moments from the lateral load tests. It is likely that the loose sand condition had larger differences in behavior because a failure condition of the soil was reached or nearly reached in all of the tests. As expected, it would take much larger loads to reach similar levels of strain in the dense sand. These results reiterate the fact that designers should be particularly cautious when soil conditions are poor.

- For the bending moment versus depth curves plotted at similar magnitudes of displacement (Figures 4.60 and 4.61), the results from the dense sand case are nearly identical for the combined and lateral load tests. However, for the loose sand tests, the results are highly variable and do not correlate to the type of test that was performed on each micropile. These results indicate that, because the stiffness of the loose sand is so small, it only takes relatively small loads to reach the allowable displacement. Thus, the behavior is likely very dependent on small differences in soil conditions (density and shear strength) and construction, such as the verticality of the micropile and disturbance to the soil surrounding the micropile. Because of this sensitivity, it would likely be difficult to predict lateral behavior in loose sand.

5. FULL-SCALE FIELD TESTING

The full-scale field testing portion of the research consisted of installation of 6 micropiles to assess the impact of combined loading on the lateral capacity of micropiles. Each of the micropiles was instrumented to determine load transfer with depth, as well as bending within the upper portion of the micropile. Specifically, testing consisted of two axial compression tests, two lateral load tests, and four combined load tests at a site in Warrensburg, Missouri. The following sections present details regarding the test site, test design, instrumentation, installation, the experimental program, and the testing results.

5.1. WARRENSBURG TEST SITE

The Warrensburg Test Site (WTS) is located on land owned by the Missouri Department of Transportation (MoDOT) and was used to test drilled shafts in conjunction with the MoDOT Geotechnics Research Program (GRP) conducted by the University of Missouri-Columbia (MU) and Missouri S&T. The WTS was chosen for full-scale field testing because it provided a unique opportunity for access to a well-characterized site where research-grade borings and laboratory testing have been completed. In addition, the drilled shafts installed at the site could be used as reaction piles for the micropile testing, thus reducing the number of micropiles that would need to be installed.

5.1.1. Site Description. The WTS is located east of Warrensburg, MO on U.S. Highway 50. Specifically, it is just west of the new intersection with the Missouri State Route 13 by-pass and approximately two miles east of the intersection with old Missouri Route 13 (Figure 5.1). The site is at the crest of a hill between the westbound (north) lanes of U.S. Highway 50 and the entrance ramp from Route 13 to westbound U.S. 50. Latitude/Longitude coordinates for the site are approximately 38°46'25.44"N,

93°41'17.92"W. Access to the site is from the aforementioned entrance ramp. Near the end of the ramp, the abandoned Route HH is present to the south of the ramp. The site is a short distance to the east along the abandoned roadway. The site is relatively flat with a slight slope toward the southwest, and a gravel working pad was constructed at the load test area by MoDOT. Prior to micropile installation, 15 drilled shafts (labeled TS-W1 through TS-W15) were installed and tested at the site. At a later date, 6 micropiles (labeled A through F) were installed between the drilled shafts. Figure 5.2 shows a plan view of the site with the layout of the drilled shafts and micropiles.

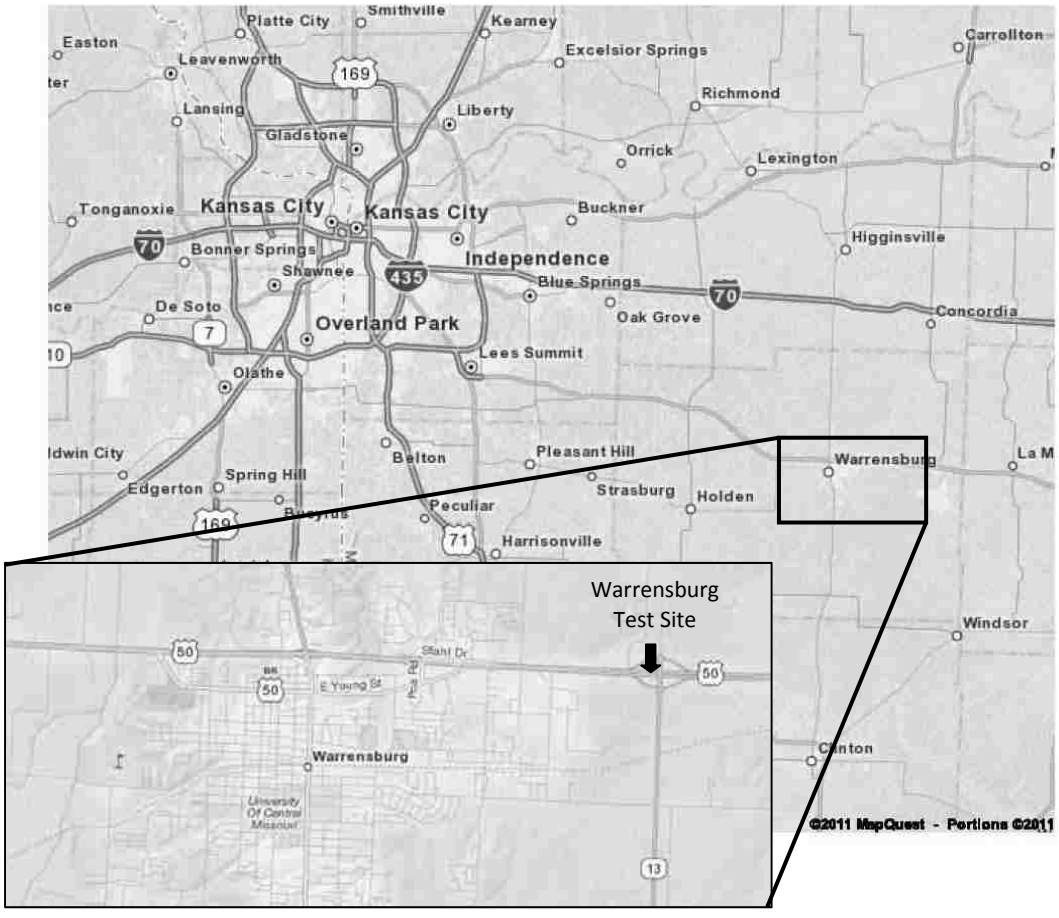

Figure 5.1. Warrensburg Test Site Vicinity Map

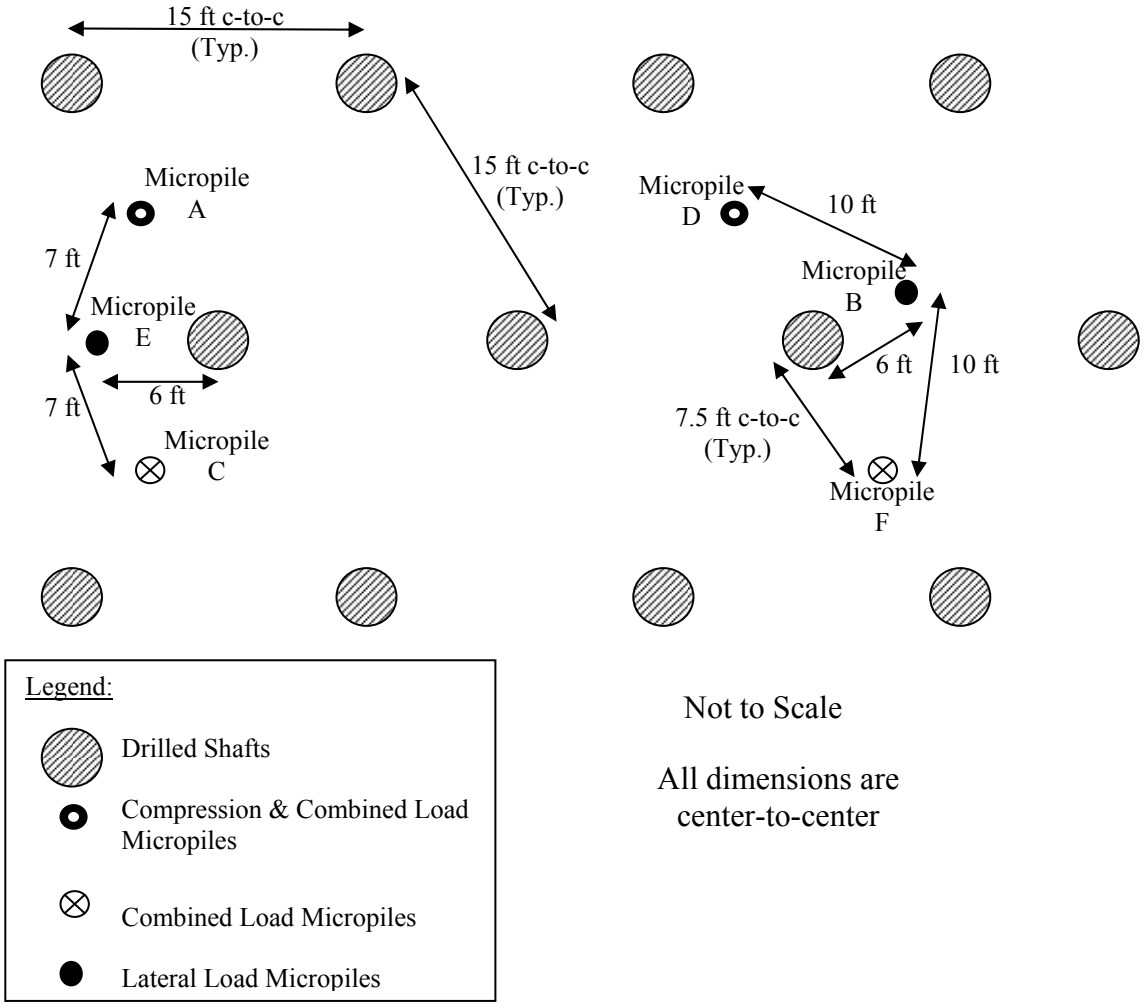

Figure 5.2. Warrensburg Test Site Layout

5.1.2. Geologic Setting. The WTS is located within the Western Plains region of Missouri, as defined and discussed in the MoDOT Geology and Soils Manual [1962]. This region is generally delineated by the Kansas border to the west, the edge of the Ozark Mountains to the east and south, and the Missouri River to the north. The site is within the eastern portion of this region. The Western Plains region is part of the larger Great Plains region that stretches through Kansas and Colorado to the eastern edge of the

Rocky Mountains. Although the region is relatively flat, it is just south of the southern limit of glaciation.

Bedrock in the region is sedimentary in nature and was primarily deposited in the Mississippian period. The Mississippian bedrock generally consists of cherty limestone and shale. In localized areas, the bedrock consists of sandstones and shales from the Pennsylvanian period. Because it dips toward the west, the near surface bedrock within the eastern portion of the region is generally older than near surface bedrock in the western portion of the region.

Soil cover in the region is generally residual or alluvial in nature and derived primarily from the Pennsylvanian shale, sandstone, and limestone. The topography of the soil cover is flat to gently undulating with wide river valleys and wide floodplains.

5.1.3. Subsurface Characterization Program. Subsurface characterization at the site was conducted by MoDOT in conjunction with the MoDOT GRP project. Information provided herein was based on the "Field Site Characterization Testing Program Data Report" [Magner et. al. 2011] and the "Site Characterization Program Interpretation Report" [Likos et. al. 2011] published in conjunction with the GRP Project. Investigations methods at the site generally included "penetration borings", "pressuremeter borings", and "core borings". Penetration borings were completed using rotary wash boring methods with Standard Penetration Tests (SPT) performed at 5-ft intervals within the shale strata. Texas Cone Penetration Tests (TCPT) were also conducted in these borings at 5-ft intervals (alternating with the SPT measurements). Pressuremeter borings were completed using rotary wash boring methods with pressuremeter tests (PMT) being performed within the shale strata at 5 to 10 foot

intervals. The core borings were generally completed using NQ size, wireline or solid stem double-tube core barrels to obtain rock core for laboratory testing. In the pressuremeter and core borings, relatively undisturbed samples were taken in the overburden soils using Shelby tubes or Osterberg samplers.

Initial subsurface investigations were performed by MoDOT in October, November, and December of 2009. These investigations included one penetration boring, one pressuremeter boring and four core borings. Three of the core borings were completed following the research protocol. The remaining core boring was completed following current MoDOT practice for site characterization in shale. Subsequent to the initial investigations, three additional borings were completed at the site to supplement the data obtained from the initial investigation. These borings were completed in April and May 2010. The primary purpose of these borings was to support the drilled shaft load test program and to further characterize the clay overburden soils. As such, a "mixed" protocol was used for sampling and testing (Table 5.1). This mixed protocol was similar to the research protocol used for other borings in this program except that shale specimens were acquired using a Pitcher sampler (as opposed to core barrel sampling) where possible. The borings that were drilled in the immediate vicinity of the micropile testing area included WAR-1(A, B, C), WAR-8, WAR-9, OFF-3, OFF-4, and OFF-5. Locations for these borings are shown in an aerial photograph in Figure 5.3 and summarized in Table 5.1.

As samples were extracted from the borings, pocket penetrometer and torvane tests were completed, when possible. Additional field tests, including unconfined compression (UC) tests and point load index tests (PLI), were conducted on select

Table 5.1. Summary of Borings Used for WTS Analysis

Borings			
Designation	**MoDOT Hole #**	**Hole Type**	**Comments**
WAR-1A	H-09-65	SPT/TCPT	MoDOT protocol
WAR-1B	H-09-72	Core	Research protocol
WAR-1C	H-09-74	PMT	Research protocol
WAR-8	H-09-75	Core	Research protocol
WAR-9	H-09-73	Core	Research protocol
OFF-3	A-10-03	Core	Mixed methods
OFF-4	H-10-10	Core	Mixed methods
OFF-5	A-10-04	Core	Mixed methods

Figure 5.3. Warrensburg Test Site Boring Locations [Likos et. al. 2011]

samples. The remaining samples were transported to MoDOT, MU, and Missouri S&T laboratories for additional testing. Tests conducted on relatively undisturbed materials sampled at the WTS included unconsolidated-undrained (UU) type triaxial compression tests and UC tests. Supplemental tests conducted on disturbed samples and specimen

trimmings included Atterberg limits, water content, specific gravity, grain size, quantitative mineralogy of bulk powder and clay fraction by X-ray diffraction (XRD), slake durability tests, and insoluble residue tests. Logs of the borings used in design and analysis of the micropiles are provided in Appendix C [Likos et. al. 2011].

5.1.4. Geotechnical Profile and Parameters. As previously stated, borings WAR-1 (A-C), WAR-8, WAR-9, OFF-3, OFF-4, and OFF-5 were drilled in the vicinity of the micropile testing area. The information from these borings and the associated laboratory testing were analyzed to develop a generalized subsurface profile and to determine the soil and rock parameters for the site. The subsurface conditions at the site generally consisted of 11 to 14 feet of very stiff to hard, lean to fat clay with scattered sand and gravel underlain by massive, generally moderate strength shale with varying amounts of silt and sand and varying degrees of weathering. Some sandstone was present at the bedrock surface in localized areas of the site and thin limestone stringers were sometimes encountered. All retrieved soil and rock samples were classified as moist. Following completion of boring OFF-3, the portion of the hole within bedrock was left open and approximately 15.5 feet of casing was left in the upper portion of the hole through the overburden. Groundwater measurements were made in the open hole over the next five days and indicated that the groundwater level was approximately 30 feet below the ground surface. Examination of cuttings during micropile installation confirmed the generalized subsurface profile described above.

The types of field and laboratory tests completed for the pertinent borings are discussed in Section 5.1.3 above. Using the data obtained from these tests, analyses were completed to determine the mean and coefficient of variation (COV) for several relevant

soil and rock parameters. These values, along with the number of data points used in the analysis are shown in Table 5.2. As shown in Table 5.2 and Figure 5.4, the undrained strength of the clay increases slightly with depth and is somewhat variable, resulting in a COV of approximately 32 percent. However, the strength of the shale is highly variable at the site (COV of 55 percent) and does not appear to have a clear relation with depth.

Table 5.2. Summary of Soil and Rock Parameters

Parameter	Units	Mean	Coefficient of Variation (%)	Number of Data Points
Clay Layer				
Depth to Rock	feet	12.6	11.7	8
N_{60}	blows/foot	14.0	20.2	2
Natural Water Content	percent	25.2	27.0	21
Peak Undrained Shear Strength (from UU triaxial)	lbs/ft^2	1716.4	32.2	15
Residual Undrained Shear Strength (from UU triaxial)	lbs/ft^2	1603.3	39.5	15
Pocket Penetrometer Reading	$tons/ft^2$	3.6	39.2	25
Torvane Reading	$tons/ft^2$	0.7	27.9	20
Pressuremeter Modulus	$kips/ft^2$	256.0	-	1
Shale Layer				
Unit Weight	lbs/ft^3	144.7	5.7	6
Natural Water Content	percent	14.8	30.0	12
Liquid Limit	percent	34.2	15.2	5
Plasticity Index	percent	14.0	38.1	5
Pressuremeter Modulus	$kips/ft^2$	1246.3	108.1	3
Peak Undrained Shear Strength (from UU triaxial)	$kips/ft^2$	6436.1	55.3	34

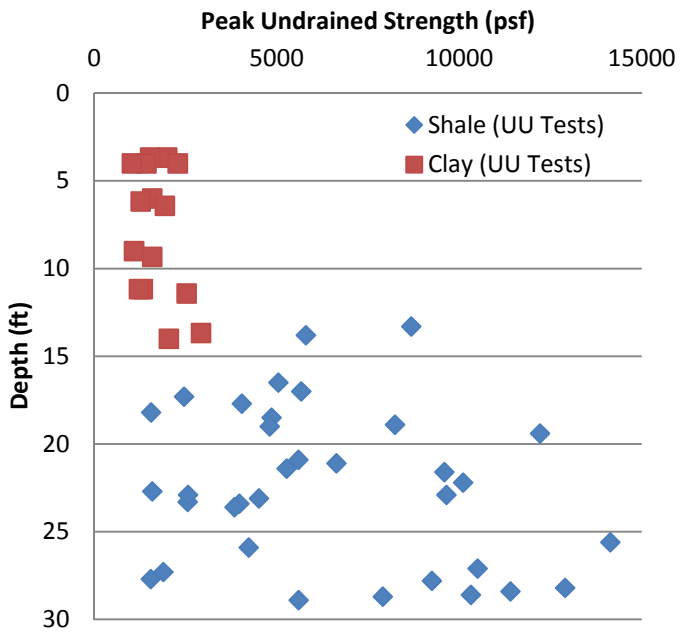

Figure 5.4. Depth Versus Undrained Shear Strength

5.2. TEST DESIGN

Design of the micropiles and testing apparatus was completed in general accordance with commonly accepted geotechnical and structural design standards, as documented in the following sections. The general design philosophy was to design the test such that the geotechnical capacity controlled and structural failure of the micropile or the load frame was avoided. This design philosophy had to be implemented within the constraints of the materials available to the project. Namely, the materials used to construct the micropiles were donated, and components of the load frame and testing apparatus were provided by the Missouri S&T Civil Engineering Laboratories. Thus, the structural capacity of these elements was first calculated, and the remaining elements of the test were designed such that the geotechnical capacity of the micropiles controlled.

The following sections provide descriptions of the test materials and further details regarding the test design.

5.2.1. Micropile Design. Because the goal of the research project is to assess the effect of combined loading on micropiles, the micropiles needed to have both a cased section and an uncased bond zone, consistent with industry practice of installing permanent casing for micropiles that will be subjected to lateral loads. The casing steel donated by LB Pipe and Coupling consisted of 7-inch-outer diameter (OD) steel pipe with a wall thickness of 0.453 inch and a minimum yield strength of 80 ksi. Both 6-foot and 10-foot sections of casing were available for the project. The central reinforcing bar provided by Dywidag-Systems International consisted of a #11 all-thread bar with a minimum yield strength of 75 ksi. Finally, Buzzi Unicem provided Type I/II Portland cement for the project. Because of the soil conditions at the site and the size of the casing, Hayward Baker, Inc. determined that the proper method of installation included the use of an 8-inch-diameter auger, resulting in an 8-inch-diameter bond zone. More details regarding micropile installation are provided in Section 5.5.

Design of the test micropiles was completed in general accordance with the FHWA Micropile Design and Construction Reference Manual [Sabatini et. al. 2005], and detailed calculations are shown in Appendix D, including hand calculations for axial design and the use of LPILE software [Reese et. al. 2004] for lateral design. Because there is no standard method for analysis of combined loading, LPILE was also used for the combined loading condition as an approximate design method.

In accordance with the design philosophy discussed above, the design of the micropile was primarily limited by the structural capacity of the micropile casing for

lateral and combined load conditions and the reaction beam for axial load conditions. Within these constraints, the design was completed in three steps (lateral, axial, and combined loading) to determine the casing and bond zone lengths. First, the micropile was designed for the lateral loading condition. The allowable bending moment capacity was calculated for the cased section of the pile (630 in-kips), the threaded connection between the two casing sections (283 in-kips), and the bond zone (10 in-kips). The cased section was then modeled using LPILE. For this model, it was assumed that two sections of casing would be used such that the threaded connection would be located approximately 8.5 feet below the ground surface (10-foot-long section of casing with 1.5 feet of stickup above the ground surface). Within the model, incrementally larger lateral loads were placed on the pile until the resulting maximum bending moment from LPILE was approximately equal to the calculated allowable moment capacity. Next, the casing length was adjusted until the bottom of the casing corresponded to the elevation at which the bending moment from LPILE was approximately equal to the allowable bending moment of the bond zone. Keeping the predicted bending moment below the allowable bending moment throughout the pile ensures that a structural failure will not occur during lateral loading.

Second, the micropile was designed for the axial loading condition. It was assumed that the cased zone would not contribute to the axial capacity of the micropile, so this step consisted of sizing the bond zone of the micropile. The two constraints for this design step included the allowable structural capacity of the reaction beam (120 kips; see Section 5.2.2 for additional information regarding the load frame design) and the diameter of the bond zone (8 inches). Given these two constraints, the length of the bond

zone was calculated assuming an ultimate bond strength of 40 psi, consistent with the published range of values for low strength shale [Sabatini et. al. 2005]. To complete the design for axial loading conditions, the axial structural strength of the cased section and bond zone were checked to make sure that the allowable strength exceeded the planned maximum load of 120 kips. Consistent with the overall design philosophy, this step in the design process was taken to ensure that geotechnical failure of the bond zone will occur prior to structural failure of the micropile or load frame.

Finally, the micropile was designed for the combined loading condition. The design method was similar to the lateral micropile design. The allowable bending moment capacity was identical to that used in the lateral analysis, and LPILE was used to model the micropile. However, a constant axial load equal to one-half of the ultimate axial capacity (60 kips) was placed on the micropile. The lateral load was then incrementally increased until the maximum bending moment from LPILE was approximately equal to the calculated maximum allowable bending moment for the cased section, threaded connection, or bond zone. As necessary, the length of the casing was adjusted to prevent significant bending within the bond zone.

The resulting micropile design consisted of a total micropile length of 26 feet, including a 10-foot-long bond zone and a 16-foot-long cased section. The central reinforcing bar was planned for the lower 25 feet of the micropile. A stick-up height of 1.5 feet was planned to accommodate the testing apparatus that will be placed on the micropile casing during loading. A schematic of the designed micropile is shown in Figure 5.5.

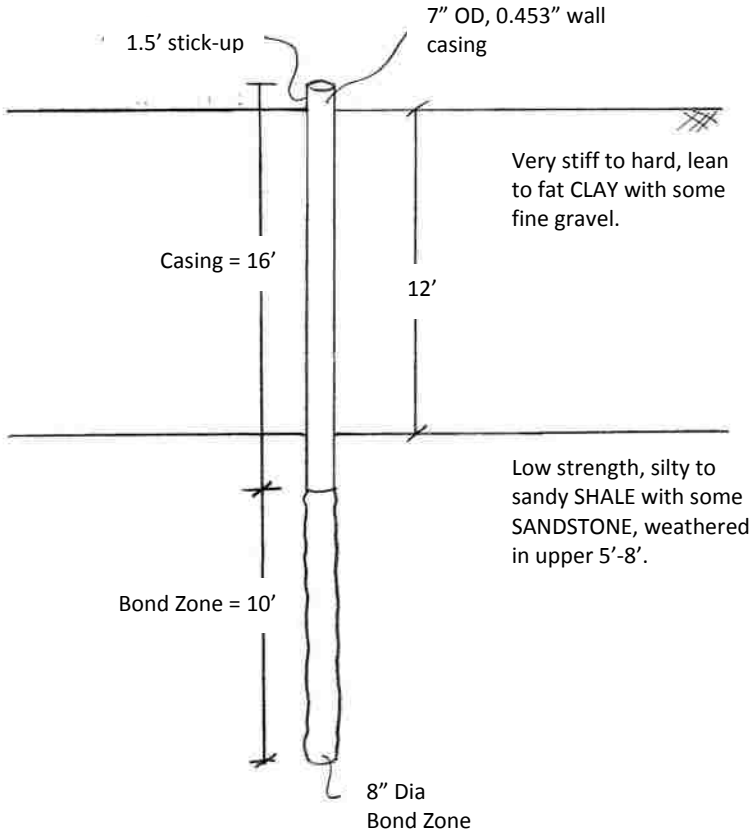

Figure 5.5. Schematic of Micropile Designed for the WTS

5.2.2. Load Frame and Testing Apparatus Design. The load frame and testing apparatus was designed such that an axial load, a lateral load, or simultaneous axial and lateral load could be applied to a micropile. Consistent with the design philosophy discussed above, the design was completed to prevent structural failure so that the geotechnical capacity of the micropile would control during loading. Detailed calculations for the design of the load frame and testing apparatus are shown in Appendix D. To minimize the number of micropiles needed at the test site, the drilled shafts that were installed for the MoDOT Geotechnics Research Program were used as reaction piles for loading (see Figures 5.2 and 5.6). Analysis indicated that the expected loads that

would be transferred from the micropiles to the drilled shafts were well below the lateral and axial capacity of the drilled shafts and would result in minimal deflection.

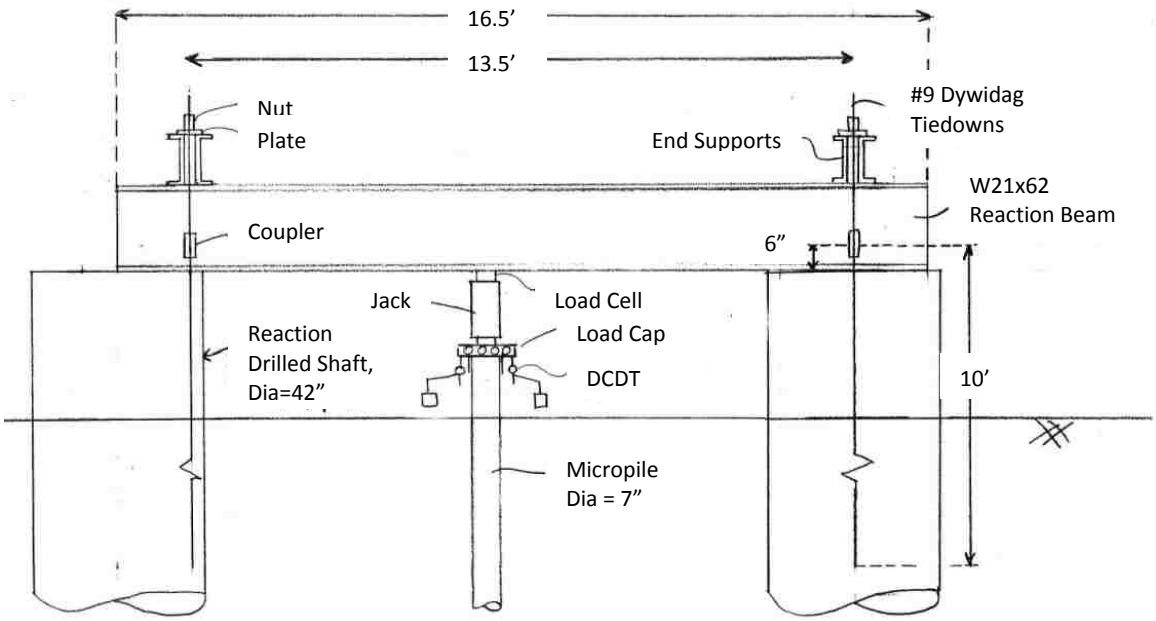

Figure 5.6. Front Elevation View of WTS Axial Load Frame

The first step in designing the load frame was to find a reaction beam that could span the drilled shafts and provide resistance for the hydraulic jack that was used to apply the downward axial load to the micropiles. The Missouri S&T Center for Infrastructure Engineering Studies (CIES) had a 16.5-foot-long, W21x62 steel beam that was made available to this project. This beam likely came from an old bridge in Missouri and was sand blasted and repainted before it was used. Because the yield strength of the steel was unknown, a conservative estimate of 36 ksi was used for design. Assuming a span length of 13.5 feet and that the load will be applied at the center of the span, the maximum

allowable vertical load was calculated to be approximately 150 kips according to the design charts in the Manual of Steel Design [AISC 1998]. To allow an additional factor of safety and to limit deflection during testing, we decreased the maximum allowable load by 20 percent to obtain the ultimate axial micropile design load (120 kips). To reduce the possibility of torsion on the beam causing buckling of the web, web stiffeners were added to the reaction beam, consisting of three 1/2-inch-thick plates welded on each side of the web at the center of the beam where the load is to be applied and at the ends where the beam is to be supported by the drilled shafts.

Because the micropiles were planned to be loaded in compression, the reaction beam needed to be tied down to the drilled shafts to resist the applied load. This was accomplished using small steel cross beams connected to two dywidag tiedowns on each end of the reaction beam (Figure 5.7). At the maximum allowable load of 150 kips, each dywidag bar would need to resist a load of 37.5 kips. A #7, 75 ksi bar was required to resist this load, but a #9 bar was chosen to increase the factor of safety of the system. A 10-foot long section of #9 dywidag threadbar, with a stick-up height of approximately 6 inches, was cast in the concrete of the drilled shafts that were used for reaction piles. During micropile testing, couplings were attached to the portion of the dywidag reaction bar sticking up out of the drilled shafts such that additional lengths of reaction bar could be installed to support the reaction beam. For axial loading, a steel swivel was placed between the top of the micropile and the base of the hydraulic jack to prevent the jack from moving or kicking out if the system was not exactly vertical. A schematic showing the design components of the axial load test frame are shown in Figures 5.6 and 5.7.

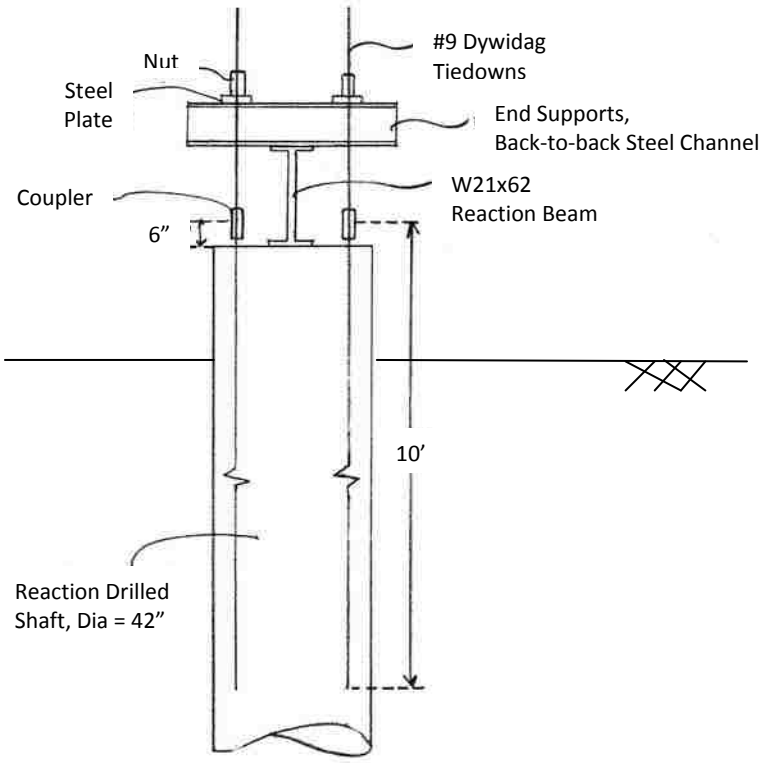

Figure 5.7. Side Elevation View of WTS Axial Load Frame

The next step of the load frame design process was to design for the lateral load condition. Based on the LPILE calculations used to design the micropiles (Section 5.2.1), the maximum lateral load that could be applied to the micropiles without approaching the maximum allowable bending moment was approximately 20 kips. The corresponding lateral deflection at this load was approximately 2 inches. Thus, the lateral load frame was designed to accommodate both the load and the expected deflection.

The basic concept for the lateral load frame was to use a hydraulic jack to pull two micropiles toward each other (Figure 5.8). Thus, if the micropiles were spaced a sufficient distance apart (at least 7 diameters) and positioned correctly during installation, a lateral load test and a combined load test could be performed simultaneously. For the

lateral load frame, Williams Form Engineering donated all-thread bars to tie to two small steel beams together on the outside of two adjacent micropiles. Loading chairs were also fabricated to provide a flat loading surface on each of the micropiles. The lateral load was applied using a hydraulic jack between the loading chair and the reaction beam on one of the micropiles. Because the two micropiles were coupled using a tension connection, identical loads were applied to each micropile by jacking from one of the micropiles. Similar to the axial load frame, a small steel swivel was placed between the hydraulic jack and the load chair to prevent the jack from moving or kicking out as the pile rotated laterally during loading.

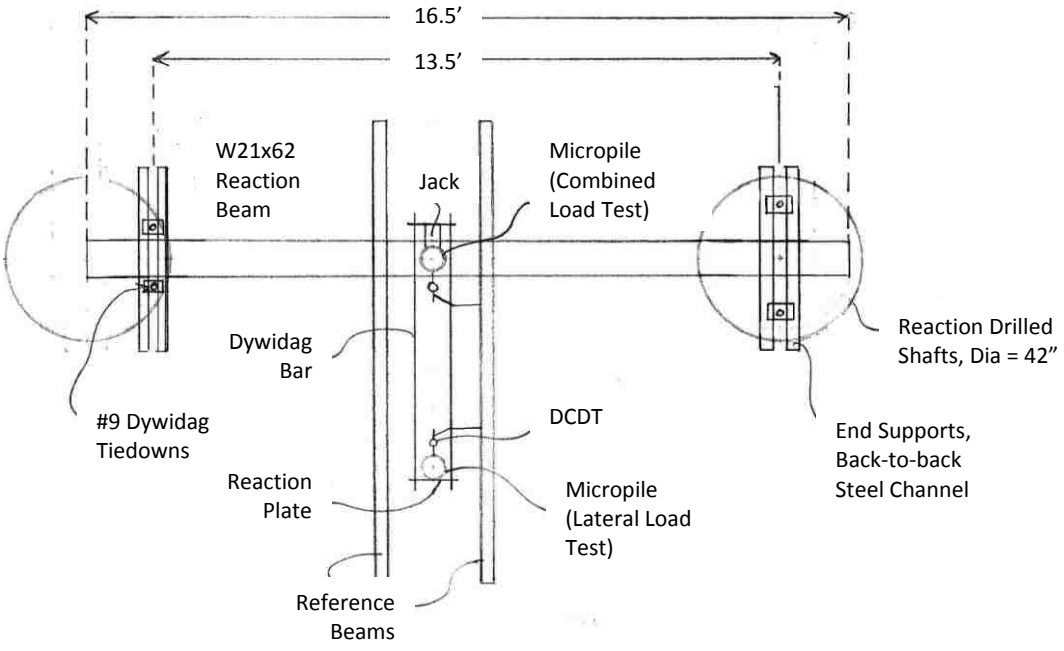

Figure 5.8. Plan View of WTS Lateral/Combined Load Frame

The final step in designing the load frame was to design the combined load testing apparatus. The load frame required for combined load testing utilized both the axial and

lateral load frames described above. The additional component of the combined load test frame was an apparatus that allows the micropile to move laterally while an axial load is applied. The design concept for the combined loading apparatus was based on the roller system designed to test piles in combined loading and presented in a paper by el-Geneidy [2009]. The design was modified to accommodate the smaller size of the micropiles installed. The resulting combined load apparatus was fabricated from a 10-inch-wide by 12-inch-long by ¾-inch-thick steel plate with rails welded on the top and bottom of the plate such that the bottom portion fit around the outside of the micropile casing and the top provided a track for the rollers. Five rollers with diameters of 1.5 inches and lengths of 7 inches were placed on the track and a free-moving, 10-inch-wide by 12-inch-long plate was placed on top of the rollers. Photographs of the roller apparatus are shown in Figure 5.9. The maximum allowed lateral movement of the roller apparatus was about 2.5 inches, consistent with the results of the LPILE analysis used for design.

Figure 5.9. Photographs of Combined Load Roller Apparatus

5.3. PREDICTION OF FIELD TEST BEHAVIOR

Prediction of micropile behavior during the field tests was completed using common design tools. As previously stated, the micropiles were designed to have an ultimate axial capacity of 120 kips. However, as further discussed in Section 5.5, the average installed bond lengths for the two micropiles that were tested in axial compression (A and D) was 9.4 feet. For the bond zone adhesion used for the original design (40 psi), the revised predicted ultimate axial capacity was 113 kips.

Prediction of micropile behavior when subjected to lateral and combined loads was completed using LPILE software [Reese et. al. 2004]. The software models the soil as non-linear springs that are modeled using individual load-deflection (p-y) curves along the length of the pile, and the structural elements are modeled as beam-columns. The required input parameters include soil and rock properties, pile geometry, and pile structural properties. The soil and rock properties and pile geometry inputs used in the analysis correspond to the values discussed in Sections 5.1.4 and 5.2.1, respectively. However, estimation of the structural properties is not as straightforward because the micropile cross-section consists of both grout and steel that interact to resist the lateral or combined loads. Determination of the properties is further complicated by the fact that the grout may crack as higher lateral loads are applied. The standard of practice for design of micropiles subjected to lateral loads is to ignore the contribution of the grout to structural bending resistance. This approach is conservative, which is appropriate for design, but likely does not account for the actual behavior during lateral loading. Because this conservative approach is typically used, there is no consensus within the micropile design community on how to account for increased bending resistance from the

grout. However, the American Concrete Institute (ACI) manual contains recommendations for concrete-filled, steel pipe columns subjected to lateral or eccentric loads. The ACI manual recommends using 70 percent of the moment of inertia that is contributed from the concrete [ACI 1999]. Therefore, the LPILE prediction of field behavior was completed using two different sets of structural properties. One prediction used the steel properties only, and the other prediction used a transformed section that included a 30 percent reduction in the moment of inertia contribution from the grout to account for cracking during bending.

The output of the program includes deflection and bending moment along the length of the pile. The program was first used to model behavior of the micropile when subjected to the planned lateral load increments for the testing program, as shown in Table 5.3. For each successive load increment, the lateral deflection at the head of the micropile and the maximum bending moment along the length of the pile were recorded. Thus, plots of load versus pile head deflection and load versus maximum bending moment could be plotted for the laterally loaded micropile tests, as shown in Figures 5.10 and 5.11, respectively. The analysis was repeated for combined loading by placing a constant load of 40 kips at the top of the pile and then incrementally applying the planned lateral loads shown in Table 5.3. The results of the combined load prediction are shown side-by-side with the lateral behavior results in Figures 5.10 and 5.11.

The results of the analyses can be used to predict behavior during field load testing of the micropiles, as well as to compare the differences in behavior between lateral and combined load tests and to evaluate the influence of the structural properties used in the analyses. Within the working load portion of the load-displacement and load-

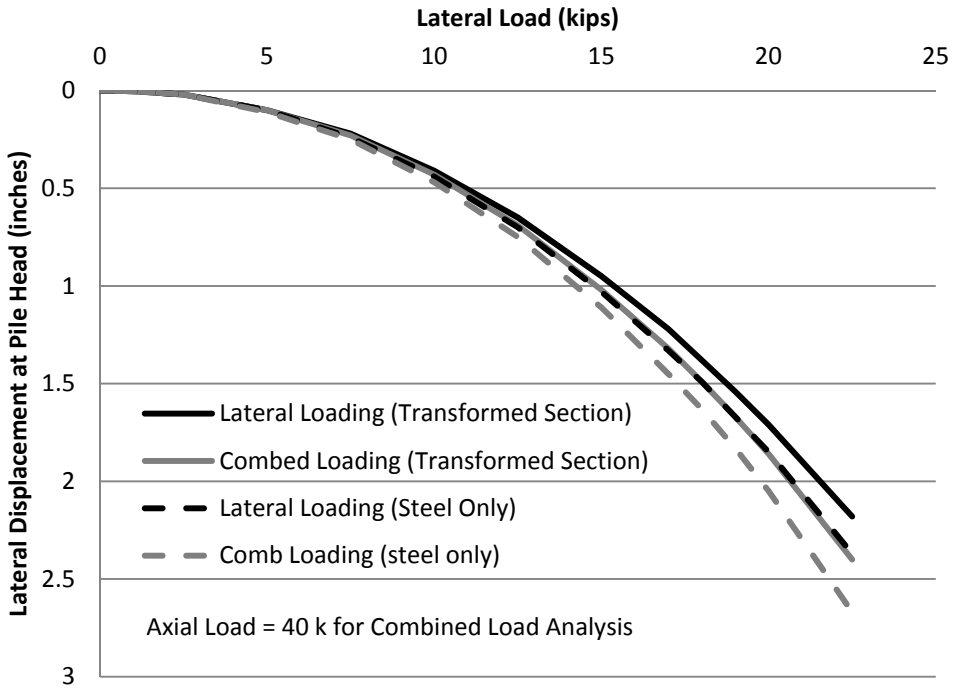

Figure 5.10. Lateral Load versus Lateral Displacement from LPILE Prediction

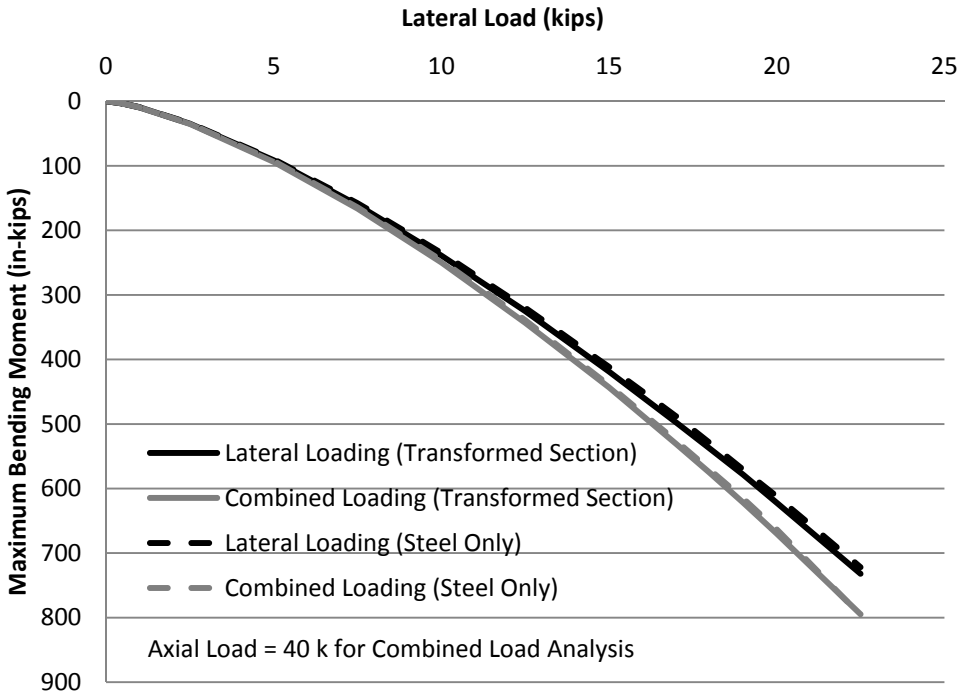

Figure 5.11. Lateral Load versus Maximum Moment from LPILE Prediction

Table 5.3. Planned Lateral/Combined Loading Sequence

Lateral Load (kips)	Hold Time (min)	Lateral Load (kips)	Hold Time (min)
Alignment Load	2.5	17	5
0.5	2.5	18	5
1	2.5	19	5
2.5	2.5	20	5
5	2.5	22.5	5
7.5	5	15	2.5
10	5	10	2.5
12.5	5	5	2.5
15	5	Alignment Load	2.5

maximum moment plots (0 kips to 10 kips), the difference between the lateral loading and combined loading curves are minimal (less than about 5 percent). However, from the design load to the maximum applied load (10 kips to 22.5 kips), the difference is more pronounced. For the load-displacement plots, the difference between the displacement at the pile head is as much as 12 percent between the lateral loading and combined loading curves. For the load-maximum moment plots, the difference between lateral and combined load plots is up to about 10 percent. In Figure 5.10, comparison of the results using a transformed section (steel and grout) and using steel only indicate that larger displacement will occur for the section where only the steel is considered for bending resistance. This result is expected because the steel-only section has less bending stiffness than the transformed section. Beyond the lowest lateral loads, the difference between pile head deflections for the two different structural sections is consistently between about 7 and 8 percent for lateral loading and between about 8 and 10 percent for combined loading. Comparison of the results for the two different structural sections

shown in Figure 5.11 indicates that the type of structural section considered in the analysis has only a minimal effect on the maximum bending moment within the micropile. For both the lateral and combined load analyses, the maximum bending moment difference is less than about 2 percent.

5.4. INSTRUMENTATION AND CALIBRATION

Each micropile was instrumented with four to seven vibrating wire strain gages that were cast into the micropile grout during installation. The vibrating wire strain gages were Model 4200 gages manufactured by Geokon, Inc. [2010]. The specifications for the gages are shown in Table 5.4. Vibrating wire strain gages were chosen for this project because of their durability during installation and the fact that wire length does not degrade the signal response of the gage. The purpose of the gages was to obtain strain measurements that could be converted into load readings and/or bending moment readings where pairs of strain gages were used. To obtain accurate bending moment readings, it is necessary to have a pair of strain gages oriented in the direction of lateral load and to have the gages placed as far from the central reinforcing bar as possible.

Table 5.4. Summary of Vibrating Wire Strain Gage Parameters

Parameter	**Value**
Gage Designation	Model 4200
Gage Factor	3.304
Batch Factor	0.97
Standard Range	3000 με
Resolution	1.0 με
Accuracy	± 0.5 %
Temperature Range	-20°C to +80°C
Active Gage Length	153 mm
Coil Resistance	80 Ω
Frequency Datum	800 Hz

Mounting bars fabricated from short sections of No. 4 reinforcing bars were used to accomplish these two objectives. Specifically, 18-inch-long bars were bent with 45 degree angles into a trapezoidal shape such that the strain gages could be attached to the mounting bars and the mounting bars could be attached to the central reinforcing bar during installation. The result was a spacing of approximately 1.7 inches from the center of the micropile to center of the gage and a clear space of approximately ¼ inch between the mounting bar and the inside of the steel casing. Figure 5.12 shows a photograph and schematic of the mounting bar and gage and the relative distance to the micropile casing and central reinforcing bar.

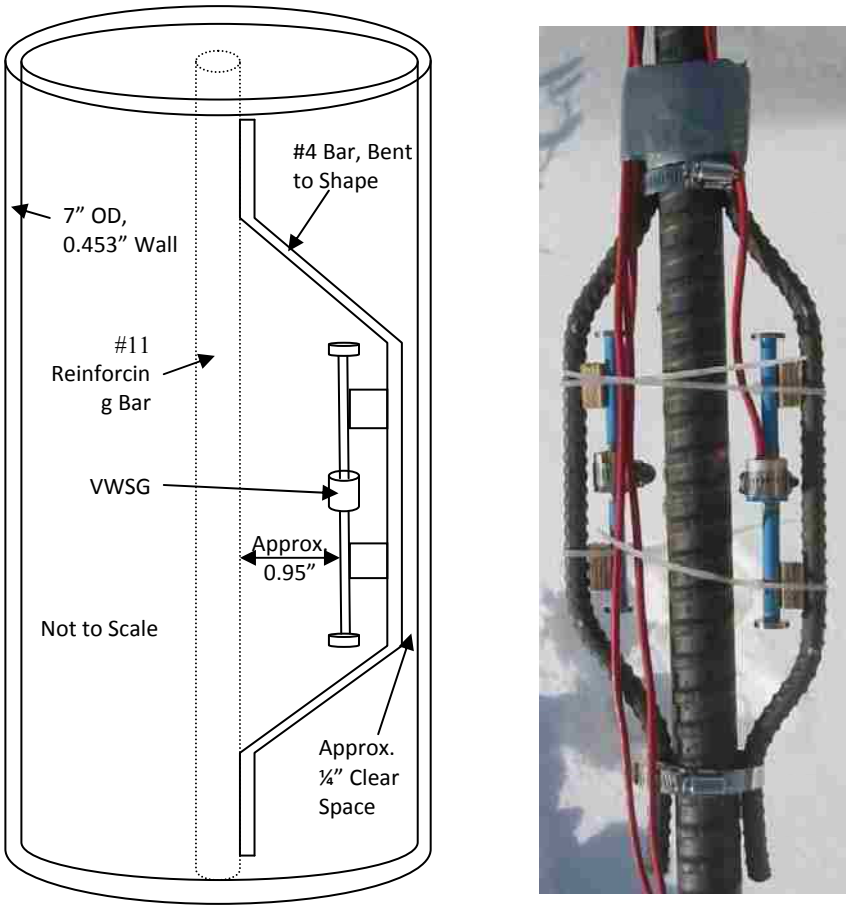

Figure 5.12. Schematic and Photograph of Strain Gage Mounting

Figure 5.13 shows the approximate locations of the gages within each micropile. As shown in this figure, the mounting bar also served as protection for the strain gages during installation. In addition, the manner in which the gages were attached to the mounting bar allowed grout to flow freely around the "barbell" ends of the strain gages such that they were fully embedded in concrete as intended by the manufacturer. Table 5.5 indicates the planned test type for each micropile. For micropiles tested in lateral only, strain gages were not needed within the bond zone.

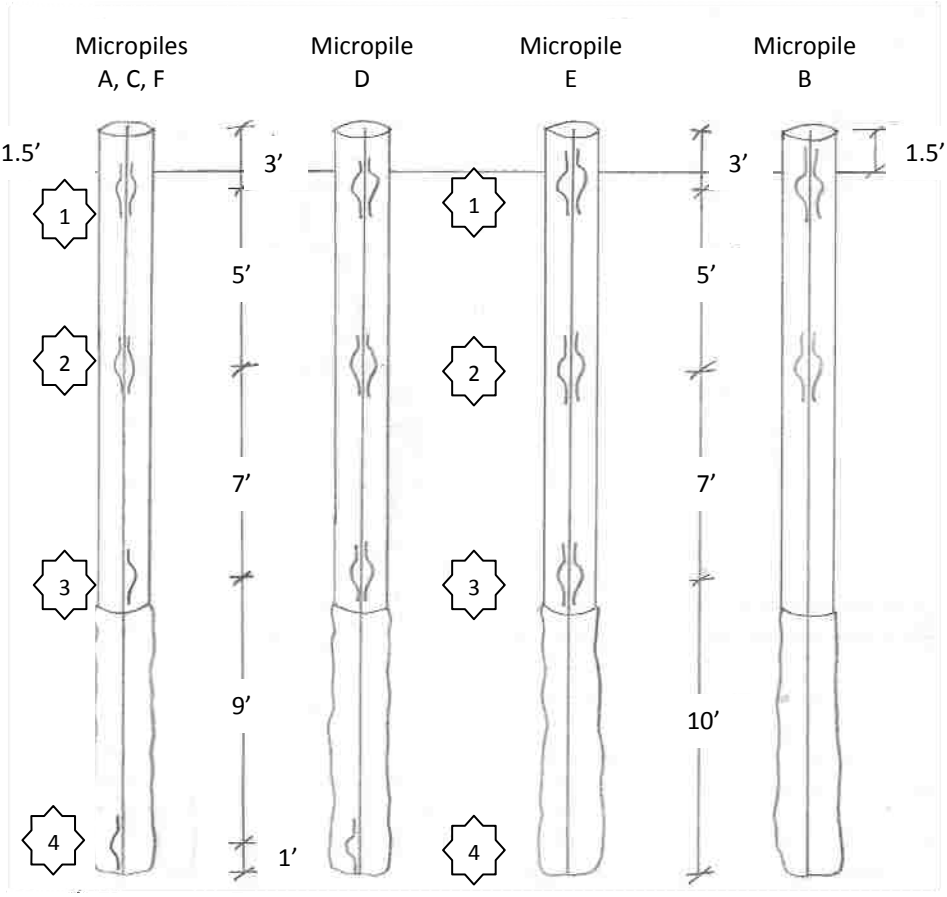

Figure 5.13. Locations of Strain Gages in Micropiles

Table 5.5. Field Testing Matrix

Micropile Designation	Vertical Compression Test	Lateral Test	Combined Load Test
A	X		X
B		X	
C			X
D	X		X
E		X	
F			X

Prior to shipping the gages to Missouri S&T, Geokon, Inc. tested the gages and provided a batch factor to be applied to the strain readings, as shown in Table 5.4. In addition, once the gages arrived at Missouri S&T, additional calibration and testing was completed. A 1-foot-long section of 7-inch-diameter casing provided by LB Pipe and Coupling was filled with grout and a single vibrating wire strain gage was embedded into the grout to simulate a short section of the planned micropiles (see photograph, Figure 5.14).

After the grout was allowed to cure, the grout surface was leveled and the piece was placed in a uniaxial compression machine along with the load cell that would be used to measure the axial compression load in the field. The specimen was loaded several times in increments and magnitudes expected in the field tests. The resulting strain values were converted to load values as discussed in Sect 5.8. The modulus value used in the equation was the modulus of steel and the area included the area of steel and the transformed area of concrete. The load input by the testing maching was then plotted against the output load from the strain gage and the load cell, as shown in Figure 5.15. To assess relationship of the measured values from the load cell and VWSG to the

applied load, statistical analysis of the data was completed. A 95 percent confidence interval was computed for the slope and intercept of best fit lines through the measured data. The slope of the applied load curve (1.0) was just outside of the confidence intervals for the data from the two devices (0.81 to 0.87 and 0.93 to 0.97 for the VWSG and load cell, respectively). The intercept of the applied load curve (zero) was within the confidence interval for the load cell (0.58 to 3.01) and well outside the confidence interval for the VWSG (8.22 to 14.35). The error associated with the intercept of the VWSG may indicate that the gage is not as reliable for low magnitudes of load. In addition, the differences between the applied and measured loads may be attributed to the strain gage not being aligned exactly vertical, the load frame being slightly out of calibration, or the load not being applied exactly vertically.

Figure 5.14. Photograph of Mock Section of Micropile for Strain Gage Calibration

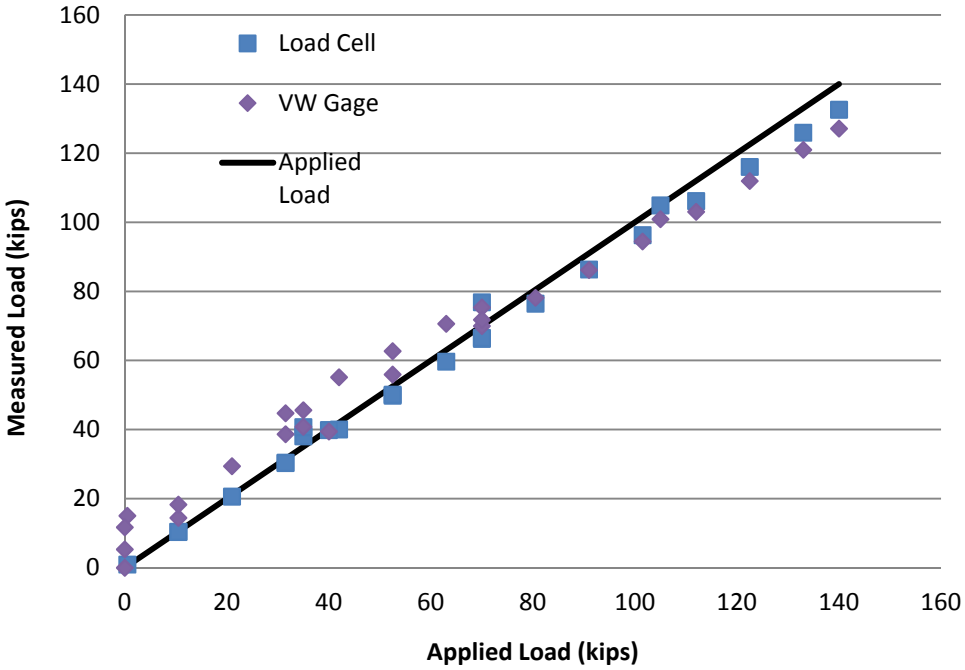

Figure 5.15. Results of Strain Gage Calibration

In addition to the strain gages, direct current displacement transducers (DCDTs) were used to monitor axial and lateral deflection at the head of the micropiles. To account for tilting during the axial load tests, twisting during the lateral load tests, and to provide redundancy, at least two DCDTs were used on each micropile in the direction of movement for each test. Each DCDT was calibrated prior to the field testing. Dial gages were used to monitor axial and/or lateral deflection to provide redundancy in case of power outages or lost data.

The applied load in the axial and lateral directions was monitored using calibrated load cells that use resistive strain gage technology. Specifically, a single load cell with a 200 kip capacity was used to monitor the axial load and two load cells, each with 50 kip capacity, were used to monitor the lateral load. For the lateral test, a load cell was placed

on each of the two tension bars in the lateral load frame. Thus, the total applied lateral load was equal to the sum of the two load cells. In addition to the load cells, the jacks were calibrated prior to the field load tests. The calibration was done by putting a pressure gage on the hydraulic line between the pump and the jack and then incrementally loading in a calibrated load cell in the Missouri S&T structures laboratory.

The digital data during the test, including vibrating wire strain data, DCDT data, and load cell data was collected and stored using the black box data acquisition system described in Section 3.3. Each of the digital data gages was calibrated to be used with this specific data acquisition box and to be used simultaneously.

5.5. MICROPILE INSTALLATION

Six micropiles were installed at the WTS on February 9 through 11, 2011 by Hayward Baker, Inc. (HBI). Based on their experience in similar soil/rock conditions, HBI recommended drilling using an 8-inch-diameter auger with a rock bit. The augers were powered by a Klemm Bohrtechnik Model 4140005 drill rig (see Figure 5.16). To the extent possible, each micropile was installed in an identical manner, as outlined below, such that the target finished product resulted in a total micropile length of approximately 25 feet, including 16 feet of casing with 1.5 feet of stickup above the ground surface and a 9- to 10-foot-long bond zone within the shale layer. The installed micropile lengths, as well as the date completed are presented in Table 5.6.

In general, installation of the micropiles was completed using the following steps, as shown in Figures 5.16 through 5.20.

1. Drill an open hole to a depth of approximately 23.5 feet using an 8-inch-diameter auger.

2. Weld rods to the sides of the casing 18 inches below the top to hold the casing in the proper location when placed.
3. Cut a V-shaped notch in the top of the casing to facilitate routing of strain gage wires.
4. Place the casing in the open hole using an extendible fork lift.
5. Attach strain gages and centralizers to the central reinforcing bar.
6. Tremie grout through the casing until grout exits at the ground surface through the annulus between the casing and the drilled hole.
7. Place the central reinforcing bar through the casing to the bottom of the open hole.
8. After initial grout set, grout to the top of the casing.

On April 20, 2011, after the grout had completely cured, the strain gage wires were routed out of the notch in the casing and non-shrink grout was placed to the top of the casing. Immediately prior to testing the surface of the non-shrink grout was smoothed and trimmed such that it was flush with the top of the casing.

Table 5.6. Summary of Micropile Installation

Pile	Bond Length (feet)	Casing Length (feet)	Casing Stickup (feet)	Date Installed
A	9.1	16	1.5	10-Feb-2011
B	10.0	16	1.5	11-Feb-2011
C	8.6	16	1.5	10-Feb-2011
D	9.7	16	1.5	10-Feb-2011
E	9.3	16	1.5	10-Feb-2011
F	9.1	16	1.5	11-Feb-2011

Figure 5.16. Micropile Drilling (Step 1)

Figure 5.17. Micropile Casing (Steps 2 and 3)

Figure 5.18. Installation of Micropile Casing (Step 4)

Figure 5.19. Attachment of Strain Gages (Step 5)

Figure 5.20. Initial Grouting (Step 6)

Figure 5.21. Placement of Central Reinforcing Bar (Step 7)

Figure 5.22. Final Grouting (Step 8)

As previously discussed, the casing consisted of 7-inch OD steel casing with a wall thickness of 0.453 inch and a minimum yield strength of 80 ksi. For each micropile, a 6-foot-long section of casing was placed at the bottom of the cased section and a 10-foot-long piece of casing was threaded to the lower casing, resulting in a 16-foot-long cased section. The lower piece of casing was outfitted with J-teeth, but they were not used because open-hole auger methods were used to install the micropiles rather than duplex drilling methods. The central reinforcing bar consisted of a 25-foot-long, #11 dywidag threadbar with a minimum yield strength of 75 ksi. The grout mix consisted of 1 bag (92 lbs) of Type I/II Portland cement for every 5 gallons of water, resulting in a 0.45 water to cement ratio. During micropile installation, six 4-inch by 8-inch grout cylinder molds were used to obtain samples of the production grout for laboratory testing. Because of the extreme cold weather during construction, the cylinders were taken inside

and allowed to cure at room temperature for 24 hours. The cylinders were then taken to Missouri S&T and allowed to further cure in a humidity controlled moist room. After curing, the cylinders were tested in the Missouri S&T laboratory in general accordance with ASTM C39 [ASTM International 2011], resulting in an average unconfined compression strength of approximately 5570 psi. The results of the grout cylinder tests are shown in Table 5.7.

Table 5.7. Summary of Grout Cylinder Testing

Pour Date	Test Date	Curing Days	f'c (psi)
10-Feb-11	21-Mar-11	39	5570
10-Feb-11	21-Mar-11	39	5820
10-Feb-11	21-Mar-11	39	5260
10-Feb-11	11-Jul-11	151	5299
10-Feb-11	11-Jul-11	151	5202
10-Feb-11	11-Jul-11	151	6278

5.6. EXPERIMENTAL TESTING PROGRAM

Testing of the micropiles at the WTS was completed on May 17 and 18, 2011. The testing program consisted of applying vertical loads, lateral loads, and simultaneous vertical and lateral (combined) loads to the micropiles. In general, the load tests were performed in accordance with commonly accepted micropile load testing methods. The loading schedule for the lateral and combined load tests is shown in Table 5.3 and the loading schedule for the axial compression tests is provided in Table 5.8. For all of the tests, deflection at the head of the micropile, applied load, and strain within the micropile were recorded continuously throughout the test. Jack gage pressure and dial gage

readings were also recorded at each load increment. A general description of the testing methods is provided in the following paragraphs.

Table 5.8. Planned Axial Loading Sequence

Load Cycle	Axial Load (kips)	Hold (min)
Alignment	AL	2.5
Cycle 1	9	2.5
	18	2.5
	27	2.5
	AL	1
Cycle 2	9	1
	27	1
	36	2.5
	45	2.5
	54	2.5
	60	2.5
	AL	1
Cycle 3	9	1
	60	1
	69	2.5
Begin Creep	78	10
End Creep	78	
	87	2.5
	AL	1

Load Cycle	Axial Load (kips)	Hold (min)
Cycle 4	9	1
	87	1
	96	1
	105	2.5
	114	2.5
	120	2.5
	135	2.5
	150	2.5
	90	2.5
	60	2.5
	30	2.5
	AL	2.5

A total of two axial compression load tests were completed on Micropiles A and D on May 17, 2011. The micropile was incrementally loaded as shown in Table 5.8 until the failure load was reached. The failure load was defined as the load at which the micropile plunged or the maximum load that can be applied to the micropile. Creep tests were conducted at approximately 65 percent of the predicted failure load (78 kips). The micropile test setup and reaction frame are shown in Figure 5.23.

Figure 5.23. Axial Load Test

A total of two lateral load tests were completed on Micropiles B and E on May 17 and May 18, 2011, respectively. The lateral load tests were performed by pulling two micropiles toward each other, as discussed in Section 5.2. Thus, each lateral load test was performed simultaneously with a combined load test. For the lateral load tests, the micropiles were incrementally loaded until a deflection of approximately 2.5 inches was reached, corresponding to the limit of the equipment that was used for the combined load test (see Section 5.2). The load test schedule for the lateral load test is shown in Table 5.3, and a photograph of the lateral load test setup is shown in Figures 5.24 and 5.25.

A total of four combined load tests were completed on Micropiles A, C, D, and F on May 17 and 18, 2011. The only difference between the load schedule for the lateral load tests and the combined load tests is that an axial load was incrementally applied to the top of the micropile prior to commencing the lateral load test schedule. The

Figure 5.24. Lateral Load Test

Figure 5.25. Simultaneous Lateral and Combined Load Tests

maximum axial load applied to the micropile during combined load testing was approximately equal to one-half of the ultimate load determined during the axial load test. As previously stated, each combined load test was performed simultaneously with a lateral load test by pulling two micropiles toward each other. Lateral movement is allowed during loading using the roller system described in Section 5.2. The micropiles were incrementally loaded until a deflection of approximately 2.5 inches was reached, corresponding to the limit of the equipment that was used for the combined load test. The load test schedule for the combined load test is shown in Table 5.3, and a photograph of the combined load test setup is shown in Figures 5.25 and 5.26.

Figure 5.26. Combined Load Test

5.7. DATA REDUCTION

As previously discussed, the data acquisition system recorded data from the load cells, DCDTs, and vibrating wire strain gages. The load cells and DCDTs were calibrated prior to testing such that the voltage in each unit that was read by the data acquisition system is converted to a load or displacement reading, respectively. Thus, the data acquisition system output from the load cells and DCVTs was in the form of pounds and inches, respectively.

Unlike the load cells and DCDTs, the output from the vibrating wire strain gages requires some post-processing to obtain the desired parameters, including load and bending moment, from the gages. Vibrating wire strain gages operate on the theory that the vibrating frequency of a wire will change as the tension in the wire is increased or decreased. The Geokon Model VCE-4200 vibrating wire strain gages were designed to measure strain in mass concrete. Thus, the gage is equipped with two barbell-type ends that are embedded in the concrete and the strain is measured between these two points. The internal wire is secured at the two barbell ends and the wire is plucked at the center of the wire. The frequency of the wire vibration is then read at the center of the wire and the value is transmitted along the instrument cable back to the data acquisition box. The data acquisition box then converts the frequency reading to a strain reading using Equation 9.

$$\mu\varepsilon = G(\Delta f^2 * 10^{-3}) \tag{9}$$

where: $\mu\varepsilon = microstrain$

$G = Gage\ Factor$ ($see\ Table$ 5.4)

$$\Delta f = Change\ in\ frequency\ of\ wire\ vibration$$

The data recorded by the data acquisition box is in the form of microstrain. The actual magnitude of microstrain is not of much use by itself. Rather, the changes in microstrain throughout the test are the desired data that can be used to obtain the load and bending moment at any point during each test. The change in microstrain is first corrected using the batch factor for the gages, a shown in Equation 10.

$$\Delta\mu\varepsilon_{corr} = B(\mu\varepsilon_i - \mu\varepsilon_0) \quad (10)$$

where: $\mu\varepsilon_0 = initial\ microstrain\ reading\ at\ beginning\ of\ test$

$\mu\varepsilon_i = microstrain\ reading\ at\ any\ point\ during\ test$

$B = Batch\ Factor\ (see\ Table\ 5.4)$

In locations where a single gage was present and bending was negligible, such as within the bond zone, the corrected change in microstrain could be used to directly compute load (P) using Equation 11.

$$P = \Delta\mu\varepsilon_{corr} * E * A \quad (11)$$

where: $E = Modulus\ of\ elasticity$

$A = Cross - sectional\ area\ of\ micropile$

To calculate bending moment, several assumptions need to be made. First, the calculations assume that the gages are located exactly within the plane where the bending

occurs and are spaced equidistant from the center of the micropile. Second, the grout in the annulus between the casing and the ground is assumed to not contribute to the bending resistance of the micropile because it is likely to crack and break away from the outside of the casing. Finally, the calculations assume that, because the grout is confined within the casing, significant cracking of the internal grout does not occur during bending. This assumption results in the neutral axis coinciding with the centerline of the micropile, as shown in Figure 5.27.

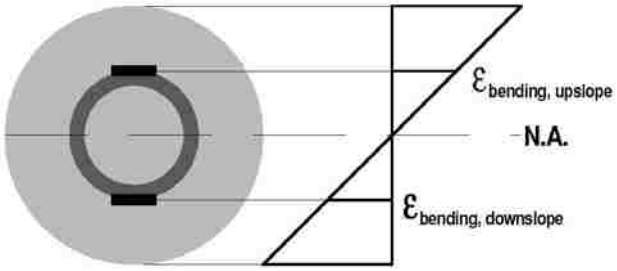

Figure 5.27. Strain Diagram for Micropile Subjected to Bending [After Textor 2007]

Because bending does not occur at the neutral axis, the strain at the neutral axis is equal to the axial strain. In addition, because the strain gages are assumed to be equidistant from the centerline (distance x), the strain resulting from bending at the gage locations should be equal and opposite (see Figure 5.27). Therefore, the axial strain can be computed by averaging the two strain readings from the pair of strain gages (Equation 12) and the bending strain can be calculated by subtracting the axial strain from the original strain reading, as shown in Equation 13. Axial load (P) and bending moment (M) can then be calculated from the resulting strains using Equations 14 and 15, respectively.

$$\varepsilon_{\text{axial}} = \frac{(\Delta\mu\varepsilon_{corr})_1 + (\Delta\mu\varepsilon_{corr})_2}{2} \quad (12)$$

$$\varepsilon_{bending} = (\Delta\mu\varepsilon_{\text{corr}})_1 - \varepsilon_{axial} \quad (13)$$

$$P = \varepsilon_{axial} * E * A \quad (14)$$

$$M = \frac{I * E * \varepsilon_{bending}}{x} \quad (15)$$

Because the cross-section of the micropile consisted of grout and steel (central reinforcing bar and/or casing), transformed sections were used to calculate the area moment of inertia (I) and the cross-sectional area (A). Specifically, the grout was transformed to an equivalent area of steel by multiplying the grout area by the ratio of steel modulus to grout modulus. The transformed area was then used to calculate an equivalent diameter and ultimately an equivalent moment of inertia. The resulting transformed areas, moments of inertia, and modulus of elasticity used in the data reduction are shown in Table 5.9.

5.8. INTERPRETATION OF RESULTS

Following data reduction, as discussed in the previous section, several plots were developed to aid interpretation of the micropile field test results. The following sections present the results of each type of test (axial, lateral, and combined), as well as comparisons between the lateral and combined load tests. In addition, the lateral and combined load tests are compared to the behavior predictions presented in Section 5.3.

Table 5.9. Micropile Parameters Used for Data Reduction

Parameter	**Value**
Modulus of Elasticity, E_{steel}	29,000 ksi
Cased Section	
Steel Area, A_{steel}	10.8 in^2
Steel Area Moment of Inertia, I_{steel}	50.3 in^4
Tranformed Area, A_{trans}	14.8 in^2
Tranformed Area Moment of Inertia, I_{trans} (Assumes 70% of I_{grout} to account for cracking)	57.2 in^4
Bond Zone	
Steel Area, A_{steel}	1.5 in^2
Steel Area Moment of Inertia, I_{steel}	0.2 in^4
Tranformed Area, A_{trans}	8.6 in^2
Tranformed Area Moment of Inertia, I_{trans} (Assumes 50% of I_{grout} to account for cracking)	14.8 in^4

5.8.1. Axial Load Test Results and Interpretation. Micropiles A and D were tested in axial compression to failure as previously discussed. Data from the load cell and DCDTs were used to produce plots of axial load versus axial displacement at the micropile head, as shown in Figure 5.28. Figure 5.29 presents the same axial load versus axial displacement data, but the plot is limited to 1 inch of displacement to more clearly show the shape of the load-displacement curves.

As previously discussed, the ultimate capacity of the micropiles tested in axial compression was defined as the load at which the pile plunged. As shown in Figure 5.28, the plunge loads for Micropiles A and D were 80.6 kips and 96.6 kips, respectively. While failure was defined as plunge for this project, the interpretation of load test data to determine the ultimate axial capacity of micropiles is an issue that is still being discussed. One alternative method for determining the ultimate axial capacity of micropiles using

load test data is Davisson's method. Davisson's method was originally developed to interpret data from driven pile load tests, but has also been widely used for micropiles. Using Davisson's method (see Figure 5.29), the ultimate axial capacities of Micropiles A and D were 56 kips and 69 kips, respectively.

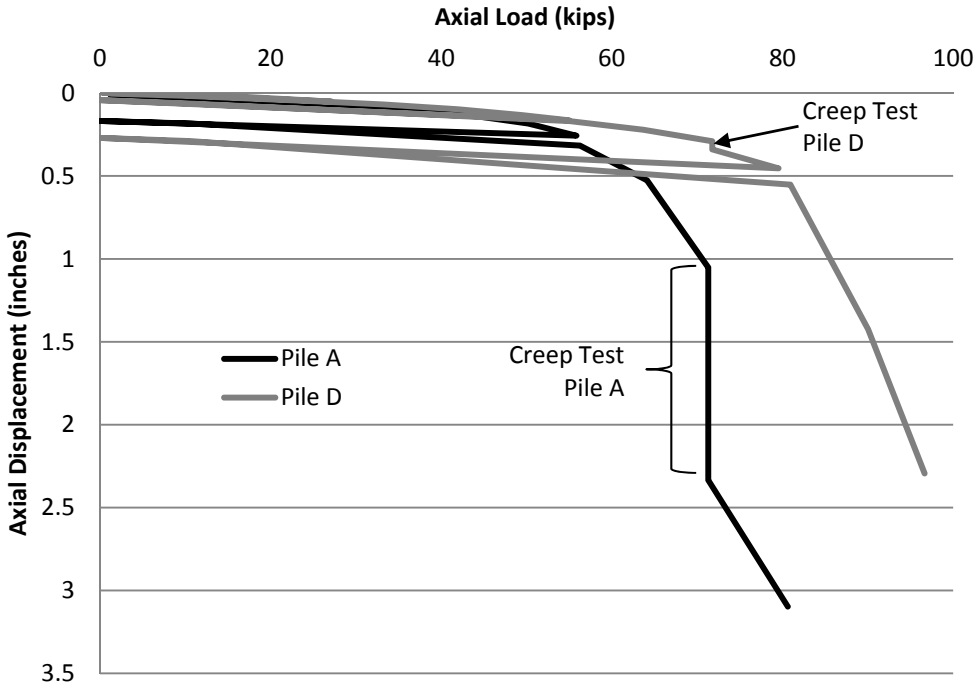

Figure 5.28. Axial Load Test Results – Load vs. Displacement

A creep test was conducted at approximately 65 percent of the predicted ultimate capacity. The FHWA Micropile Manual [Sabatini et. al. 2005] states that the acceptance criterion for the creep test is that deflection should not exceed 0.04 inches between 1 minute and 10 minutes of hold time. The recorded deflections for this time period for Micropiles A and D were 1.3 inches and 0.05 inches, respectively. The creep test for Micropile A clearly does not meet the criteria. These results are expected because the

failure load of Micropile A was approximately 30 percent lower than predicted. Therefore, the creep test was performed at a load level close to the failure load. The creep test results for Micropile D were close to the acceptance criteria but did not pass. Again, the failure load for Micropile D was approximately 20 percent lower than predicted, so the creep test was run closer to the ultimate capacity than typical.

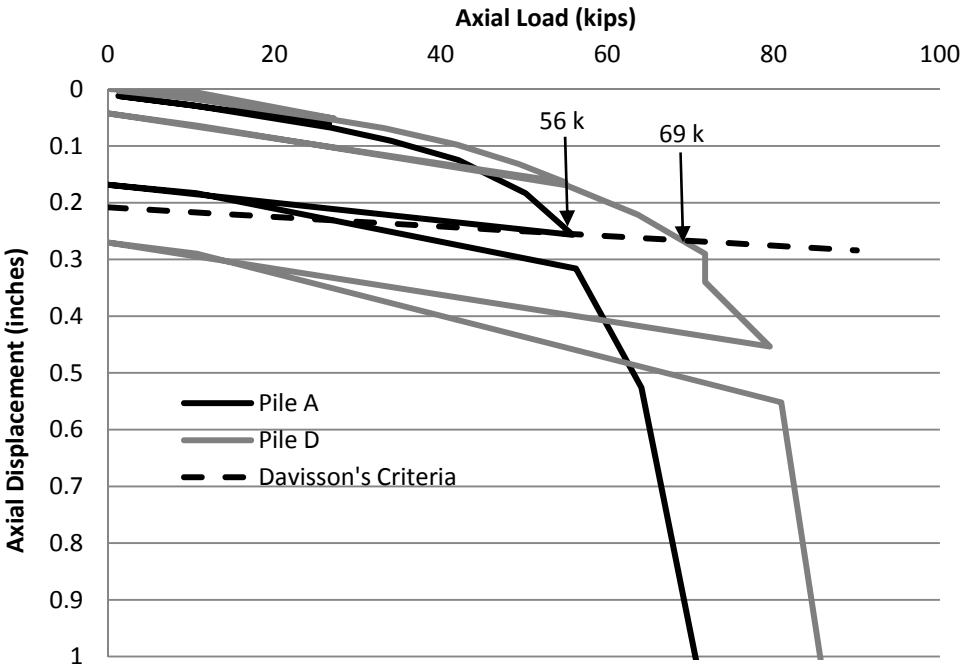

Figure 5.29. Axial Load Test Results – Load vs. Displacement with Davisson's Criteria

Using reduced data from the strain gages, load transfer plots (load versus depth) were prepared, as shown in Figures 5.30 and 5.31 for Micropiles A and D, respectively. A schematic showing the approximate locations of the casing, bond zone, and strain gages is provided on each figure. The text box shown at the top of each line is the applied axial load, and each data point along a single line represents the locations of

strain gages within the micropile. As can be seen in the plots, the load is transferred deeper as the load increases. The reason for this phenomenon is that displacement must occur to mobilize the side friction resistance along the length of the pile. Thus, as a load is applied to the top of the micropile, the pile itself will elastically compress and begin to mobilize side friction in the upper portion of the micropile. When the full side friction is mobilized in the upper portion of the micropile, additional load is transferred deeper. This iterative effect continues until load reaches the toe of the micropile where end bearing may then be mobilized. The micropile will fail when the applied load increases beyond the available side friction and end bearing resistance.

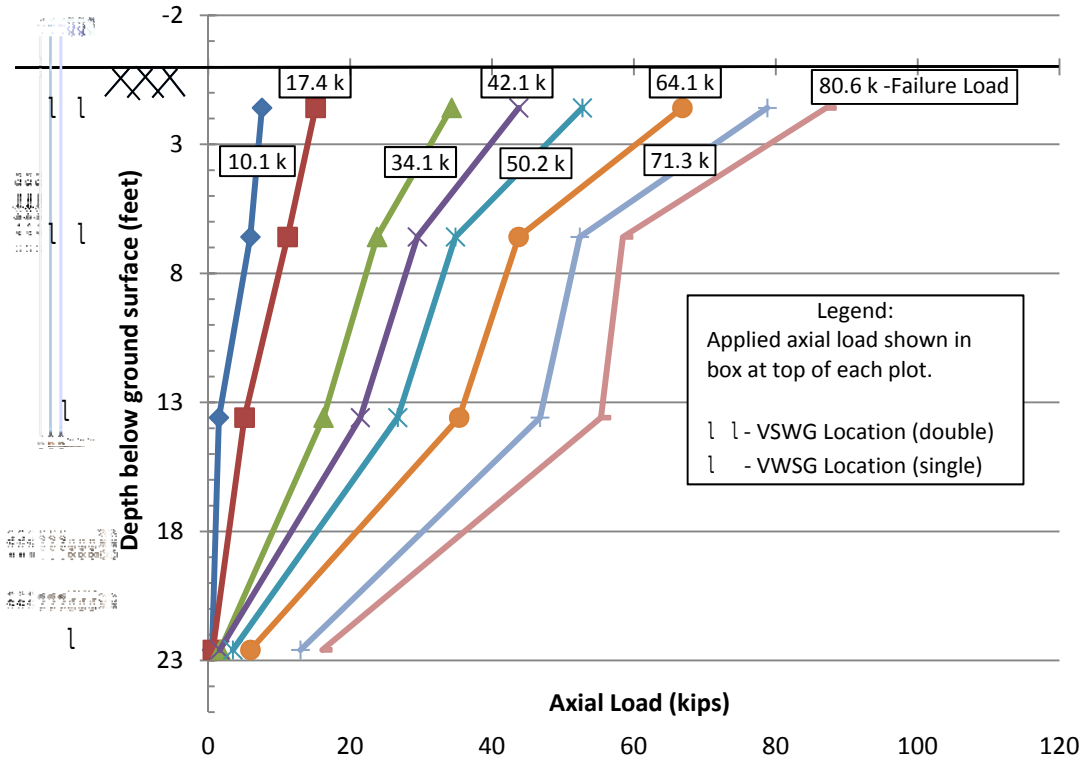

Figure 5.30. Micropile A Axial Load Test Results – Load vs. Depth

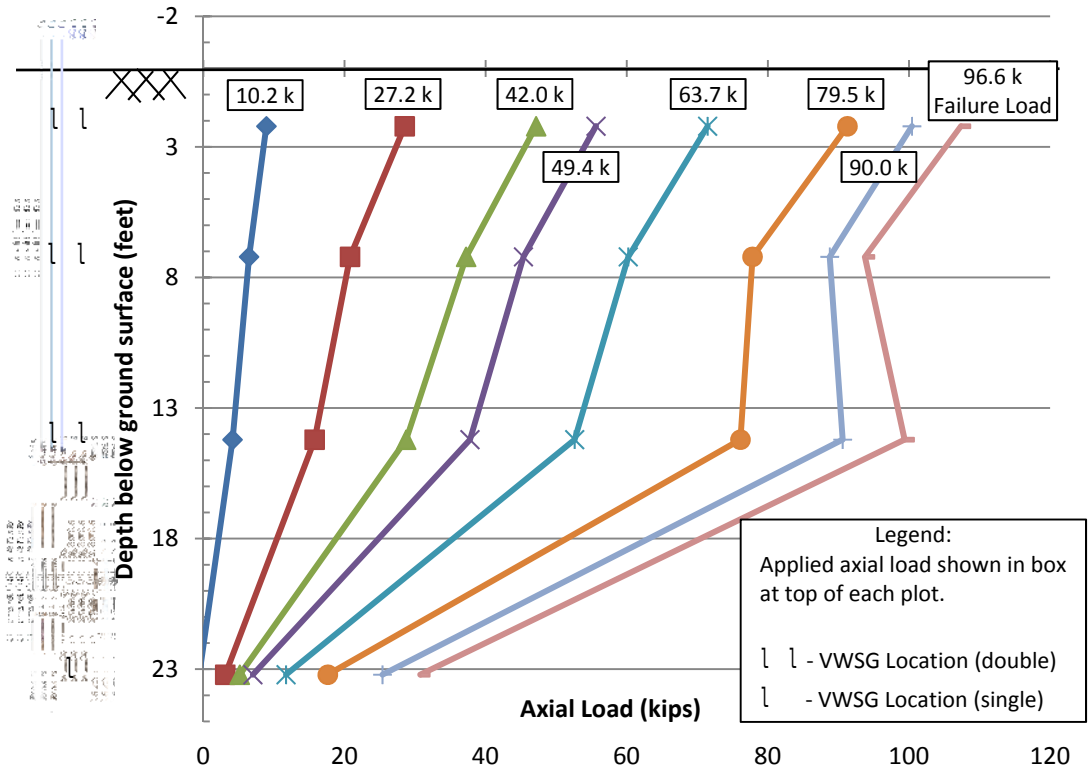

Figure 5.31. Micropile D Axial Load Test Results – Load vs. Depth

Although the two micropiles failed at different axial loads, there are some similarities between the results of the two axial load tests. The instrumentation along the length of the micropiles yields particularly valuable information that can be interpreted to gain insight into axial micropile behavior. The following paragraphs discuss several conclusions that can be drawn from the similarities and differences between the results of the two load tests.

First, the slope of the load versus depth curves in Figures 5.30 and 5.31 give an indication of load transfer along the length of the micropile. In general, the load versus depth curves are steeper within the bond zone. This behavior is expected because the side resistance is typically much greater in the bond zone and more load is transferred

from the micropile to the adjacent ground. This effect is especially apparent for the higher loads in the Micropile D load test where nearly the entire load is transferred through the casing down to the bond zone. Conversely, because the load transfer curves within the upper portion of the cased section of Micropile A are relatively steep, it is apparent that load transfer was occurring within this zone. It is likely that the increased bond strength was a result of the construction method used for the micropiles. As discussed in Section 5.2, the drill hole for the micropiles was oversized, resulting in an approximate ½ inch annulus around the casing. As the pile was tremie grouted, the annulus filled with grout. Because the grout around the casing was relatively thin and the bond between the grout and the smooth outside of the casing was likely minimal, the load transfer in the cased zone was ignored for the prediction of axial capacity. However, the load transfer between the upper two pairs of VWSGs for Micropile A was nearly equal to the load transfer in the bond zone. Despite this fact, the resistance will likely not be consistent and should not be relied on for design.

Second, the loads calculated from the vibrating wire strain gages (P_{VWSG}) during the failure condition within the bond zone can be used to back-calculate the ultimate unit side resistance (α_{bond}) using Equation 16.

$$\alpha_{bond} = \frac{\Delta P}{\pi * D_{bond} * L_{VWSG}} \tag{16}$$

where: $D_{bond} = Diameter\ of\ bond\ zone$

$L_{VWSG} = Distance\ between\ lower\ two\ VWSGs$

The resulting α_{bond} calculated from the load test data on Micropiles A and D was 14.6 psi and 25.3 psi, respectively. The summary of typical α_{bond} values listed in the FHWA Micropile Manual indicates a range of 30 psi to 80 psi for soft shales. Based on drill action, drill advancement rates, and cuttings observed during construction, the bond zone for Micropiles A and D was completely within the shale layer. There may be several reasons why the calculated bond strengths were lower than typical values. The method of drilling may have inadvertently lowered the bond strength because the augers were spun up and down in the hole to remove spoils from the bottom of the hole. This spinning action may have smeared the sides of the hole, resulting in reduced α_{bond}. Further, as discussed in Section 5.1.4, the undrained shear strength of the shale layer was highly variable, ranging from 1,550 psf to 14,130 psf. Therefore, if the bond zones of the two tested micropiles were within a region of the shale layer with lower undrained shear strength, the α_{bond} would also be lower. Typically, a shale with undrained shear strength lower than approximately 5,000 psf would be considered a hard clay. For comparison, typical values of α_{bond} in stiff silt and clay with some sand are between about 5 psi and 17.5 psi. Thus, based on the back-calculated bond strengths, the shale material within the bond zone at Micropiles A and D may classified as a hard clay or very soft shale. Perhaps the most important conclusion that can be drawn from the differences in α_{bond} is that variable ground conditions lead to variable bond strengths. This conclusion may seem rather obvious, but could be of vital importance on a micropile project. At the WTS, the shale strength variability was high and did not appear to follow any recognizable patterns, such as variation with depth or variation with lateral distance. For future load testing activities at a highly variable site, it would be beneficial to include

more strain gages within the bond zone to delineate areas of high or low bond strength. If a highly and randomly variable site is encountered in practice, the likely remedy is an increased level of testing. An increased number of verification and proof load tests will reduce the likelihood of an under-designed micropile.

Third, despite the generally accepted design premise that the toe bearing of micropiles is minimal and should be ignored, toe bearing was observed in the test results. If toe bearing was not occurring, the load calculated from the lowest level of VWSGs would approach zero throughout the test. Rather, using the loads shown in the figures at the toe of the micropiles during the failure condition, values of toe bearing can be calculated. The ultimate net toe bearing back-calculated from the Micropile A and D tests were 33,250 psf and 66,130 psf, respectively. Because toe bearing is typically ignored for micropiles, there is not a widely accepted analytical method for estimating toe bearing. Therefore, analytical methods developed for drilled shafts were used to compare a theoretical toe bearing to the observed toe bearing during axial load tests. Because the strength of the shale layer was highly variable, two different methods, both developed by O'Neill and Reese [Coduto 2001], were used to calculate the theoretical unit toe bearing (q_t'). The first method, shown in Equation 17, is used to estimate toe bearing of drilled shafts in clay, applicable for undrained shear strength (s_u) less than 5,000 psf.

$$q_t' = N_c^* s_u \tag{17}$$

where: $N_c^* = Bearing\ capacity\ factor$

$= 8.5\ for\ s_u = 1{,}500\ psf$

$= 9.0\ for\ s_u > 2{,}000\ psf$

For undrained shear strength between 1,545 psf and 5,000 psf, as determined for the WTS, the resulting range of unit toe bearing was 13,130 psf to 45,000 psf. The back-calculated unit toe bearing from the Micropile A load test lies within this range. The second method [Coduto 2001], shown in Equation 18, is used to estimate unit toe bearing of drilled shafts in cohesive intermediate geomaterial and rock. It is applicable for undrained shear strength greater than 5,000 psf.

$$q_t' = 5.0 s_u \tag{18}$$

For undrained shear strength between 5,000 psf and 14,130 psf, as determined for the WTS, the resulting range of unit toe bearing was 25,000 psf to 70,670 psf. The back-calculated unit toe bearing from both of the micropile axial load tests lie within this range. For the average value of undrained shear strength (6,400 psf) at the site, the theoretical unit toe bearing was calculated to be 32,000 psf which is very close to the back-calculated value from the Micropile A load test (33,250 psf). Provided good construction techniques are used during installation, it is reasonable to expect that some toe bearing will be present during axial loading. If further research is conducted to assess the effect of different construction methods in different soil types, undue conservativism in certain micropile designs may be eliminated. Designers will also need to assess the amount of deflection that is required to mobilize toe bearing and compare it to the allowable settlement of the supported structure.

5.8.2. Lateral Load Test Results and Interpretation. Micropiles B and E were tested by applying a lateral load near the head of the pile in the absence of an axial load,

as previously discussed. Data from the load cells and DCDTs were used to produce plots of lateral load versus lateral displacement near the micropile head, as shown in Figure 5.32. The figure also includes the results of the LPILE prediction of lateral micropile behavior discussed in Section 5.3.

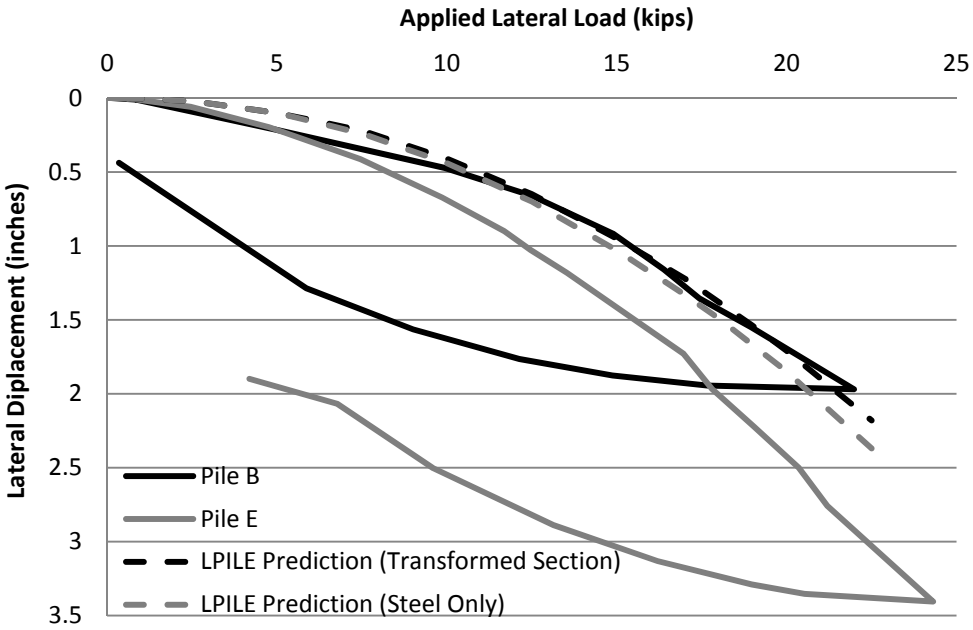

Figure 5.32. Lateral Load Test Results – Load vs. Displacement

The test results shown in Figure 5.32 indicate that the behavior of the two piles subjected to lateral loads was somewhat different for lateral loads greater than approximately 5 kips. The differences are likely a result of slight differences in ground conditions between the two piles. Comparison of the LPILE prediction with results from the two lateral load tests indicates that the field tests behaved less stiff than predicted in the early portions of the test (lateral load less than about 5 kips). Beyond a load of about

5 kips, the LPILE prediction matched the behavior of Micropile B. Micropile E behaved less stiff than the LPILE prediction for the entire range of applied lateral loads.

In addition to the load lateral load versus lateral displacement curve, the data obtained from the load cells and the VWSGs was used to plot lateral load versus maximum bending moment. At each VWSG level and for each applied lateral load, bending moments were calculated as discussed in Section 5.7 and used to develop the plot shown in Figure 5.33. The figure also includes the results of the LPILE prediction of lateral micropile behavior discussed in Section 5.3.

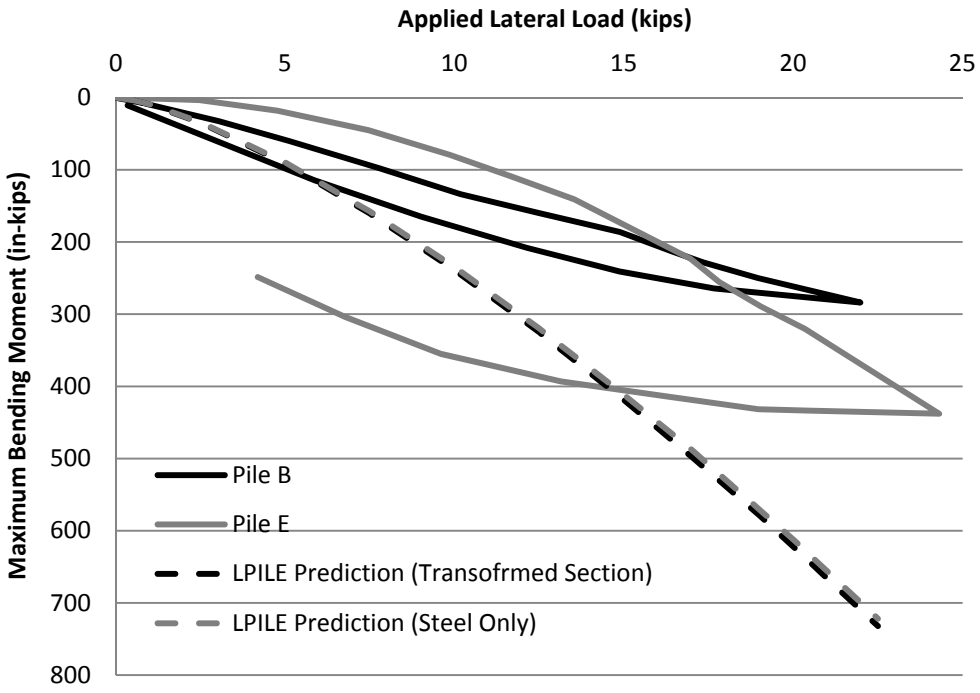

Figure 5.33. Lateral Load Test Results – Load vs. Maximum Bending Moment

The results shown in Figure 5.33 indicate that, at lower lateral loads (below about 15 kips), the maximum bending moments in Micropile E and Micropile B are similar. However, at larger loads, Micropile E experienced larger bending moments. This result

is expected because Micropile E also experienced greater lateral deflection than Micropile B, as shown in Figure 5.32. Comparison of the LPILE prediction to the measured bending moments shows that LPILE over predicts the bending moment for all but the lowest lateral loads. This overprediction is probably exaggerated because it is unlikely that the location of the strain gages corresponded to the exact location of the maximum bending moment within the test micropile.

Using the VWSG data, plots of bending moment versus depth were also prepared for several different magnitudes of lateral load, as shown in Figures 5.34 and 5.35. Because the micropiles had a free head condition, the bending moment was assumed to be zero at the location where the lateral load was applied (approximately 6 inches above the ground surface. In addition, the bending moment was assumed to be zero at the casing-bond zone interface for Micropile B, where a third level of strain gages was not present. Based on the results of the Micropile E lateral test (Figure 5.35), the bending moment approaches zero at the third level gages in the vicinity of the casing-bond zone interface, so the assumption is valid. Sketches showing the approximate locations of the casing, bond zone, and VWSGs are provided in each figure.

Comparison of the two bending moment versus depth plots indicates that, for the Micropile E lateral load test, the bending moment is both larger and transferred deeper than the bending moment within Micropile B. As previously stated, the larger bending moments are expected because of the larger lateral deflection that occurred during the Micropile E test.

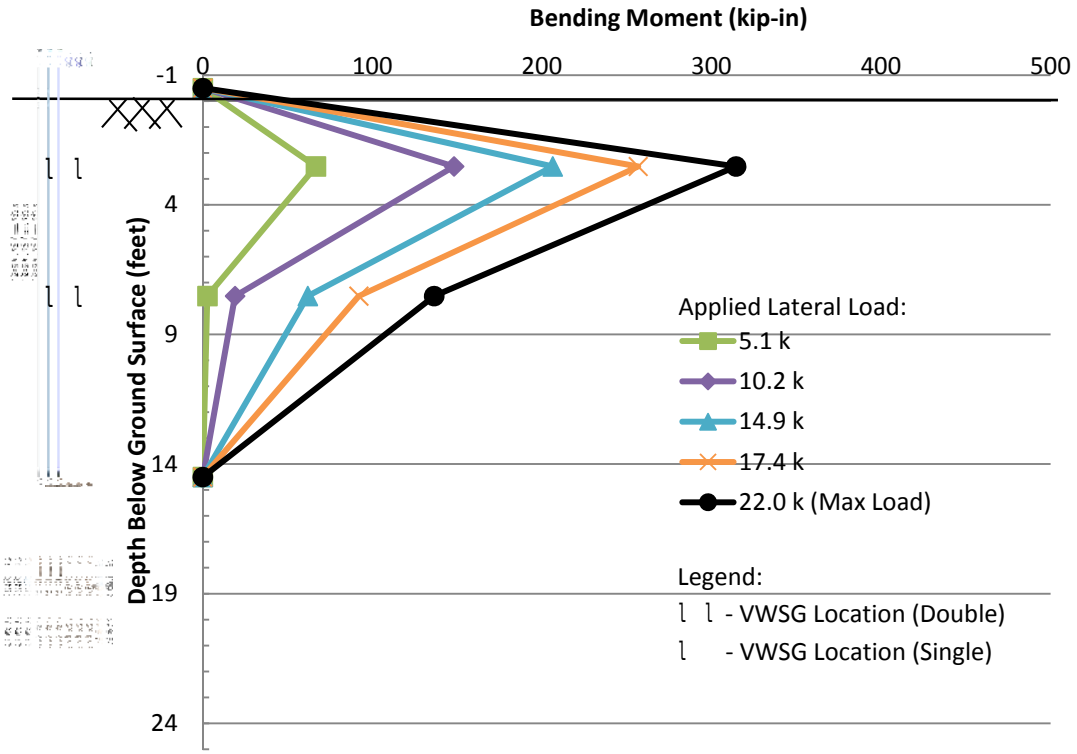

Figure 5.34. Micropile B Lateral Load Test Results – Bending Moment vs. Depth

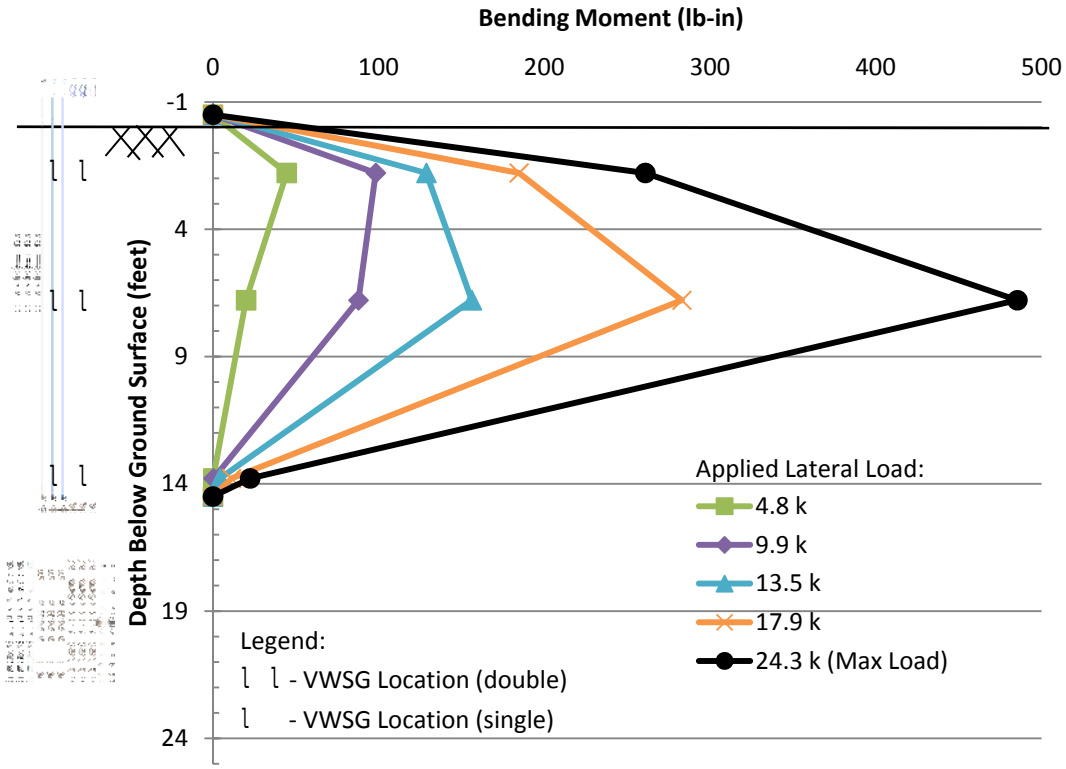

Figure 5.35. Micropile E Lateral Load Test Results – Bending Moment vs. Depth

Finally, Figures 5.36 and 5.37 were prepared to further compare the results of the two tests and to compare the measured bending moments to the predicted bending moments from LPILE. Figure 5.36 compares the bending moment diagrams at similar applied lateral loads (approximately 22 kips) for each test and the LPILE analysis. However, lateral failure is typically defined in terms of a maximum allowable deflection. Therefore, Figure 5.37 was prepared to compare the bending moment diagrams at similar lateral displacement (approximately 1.5 inches). The 1.5-inch lateral displacement was chosen because it is likely the highest deflection that would be allowed for production micropiles. The text on both plots indicates the lateral load and lateral displacement for each bending moment diagram. In both of the plots, the maximum bending moments predicted in LPILE are significantly larger than the measured bending moments and the location of the maximum bending moment is at a depth between the maximum bending moments measured in Micropiles B and E. A comparison of the bending moment diagrams for the two lateral tests shows that the maximum bending moments at a similar lateral displacement are very close, but the depth to the maximum bending moment are different.

The results of the two lateral load tests were somewhat different, but interpretation of the tests and comparison to predictive methods can be used to develop some basic conclusions. The major difference between the two tests was the magnitude of lateral displacement measured at the head of the micropiles. For low levels of lateral load (less than about 5 kips) the load deflection curves were identical, but Micropile E experienced higher lateral deflection at similar levels of lateral load loads. For the largest applied loads, lateral deflection for Micropile E was approximately 30 to 40 percent

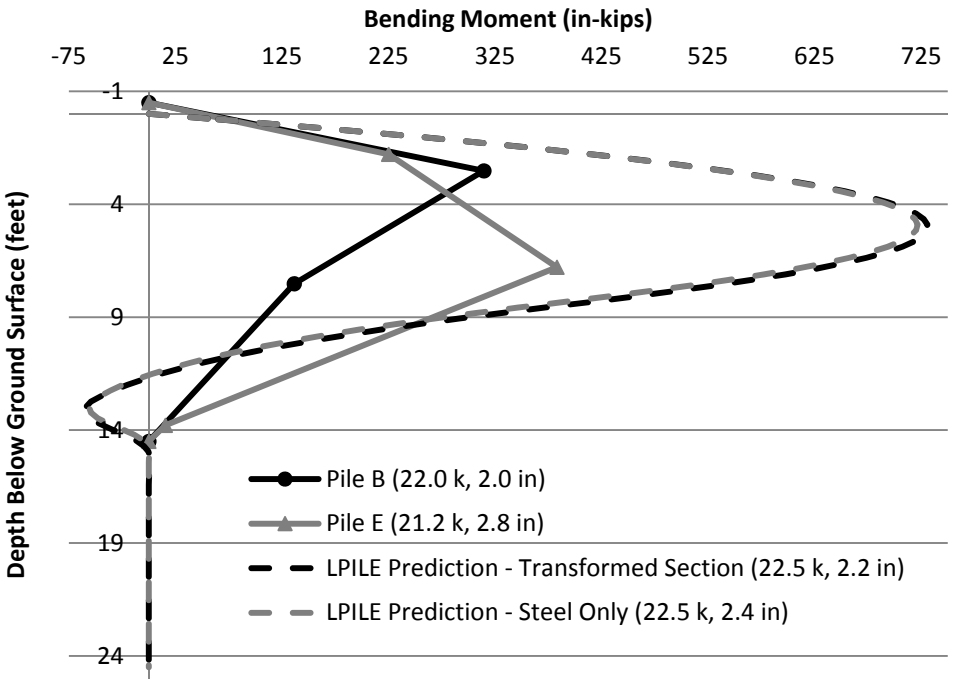

Figure 5.36. Bending Moment vs. Depth at Maximum Lateral Load (Approx. 22 kips)

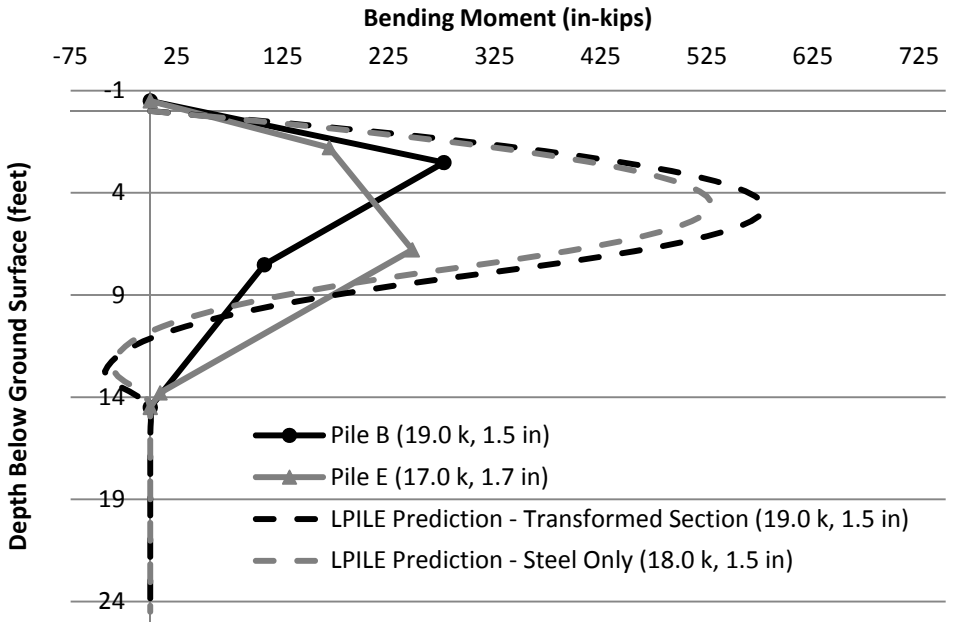

Figure 5.37. Bending Moment vs. Depth at Allowable Deflection (Approx. 1.5 in)

greater than that for Micropile B. It is difficult to definitively conclude the reasons for the discrepancy, but one major contributor to the differences in behavior is likely differences in near-surface soil properties adjacent to the micropiles. The structural stiffness of the two micropiles should be nearly identical which leaves the soil stiffness as the most probably reason for differences in the stiffness of the soil-structure system.

Differences in maximum bending moment between the two tests were much less than the differences in deflection, as shown in Figure 5.33. In fact, Micropile B had higher maximum bending moment during the lower portion of the lateral loading sequence and Micropile E had higher maximum bending moment during the higher portion of the loading sequence. Similarities in the magnitude of the maximum bending moment can also be seen in the plots in Figure 5.37 where the diagrams were plotted and compared for similar levels of lateral deflection. The shape of the two experimental data curves shown in the figure is slightly different with the maximum bending moment occurring deeper in Micropile E than in Micropile B. This discrepancy is expected for the inferred differences in near-surface soil stiffness. For less stiff soil (Micropile E), the lateral load would be transferred deeper in the micropile because of the increased movement near the head of the pile. As the load is transferred deeper, bending occurs at greater depths and the location of the maximum bending moment also is transferred deeper.

Finally, conclusions can be drawn regarding the adequacy of the LPILE software in predicting lateral behavior of micropiles. As shown in Figure 5.32, LPILE accurately predicted the deflection of Micropile B for loads greater than about 5 kips. For lower loads, the LPILE model exhibited stiffer behavior than the experimental data. LPILE

under-predicted lateral deflection for Micropile E, but this can likely be explained by the presence of less stiff near-surface soil surrounding Micropile E, as previously discussed. While LPILE generally did well predicting deflection, it greatly over-predicted the bending moment. This difference can be seen in Figures 5.33, 5.36, and 5.37. These figures also show that the bending moment is not highly dependent on the type of structural cross-section (transformed section vs. steel only) that is input into the software.

5.8.3. Combined Load Test Results and Interpretation. Micropiles A, C, D, and F were tested by applying an axial load of 40 kips and then incrementally applying lateral loads near the head of the pile as the axial load was held constant, as previously discussed. Prior to the combined load testing, Micropiles A and D were tested in axial compression. Data from the load cells and DCDTs were used to produce plots of lateral load versus lateral displacement near the micropile head, as shown in Figure 5.38. The figure also includes the results of the prediction of combined load micropile behavior discussed in Section 5.3. Except for some anomalies in the combined load test results for Micropile F, the remainder of the micropiles exhibited very similar behavior from initial lateral loading to loads of approximately 15 to 20 kips. In addition, the LPILE analysis of the combined load test accurately predicted the load-deflection behavior for the majority of the applied lateral loads. The exception is between approximately 5 and 15 kips where the LPILE prediction slightly underestimated the lateral deflection.

Figure 5.39 presents lateral load versus maximum bending moment for the four combined load tests and the LPILE prediction. The behavior of all four combined load tests is nearly identical. However, the LPILE analysis over predicts the maximum bending moment during the combined load test.

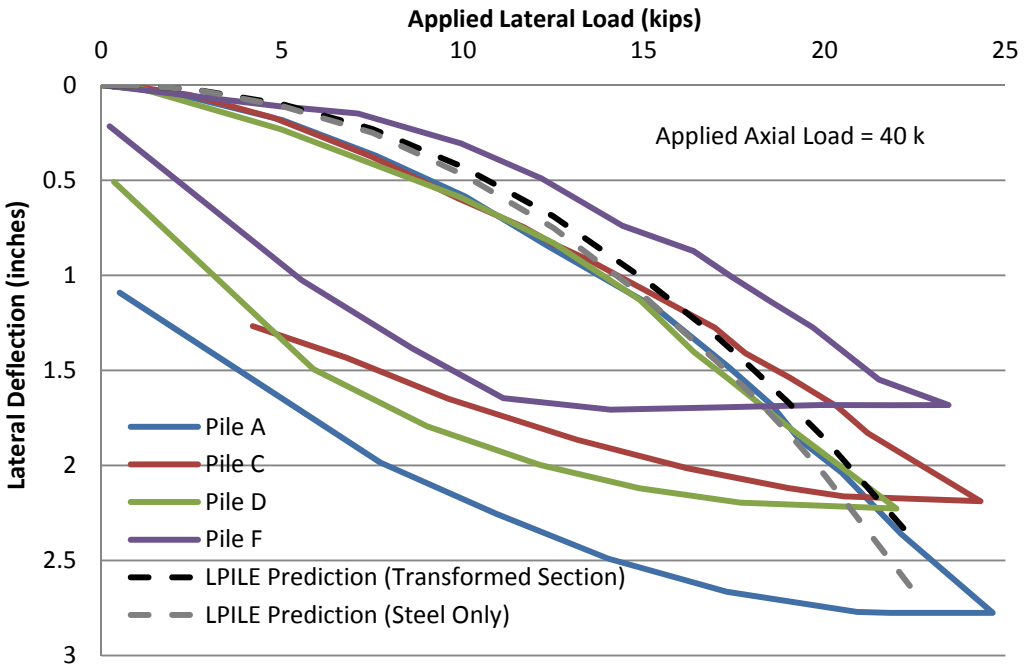

Figure 5.38. Combined Load Test Results – Load vs. Displacement

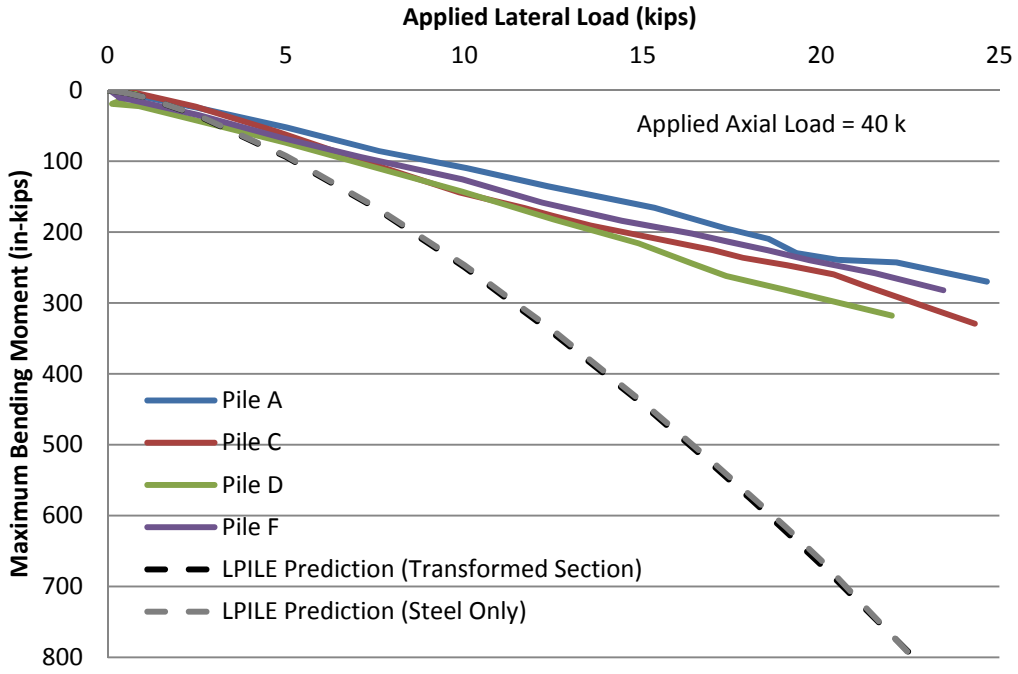

Figure 5.39. Combined Load Test Results – Load vs. Maximum Bending Moment

Using the VWSG data, plots of bending moment versus depth were also prepared for several different magnitudes of lateral load. The plots for combined load tests on Micropiles A, C, D, and F are shown in Figures 5.40, 5.41, 5.42, and 5.43, respectively. The testing apparatus was designed to try to model a free head condition by incorporating a swivel and rollers (see Section 5.2.2). However, it is likely that application of a simultaneous axial and lateral load induced a slight moment at the top of the pile. Nevertheless, because we did not directly measure the moment at the pile head and because it is likely small, the bending moment was assumed to be zero at the location where the lateral load was applied (approximately 6 inches above the ground surface). In addition, the bending moment was assumed to be zero at the casing-bond zone interface in micropiles where a third level of strain gages were not present. Sketches showing the approximate locations of the casing, bond zone, and VWSGs are provided in each figure.

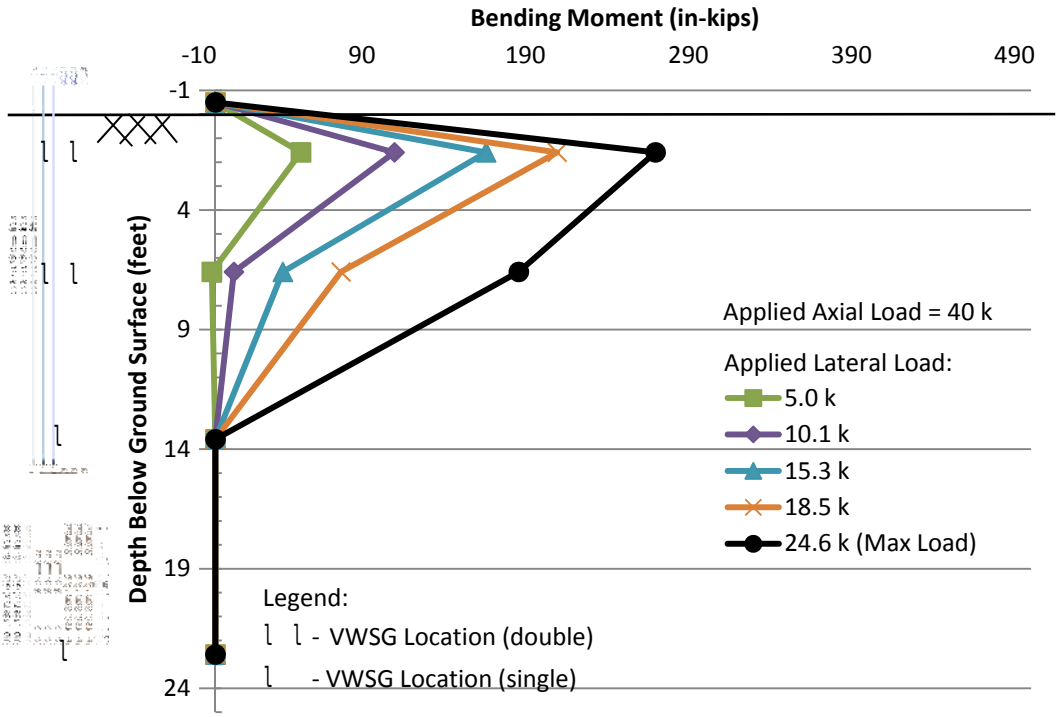

Figure 5.40. Micropile A Combined Load Test Results – Bending Moment vs. Depth

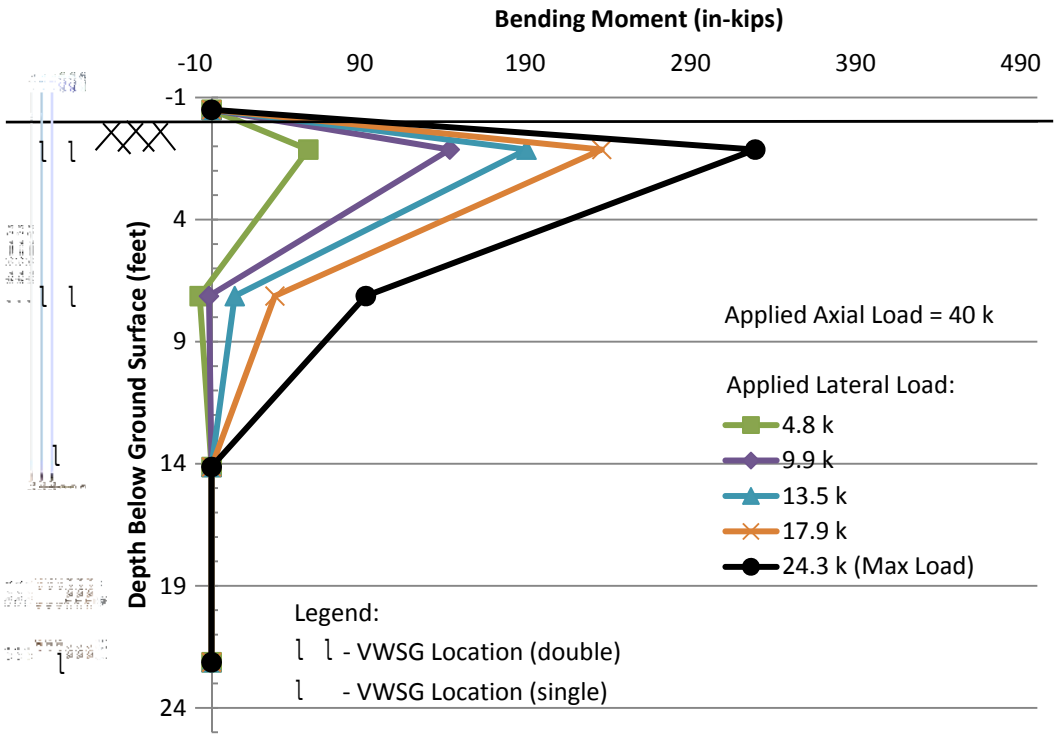

Figure 5.41. Micropile C Combined Load Test Results – Bending Moment vs. Depth

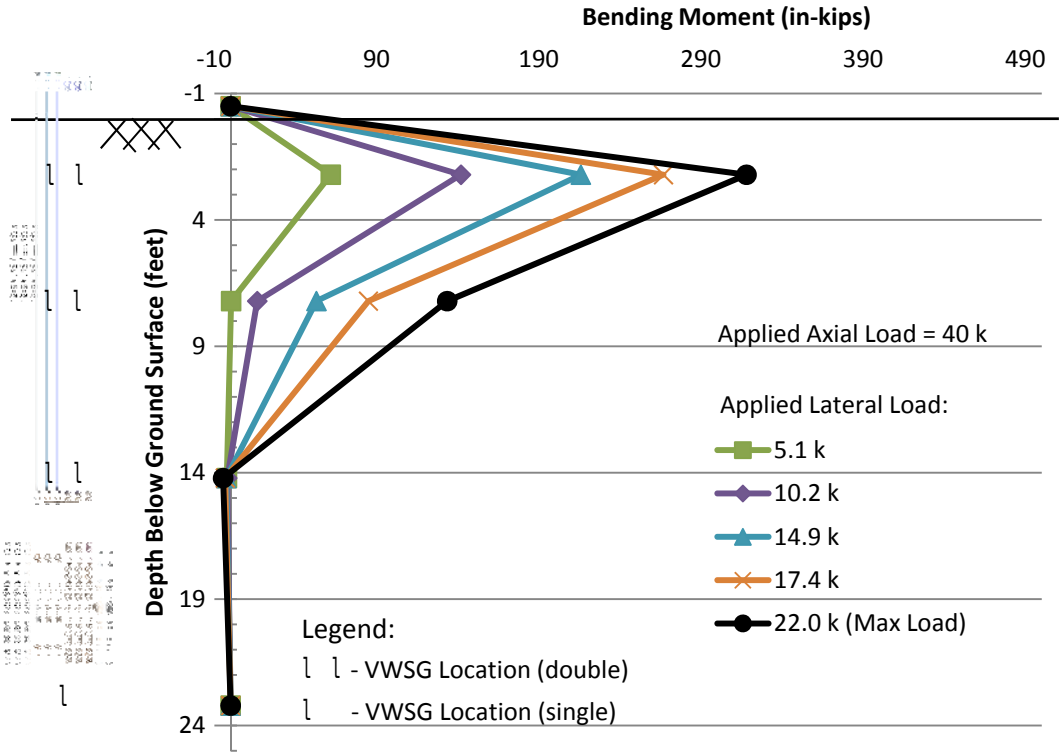

Figure 5.42. Micropile D Combined Load Test Results – Bending Moment vs. Depth

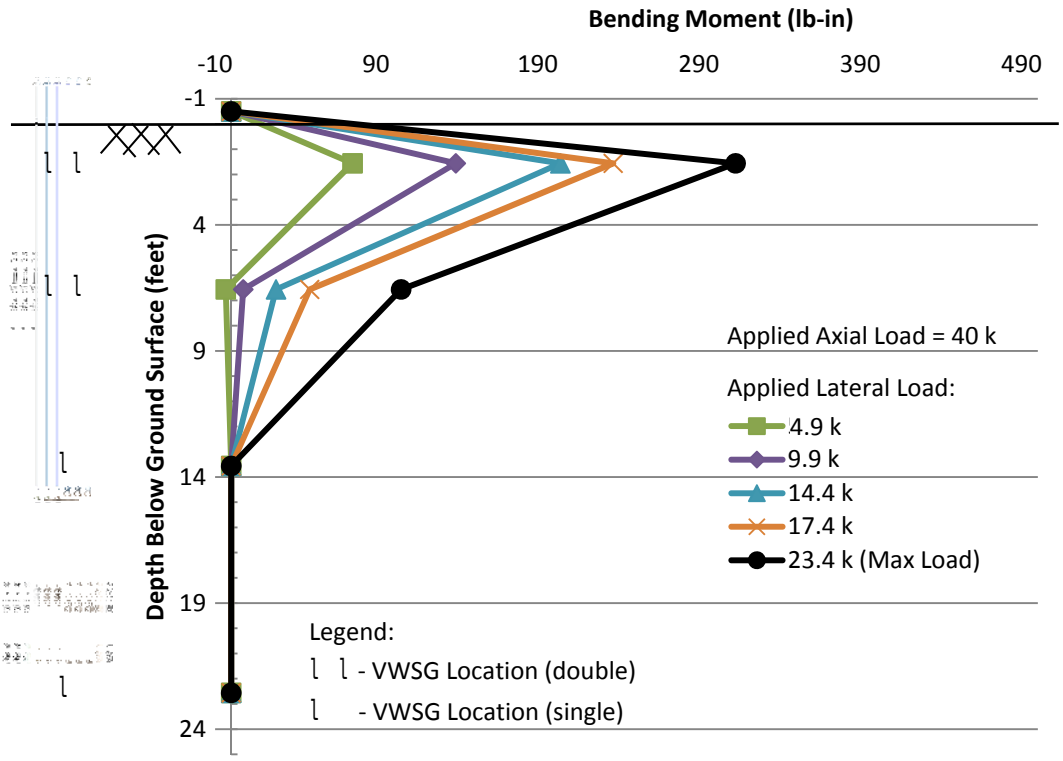

Figure 5.43. Micropile F Combined Load Test Results – Bending Moment vs. Depth

Comparison of the four bending moment versus depth plots indicates that the maximum being moment occurs in the vicinity of the highest level of strain gages at a depth of approximately two feet below the ground surface. The shape of the bending moment curves and the magnitudes of the measured bending moments are also similar for the four combined load tests.

Finally, Figures 5.44 and 5.45 were prepared to further compare the measured bending moments for each of the four tests and to compare to the predicted bending moments from LPILE. Figure 5.44 compares the bending moment diagrams at similar applied lateral loads (approximately 22 kips) for each test and the LPILE analysis. However, lateral failure is typically defined in terms of a maximum allowable deflection.

Therefore, Figure 5.45 was prepared to compare the bending moment diagrams at similar head lateral displacement (approximately 1.5 inches). The 1.5-inch lateral displacement was chosen because it is likely the highest deflection that would be allowed for production micropiles. The text on both plots indicates the lateral load and lateral displacement for each bending moment diagram.

The results of the four combined load tests were very similar, indicating that the combined load test is highly reproducible. The reproducibility of the tests indicates that the combined load test is likely not affected by variability of the subsurface conditions. Specifically, the deflection at the head of the piles was nearly identical up to lateral loads of about 15 kips for all piles except Micropile F. Because the load-deflection curve for Micropile F is not as smooth as the curves for the other three tested piles, it may have been acting in a stick-slip mode of deflection which could account for some of the discrepancy in the results. In addition, it is apparent from the graph that the soil-structure system exhibited a stiffer response for Micropile F, especially for applied lateral loads below about 7 kips. The bending moments measured in the four tests are very similar, as shown in Figures 5.39, 5.44, and 5.45. The magnitudes of the maximum bending moments are nearly identical, the location of the maximum bending moments is nearly identical, and the shape of the bending moment versus depth curves are also very similar.

Finally, conclusions can be drawn regarding the adequacy of the LPILE software to predict the behavior of micropiles subjected to combined loads. Similar to the lateral load test results, Figure 5.38 shows that LPILE predicted the load-deflection behavior of the micropiles fairly accurately. The predicted micropile response was slightly stiffer than the measured response for the load below about 12 kips. Also analogous to lateral

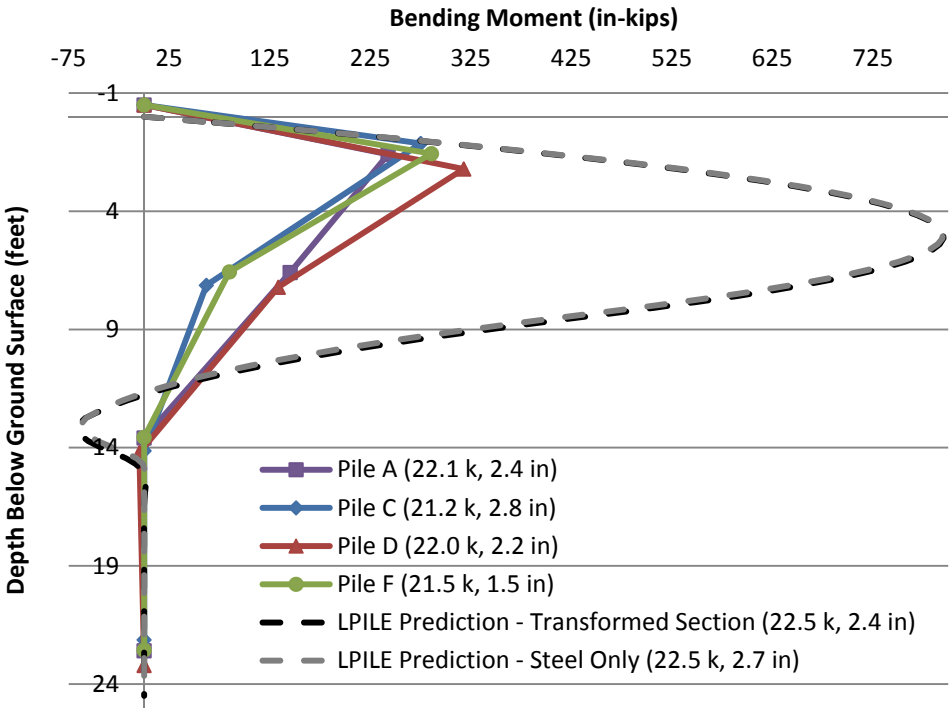

Figure 5.44. Bending Moment vs. Depth at Maximum Lateral Load (Approx. 22 kips)

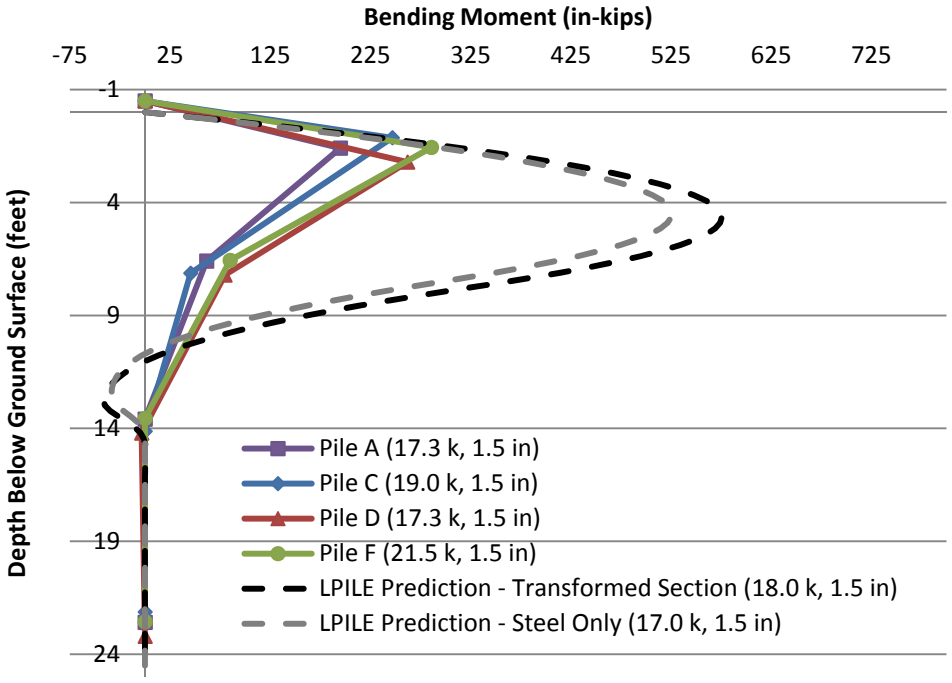

Figure 5.45. Bending Moment vs. Depth at Allowable Deflection (Approx. 1.5 in)

load test results, the maximum bending moment predicted in LPILE is much larger than the measured bending moments from the four combined load tests as shown in Figures 5.39, 5.44, and 5.45. In addition, the location of the predicted maximum bending moment is lower than the measured maximum bending moments. Based on the results of the lateral and combined load tests, LPILE adequately predicts lateral deflection, but should not be relied upon for accurate bending moment predictions. As previously discussed, the over-prediction of bending moments was likely exaggerated because the strain gage locations were likely not located at the exact point of maximum bending moment.. Therefore, while the magnitude of bending moment over-prediction is unknown, it is apparent that LPILE does over-predict bending moments. Using the over-predicted bending moments for design would result in micropile cross-sections that are larger and/or contain more steel than is needed. While this approach may be conservative, it may also results in increased construction costs.

5.8.4. Comparison of Lateral and Combined Load Test Results. Because the lateral load tests and combined load tests were performed simultaneously and within close proximity to each other, the results of the tests can be compared to assess the effect of an axial load on the lateral behavior of micropiles (combined loading). In each of the following plots, the combined load tests are represented by solid lines and the lateral load tests are represented by dashed lines. The plots used to compare the two test types are shown below and include lateral load versus lateral displacement (Figure 5.46), lateral load versus maximum bending moment (Figure 5.47), and bending moment versus depth (Figures 5.48 and 5.49).

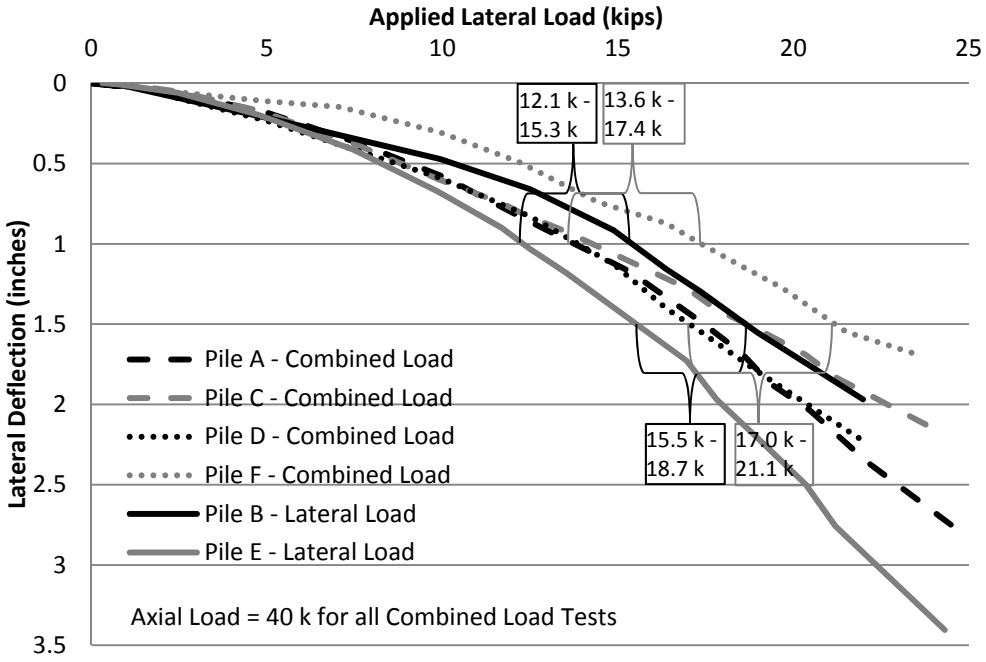

Figure 5.46. Comparison of Lateral and Combined Load Test Results, Lateral Load vs. Lateral Displacement

A cursory visual comparison of the load-deflection results shown in Figure 5.46 did not yield clear differences between the lateral and combined load tests. To quantitatively assess the differences, brackets of data were added to the figure. Specifically, the range of applied lateral loads corresponding to specific magnitudes of lateral deflection (1.0 and 1.5 inches) are shown for each of the two test types. The black and grey brackets correspond to the range of loads for the lateral and combined load tests, respectively. The spread of each of the ranges (upper value minus lower value) are similar for both of the load test types and both of the chosen levels of deflection (3.2 to 4.1 kips). While the ranges overlap at each of the deflection magnitudes, it is clear that the median of the ranges for the combined load tests is slightly higher than the ranges for the lateral load tests. Because it takes slightly more load to get the same deflection, it can

be concluded that the micropile behaves slightly stiffer when subjected to combined loading, as compared to lateral loading only.

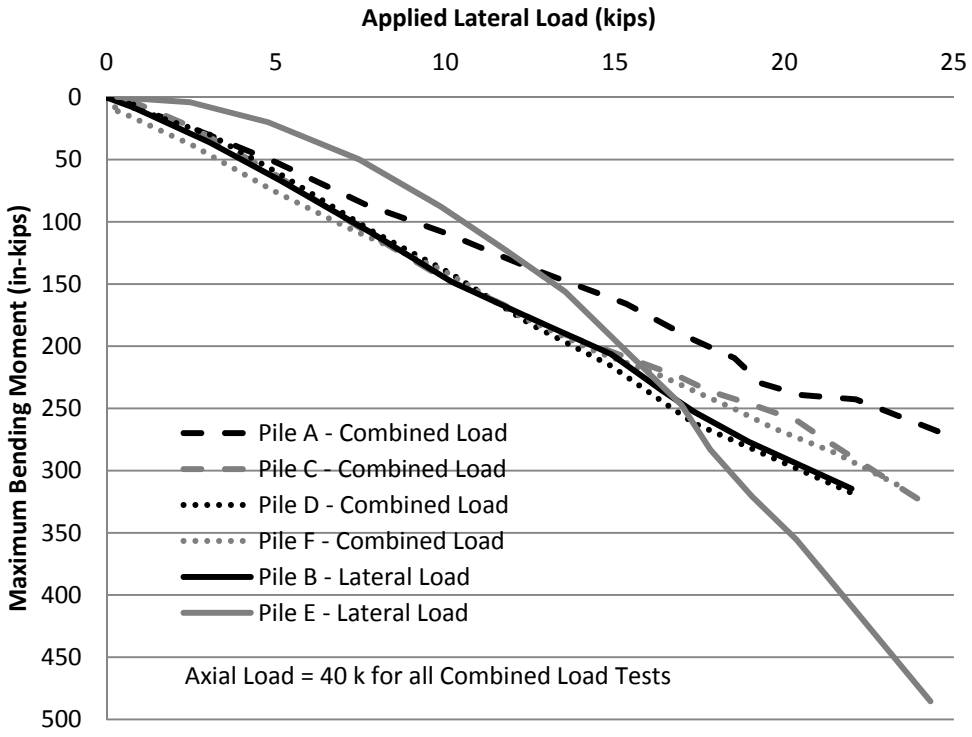

Figure 5.47. Comparison of Lateral and Combined Load Test Results, Lateral Load vs. Maximum Bending Moment

Comparison of the plots of applied lateral load versus maximum bending moment in Figure 5.47 indicate that there is perhaps a slight reduction in maximum bending moment in the combined load tests, except for Micropile E which behaved differently than the other tests. In general, the plots fit within a relatively tight range. Micropile E behaved less stiff than the other tests, likely because of softer soil, as previously discussed. Thus, because the lateral deflection was greater for each of the load steps, the bending moment was also greater than the other tests.

The Figure 5.48 compares the bending moment diagrams at similar applied lateral loads (approximately 22 kips) for each combined load and lateral load test. Because the bending moment is more closely related to the lateral deflection than the applied lateral load, Figure 5.49 was prepared to compare the bending moment diagrams at similar lateral displacement (approximately 1.5 inches). The 1.5-inch lateral displacement was chosen because it is likely the highest deflection that would be allowed for production micropiles. The text on both plots indicates the lateral load and lateral displacement for each bending moment diagram. Similar to Figure 5.47, it appears that there is a slight reduction in bending moment in the micropiles that were subjected to combined loading conditions when compared to the lateral load tests.

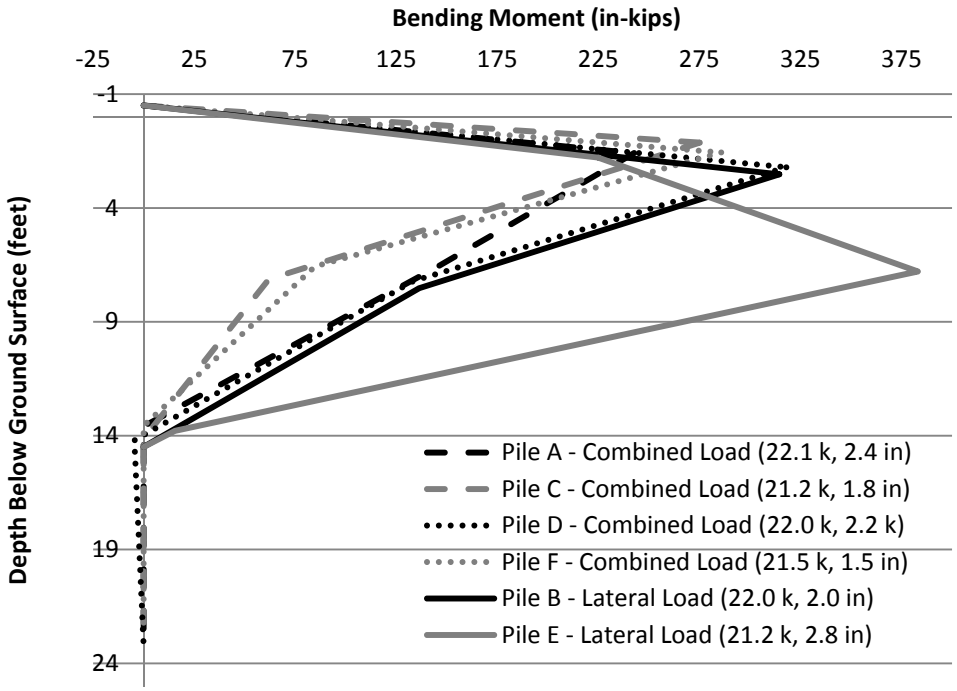

Figure 5.48. Comparison of Lateral and Combined Load Test Results, Bending Moment vs. Depth at Maximum Lateral Load (Approx. 22 kips)

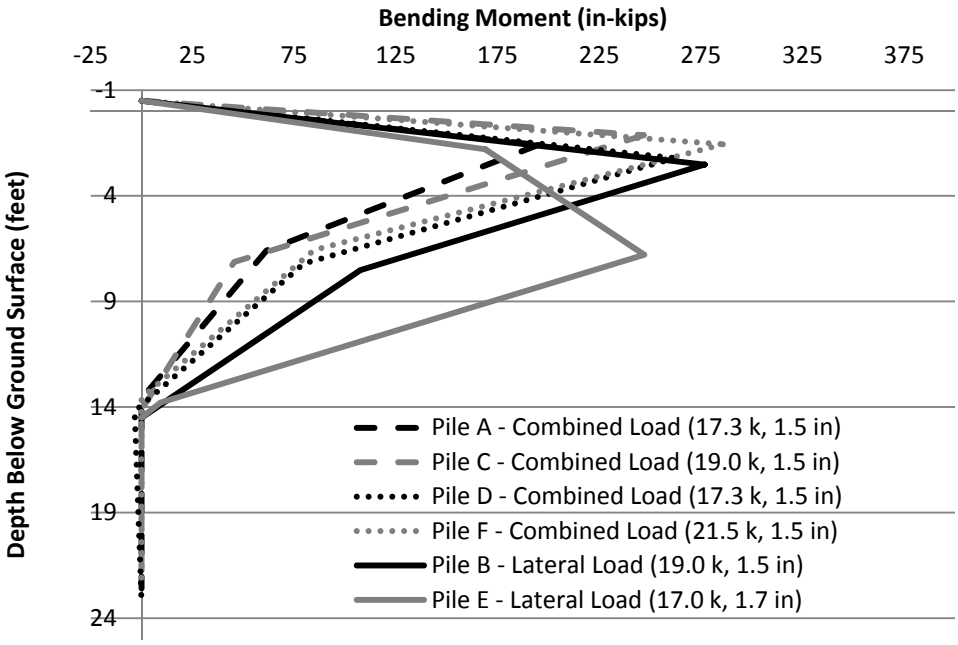

Figure 5.49. Comparison of Lateral and Combined Load Test Results, Bending Moment vs. Depth at Allowable Deflection (Approx. 1.5 in)

Results from the four combined load tests and two lateral load tests were analyzed and the four plots shown above were developed to compare the results of the tests. Based on examination of the four plots discussed above, the differences between the results of the lateral load tests and the combined load tests are minimal. The load-deflection data indicates that the addition of an axial load onto the micropile, as in the combined load test, results in a stiffer lateral response. This behavior is the opposite of what was predicted by LPILE, as discussed in Section 5.3. The LPILE software uses a beam-column model for the pile that results in a P-delta effect such that application of an axial load in conjunction with a lateral load results in larger lateral deflections [Reese et. al. 2004].

The bending moment versus depth curves and the lateral load versus maximum bending moment curves from the two types of tests indicate that the magnitude of the maximum bending moment, location of the maximum bending moment, and the shape of the bending moment envelope are similar for all six of the tests. It appears that the addition of an axial compression load on top of the micropile slightly reduces the bending moment and shifts the maximum bending moment slightly higher within the micropile.

6. INSTRUMENTATION OF PRODUCTION MICROPILES

This portion of the research consisted of instrumentation of production micropiles installed for foundation support of Foothills Parkway Bridge No. 2 in Great Smoky Mountains National Park in Blount County, Tennessee. The bridge is part of a high profile Federal Highway Administration (FHWA), Eastern Federal Lands Highway Division project. The purpose of this task was to monitor the micropiles during and after construction to assess micropile response to combined loading, depth of load transfer, and residual loads resulting from cyclic or live loads. Data from instrumented production micropiles is relatively rare, especially data that includes readings throughout construction and after the structure is put into service. The information gained from this project, along with similar data from subsequent projects, will assist designers and contractors in producing more efficient micropile designs. Instrumentation design and installation, as well as establishment of the monitoring program were completed as part of this research task. The remainder of the data collection, analysis, and interpretation will be completed by others.

6.1. FOOTHILLS PARKWAY

Prior to commencement of this research task, the bridge design was complete (including micropile foundations) and initial construction activities had begun. Thus, the first step for this task was obtaining the necessary permissions and permits to install instrumentation and access the site during and after construction. Missouri S&T teamed with Dan Brown and Associates (micropile design engineers) to execute this task, and the general contractor (Bell & Associates Construction) and Federal Highway Administration (FHWA) both expressed support for this research task. Based on this support and the

merit of the project, U.S. Department of the Interior / National park Service issued a Scientific Research and Collecting Permit.

The information presented herein regarding subsurface conditions, micropile design, and the pier load conditions were provided by the micropile design engineers (Dan Brown and Associates) and the superstructure engineers and constructors (VSL International). At the time of publication, instrumentation had been installed in four micropiles at Piers 1 and 2 (eight total) and the micropile caps at Piers 1 and 2 had been poured. Construction of the superstructure had not yet begun.

6.1.1. Site and Superstructure Description. Foothills Parkway Bridge No. 2 is located in eastern Tenessee along the northwest border of Great Smoky Mountain National Park. The site is approximately 12 miles from Pigeon Forge, Tennessee and the closest town to the site is Wear Valley, as shown on Figure 6.1. The eastern portion of Tennessee, including the project site, is mountainous and heavily wooded. The topography at the bridge location was steeply inclined toward the southwest and vegetation included a combination of deciduous trees, coniferous trees, and dense underbrush.

Bridge No. 2 will be a five-span structure with a total length of 790 feet, and the bridge deck will be up to about 50 feet above the ground surface. Because the purpose of the two-lane roadway is a scenic parkway within the national park, one of the main goals of the project is to preserve the natural beauty of the area. Thus, the type of superstructure and corresponding construction method selected for the project needed to minimize disturbance of the slope. The bridge will be a reinforced concrete structure constructed using pre-cast, post-tensioned segments. Disturbance was minimized by

utilizing a temporary, elevated steel structure that served as an access way and track for cranes that lowered the concrete segments into place to construct the piers and bridge deck.

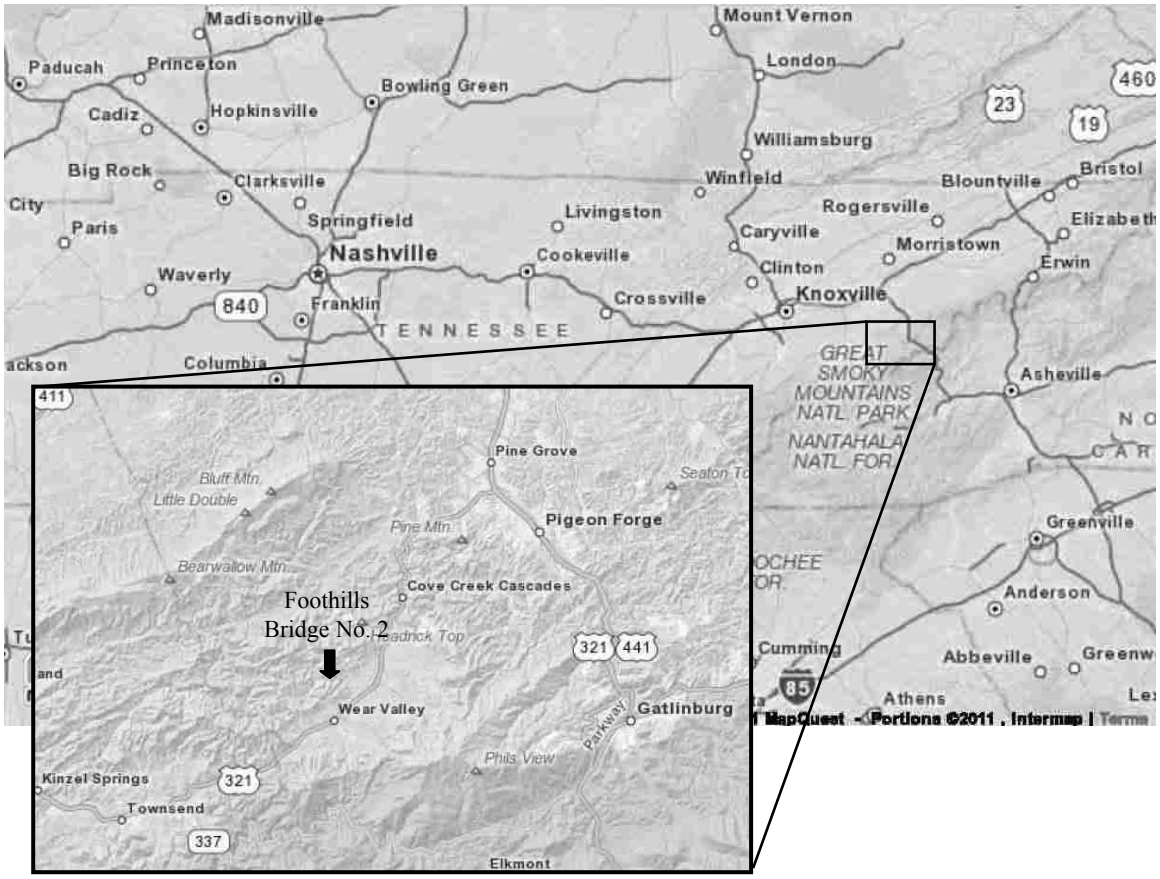

Figure 6.1. Foothills Parkway Bridge No. 2 Vicinity Map

6.1.2. Subsurface Conditions. The subsurface conditions at the site were based on information provided in a geotechnical report provided by Dan Brown and Associates [Siegel et. al. 2010]. According to the report, six borings were completed in the vicinity of each of the two piers where the instrumented micropiles were installed. Based on these twelve borings, the subsurface conditions generally consisted of approximately 4 to

50 feet (average of about 35 feet) of overburden soils overlying bedrock. The soil overburden is somewhat variable with the predominant soil type being medium dense to very dense, sand and gravel with varying amounts of silt and clay. Because of the variability of the overburden soil, it is difficult to determine the nature of the soil, but it is likely a combination of colluvium and residuum with possible isolated fill deposits. The bedrock encountered in the borings was predominantly sedimentary rock that had experienced varying degrees of metamorphosis and was classified as metasandstone and metaconglomerate with occasional layers of phyllite. The upper portions of the bedrock were moderately to severely weathered as evidenced by low recovery and RQD in the rock cores obtained in the borings.

6.1.3. Micropile Design. Because of the variability of the overburden soils, deep foundations were needed to transfer the superstructure loads to the underlying fresh, competent bedrock. In conjunction with the project goals to minimize the disturbance, micropiles were the chosen deep foundation type because they could be installed using a small drill rig that could be lowered into place using the overhead crane. Using the anticipated pier loads, the foundation design included a group of twenty (20) vertical micropiles to support each pier. The micropiles were designed to resist vertical loads of approximately 310 kips each from the superstructure only. Horizontal ground anchors were also installed at each bent location to resist the potential lateral loads resulting from unbalanced soil loads on the pile cap and sliding of the surficial soils. Each micropile consisted of permanent casing with an outside diameter of 9.625 inches and a wall thickness of 0.472 inch to transfer loads through the overburden soils and weathered rock. Below the permanent casing, the rock-socketed bond zone had diameter of 9.625

inches and a minimum length of 15 feet. The casing and bond zone were filled with grout and were designed with a full-length central reinforcing bar that had a diameter of 2.5 inches (#20) for Pier 1 and 1.75 inches (#14) for Pier 2. The micropiles at each pier were connected by a circular concrete pile cap with a diameter of 20 feet and thickness of 5 feet. Below this pile cap, a concrete pad of varying thickness was constructed as a drill pad. Because of the potential lateral loads imposed on the pile cap from the steeply sloping ground, four (4) ground anchors were included for Pier 1 and two (2) anchors were included in the pile cap for Pier 2. These anchors were designed to resist the entire anticipated lateral load, and the micropiles were designed to only resist the vertical loads from the superstructure.

To assess the adequacy of the design, an axial, vertical compression load test was completed on October 20, 2010. The test micropile was constructed near Abutment 1 using the same materials as a Pier 1 micropile, as described above, with a cased length of 15 feet and a bond zone length of 15 feet. Load was incrementally applied using a hydraulic jack to a maximum load of 619 kips. The axial load was monitored using a load cell and axial deflection was monitored using three dial gages. The measured deflection was greater than the calculated theoretical structural deflection but less than the failure criterion calculated using Davisson's Method. While the micropile test load was not large enough to back-calculate the bond strength at the bond zone-rock interface, the results indicated that the design was adequate to resist the anticipated axial loads for the project.

6.1.4. Instrumentation. A total of eight micropiles were instrumented, including four each at Pier 1 and Pier 2. The four instrumented micropiles were generally located

90 degrees from each in each pile cap, as shown in Figure 6.2. However, because Micropile 6 at Pier 1 had been grouted prior to arrival of instrumentation at the site, gages were installed in Micropile 4 instead of Micropile 6. Two of the micropiles were generally aligned with the centerline of the bridge (Micropiles 4/6 and 16) and two of the micropiles were generally aligned with the dip direction of the slope (Micropiles 1 and 11). This configuration was chosen because it is likely that, if bending is present in the micropiles, it will be at its greatest either along the bridge alignment resulting from superstructure loads or parallel to the slope dip direction resulting from slope movement in the overburden soils.

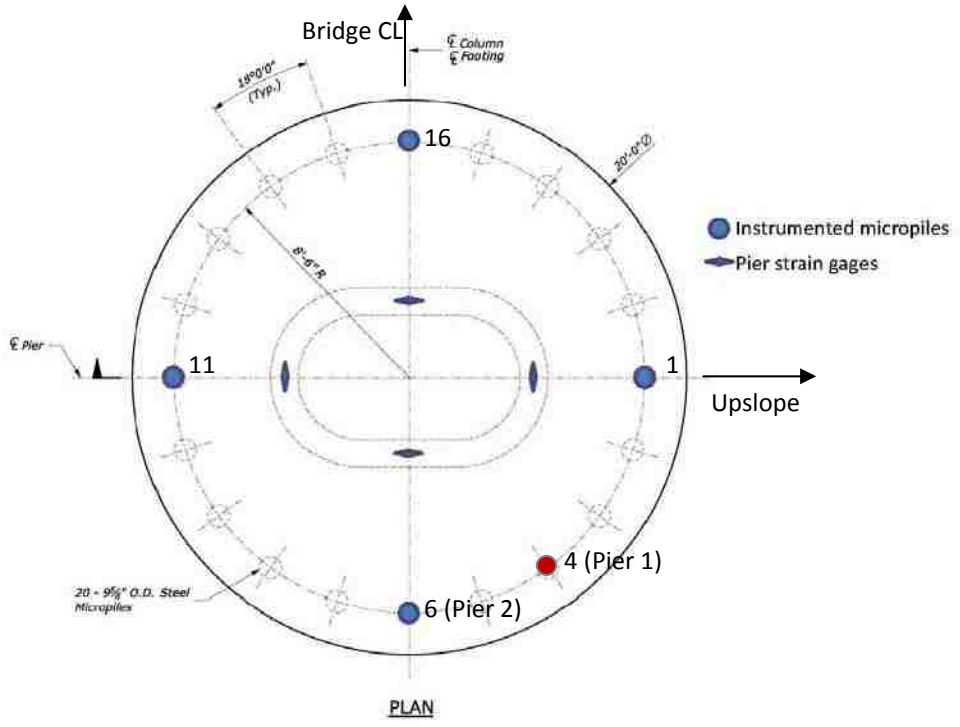

Figure 6.2. Locations of Instrumented Micropiles

Each micropile was instrumented with seven vibrating wire strain gages (VWSG) that were cast into the micropile grout during installation. The vibrating wire strain gages were Model 4200 gages manufactured by Geokon, Inc. [2010]. The specifications for the gages were discussed in Section 5.4 and shown in Table 5.4. VWSG were chosen for this project because of their durability during installation, their longevity, and the fact that wire length does not degrade the signal response of the gage.

The purpose of the gages was to obtain strain measurements that could be converted into load and/or bending moment where pairs of strain gages were used. To obtain accurate bending moment readings, it is necessary to have a pair of strain gages oriented in the direction of lateral load and to have the gages placed as far from the central reinforcing bar as possible. Mounting bars fabricated from short sections of No. 4 reinforcing bars were used to accomplish these two objectives. Specifically, 18- to 24-inch-long bars were bent with 45 degree angles into a trapezoidal shape such that the strain gages could be attached to the mounting bars and the mounting bars could be attached to the central reinforcing bar during installation. The result was a spacing of approximately 2.5 to 3.0 inches from the center of the micropile to center of the gage and a clear space of approximately ¼ inch between the mounting bar and the inside of the steel casing. Figure 6.3 shows a schematic of the mounting bar and gage and the relative distance to the micropile casing and central reinforcing bar.

As shown in Figure 6.3, the mounting bar also served as protection for the strain gages during installation. In addition, the manner in which the gages were attached to the mounting bar allowed grout to flow freely around the "barbell" ends of the strain gages such that they were fully embedded in concrete as intended by the manufacturer. Figure

6.4 shows a photograph of gages being installed on the central reinforcing bar, and Figure 6.5 shows a schematic of the locations of the different levels of strain gages within each micropile.

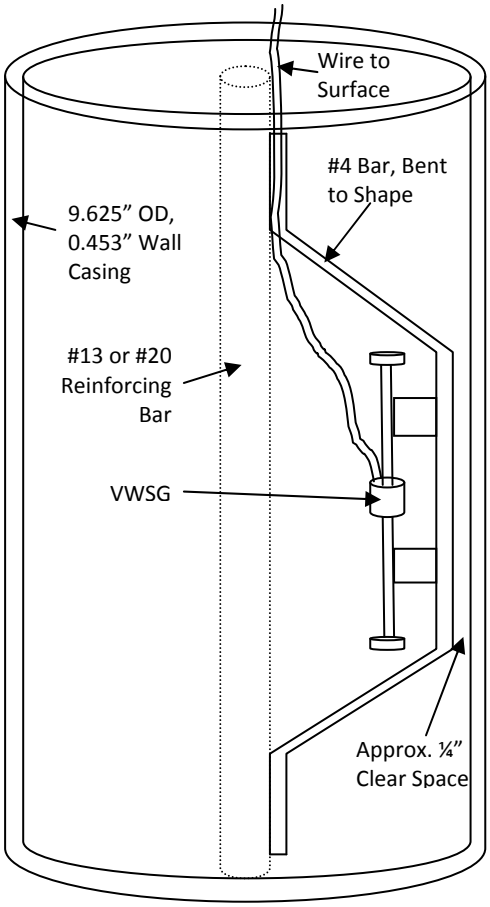

Figure 6.3. Schematic of Strain Gage Mounting

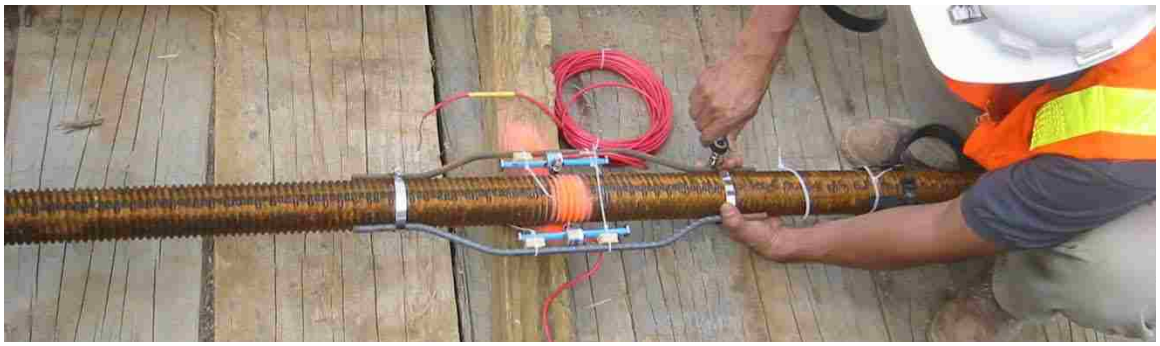

Figure 6.4. Photograph of VWSG Installed on Central Reinforcing Bar

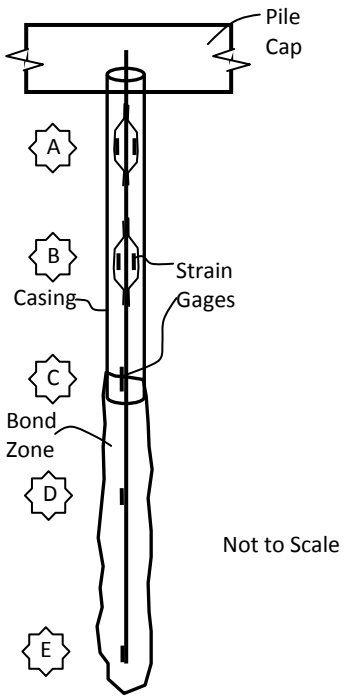

Figure 6.5. Schematic of VWSG Locations with Depth

Table 6.1 provides the location and configuration of each installed strain gage. The VWSG nomenclature includes the pier number, micropile number, gage level, and gage orientation such that "**01B1 Pier1**" indicates that the gage is installed in Micropile 1, level B, side 1 at Pier 1. For micropiles installed in the same plane as the bridge centerline, the pairs of gages were installed parallel to the bridge alignment and side 1 was oriented to the west. For micropiles installed in the dip direction of the slope, the pairs of gages were installed perpendicular to the bridge with side 1 oriented uphill.

In addition to the strain gages installed in the micropiles, vibrating wire strain gages were planned to be attached to the pier near the connection with the pile cap to monitor loads transferred from the superstructure to the pile cap. Four strain gages, installed 90 degrees from each other (see Figure 6.2), are required to simultaneously

monitor axial loads and bending moments. Because the pier sections were pre-cast concrete that were not constructed at the site, installation of embedment strain gages within the concrete would be difficult and surface-mount gages were chosen. At the time of writing, Model 4151 surface-mount VWSG, manufactured by Geokon, Inc. [2008], are planned for the piers. They are installed by drilling a small hole in the concrete and using epoxy to secure the mounting pins. Specifications for the VWSG are shown in Table 6.2.

Table 6.1. Summary of Vibrating Wire Strain Gage Locations

Micropile Name and Length	Gage Name	Distance from Pile Toe (ft)
Pier 1 Pile 1 45 feet	01A1 Pier1	40
	01A2 Pier1	40
	01B1 Pier1	35
	01B2 Pier1	35
	01C1 Pier1	15
	01D1 Pier1	9
	01E1 Pier1	3
Pier 1 Pile 4 95 feet	06A1 Pier1	90
	06A2 Pier1	90
	06B1 Pier1	85
	06B2 Pier1	85
	06C1 Pier1	35
	06D1 Pier1	15
	06E1 Pier1	6
Pier 1 Pile 11 93 feet	11A1 Pier1	90
	11A2 Pier1	90
	11B1 Pier1	85
	11B2 Pier1	85
	11C1 Pier1	36
	11D1 Pier1	9
	11E1 Pier1	3
Pier 1 Pile 16 93 feet	16A1 Pier1	85
	16A2 Pier1	85
	16B1 Pier1	80
	16B2 Pier1	80
	16C1 Pier1	35
	16D1 Pier1	13
	16E1 Pier1	3
Pier 2 Pile 1 98 feet	01A1 Pier2	95
	01A2 Pier2	95
	01B1 Pier2	90
	01B2 Pier2	90
	01C1 Pier2	35
	01D1 Pier2	15
	01E1 Pier2	6
Pier 2 Pile 6 99 feet	06A1 Pier2	95
	06A2 Pier2	95
	06B1 Pier2	90
	06B2 Pier2	90
	06C1 Pier2	35
	06D1 Pier2	15
	06E1 Pier2	6
Pier 2 Pile 11 106 feet	11A1 Pier2	101
	11A2 Pier2	101
	11B1 Pier2	96
	11B2 Pier2	96
	11C1 Pier2	37
	11D1 Pier2	17
	11E1 Pier2	7.5
Pier 2 Pile 16 98 feet	16A1 Pier2	95
	16A2 Pier2	95
	16B1 Pier2	90
	16B2 Pier2	90
	16C1 Pier2	35
	16D1 Pier2	15
	16E1 Pier2	6

Table 6.2. Summary of Model 4151 VWSG Parameters

Parameter	**Value**
Gage Designation	Model 4151
Gage Factor	0.391
Batch Factor	0.90
Standard Range	3000 με
Resolution	0.4 με
Accuracy	± 0.5 %
Nonlinearity	< 0.5 %
Temperature Range	-20°C to +80°C
Active Gage Length	51 mm
Coil Resistance	50 Ω

Following installation of the gages within the micropile, the wires were attached along the length of the central reinforcing bar and exited the top of the casing as a bundle. The wire bundles for each of the micropiles were then routed to a single location where they exited the pile cap. The wires were then attached to a weather resistant terminal box at a location that was accessible throughout construction and upon completion of the project. The junction box is a model 4999 Terminal Box manufactured by Geokon, Inc. [2009] that has external connections that allow quick readings throughout the project life. A photograph of an installed terminal box is provided below in Figure 6.11.

A new data acquisition box (the black box) was recently built for the dual purpose of collecting data during load tests and monitoring micropiles subjected to service loading, as discussed in Section 3.3. The black box is capable of reading and recording data VWSG and is very portable such that it can be used to take readings by connecting to the terminal box. In addition to the black box, a simple hand-held readout box was used to take readings at the site. Although the hand-held device cannot simultaneously

take readings of several strain gages at once like the black box or internally record data, it can be used to obtain additional data points from the strain gages during construction, where simultaneous readings are not needed. The hand-held device was a Model GK-404 Vibrating Wire Readout manufactured by Geokon, Inc. [2003]. Operation of the device is relatively simple and the gage factors for each of the gages manufactured by Geokon are programmed into the device such that the readout is microstrain.

6.1.5. Micropile Installation. The micropiles for support of Bridge No. 2 were installed by Strucutral Preservations Systems from May through July 2011. They were installed using a rotary percussive duplex drilling methods with internal flush powered by a Davey Kent 620 (see Figure 6.6) and grouted using Type A methods (gravity grouting without pressurizing). To the extent possible, each micropile was installed in an identical manner, as outlined below. The lengths of the installed instrumented micropiles, as well as the date completed are presented in Table 6.3. In general, installation of the micropiles was completed using the following steps, as shown in Figures 6.6 through 6.11.

1. Use duplex drilling methods through the overburden down to competent rock.
2. Drill the rock socket using a rock hammer drill and clean out hole using air.
3. Attach strain gages and centralizers to the central reinforcing bar and mark the bar showing the orientation of the strain gage pairs.
4. Place the instrumented bar through the casing to the bottom of the rock socket using a crane operating on the temporary access structure.
5. Tremie grout through the casing until grout exits at the top of the casing.
6. After all micropiles at a pier location are installed, route the VWSG wires to a single location and exit the wires through a hole in the pile cap formwork and seal around the hole using expansive foam.
7. After pile cap is poured, install the VWSG terminal box.

Table 6.3. Summary of Micropile Installation

Pile Name	Total Length (feet)	Bond Length (feet)	Casing Length (feet)	Date Completed
Pier 1 Micropile 1	45	15	30	24-May-2011
Pier 1 Micropile 4	95	20	75	24-May-2011
Pier 1 Micropile 11	93	18	75	24-May-2011
Pier 1 Micropile 16	93	23	70	5-Jun-2011
Pier 2 Micropile 1	98	18	80	15-Jul-2011
Pier 2 Micropile 6	99	24	75	15-Jul-2011
Pier 2 Micropile 11	106	21	85	15-Jul-2011
Pier 2 Micropile 16	98	18	80	15-Jul-2011

Figure 6.6. Photograph of Micropile Drilling (Steps 1 and 2)

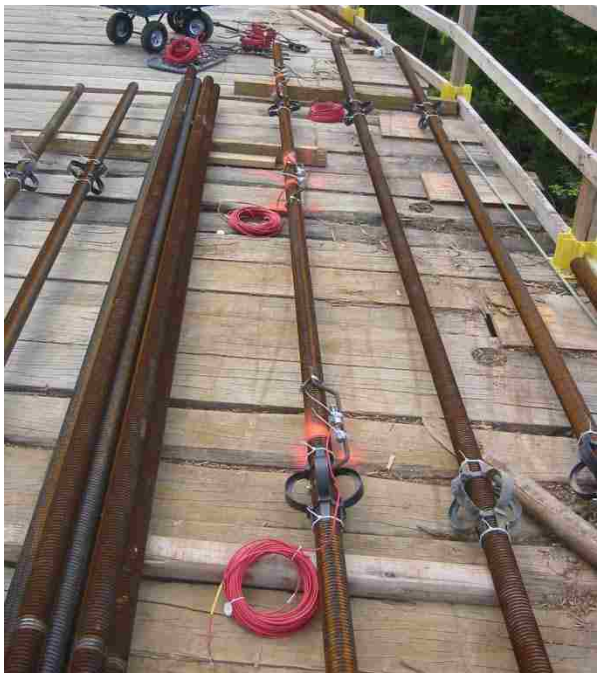

Figure 6.7. Photograph of Instrumented Central Reinforcing Bar (Step 3)

Figure 6.8. Photographs of Central bar Installation (Step 4)

Figure 6.9. Photograph of Grouted Micropiles (Step 5)

Figure 6.10. Photograph of VWSG Wire Routing through Pile Cap (Step 6)

Figure 6.11. Photograph of Installed Terminal Box (Step 7)

As previously discussed, the casing consisted of 9.625-inch OD steel casing with a wall thickness of 0.472 inch and a minimum yield strength of 80 ksi. For all micropiles, 5-foot-long sections of casing were used. The lowest piece of casing for each pile was outfitted with J-teeth to aid in casing advancement. The central reinforcing bars consisted of 50-foot-long sections of #20 (Pier 1) or #14 (Pier 2) threadbar manufactured by Willams Form Engineering Corp. with a minimum yield strength of 75 ksi. The grout mix consisted of 1 bag (94 lbs) of Type I/II Portland cement for every 5 gallons of water, resulting in a 0.44 water to cement ratio.

6.1.6. Monitoring Program. The objectives of the monitoring program are to examine the progressive load transfter from the superstructure to the micropiles as the bridge is being built and to evaluate the response of the micropiles to combined loading. As stated in Section 6.1.3, the micropiles were designed to resist the vertical loads of the

superstructure and horizontal ground anchors were installed to withstand the lateral loads at the piers. However, there will likely be small lateral loads transferred to the micropiles as a result of the lateral deflection required to mobilize the anchor bond strength and differential bridge longitudinal loads from traffic. The two conditions that could occur within the micropiles as a result of small the lateral loads are bending within each individual micropile or a couple that is formed within the pile cap such that micropiles on one side act in tension and the other side act in compression to resist the lateral loads. Typical of most bridges, the majority of the load supported by the foundation is a result of the dead load of the structure. At the time of publication, all of the instrumented micropiles had been installed and the two pile caps had been poured. However, construction of the superstructure had not yet begun. Thus, discussion of the monitoring program is a combination of readings that had been taken and future readings.

The strain gages will be read using the black box or the hand-held readout box, as discussed in Section 6.1.4. The first reading occurred prior to delivery of the VWSGs to the site to assess whether the gages were working properly. The second reading occurred immediately after installation of the micropiles while the grout had not yet set. This reading could be used to determine the effect of grout shrink during curing. A third reading was taken after curing of the micropile and before application of additional loads to establish a baseline that will be used to compare subsequent readings throughout the project. The first load applied to the micropiles was from the dead weight of the 5-foot-thick pile cap, and an additional reading was taken after the concrete in the pile cap had cured.

As previously discussed, the superstructure of the bridge will be constructed using pre-cast, post-tensioned concrete segments for both the piers and the bridge deck. Ideally, strain gage readings will be taken after placement of every segment placed for construction of Piers 1 and 2 and for each segment used to construct the bridge deck. This monitoring program would give a clear picture of load transfer throughout construction, but would also require significant cooperation from the engineers and/or contractors on the project site. Because the level of cooperation is unknown, the minimum number of readings for the monitoring program includes 2 during construction of each pier and 4 during construction of the bridge deck. A reading will be taken at the end of construction, and the contractor has stated that they will be willing to drive a fully-loaded transport truck onto the bridge to obtain strain gage readings. Because of the longevity of the VWSGs, it is possible to get readings periodically throughout the life of the bridge to assess changes in load transfer over time.

6.1.7. Monitoring Data. At the time of publication, VWSG readings had been taken at Pier 1 and Pier 2 immediately after installation and after curing of the micropile grout. Of the 56 VWSG installed at the site (8 instrumented micropiles and 7 VWSG per micropile), only one gage is not reading (Pier 1, 04D1) because the cable for the gage was lost in the pile cap when it was poured. Data was also obtained at Pier 1after the concrete pile cap was poured. Using the data reduction methods described in Section 5.7, the strain readings from the VWSG were converted to axial load readings. The strain readings after the grout had cured were used as the baseline (zero load) readings and the axial loads were calculated from the August 10, 2011 readings at Pier 1 after the pile cap had been constructed, as shown in Figure 6.12. Based on the size of the pile cap (20 feet

diameter and 5 feet thick), the total dead load of the piles cap was approximately 300 kips or about 15 kips on each micropile. The measured loads for each micropile are shown in relation to the design load (310 kips) and appear to be relatively close to the calculated dead load of the pile cap. Deviations from the expected load may be a result of the interaction between the pile cap and the concrete drill pad of varying thickness, as well as interaction between the drill pad and the ground surface.

Because the pile cap has not yet been constructed at Pier 2, the micropiles are in a no-load condition. Therefore, the VWSG readings cannot yet be interpreted and converted to load or bending moment. The initial VWSG readings that were taken after installation (wet grout) and after the grout had cured are provided in Table 6.4.

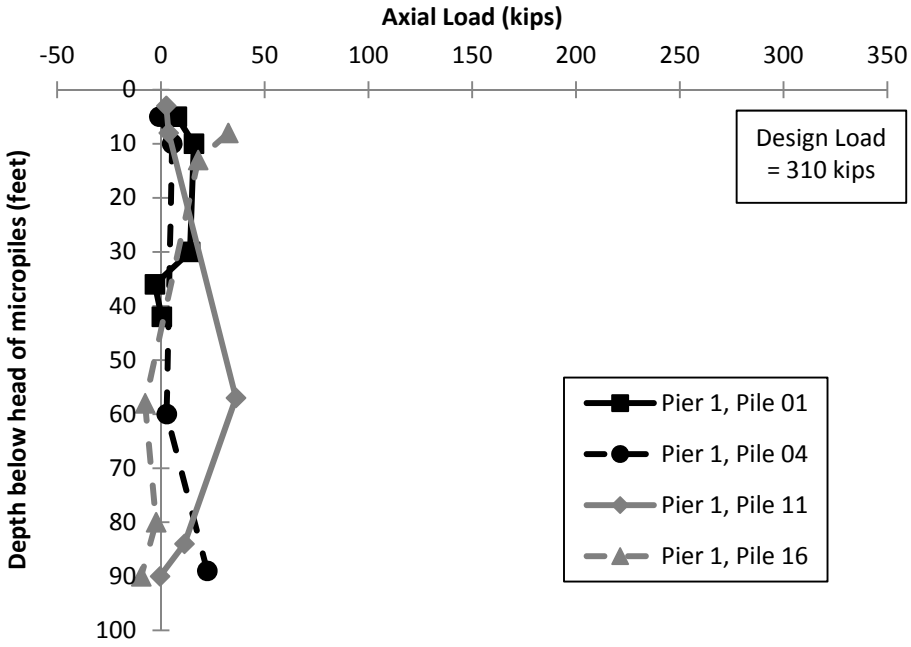

Figure 6.12. Load Interpreted from VWSG Readings with Pile Cap Constructed

Table 6.4. Pier 2 VWSG Readings

	Reading Date	6/15/2011	8/10/2011
	Load Condition	Wet Grout	Cured Grout
Location	Gage Name	Microstrain	
Pile 1	01A1	2868.6	2859.5
	01A2	2644.7	2633.5
	01B1	3061.0	3060.0
	01B2	3008.7	3006.3
	01C1	2789.6	2778.6
	01D1	2780.1	2753.8
	01E1	2672.9	2670.7
Pile 6	06A1	2836.4	2796.8
	06A2	2857.6	2842.3
	06B1	2803.2	2790.1
	06B2	2973.7	2959.5
	06C1	3265.4	3258.3
	06D1	3041.1	3072.2
	06E1	2670.8	2660.6
Pile 11	11A1	2911.6	2907.6
	11A2	2985.7	2984.3
	11B1	2763.0	2757.5
	11B2	2969.5	2968.7
	11C1	2931.7	2927.3
	11D1	No Reading	3046.5
	11E1	3001.7	3036.8
Pile 16	16A1	2803.8	2747.7
	16A2	2961.9	2897.5
	16B1	2584.7	2567.9
	16B2	2941.6	2920.5
	16C1	2876.5	2858.3
	16D1	2916.9	2904.4
	16E1	2843.2	2838.1

7. SYNTHESIS AND CONCLUSIONS

This section presents a summary and synthesis of the results of the research tasks. A synthesis of results is necessary because the three tasks were completed relatively independent from each other, but the scope and purpose of each task are inter-related. In addition, this section provides comparisons of the results to previous research. Based on the synthesis and comparisons, general conclusions can be drawn regarding the behavior of micropiles subjected to combined loading conditions.

7.1. SUMMARY OF RESULTS

7.1.1. Effect of Combined Loading in Loose Sand. As discussed in Section 4, testing was completed on model micropiles installed in relatively loose sand, including four (4) lateral load tests and four (4) combined load tests. The casing thickness of the micropiles was also varied such that half of the tests were completed on micropiles with higher flexural stiffness and half were completed on micropiles with lower flexural stiffness. The applied axial load was equal to approximately one-half of the ultimate axial compressive capacity of the micropiles subjected to axial loading. With the axial load held constant, the lateral load was incrementally increased until excessive deflection or complete failure was achieved. Excessive lateral deflection was defined as greater than about five pile diameters and complete failure was defined as the largest lateral load that the micropile could withstand. The maximum applied lateral loads for the four combined load tests resulted in maximum ratios of lateral load to axial load (P_{lat}/P_{ax}) ranging from 0.80 to 0.96 with a mean value of 0.91.

The results presented in Figure 4.53 indicate that an axial load applied to the micropiles in loose sand did not have an appreciable effect on the lateral load-deflection

behavior for the majority of the lateral load sequence. However, the failure of micropiles subjected to combined loading was dramatic and precluded the incremental unloading of the micropiles, as shown by the steepness of the curves in Figure 4.53 and the larger lateral deflections at high lateral loads. To further assess the effect of combined loading at low lateral loads, Figure 7.1 was prepared by zooming in on the data shown in Figure 4.53.

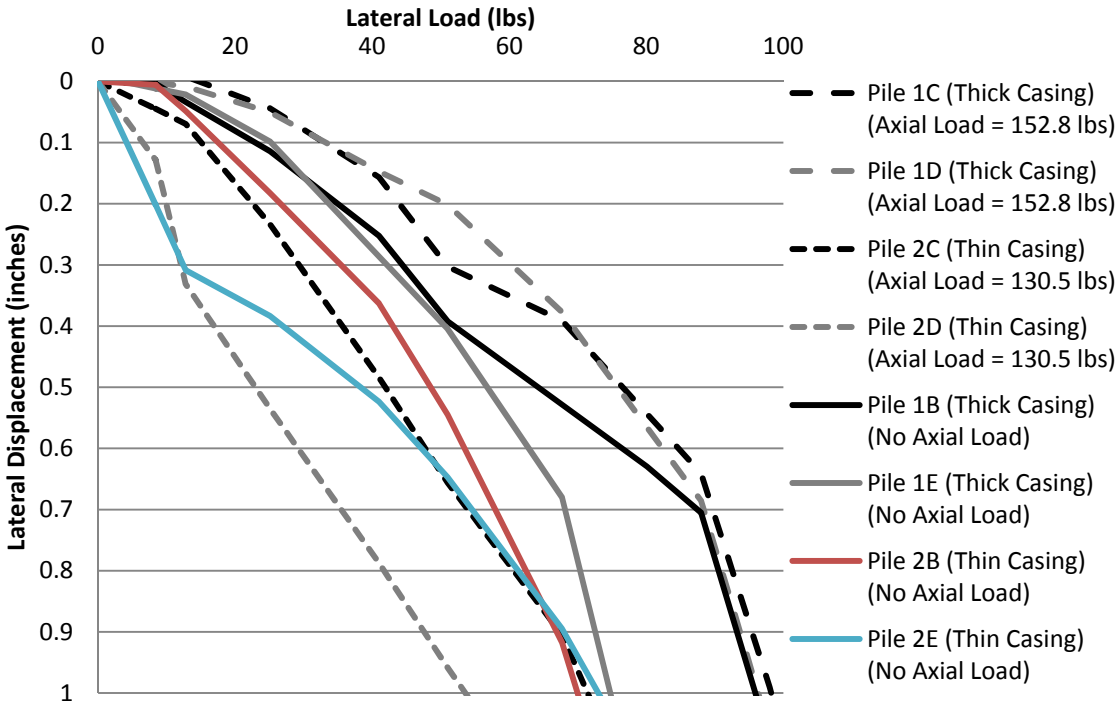

Figure 7.1. Comparison of Lateral and Combined Load Test Results for Loose Sand, Lateral Load vs. Lateral Displacement (zoomed version)

Based on the results in Figure 7.1, it appears that, for the tests on the relatively stiff micropiles (thick casing), the presence of an axial load caused a slight increase in the lateral stiffness of the micropiles compared to the lateral load tests. This increase in

lateral stiffness is not apparent in the micropiles with thinner casing. Finally, the micropiles with thicker casing exhibited greater lateral stiffness than those with thinner casing, as expected.

The results presented in Figures 4.55 and 4.57 indicated that micropiles installed in loose sand and subjected to combined loading conditions exhibited higher maximum bending moments than micropiles subjected only to lateral loads. This effect was more distinct for higher lateral loads where there was an increase in maximum bending moment of 22 to 40 percent.

7.1.2. Effect of Combined Loading in Dense Sand. Testing was completed on model micropiles installed in relatively dense sand, including two (2) lateral load tests and two (2) combined load tests (see Section 4). The casing thickness of the micropiles was also varied such that half of the tests were completed on micropiles with higher flexural stiffness and half were completed on micropiles with lower flexural stiffness. The applied axial load was equal to approximately one-half of the maximum applied axial load applied to the micropiles during axial compression testing. With the axial load held constant, the lateral load was incrementally increased until the maximum lateral load of the testing equipment was reached. The maximum applied lateral loads for the two combined load tests resulted in maximum ratios of lateral load to axial load (P_{lat}/P_{ax}) of 1.4 and 1.5.

The results presented in Figure 4.54 indicate that an axial load applied to the micropiles in dense sand did not have an appreciable effect on the lateral load-deflection behavior for the majority of the lateral load sequence. However, similar to the effect of combined loading on micropiles in loose sand, a relatively small effect from combined

loading was apparent for lateral loads at the smallest and largest ends of the lateral load range used for the tests. As shown in Figure 4.54, the micropiles subjected to combined loading experienced greater lateral deflections at large lateral loads than the micropiles subjected only to lateral loads only. In addition, based on the plot of lateral load versus deflection for small lateral loads shown in Figure 7.2, the micropiles tested with combined loads exhibited a slightly stiffer response than the laterally loaded micropiles. As expected, the micropiles with thicker casing exhibited greater lateral stiffness than those with thinner casing for the entire lateral loading sequence.

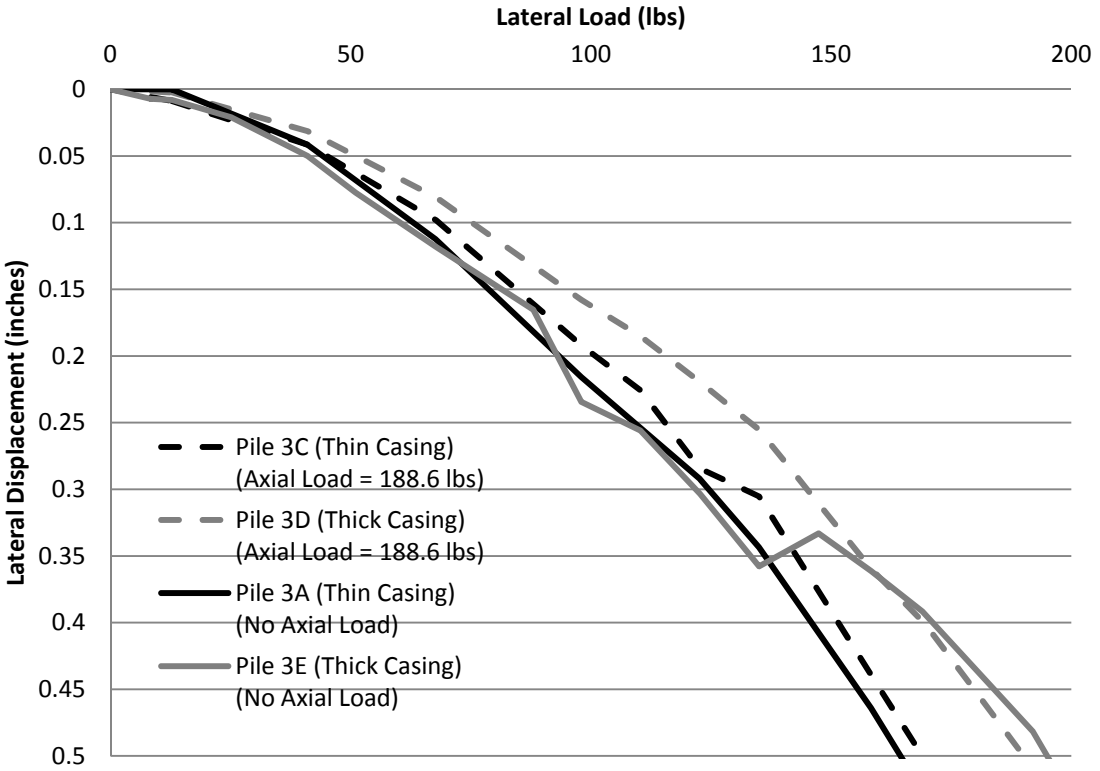

Figure 7.2. Comparison of Lateral and Combined Load Test Results for Dense Sand, Lateral Load vs. Lateral Displacement (zoomed version)

The results presented in Figures 4.56 and 4.58 indicated that micropiles installed in dense sand and subjected to combined loading conditions exhibited higher maximum bending moments than micropiles subjected only to lateral loads. This effect was more distinct for higher lateral loads where there was an increase in maximum bending moment of 5 to 30 percent.

7.1.3. Effect of Combined Loading in Stiff Clay. As discussed in Section 5, load tests were completed on full-scale micropiles installed in very stiff clay underlain by low strength shale. The testing program included two (2) lateral load tests and four (4) combined load tests. The applied axial load for the combined load tests was equal to approximately one-half of the ultimate failure load from the axial compression load tests completed at the site. With the axial load held constant, the lateral load was incrementally increased until the maximum lateral deflection of the testing equipment was reached (approximately 2.5 inches). The maximum applied lateral loads for the four combined load tests resulted in a maximum ratio of lateral load to axial load (P_{lat}/P_{ax}) of about 0.6.

The results presented in Figure 5.46 indicate that, for stiff clay near-surface conditions, a combined axial and lateral load applied to micropiles resulted in increased lateral stiffness compared to micropiles subjected to a lateral load only. However, the increase in stiffness appears to be minimal and was not apparent in all comparisons between lateral and combined load tests. In addition to the comparison of lateral load-deflection behavior for the combined and lateral load tests, Section 5 also provided a comparison of bending moment between the two test types. Based on Figures 5.47, 5.48, and 5.49, micropiles installed in stiff clay and subjected to combined loading conditions

exhibited slightly reduced bending moments compared to micropiles subjected only to lateral loads. However, similar to the load-deflection behavior, the reduction in bending moment was minimal and was not shown in every combined load test. Finally, the maximum bending moment for the combined load tests was slightly shallower (closer to the ground surface) than the maximum bending moment for the lateral only load tests.

7.2. COMPARISONS OF TESTS IN SAND TO PREVIOUS WORK

The results of the scale model testing of micropiles installed in sand indicated that the combined loading had a minimal effect on the lateral load-deflection behavior (Sections 7.1.1 and 7.1.2). The lateral deflection in the combined load tests had a very slight decrease at low lateral loads and a slight increase at high lateral loads compared to the lateral load tests. The maximum bending moments were increased by the inclusion of an axial load for both loose (22 to 40 percent increase) and dense (5 to 30 percent increase) sand. As discussed in Section 2.3, the results of previous work were varied and conflicting. For the ten studies that specifically analyzed the combined load behavior of deep foundations installed in sand, one paper reported that application of an axial load had no effect on lateral behavior [You et. al. 2003], four studies indicated that lateral deflection and/or bending moment increased for the combined load conditions [Karthigeyan et. al. 2006 and 2007, Chik et. al. 2009, Jain et. al. 1987, Lee 2008], and five studies resulted in decreased lateral deflection when subjected to combined load conditions [Klein and Karavaev 1979, Karasev 1977, Pise 1975, Majumdar 1980, Saxena 1982]. However, Jain et. al. [1987] surmised that the data from four of the studies that reported decreased lateral deflection was skewed because of unintentional restraint at the pile head that resulted from the combined load application method. Because the

micropile head was allowed to translate and rotate freely after application of the axial load, head restraint was not a factor in the scale model micropile study discussed in Section 4.

7.3. COMPARISONS OF TESTS IN CLAY TO PREVIOUS WORK

As summarized in Section 7.1.3, the full-scale micropiles installed in stiff clay had a slight increase in lateral stiffness (decrease in lateral deflection) and a slight decrease in bending moment for combined loading conditions, as compared to lateral loading conditions. These results are supported by the full-scale testing of driven piles in clay soil by Zhukov and Balov [1978], Sarochen and Bykov [1976], and Bartolomey [1977]. In addition, full-scale tests on piles in mixed clay/sand soil by Lehane et. al. [1999], Evans [1953], and McNulty [1956] yielded similar results. Jain et. al. [1987] argued that the reduction in deflection may have been a result of pile head restraint in the load tests, but restraint was minimized in the combined load tests discussed herein because of the presence of the roller system combined with the swivel. While all of the full-scale tests on piles in clay had similar results, two other studies on piles in clay had conflicting results from the combined load results presented above, including scale model testing on piles in clay [Anagnostopoulos and Georgiadis 1993] and three-dimensional finite element analysis of piles in clay [Karthigeyan et. al. 2006 and 2007]. However, both of the studies indicated that the increases in deflection and bending moment were small. Finally, two finite element studies [Shahrour and Meimon 1991, Shahrour and Ata 1994] concluded that the presence of an axial load does not have an effect on the lateral behavior of micropiles.

7.4. CONCLUSIONS

The increase in popularity of micropiles has led to increased usage as traditional foundation elements, as well as in new, non-traditional applications. The foundation elements are commonly subjected to combined (axial and lateral) loading. This loading scheme can be critical for design because micropiles are slender elements with relatively small lateral stiffness that are sensitive to changes in bending moment. However, the research regarding combined load behavior of micropiles is sparse. Research regarding all deep foundation elements subjected to combined loading is also minimal, and the results are conflicting.

The main objective of this research was to assess the effect of combined loading on lateral behavior of micropiles. To this end, three research tasks were completed, including scale model testing of micropiles installed in loose and dense sand, full-scale field testing of micropiles installed in very stiff clay, and instrumentation of production micropiles. Because the structure supported by the instrumented production piles had not been completed at the time of publication of this document, conclusions based on the results of that task are not possible.

Based on the results of the aforementioned tasks, as well as comparison of results to previous work, some basic conclusions can be made regarding the behavior of micropiles subjected combined loading as follows.

1. For micropiles in clay, the presence of an axial load results in limited changes in lateral behavior. The small changes that were observed included small decreases in both lateral deflection and bending moment compared to the lateral load tests.

2. For micropiles in sand, the lateral deflection was not significantly affected by introduction of a constant axial load. However, bending moments in the micropiles were significantly increased for combined load conditions. The increase in bending moment was more significant for micropiles in loose sand than micropiles in dense sand.

3. For micropiles in sand, the density (and therefore strength and modulus) of the sand has a much larger effect on the lateral behavior than the bending stiffness of the steel casing. Therefore, proper characterization of the soil is extremely important for design of micropiles with lateral or combined loads.

4. P-y computer analysis predicts the lateral load-deflection behavior of micropiles in clay subjected to lateral loads and combined loads relatively accurately. However, for both lateral and combined load cases, the maximum bending moment within the micropile is over-predicted by p-y analysis.

5. For axial load conditions in both clay and sand, end bearing contributed approximately 14 to 24 percent of the ultimate capacity of the micropiles at the plunge failure load.

8. RECOMMENDATIONS FOR FUTURE RESEARCH

The research discussed herein consisted of experimental studies to assess the response of micropiles to axial, lateral, and combined loads. Based on the results of these studies, several areas of further study were identified. The recommendations listed below are divided into three categories, including the author's future research plans, continuation of research at Missouri S&T, and continuation of research at the Warrensburg test site.

8.1. FUTURE RESEARCH PLANS

The author's future research plans include additional analysis of the data obtained during this research project, as well as continuation of research regarding combined loading, as listed below.

1. The effect of combined loading on micropiles could be further investigated using finite element or finite difference numerical modeling methods, including two- and three-dimensional analysis. The data from the scale model and full-scale load tests could be used to calibrate the models. Following calibration, a wider range of loading conditions could be applied to the micropiles to assess other phenomena such as the effect of a static lateral load on the axial behavior of micropiles. In addition, the numerical modeling could be extended to evaluate the behavior of micropile groups subjected to combined loading.

2. The effect of combined loading on a group of micropiles in sand could be investigated using scale model testing. The model micropiles, sand placement technique, and micropile installation method would be similar to the scale model

testing described herein. Because of the larger loads required to fail the micropile groups, new methods of micropile loading would need to be developed.

8.2. CONTINUATION OF RESEARCH AT MISSOURI S&T

Development of the load testing capabilities discussed in Section 3 gives the Department of Civil Engineering at Missouri S&T unique capabilities for future research opportunities, as listed below.

1. First and foremost, the instrumentation installed in the micropiles at Foothills Bridge No. 2 should continue to be monitored. The data obtained from the instruments should be interpreted to assess the depth of load transfer, potential bending in the upper portion of the micropile, and the presence of combined loading on the micropiles that were designed for axial loads only. The project has been passed on to Devin Dixon, a M.S. student at Missouri S&T.

2. Using the relationships that have been developed with micropile designers and constructors, additional production micropiles could be instrumented and monitored. The instrumented micropiles could be used for foundation support, slope stabilization, or retaining structures.

8.3. CONTINUATION OF RESEARCH AT WARRENSBURG TEST SITE

Because of the durability and longevity of the vibrating wire strain gages installed in the micropiles at the Warrensburg test site, additional testing could be completed on the installed micropiles. Recommendations for further research on the micropiles are listed below.

1. The micropiles could be re-tested with axial compression and lateral loads to better define the re-use of micropiles. Re-use of existing foundations is currently of interest because of the push for sustainable design. Because the micropiles at the site were taken to practical failure, re-testing could be used to develop a relationship between the original capacity and the post-failure capacity. Nondestructive testing would also be valuable to assess the condition of the failed micropiles.

2. The micropiles could be re-tested using cyclic loading conditions. Because the response of the strain gages is not sufficient to apply high frequency earthquake loading, the cyclic load tests would need to be limited to low frequency that more closely models cyclic loads such as wind.

APPENDIX A

LABORATORY TESTING REPORT FOR P-57 SAND

USED FOR SCALE MODEL TESTING

Micropile Sand Testing

Opportunity for Undergraduate Research 2010-2011

Prepared By:

Skylar Knickerbocker

Advisor:

Ronaldo Luna

Department of Civil, Architectural and Environmental Engineering

Missouri University of Science & Technology

Rolla, MO

April 2011

Table of Contents

1.0 Introduction

Civil engineering encompasses a wide variety of fields including geotechnical engineering. Within geotechnical engineering is foundations in which a rapidly developing type of foundation is the micropile. Micropiles are a smaller diameter type of deep foundation that can be used in a many situations that a typical deep foundation could not. One way that this is possible is the compact drilling that can be done making it possible to underpin a building. This type of foundation can be used in a variety of situations and commonly is being used in ways that haven't been researched adequately enough. Kyle Kershaw is researching the reaction of vertical, axial, and combination loading have on the micropiles.

My contribution to his research is to determine the soil characteristics of the sand that is being used in the scale model testing of these micropiles. The scale model testing used a very fine silica sand that is from the U.S. Silica Company in Pacific, Missouri. Testing started by performing index property tests then determining a range of density that sand can be. From the maximum and minimum density a high and low density were determined that would be used for the rest of the scale and laboratory testing so that a range of conditions could be found.

Determining the shear strength of the sand was a major part of the research. This was done in the lab by performing direct shear testing and also a triaxial consolidated undrained test. Tests were ran on both the high and low density and compared. Another check on the shear strength was done in the scale model testing using the cone penetration test. The scale model test consisted of 4' deep sand pit that scale model micropiles were installed and built in. The cone penetration test was then used to determine the sands shear strength and also to make sure the sand was uniform.

This research will help to determine what the properties of the sand that were used in the scale tests. With scale model testing data done in the lab it will be possible to get an accurate depiction of how the micropiles would behave in full scale situations.

2.0 Abstract

Micropiles were first developed in the 1950's in Italy to underpin historic buildings where conventional piles could not be used. Since then, micropiles have grown in popularity and are being used in a wide variety of applications. The response of micropiles used in these new applications have not been adequately researched enough which is why Kyle Kershaw is researching the effects of combined, axial, and lateral loads. My part in this research is to determine the soil properties and strength characteristics of the sand used for scale model tests and correlate the model soil parameters to the prototype soil parameters. This will be done by running direct shear testing, cone penetration and triaxial consolidated undrained testing along with index testing and density tests.

3.0 Testing Procedure

The testing done on the sand was done in the following progression. The index properties were first determined in the lab to get a starting point of what the sand was like and how it compared to the manufacturers data. Once this was done density tests were performed to get a range of the density possible for the sand. This range of densities would be used for the remainder of the tests. A maximum and minimum density that could be achieved in the lab was chosen to be tested in direct shear and triaxial so that the shear strength could be determined. The two densities would allow a range of shear strength that could be achieved with this sand. The direct shear tests were performed first followed by a consolidated drained triaxial tests.

All while the testing in the lab was being done, scale model testing was being performed in a 4' deep sand pit that can be seen in Figure 1. The scale model testing consisted of creating and installing scale micropiles and testing different loading combinations. This testing was performed in three different rounds. The first two rounds of testing tried to simulate the low density sand behavior. This was done by using a box that would spread the sand out evenly at a drop height of approximately one foot. During the third round a vibratory compactor was rented so that the sand would simulate high density sand behavior. Before the scale micropiles were installed cone penetration tests along with density mold were used to determine the density of the sand and shear strength of the sand while also ensuring that the sand was uniform all the way down.

Figure 1:Sand Pit

4.0 Laboratory Test

4.1 Particle Size

The first analysis performed on the sample was a sieve analysis that was done in accordance to ASTM D 422. The results were compared to the product data provided by U.S. Silica Company (Figure 17 Appendix A). Six sieves from the U.S. Silica Company's product data were used based on what would give the best representation of the sand and collect the most material. Sieve No. 20, 40, 50, 70, 100, and 200 were chosen to meet the requirements. Table 1 shows that the two trials are close to the percent passing that was provided by U.S. Silica Company. Figure 2 is a plot of the percent passing and both of the curves are close together and show that the sand is very fine and well graded.

Sieve Size	Percent Passing		
	Trial 1	Trial 2	U.S. Silica
20	100.0%	100.0%	100.0%
40	97.3%	96.8%	95.8%
50	84.2%	82.4%	73.8%
70	47.4%	45.4%	37.8%
100	15.9%	14.7%	7.8%
200	0.1%	0.1%	0.3%

Table 1: Summary of Particle Size Analysis

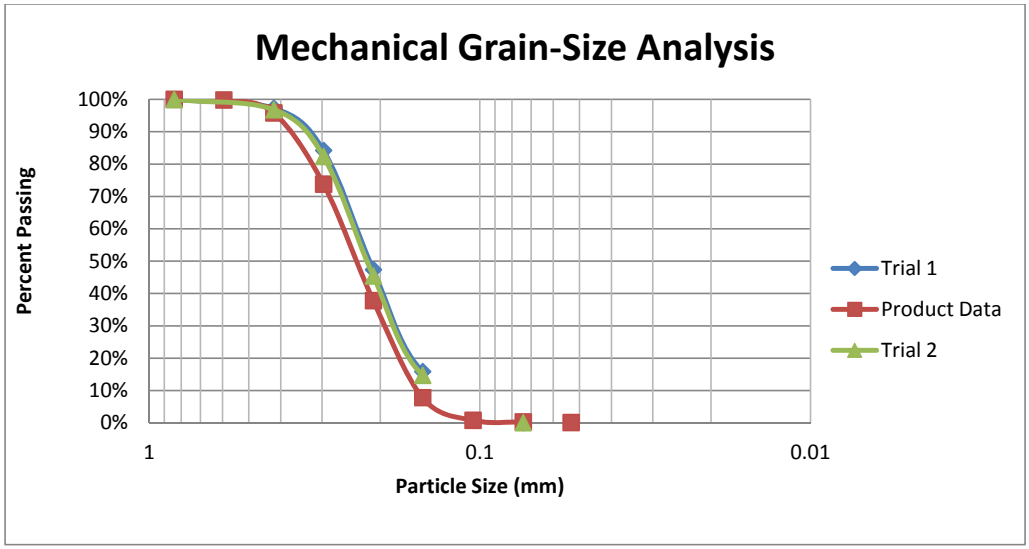

Figure 2: Particle Size Analysis

4.2 Density

For all of the testing that would be done on the sand both in the lab and in the scale testing a high and low density was needed so that a comparison of the shear strength could be performed. To do this the maximum and minimum density were determined in the lab in multiple ways. The maximum density was performed twice, once according to ASTM D 4253 and the other manually compacting the sand. The manually compacted sand was done first to determine a range that could physically be made to be run in the direct shear test and triaxial test. To manually compact the sand a cylinder with a known volume was filled in 1" lift and then compacted with a weight and roding. The maximum density achieved manually was 106.1 pcf. Following ASTM D 4253 Method 2A was used, utilizing the vibratory table. The specimen was oven dried then filled in the mold at five 1" lifts. The soil was compacted by hand after each layer. The mold, with soil, was then placed in the vibratory table and vibrated at 50 Hz for 12 minutes. Once complete the excess sand was removed and the weight of sand in the mold was measured. This lead to a maximum density of 115.5 pcf.

The minimum density was also done two different ways using ASTM D 4254 Method A and Method B. Method A was performed exactly according to ASTM D 4254 using a ½" funnel to place the sand in a circular motion with approximately a ½" drop height. This method allowed a minimum density to be found that could be duplicated in the direct shear test and triaxial test. The minimum density found was 99.9 pcf. Finally Method B was used with a slight variance. Water was used in the tube instead of air to get the minimum density. This allowed the sand to free fall slower and get a lower density. This method was performed twice and got a minimum average density of 94.4 pcf. A chart of the minimum and maximum density is shown in Table 2.

Maximum Density	(lb/ft^3)
ASTM 4254 Method 2A	115.5
Manual Compaction	106.1
Minimum Density	(lb/ft^3)
ASTM 4253 Method A	99.9
ASTM 4253 Method B-Trial 1	94.7
ASTM 4253 Method B Trial 2	94.1
ASTM 4253 Method B Average	94.4

Table 2: Maximum and Minimum Density

From this data the high and low densities were determined to be 106 pcf and 100 pcf, respectively. They were chosen because they would give a fairly wide range in the density for this sand but also for their ability to be replicated in the lab testing. These densities will be used for the direct shear testing, the triaxial testing, and scale model testing.

4.3 Shear Strength

4.3.1 Direct Shear

The direct shear testing was part of the laboratory testing that was performed to determine the shear strength of the sand. Testing was ran according to ASTM D 3080. It was determined that two densities would be tested to get both a maximum density and minimum density result. This would allow a range of shear strength in the scale testing to be determined. Both densities were tested at normal stresses of 200 psf, 400 psf, 600 psf, and 1200 psf. Along with that, a 900pcf test was done on the 100 pcf to better shape the line determining the friction angle.

The data from the direct shear was used to create a plot of the shear stress vs shear displacement. With this plot the failure stress could be found as the peak. All shear stress vs shear displacement graphs are in Appendix B Figure 18-26. Once having the peak shear stress another plot was created that had the failure stress and the normal stress for both densities as shown in Figures 3 and 4. From the points plotted a linear relationship was seen for both densities allowing a best fit line to be drawn. The friction angle was found from these graphs to be 29.9° for the 100 pcf sand and for the 106pcf sand it was 39.1°. In both graphs there appears to be cohesion but this has to do with the fact that this relationship is not perfectly linear in sands. Typically sand has a curve at the beginning of the graph that could not be shown with this testing data. If lower normal stresses were tested this relationship would be seen.

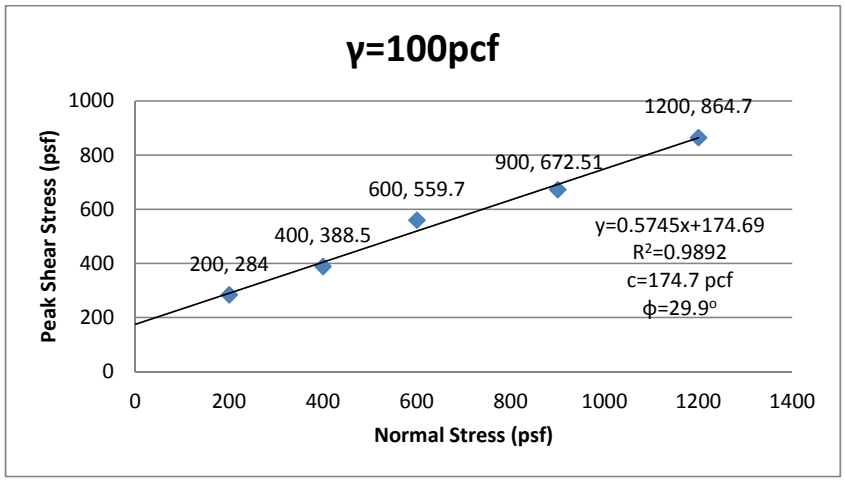

Figure 3: Peak Shear Stress vs. Normal Stress

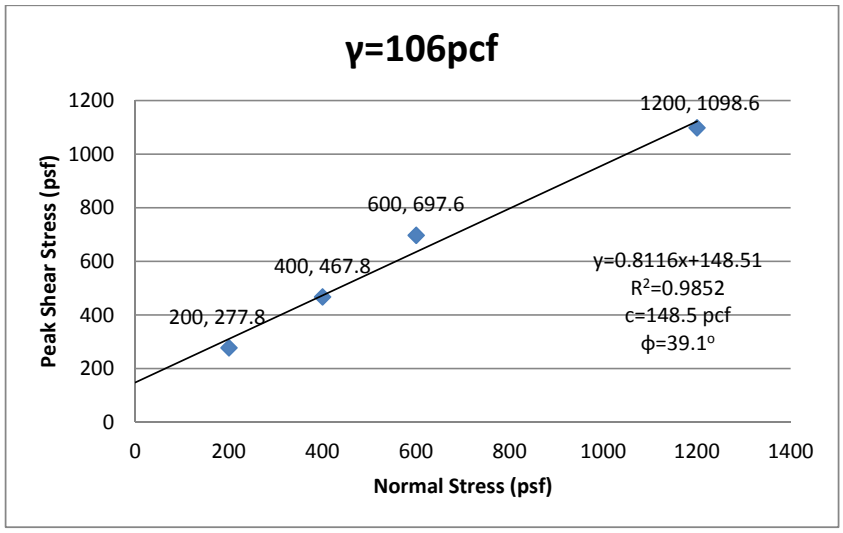

Figure 4: Peak Shear Stress vs. Normal Stress

There is a relationship between the shear stress and normal stress that when put in a ratio can be compared to the other direct shear tests on the same sample. Figure 5 and 6 shows that they all have similar shapes and are relatively close together. It can be seen too that in the 100pcf graph that all tests seem to not have as defined of a peak as in the 106pcf sample. This is typical because dense sands should have a more defined peak then the loose sand. The only tests that seem to be off are the normal stresses of 200psf in both densities. This could be because the normal stress was too low and the shear stress was not affected by the normal stress as it was in the other tests.

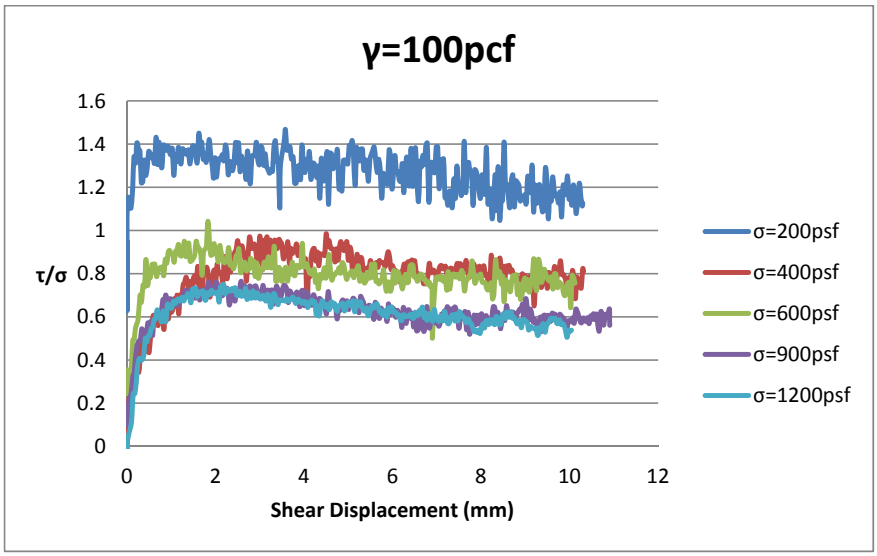

Figure 5:Shear Stress/Normal Stress vs. Shear Displacement

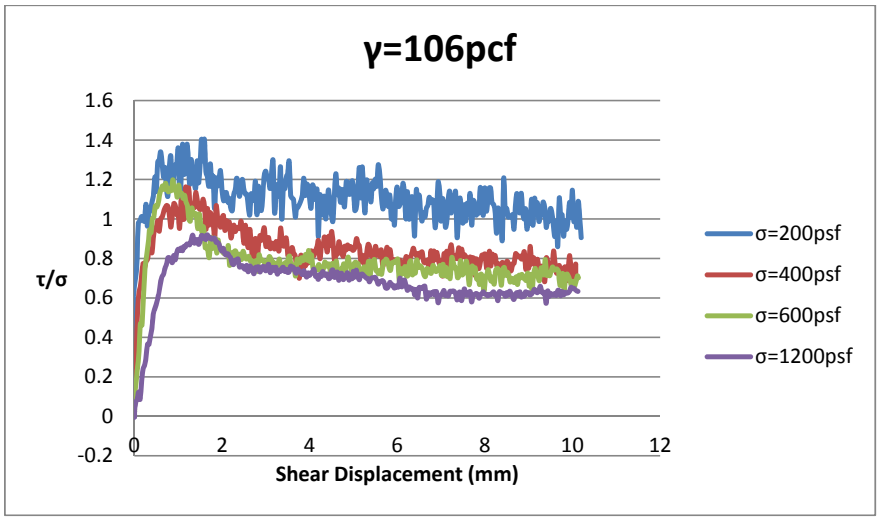

Figure 6:Shear Stress/Normal Stress vs. Shear Displacement

Looking at the shear displacement vs normal displacement graphs, Appendix B Figures 27-35, you can see a difference from the high density and low density sand. In the low density sand the graphs initially contract then dilate to a peak then contract till failure. The only exception to this is the graphs with normal stress of 200psf and 400psf. The 200psf normal stress test had dilation which is most likely because there wasn't enough normal stress to behave like a loose sand. Looking at the graph for the normal stress of 400psf, the graph seems to jump around the shear displacement of 4mm. The cause of this is believed to be the instrumentation error because of the sudden change that is perfectly straight down. If the jump would be removed it would behave like all the other loose sands. All of the high density sand behaved like they should have. The graphs show that the sand expanded during shearing which is expected because the sand is dense and the particles have nowhere to go but to dilate.

4.3.2 Triaxial Testing

The triaxial test was also performed to determine the shear strength but this test would simulate what a full scale test would be like. To reference the scale model testing the sand was tested dry using the consolidated drained method. The sand was again tested at both a low and high density which was attained by manually compacting in lifts to meet the high density specimen and using a funnel with a small drop height for the low density. Once the specimen was prepared both the bottom and top valve were left open so that the test would be drained. The testing started with a consolidation stage consisting of 30 minutes at the three different stresses for each density. The three stresses tested were 300 psf, 600 psf, and 1200 psf. The strain rate was determined to be .5% per minute until it reached a failure strain of 20%. Since the specimen is dry and the air coming out of the sample could not be measured the volume change was measured indirectly by the volume change of the cell. This volume was read every 30 seconds until the strain reached 20%.

Figure 7:Triaxial Testing

A difficult part during the testing was being able to get the correct density for each test. Table 3 shows the breakdown of what densities were achieved for each test that was ran.

γ=100pcf			γ=106pcf	
Testing Stress	Testing Density		Testing Stress	Testing Density
300psf	98.7		300psf	105.1
600psf	100.1		600psf	105.9
1200psf	98.8		1200psf	104.4

Table 3:Triaxial Testing Density

Once the testing was complete the deviatoric stress needed to be calculated by dividing the axial force by the corrected cross sectional area using equation 6.26 from “Introduction to Soil Mechanics Laboratory Testing” by Dante Fratta, Jennifer Aguettant and Lynne Foussel-Smith. The total axial stress was found, which is needed to calculate the peak axial stress which will then be used to create the Mohr Circle. The graphs used to find the peak total axial stress are shown in Appendix C

Figures 36-41. Using the peak axial stress plus each respective confining stress the Mohr Circles in Figure 8 and 9 were created. From the Mohr Circle is was found that the friction angle in the 100pcf density sand was 35.1° while the 106pcf density sand had a friction angle of 39.4°.

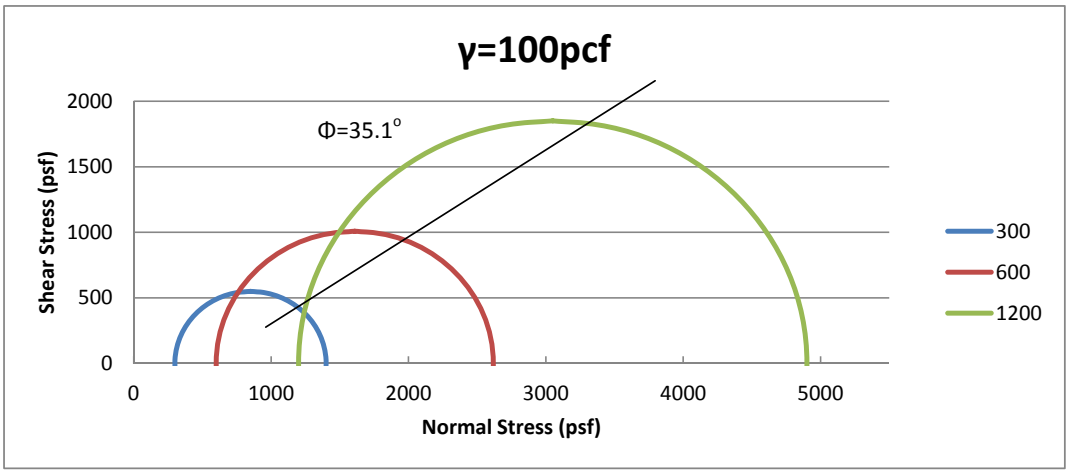

Figure 8:Mohr Circle-γ=100pcf

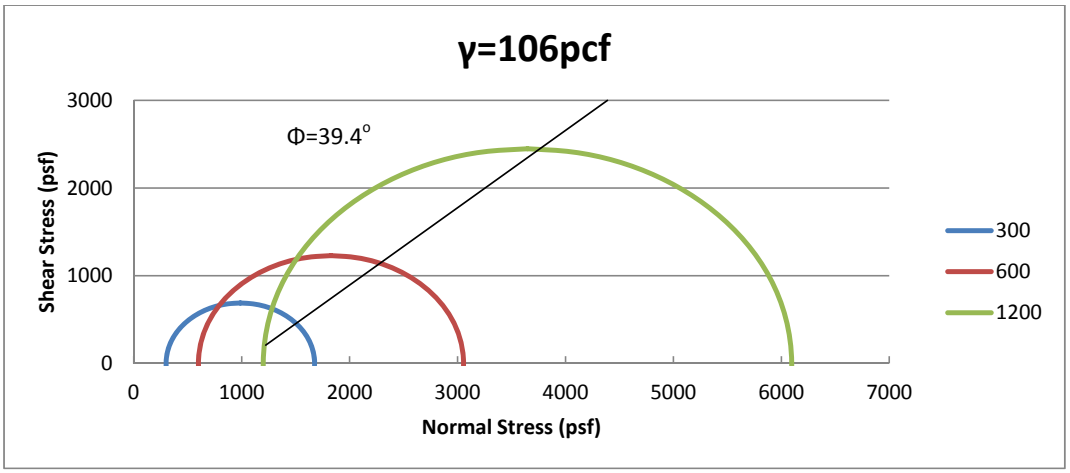

Figure 9:Mohr Circle-γ=106pcf

It is also standard to plot the principal stress ratio which is the total axial stress divided by the confining stress. This can be seen in Figure 10 and 11. The lower density principal stress graph shows that all the curves are fairly close and that none of them have a really defined peak. But in the higher density principal stress ratio graph the curves all have a better defined peak and also have a higher ratio that peak around 5.5 while the lower density peaks around 4.5. The higher ratio is seen in the Mohr's Circle and also that the higher density has a higher friction angle.

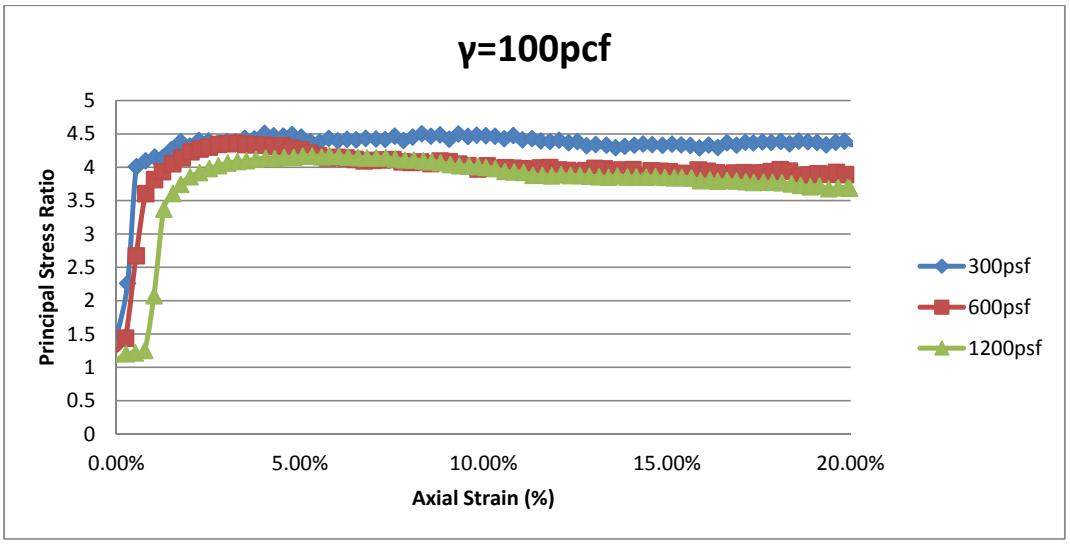

Figure 10:Principal Stress Ratio vs Axial Strain

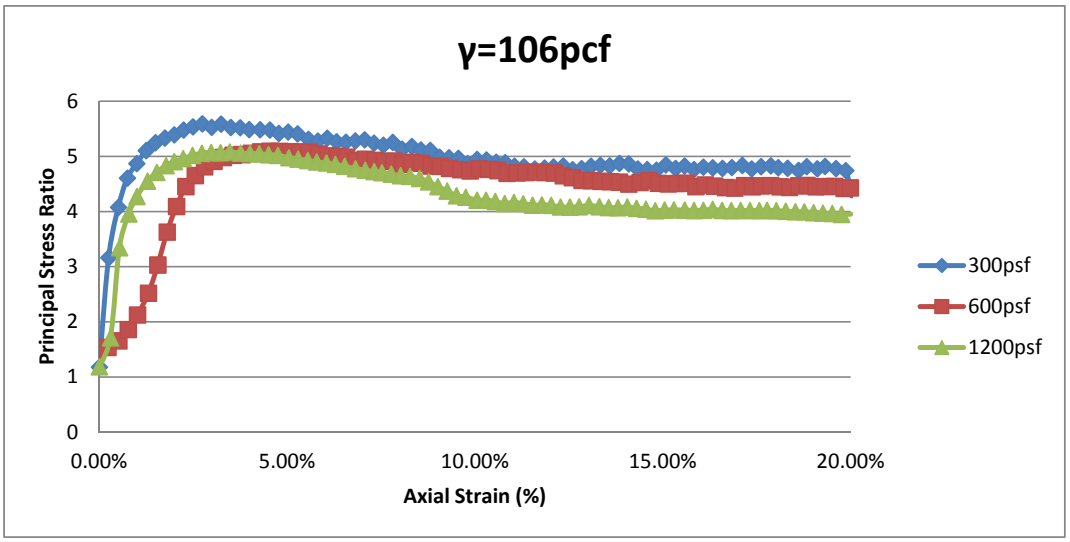

Figure 11:Principal Stress Ratio vs Axial Strain

5.0 Scale Test (In-Situ)

5.1 Density

For the scale model testing a pit 4' deep was used for testing of the micropiles. There were three different rounds of testing. The first two rounds consisted of developing a low density sand pit while the third round of testing aimed at getting the sand as dense as possible. The first major task in doing the small scale testing is placing the sand. To achieve a low density in the first two rounds the sand was placed by letting the sand fall a consistent distance of approximately one foot. This was done using a box that had holes in the bottom and a screen to separate the sand which can be seen in Figure 12. During the third round of testing a higher density was wanted and a compactor was used to achieve this. The compactor was allowed to run for approximately 8 second in a single place and was then moved to the next uncompacted spot. The compactor was used on every six inch lift. A photo of the compactor is also shown in Figure 12. Table 4 gives a breakdown of what tests were ran in each round of testing

	Density Molds	Cone Penetration Test
Round 1 (low density)	4	2
Round 2 (low density)	4	2
Round 3 (high density)	0	3

Table 4: Summary of Scale Testing

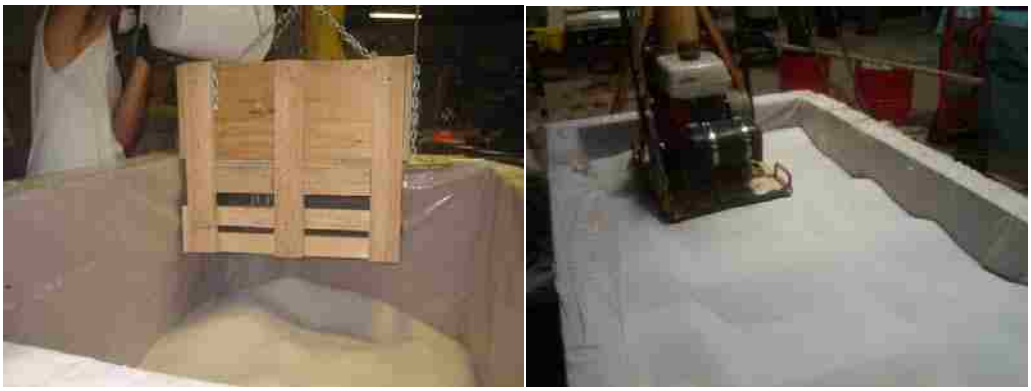

Figure 12: Round 1&2 (left) Round 3 (right)

A single test performed on rounds 1 and 2 was to place a density mold in the sand during filling. This allowed the sand to fall into the mold just like the rest of the box. With a known volume the density was determined of the sand after testing was concluded. When the box was emptied the density molds were recovered and weighed to determine an average density. Each round had four

density molds placed in the northeast and southwest corner and placed 1.5' and 2.75' deep in the sand. From round 1 the average density of the box was 111.3 pcf while round 2 had an average density of 108.4 pcf. During lab testing the maximum density was 115.5 pcf so both of these densities are on the high side but are fairly close together to compare data. The densities molds were not placed during round 3 because it was not possible for them to get an accurate reading while using the compactor.

5.2 Cone Penetration Testing

The cone penetration test was used in this lab for two purposes: to make sure the sand is uniform and to check the strength compared to the direct shear testing. Raw data from the CPT can be seen in Figures 47-53 in Appendix D. From the raw data it can be seen that the tip stress increases with depth on all the tests and has a consistent shape. The sleeve stress in all of the test do not seem to vary with depth and stays very low. One thing to notice in all of the data and interpretations with the CPT is that the values in the first foot are erratic. This may be due to the sand being so loose near the top of the pit but also could be that the sleeve recording the friction stress is not entirely in the sand and gives erratic readings.

5.2.1 Friction Angle

To compare the CPT test results to the direct shear and triaxial testing done in the lab the data must be interpreted to find a friction angle. Since most interpretations on CPT data for sand was done in the early 90's most of the interpretations used are from around then. The friction angle can be determined using the following equation(Mayne, P.W. 2006 Geomechanics and Geoengineering).

$$\Phi'(\text{deg})=17.6+11*\log(q_t/\sqrt{\sigma vo' * \sigma atm})$$

From this equation the friction angles are calculated and plotted vs depth. The raw data for the effective friction angle is in Appendix D Figure 42-44 but a summary of all the rounds is shown in Figure 13. As in most of the data collected, the top foot never shows any uniformity and this is because the sand is loose at the top and accurate reading are not being made with the CPT. Below one foot the friction angle stays constantly around 27° and 28° for the first round of testing. Round 2 testing, which was placed the same way as round 1, is almost identical to round 1. The friction angle in round 2 is around 26° the entire way down and like round 1 will also seem to be behaving similarly to a low density silica sand. Round 3 of testing aimed at getting a high density sand reaction. The raw data shows that the again the first foot of data is erratic but below that the friction angle is almost exactly 39° all the way down.

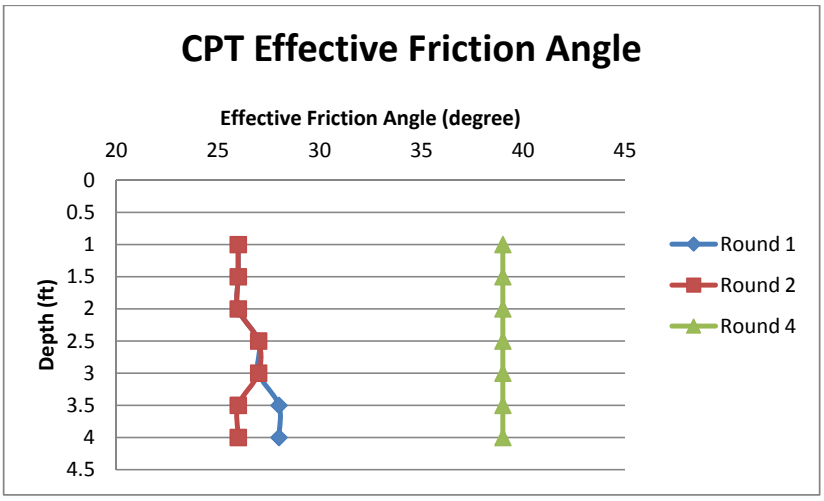

Figure 13:CPT Effective Friction Angle

5.2.2 Relative Density

To make sure the sand is uniform the relative density was found using the CPT data. A recent interpretation from ASCE GSP 119 by Jamiolkowski in 2001 was initially used.

$$D_R=100*[.268*\ln((q_t/\sigma_{atm})/(\sqrt{\sigma vo'/\sigma atm}))-.675]$$

When using this interpretation the data for rounds 1 and 2 were both negative which is not possible. But when used with the high density sand in round 3 the data is almost constant around 50% below 1 foot (Figure 14) which shows that the sand is uniform throughout the box. Since the interpretation worked for the high density sand but not the low density sand then it was determined that the interpretation may not work for the low density sand.

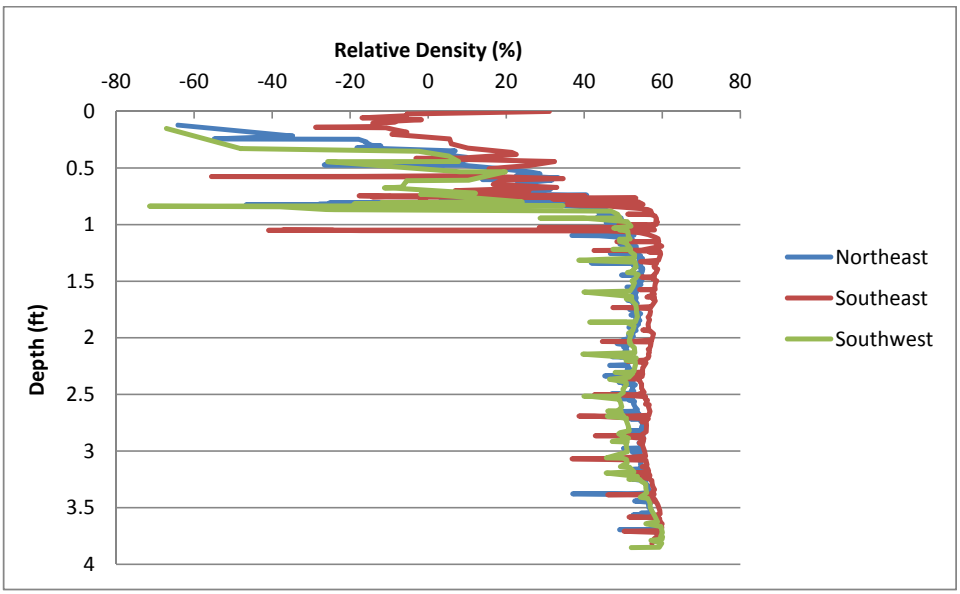

Figure 14:Round 3 Relative Density (Jamiolkowski 2001)

Since the first interpretation did not work for the low density sand a second interpretation was used from the 11th International Conference on Soil Mechanics and Foundation Engineering in San Francisco. This interpretation was from Jamiolkowski, Ladd, Germaine and Lancellotta.

$$D_R=-98+56\log(q_c/\sigma_{vo}'^{0.5})$$

The same thing occurs with this interpretation as the initial interpretation for rounds 1 and 2. The low density must not give accurate enough reading to use the relative density equations. For round 3 the relative density was consistent again but this time around 15%(Figure 15). With this it cannot be determined what the actual relative density is but that is not needed for this analysis. Both interpretations show a constant relative density which shows that the sand in round 3 is uniform

throughout the entire box, meeting the second objective of this testing. The graphs for round 1 and 2 relative densities are in Appendix D Figure 45-46.

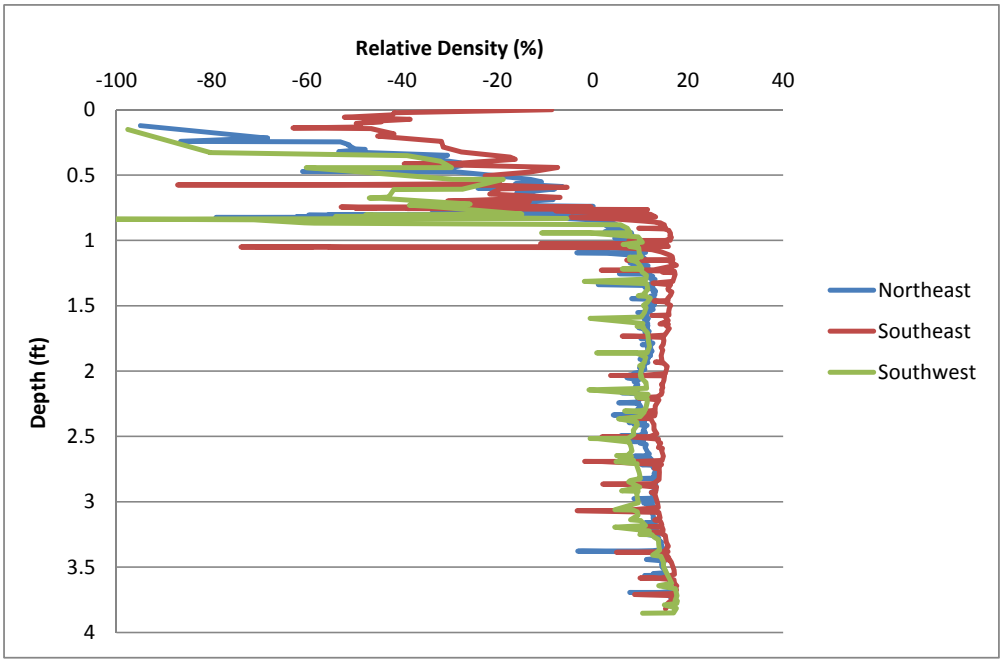

Figure 15:Round 3 Relative Density (Jamiolkowski, Ladd, Germaine and Lancellotta 1985)

6.0 Summary of Results

The data from this research has provided a good understanding of what the sand is like and also the shear strength of the sand. It started with the sieve analysis that matched up to the data provided by the U.S. Silica Company. The sand was a very well graded material that was all smaller than a sieve size of 20.

The density testing showed that the sand could range in density from 94.4 pcf to 115.5 pcf. For the testing in the lab the density that was aimed at was at 100 pcf for the low density and 106 pcf for the high density. It showed during the triaxial testing where the average low density was 99.2 pcf while the average high density was 105.1 pcf. Though the high density wasn't as high as wanted it still gave an accurate representation of the high density sand. During the scale model testing the sand in the first two rounds of testing that was aimed at achieving a low density, the density molds had an average density of 109.8 pcf which is fairly high but later data showed that the sand behaved more like a low density sand. The accuracy of the density molds do not seem to be very high.

The shear strength was a main objective of this research. From the data, similarities were looked for and the data seemed to show some. The direct shear testing would best show how the soil shear strength would behave in a small scale testing while the triaxial test give a better representation of a full scale test shear strength. The cone penetration test data was from the small scale test and was very similar to the direct shear testing done which is what the data should be like. As seen in Figure 16 the direct shear testing and cone penetration testing seemed to be exactly the same for the high density and low density. This was expected since the direct shear should give a more accurate showing of how the sand would behave in a small scale test. The low density triaxial test seemed to have a much higher friction angle than the direct shear and cone penetration but since triaxial tests are suppose to give a better representation of what a full scale test then this will have to be a consideration when looking at the test data. The high density had similar friction angles in the direct shear, triaxial and cone penetration testing. This shows that the friction angle for the sand seems to have a maximum around 39^{o}. With this data the small scale tests can be used more effective in relating to how a micropile will behave in a full scale test.

Low Density			High Density	
Direct Shear	29.9^{o}		Direct Shear	39.1^{o}
Triaxial	35.1^{o}		Triaxial	39.4^{o}
CPT	26^{o}-28^{o}		CPT	39^{o}

Figure 16:Summary of Friction Angles

7.0 Acknowledgments

I would like to thank Ronaldo Luna for giving me this opportunity that most others would not get. Without him I would never have gotten this sort of insight, experience and knowledge into geotechnical engineering and researching. He was also a major help in leading me in which direction to go and instrumental in showing me how researching is undertaken. I would also like to thank Shuying Wang for his support during my laboratory testing and the patience and guidance he gave to help me with this research. Kyle Kershaw was a major contributor to helping me with all of my research. Without him and giving me the chance to work with him on his research this would not be possible. He was always there to lend me advise and answer questions I was unfamiliar about. The geotech faculty and graduate students were also very supportive throughout this entire process. Finally I would like to thank my family who always have been supportive.

8.0 References

Bardet, Jean-Pierre (1997). *Experimental Soil Mechanics,* Prentice Hall, Upper Saddle River, NJ.

Coduto, Donald P. (2010). *Geotechnical Engineering: Principles and Practices Second Edition,*Prentice Hall, Upper Saddle River, NJ.

Fratta, Dante ,Aguettant, Jennifer ,Roussel-Smith, Lynne (2007). *Introduction to Soil Mechanics Laboratory Testing*. CRC Press, Boca Raton, FL.

Holtz, Robert D., Kovacs, William D. (1981). *An Introduction to Geotechnical Engineering*, Prentice Hall, Englewood Cliffs, NJ.

Jamiolkowski (2001). ASCE GSP 119

Jamiolkowski, Ladd, Germaine, and Lancellotta (1985). 11th International Conference on Soils Mechanics and Foundation Engineering, Vol. 1, San Francisco, 57-153

Lambe, T. William and Whitman, Robert V. (1969). *Soil Mechanics,* Johny Wiley & Sons, New York.

Mayne, P. W. (2006) 'The Second James K. Mitchell Lecture Undisturbed sand strength from seismic cone tests', Geomechanics and Geoengineering, 1:4, 239 - 257

Mayne P.W., *Geotechnical Site Characterization by Seismic Piezocone.* GeoMO 2009

Mayne, P.W., Mitchell, J.K., Auxt, J.A., and Yilmaz, R. (1995). U.S. National Report on CPT, *Proceedings, International Symposium on Cone Penetration Testing* (CPT'95), Vol. 1, Swedish Geotechnical Society Report No. 3:95, Linkoping, 263-276

Transportation Research Board of the National Academies. National Cooperative Highway Research Program Synthesis 368: Cone Penetration Testing (2007).

Test Method Designation

ASTM D 422: Standard Test Method of Sieve Analysis of Soils

ASTM D 4253 Standard Test Methods for Maximum Index Density and Unit Weight of Soils Using a Vibratory Table

ASTM D 4254: Standard Test Mehods for Minimum Index Density and Unit Weight of Soils and Calculation of Relative Density

ASTM D 3080: Standard Test Method for Direct Shear Test of Soils Under Consolidated Drained Conditions

Appendix A:Product Data

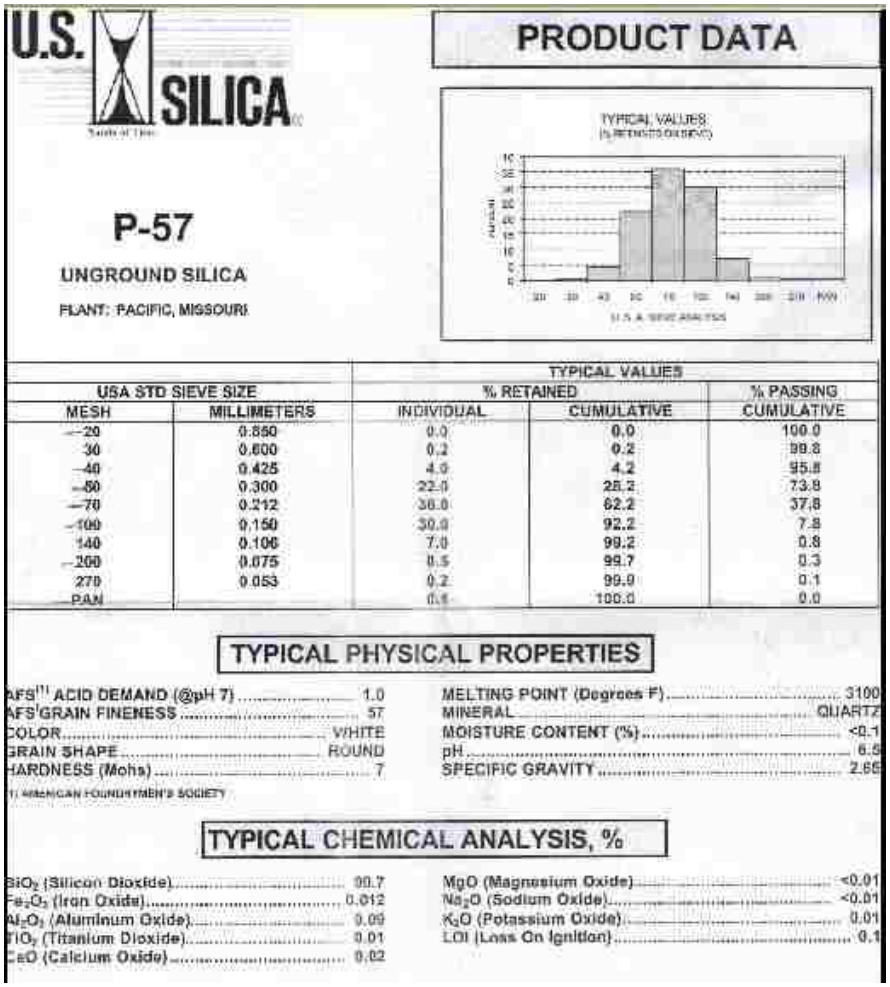

U.S. SILICA

PRODUCT DATA

P-57

UNGROUND SILICA

PLANT: PACIFIC, MISSOURI

USA STD SIEVE SIZE		TYPICAL VALUES % RETAINED		% PASSING
MESH	MILLIMETERS	INDIVIDUAL	CUMULATIVE	CUMULATIVE
–20	0.850	0.0	0.0	100.0
30	0.600	0.2	0.2	99.8
–40	0.425	4.0	4.2	95.8
–50	0.300	22.0	26.2	73.8
–70	0.212	36.0	62.2	37.8
–100	0.150	30.0	92.2	7.8
140	0.106	7.0	99.2	0.8
–200	0.075	0.5	99.7	0.3
270	0.053	0.2	99.9	0.1
PAN		0.1	100.0	0.0

TYPICAL PHYSICAL PROPERTIES

AFS[1] ACID DEMAND (@pH 7)	1.0	MELTING POINT (Degrees F)	3100
AFS GRAIN FINENESS	57	MINERAL	QUARTZ
COLOR	WHITE	MOISTURE CONTENT (%)	<0.1
GRAIN SHAPE	ROUND	pH	6.5
HARDNESS (Mohs)	7	SPECIFIC GRAVITY	2.65

[1] AMERICAN FOUNDRYMEN'S SOCIETY

TYPICAL CHEMICAL ANALYSIS, %

SiO_2 (Silicon Dioxide)	99.7	MgO (Magnesium Oxide)	<0.01
Fe_2O_3 (Iron Oxide)	0.012	Na_2O (Sodium Oxide)	<0.01
Al_2O_3 (Aluminum Oxide)	0.09	K_2O (Potassium Oxide)	0.01
TiO_2 (Titanium Dioxide)	0.01	LOI (Loss On Ignition)	0.1
CaO (Calcium Oxide)	0.02		

Figure 17:Sand Product Data

Appendix B:Direct Shear

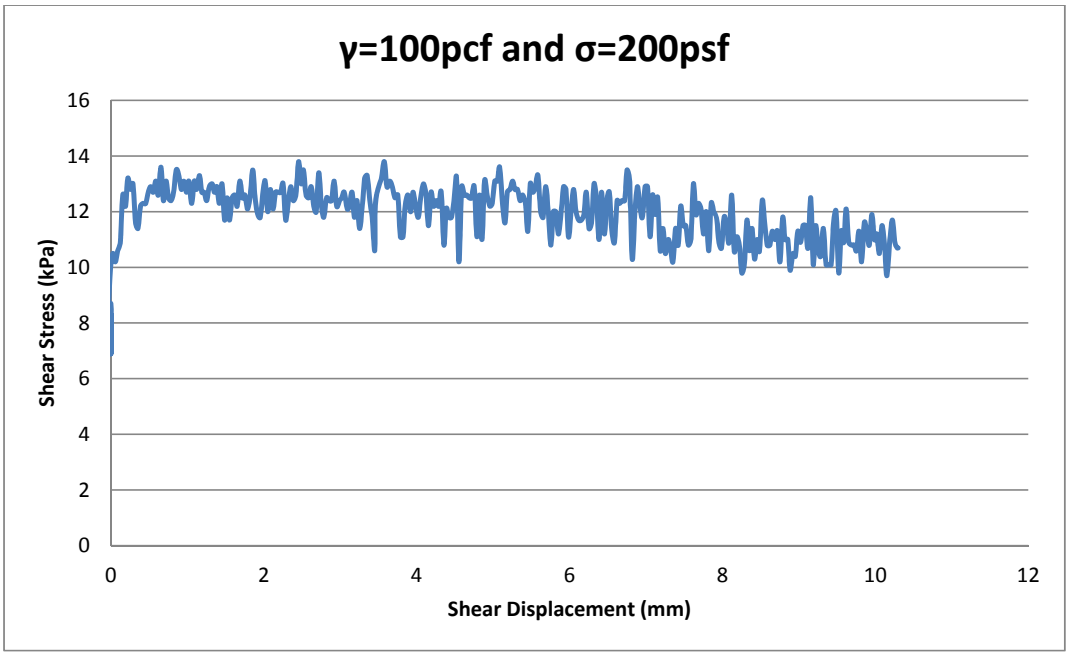

Figure 18:Shear Stress vs Shear Displacement

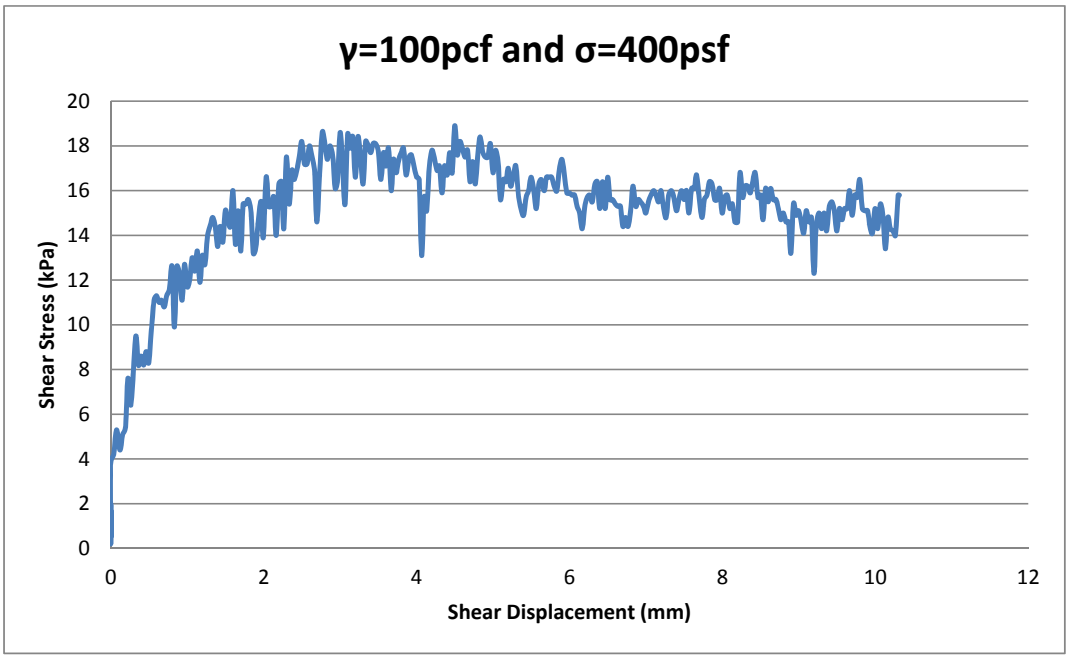

Figure 19:Shear Stress vs Shear Displacement

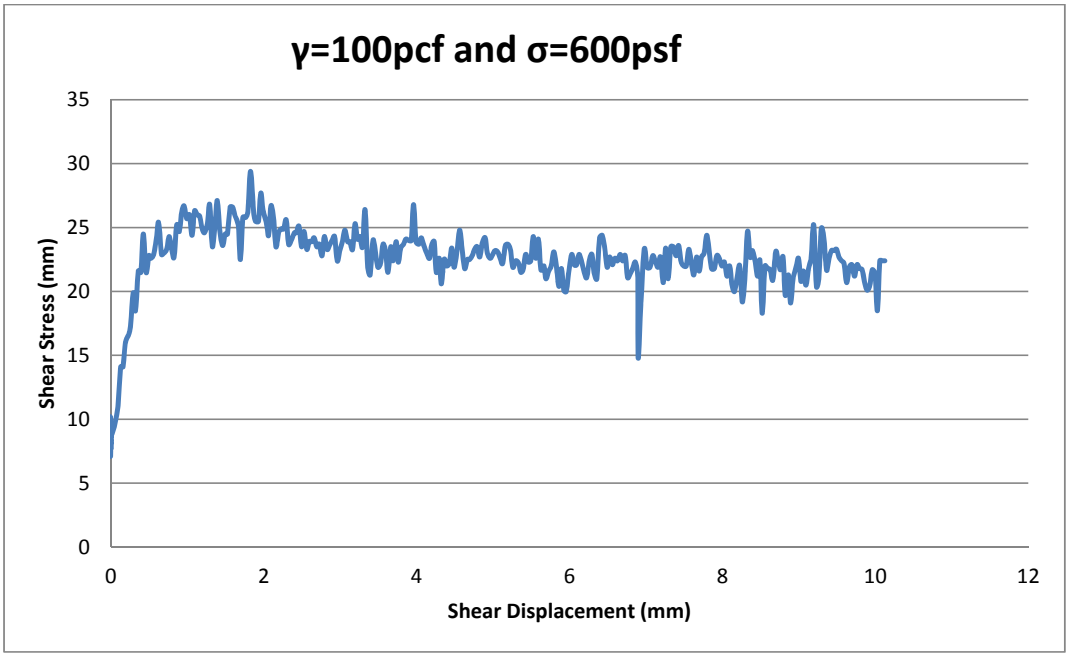

Figure 20:Shear Stress vs Shear Displacement

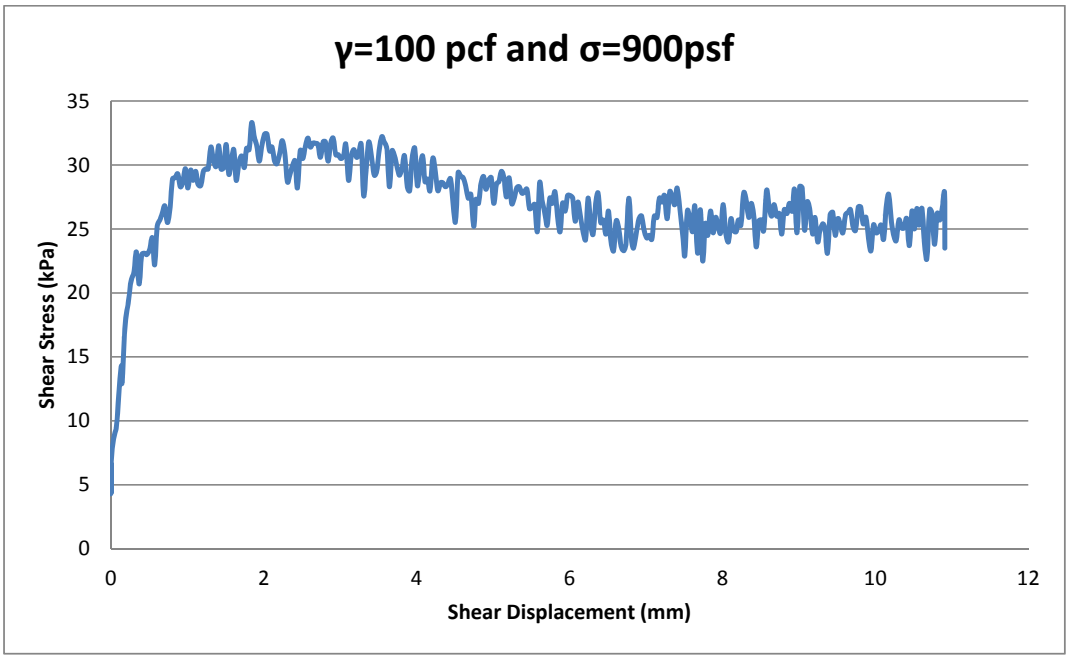

Figure 21:Shear Stress vs Shear Displacement

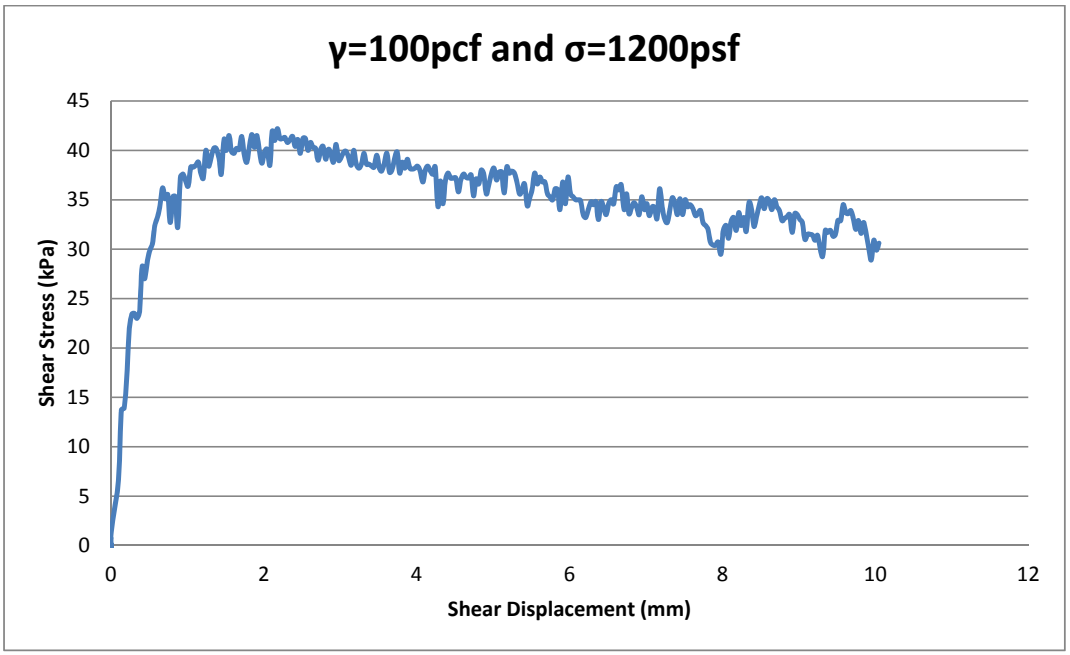

Figure 22:Shear Stress vs Shear Displacement

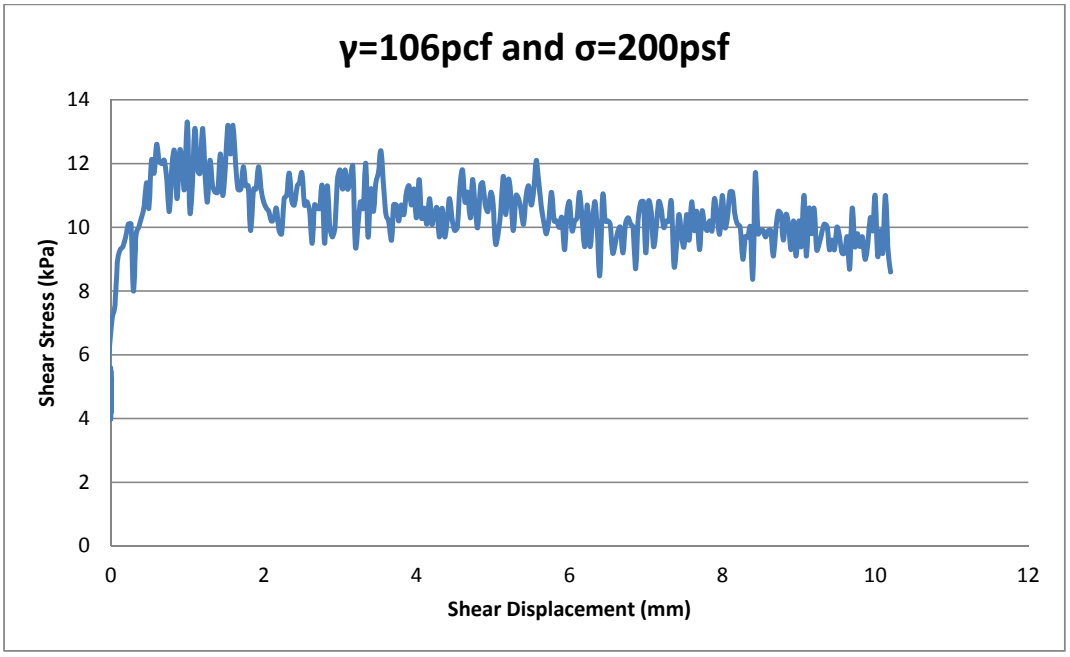

Figure 23:Shear Stress vs Shear Displacement

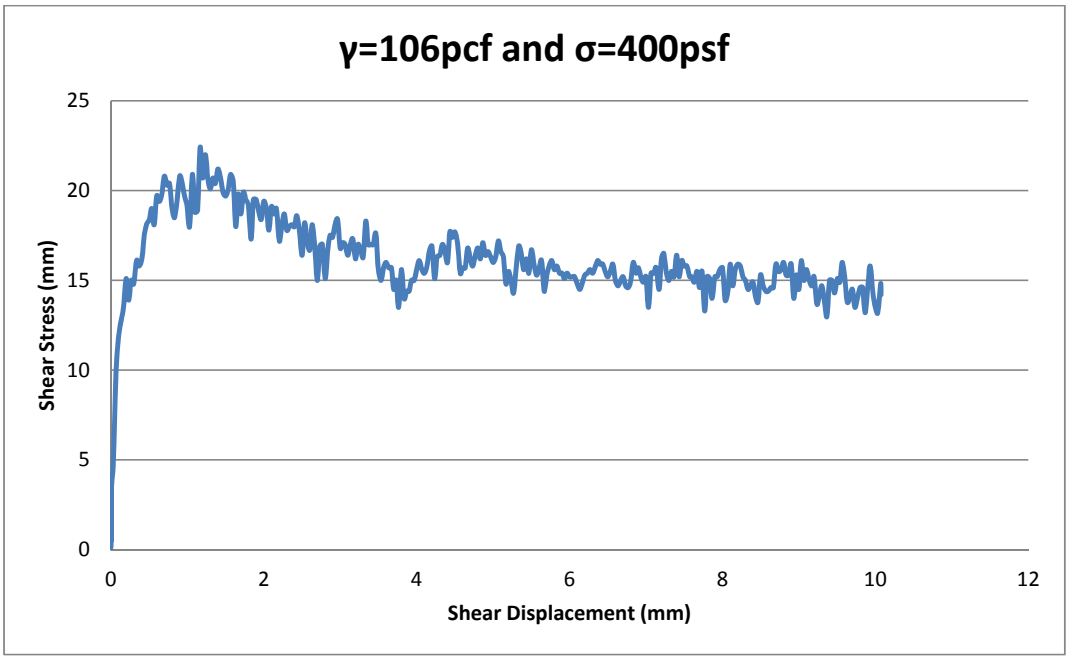

Figure 24:Shear Stress vs Shear Displacement

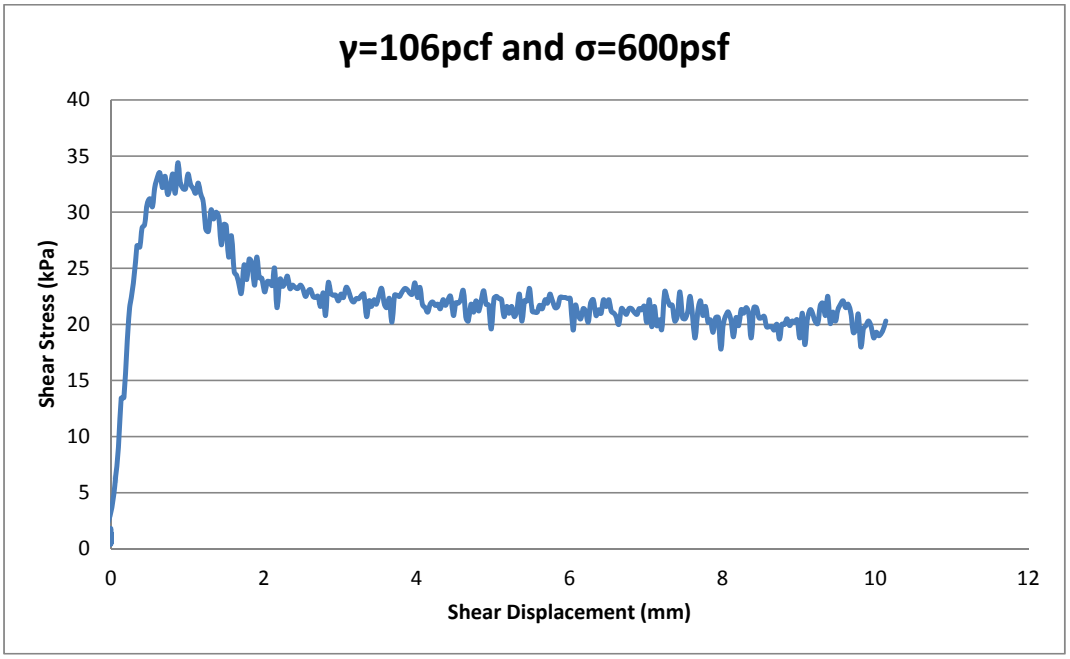

Figure 25:Shear Stress vs Shear Displacement

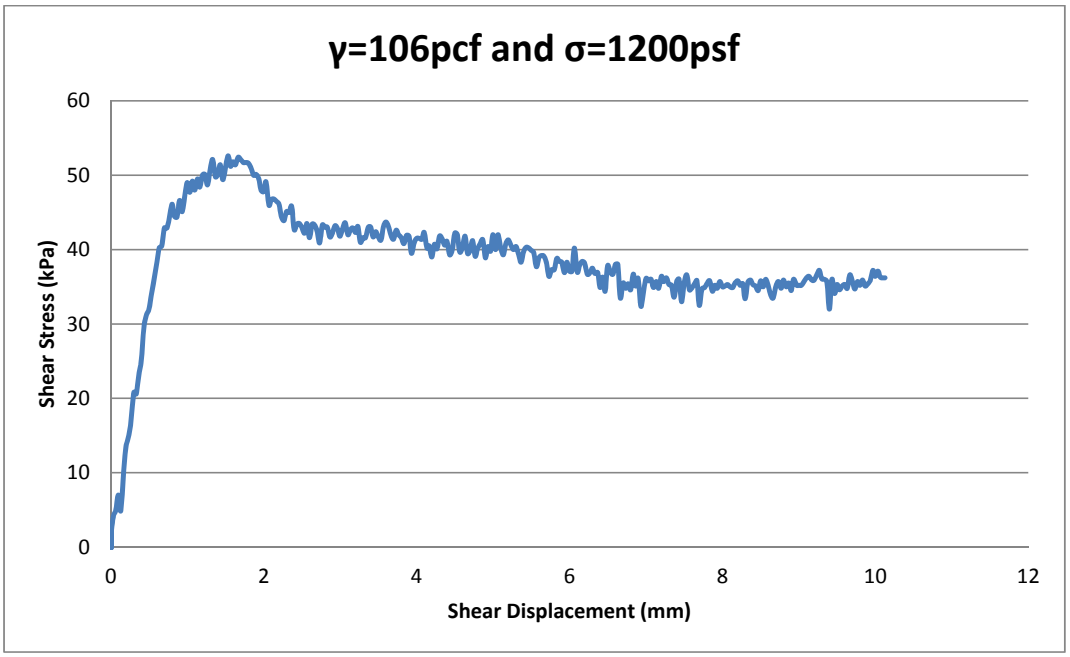

Figure 26:Shear Stress vs Shear Displacement

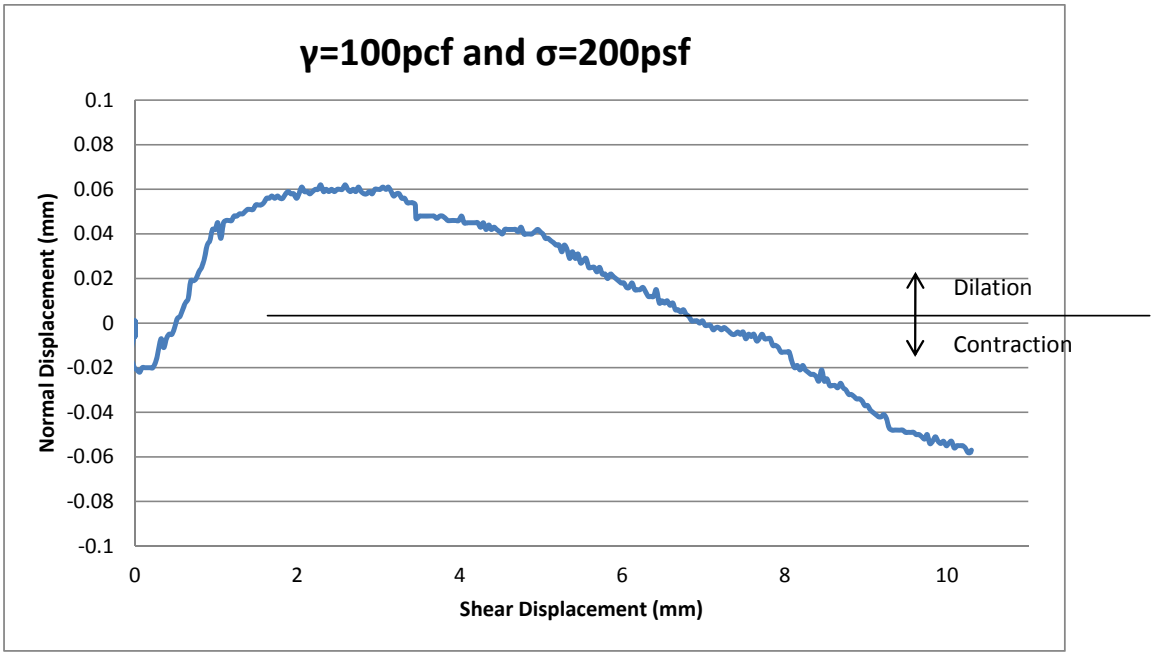

Figure 27:Normal vs Shear Displacement

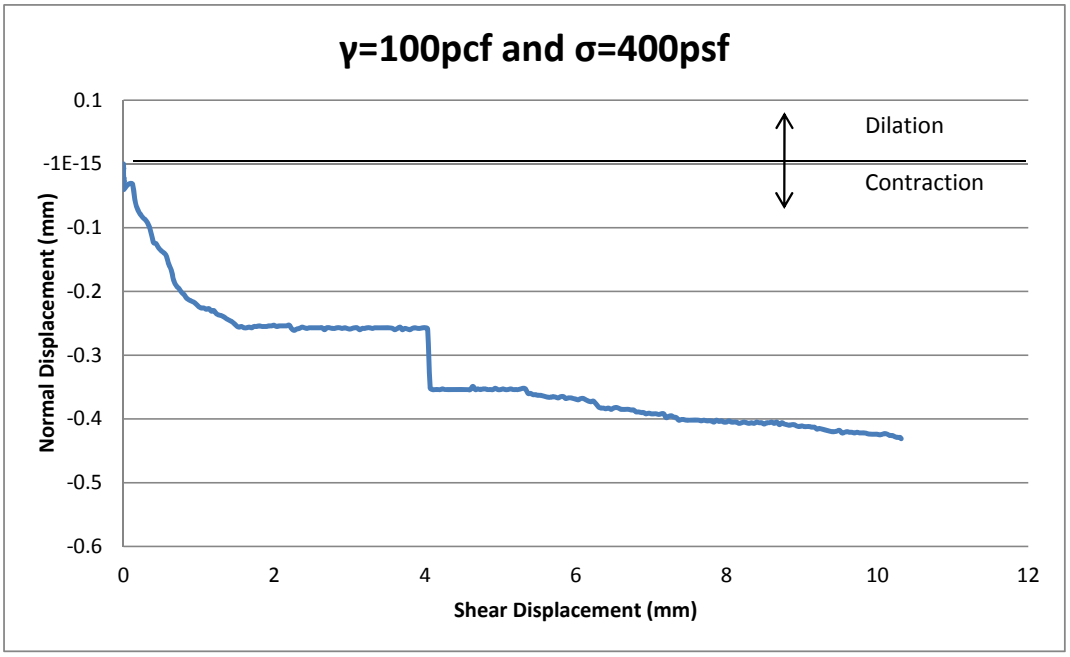

Figure 28:Normal vs Shear Displacement

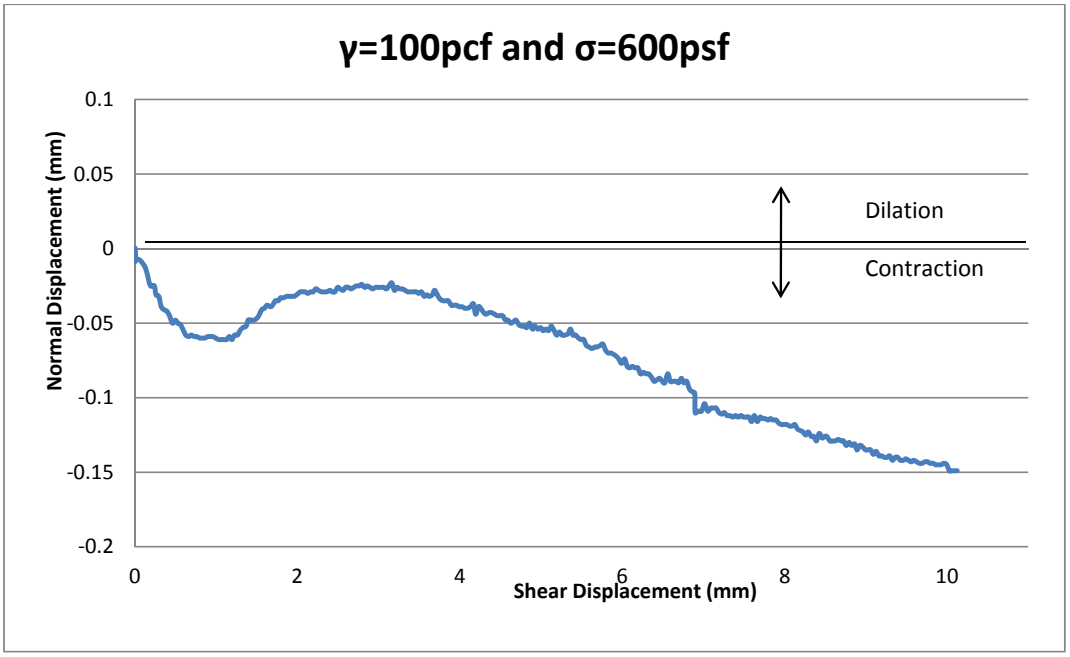

Figure 29:Normal vs Shear Displacement

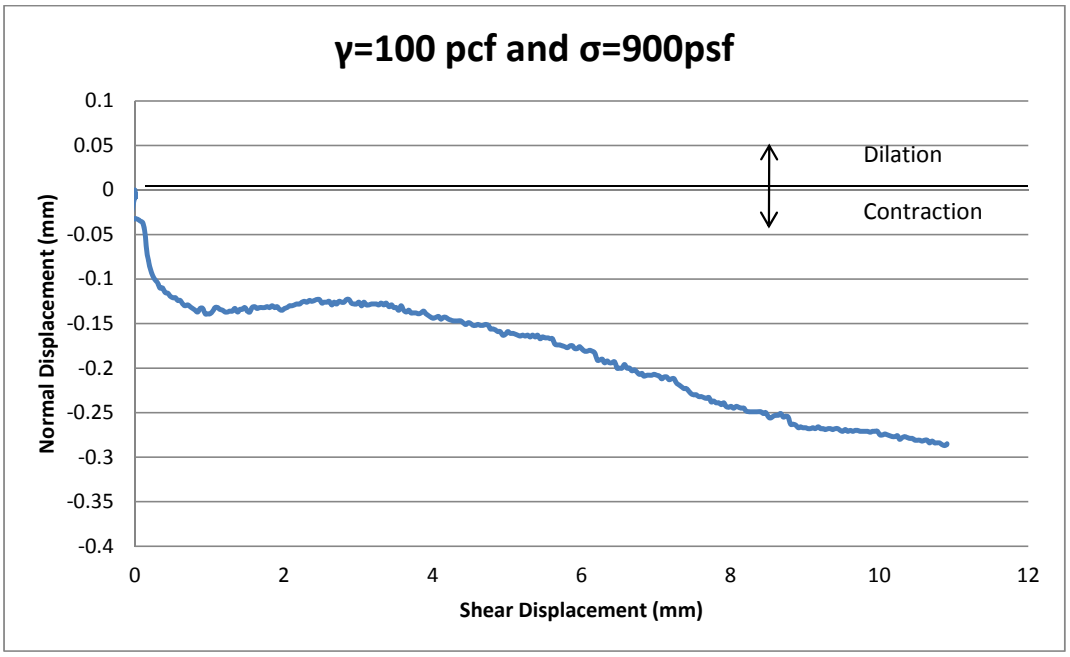

Figure 30:Normal vs Shear Displacement

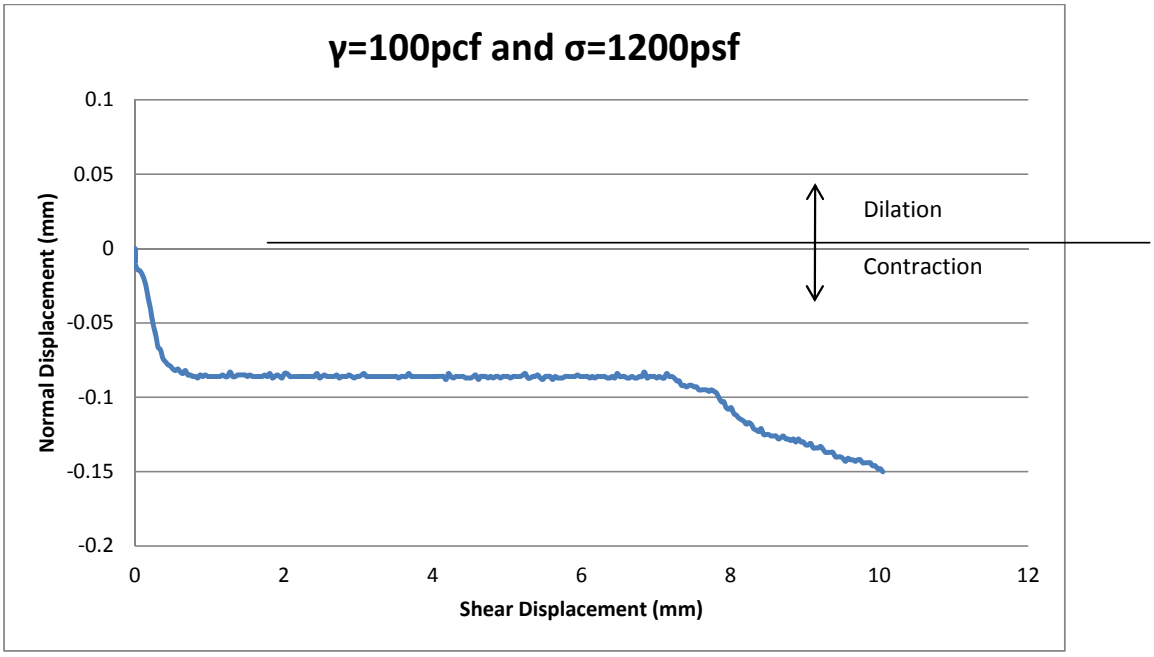

Figure 31:Normal vs Shear Displacement

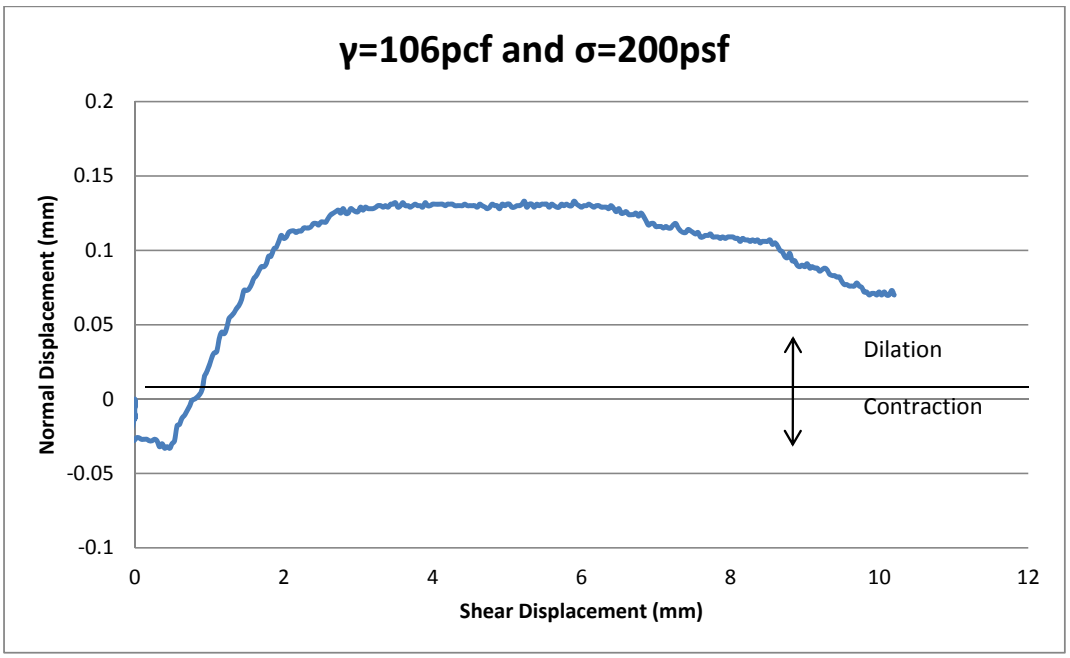

Figure 32:Normal vs Shear Displacement

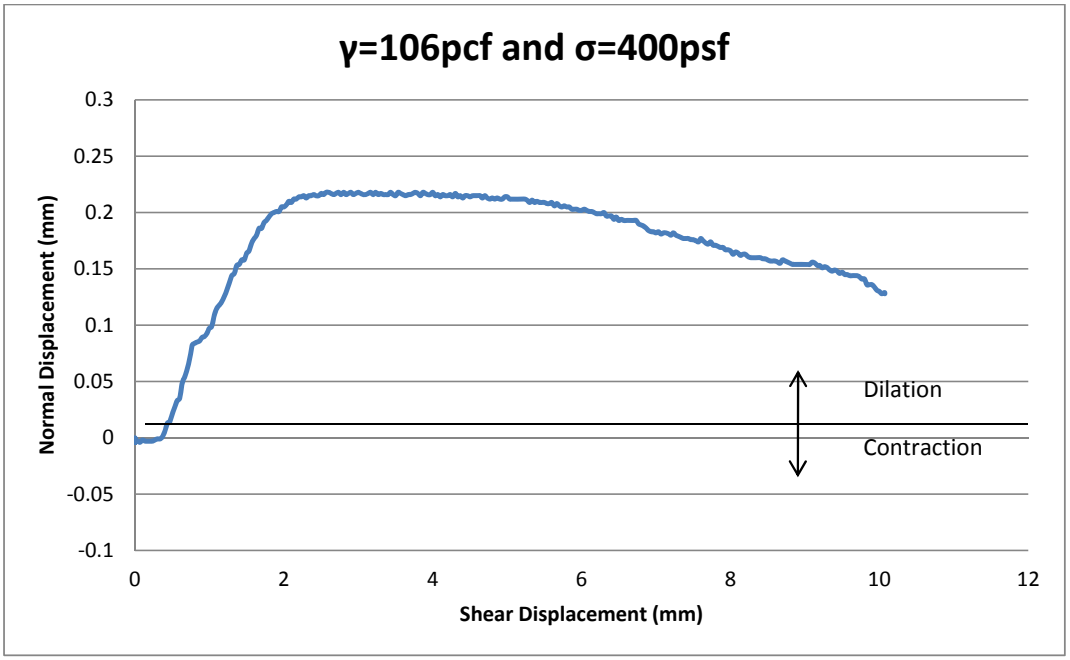

Figure 33:Normal vs Shear Displacement

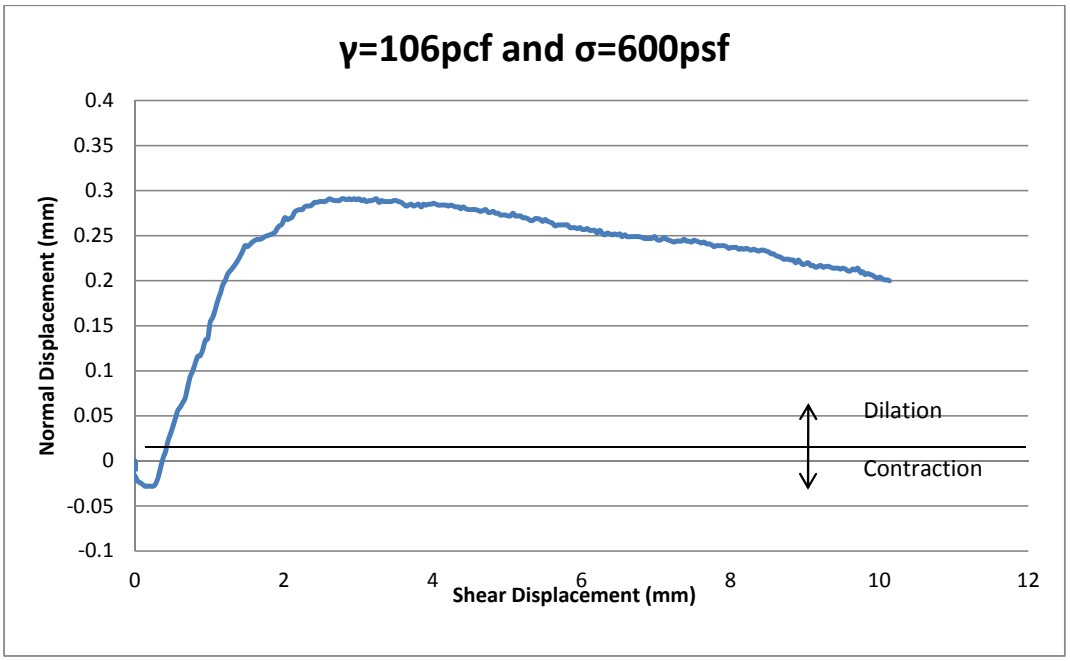

Figure 34:Normal vs Shear Displacement

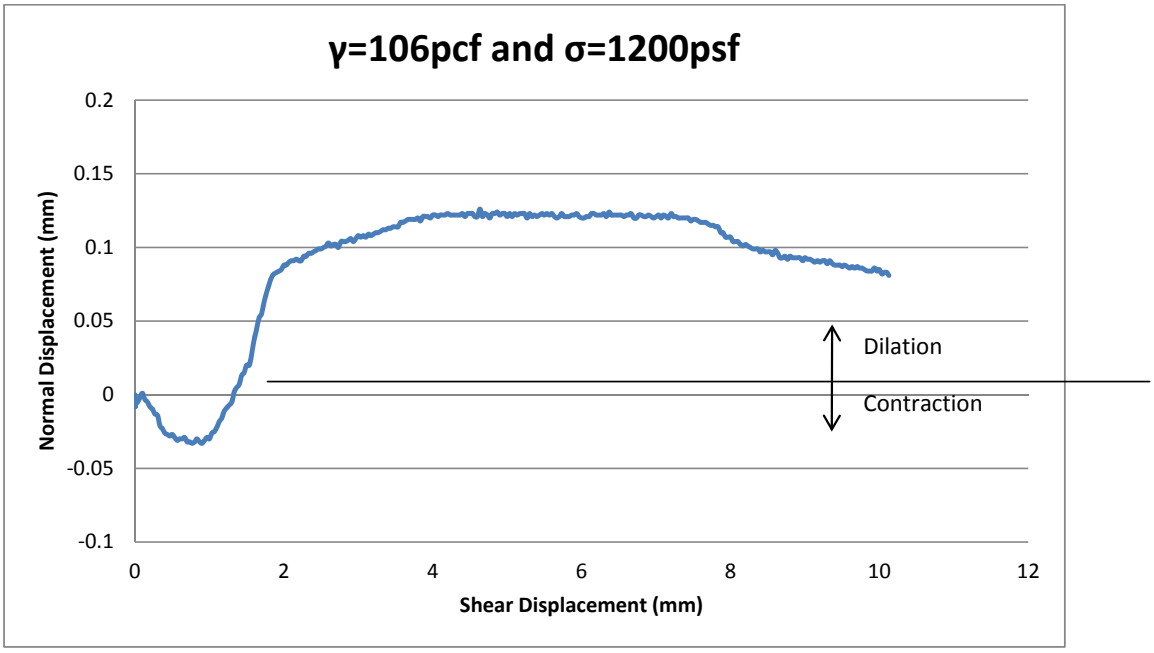

Figure 35:Normal vs Shear Displacement

Appendix C:Triaxial Data

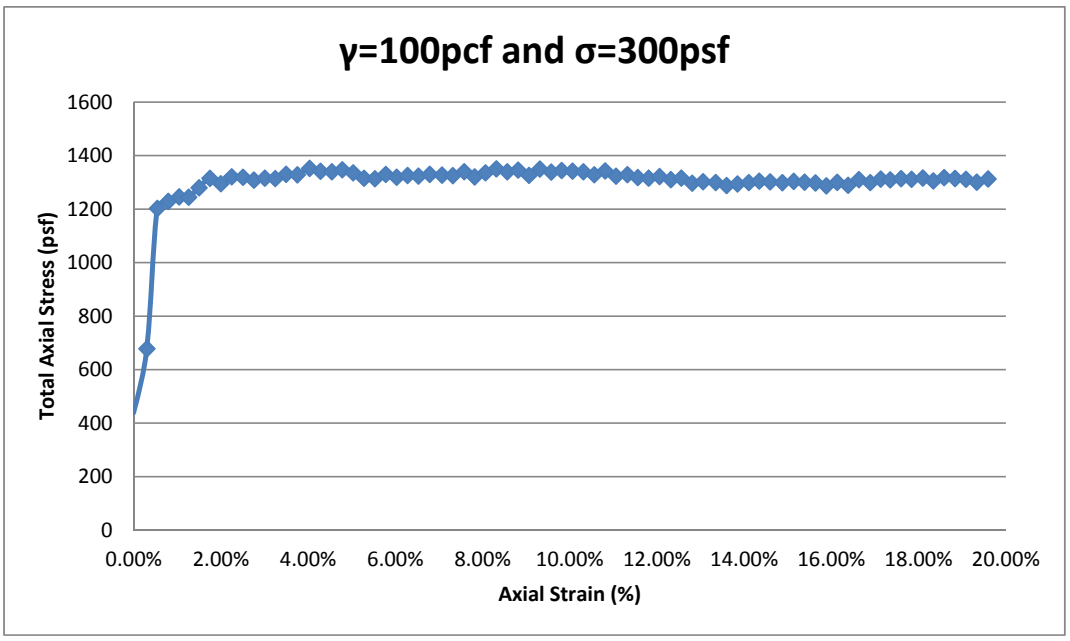

Figure 36:Total Axial Stress vs Axial Strain

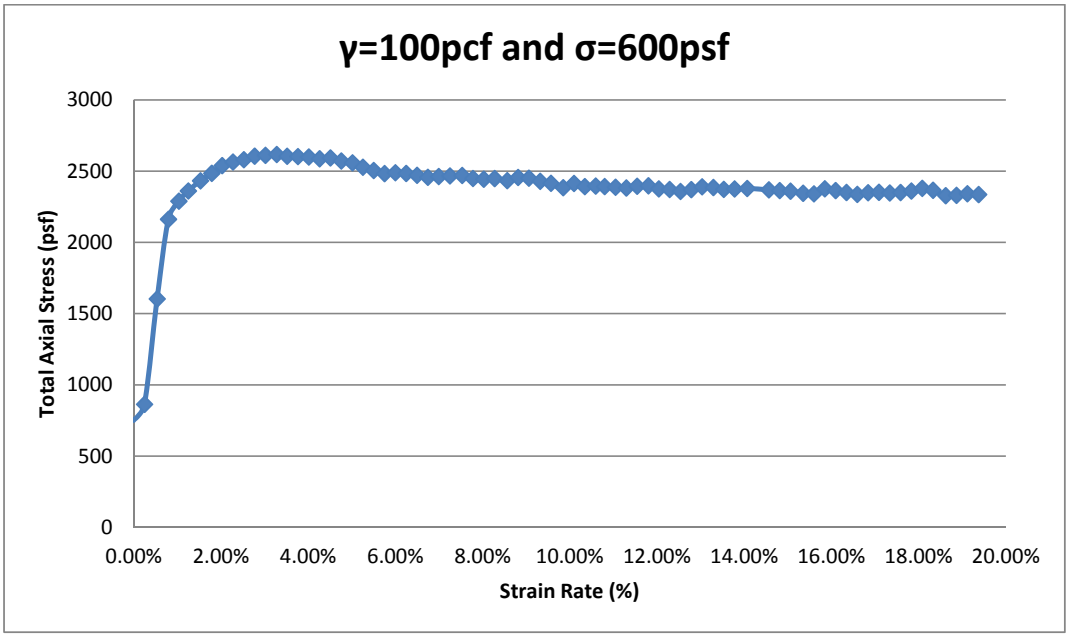

Figure 37:Total Axial Stress vs Axial Strain

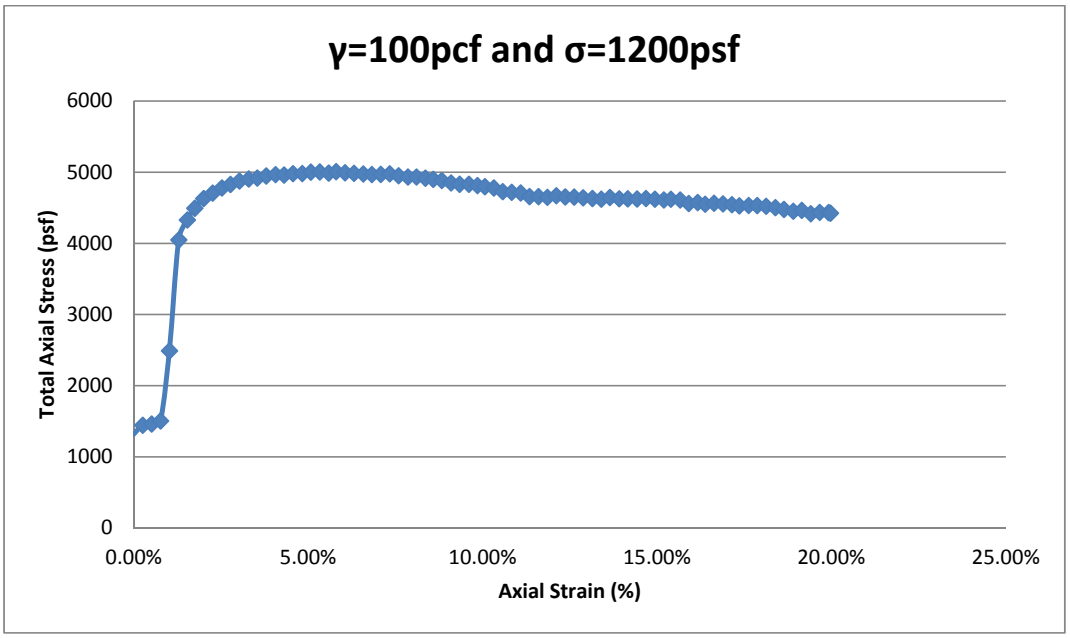

Figure 38:Total Axial Stress vs Axial Strain

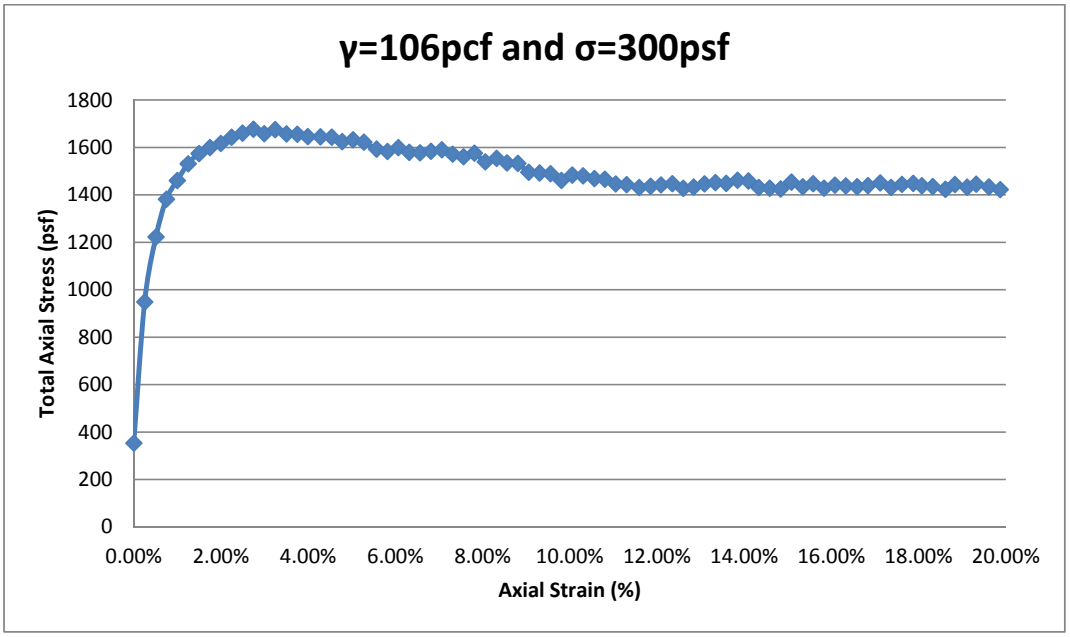

Figure 39:Total Axial Stress vs Axial Strain

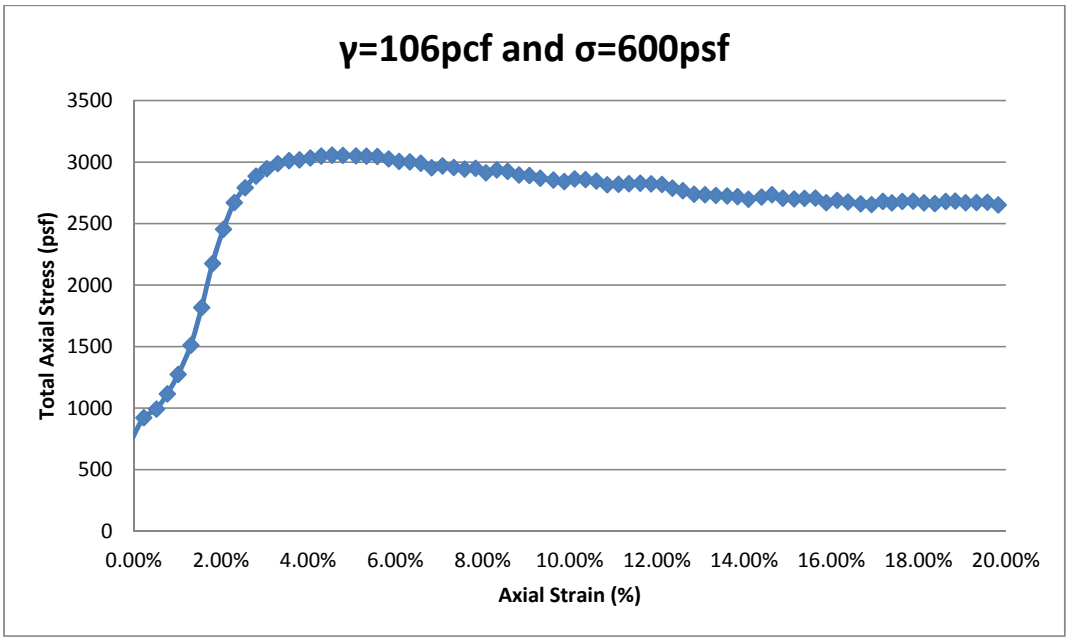

Figure 40:Total Axial Stress vs Axial Strain

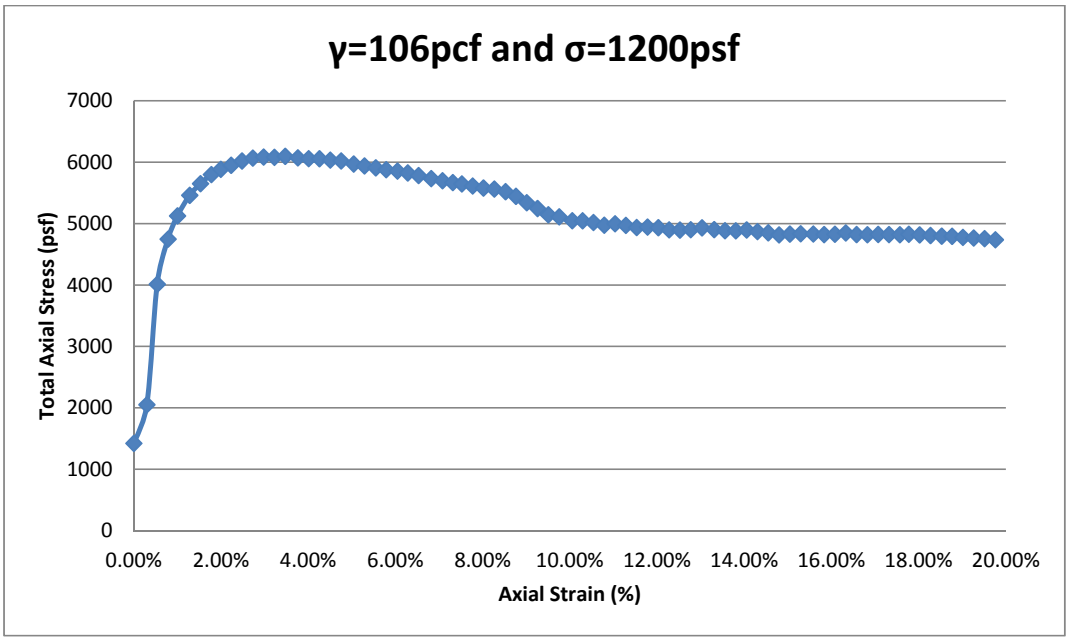

Figure 41:Total Axial Stress vs Axial Strain

Appendix D:CPT Data

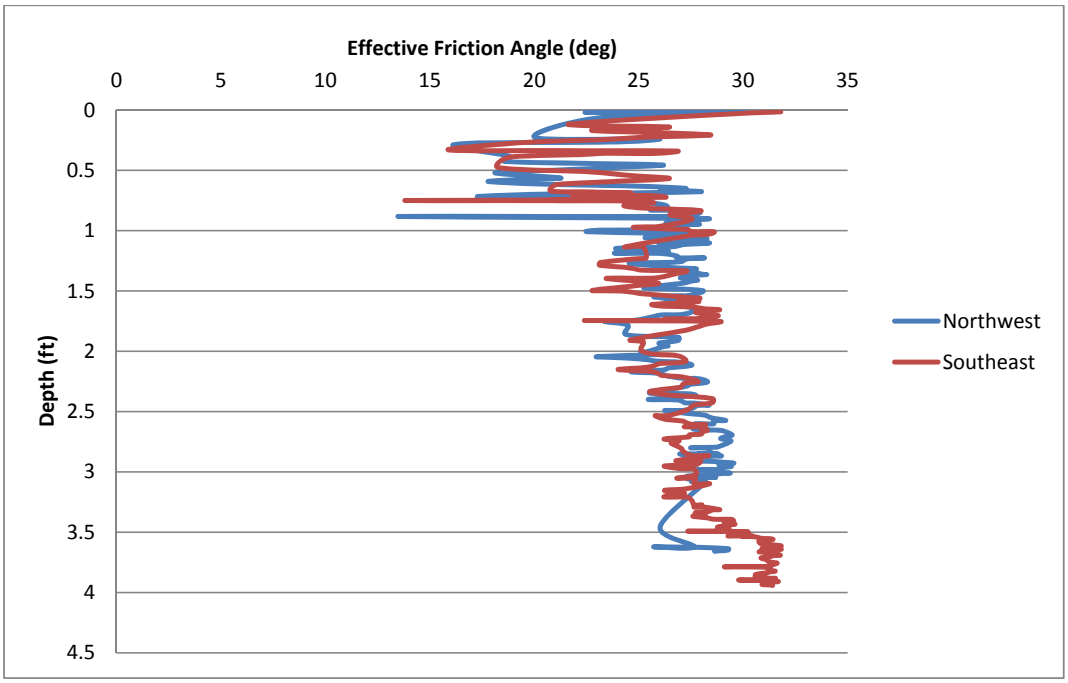

Figure 42:Round 1 Effective Friction Angle

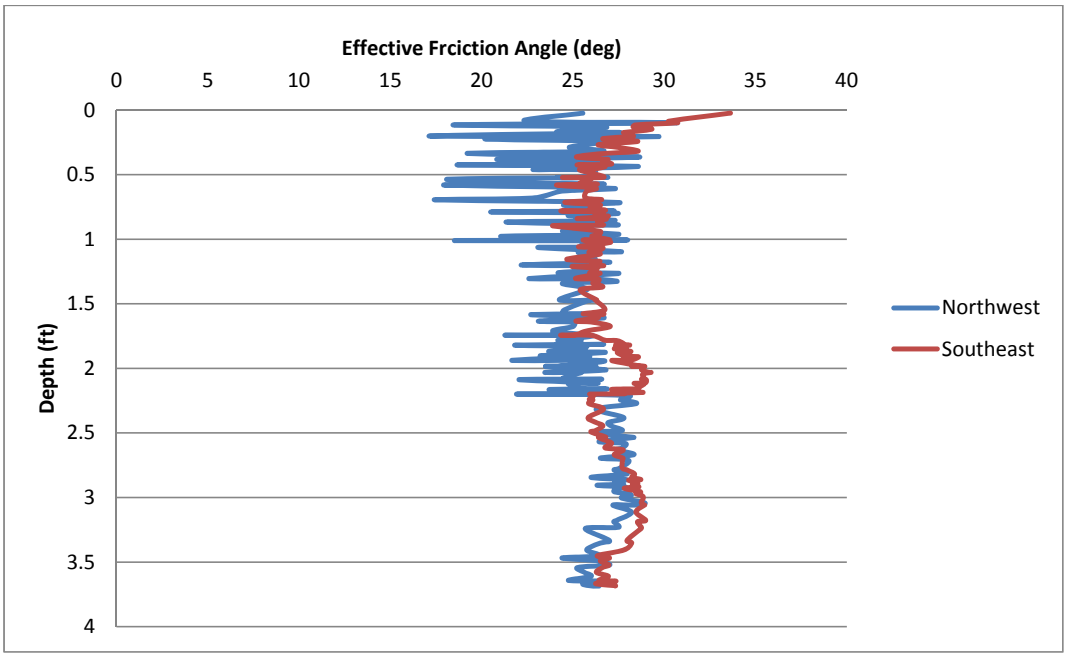

Figure 43:Round 2 Effective Friction Angle

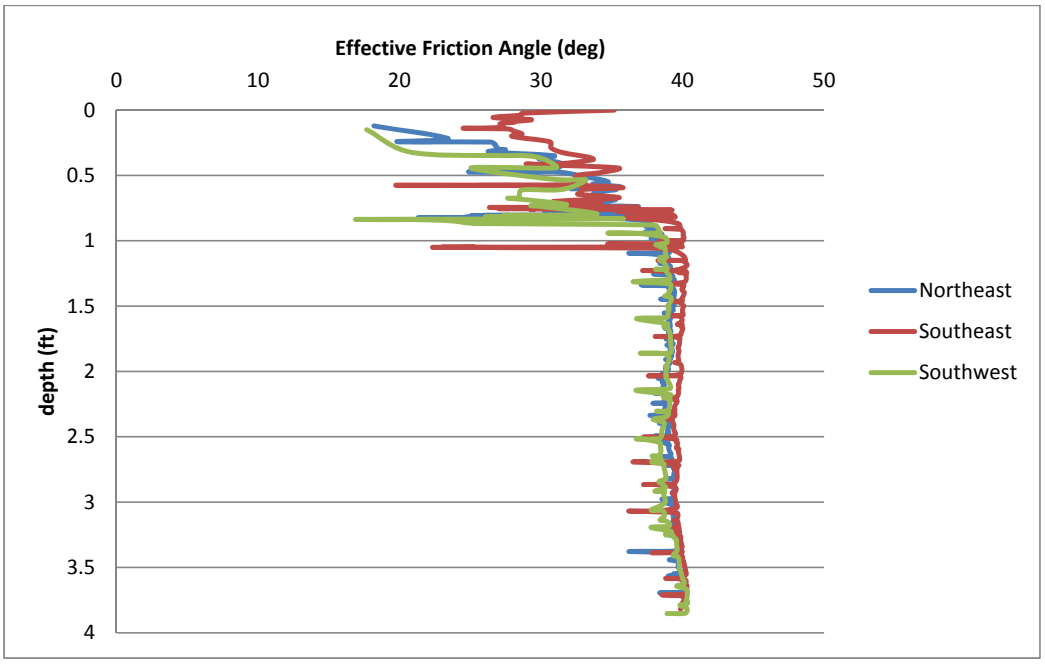

Figure 44:Round 3 Effective Friction Angle

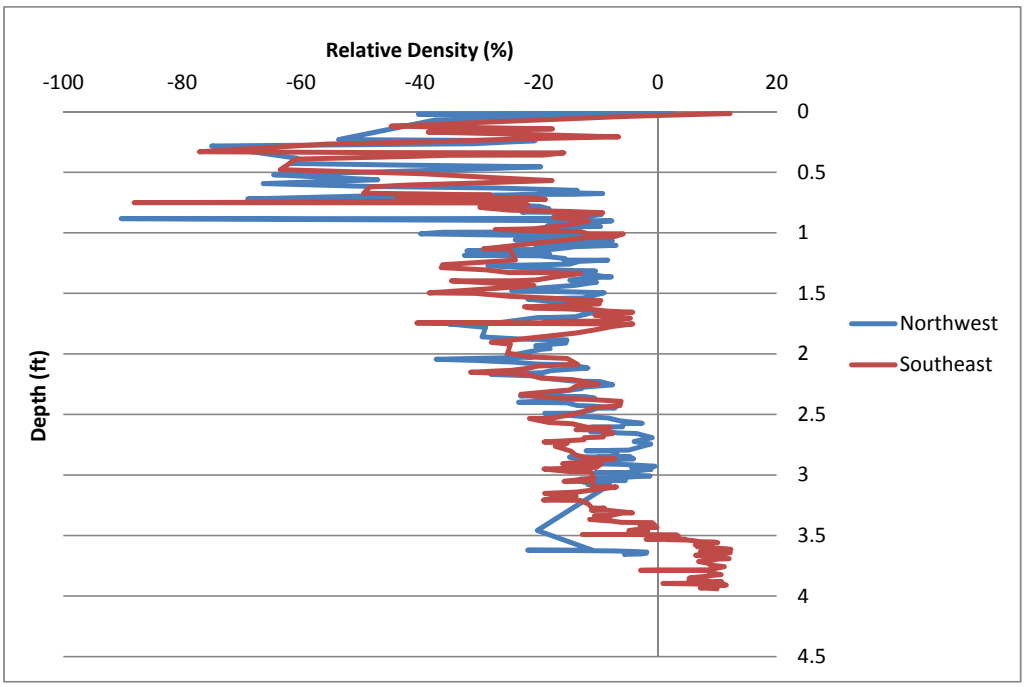

Figure 45:Round 1 Relative Density(Jamiolkowski 2001)

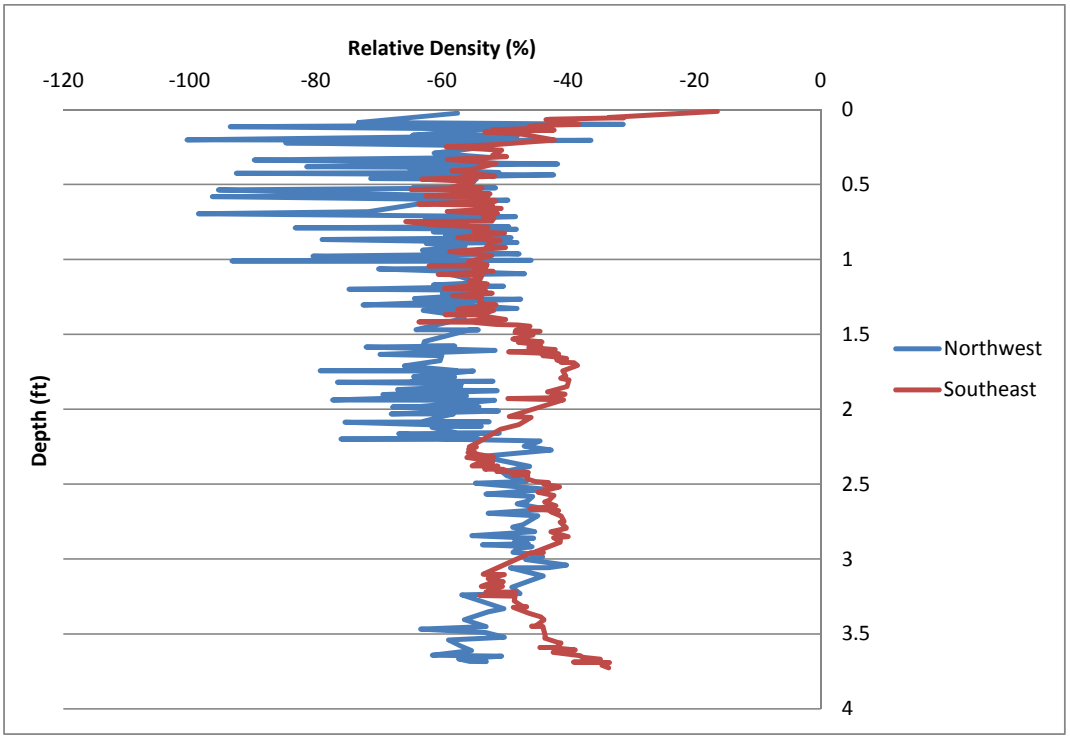

Figure 46:Round 2 Relative Density(Jamiolkowski 2001)

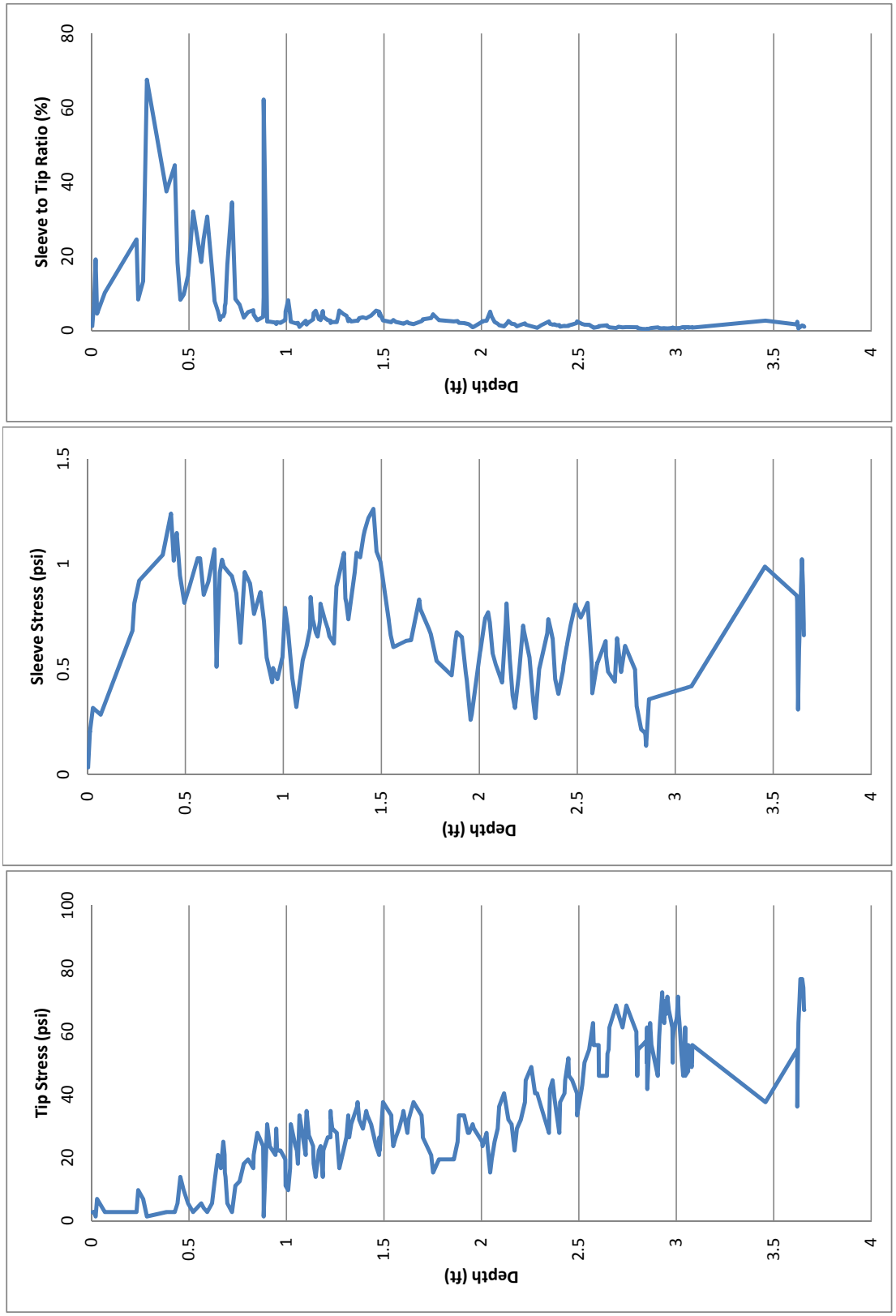

Figure 47:CPT #1 Round 1 Data

41

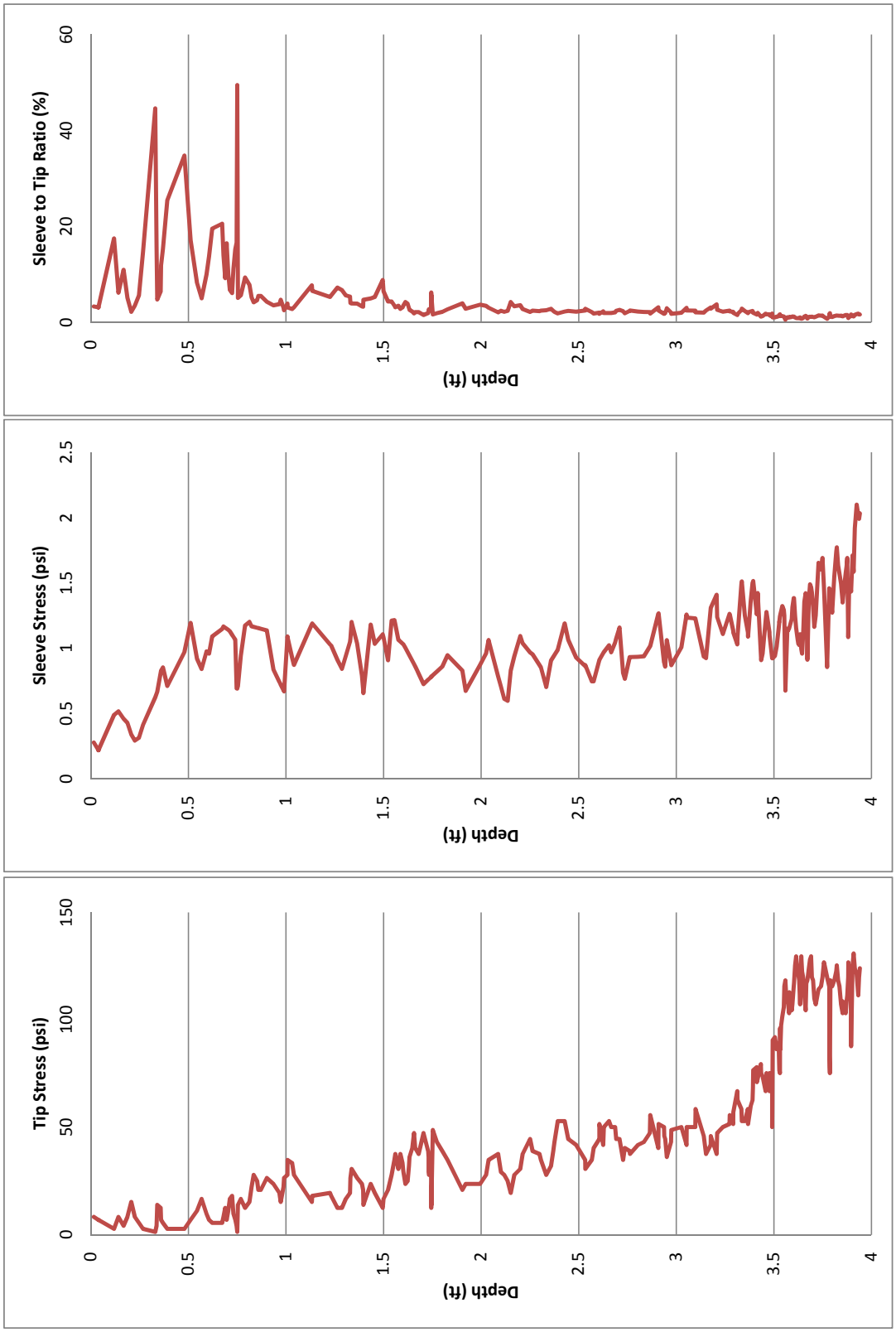

Figure 48:CPT #2 Round 1 Data

42

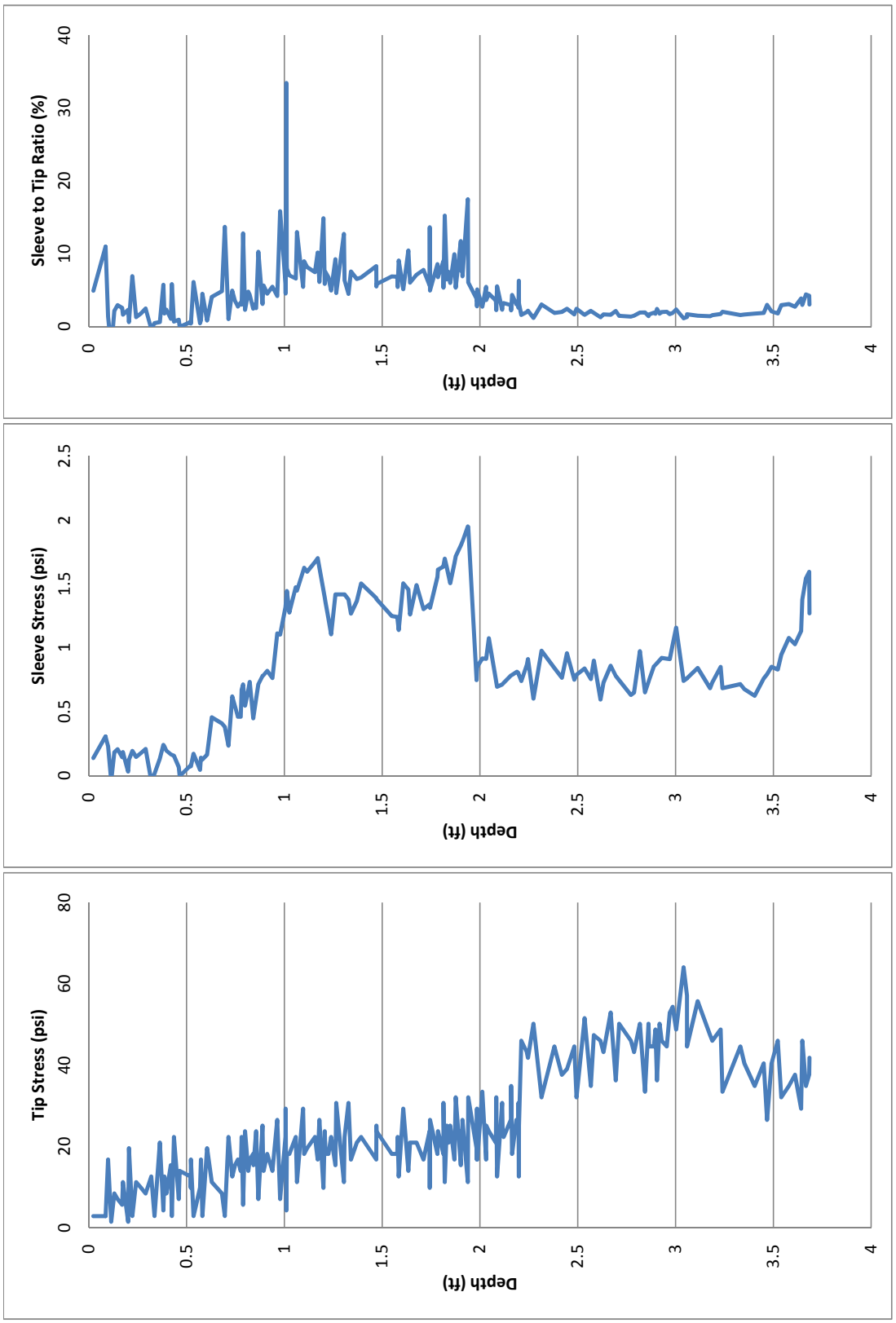

Figure 49:CPT #1 Round 2 Data

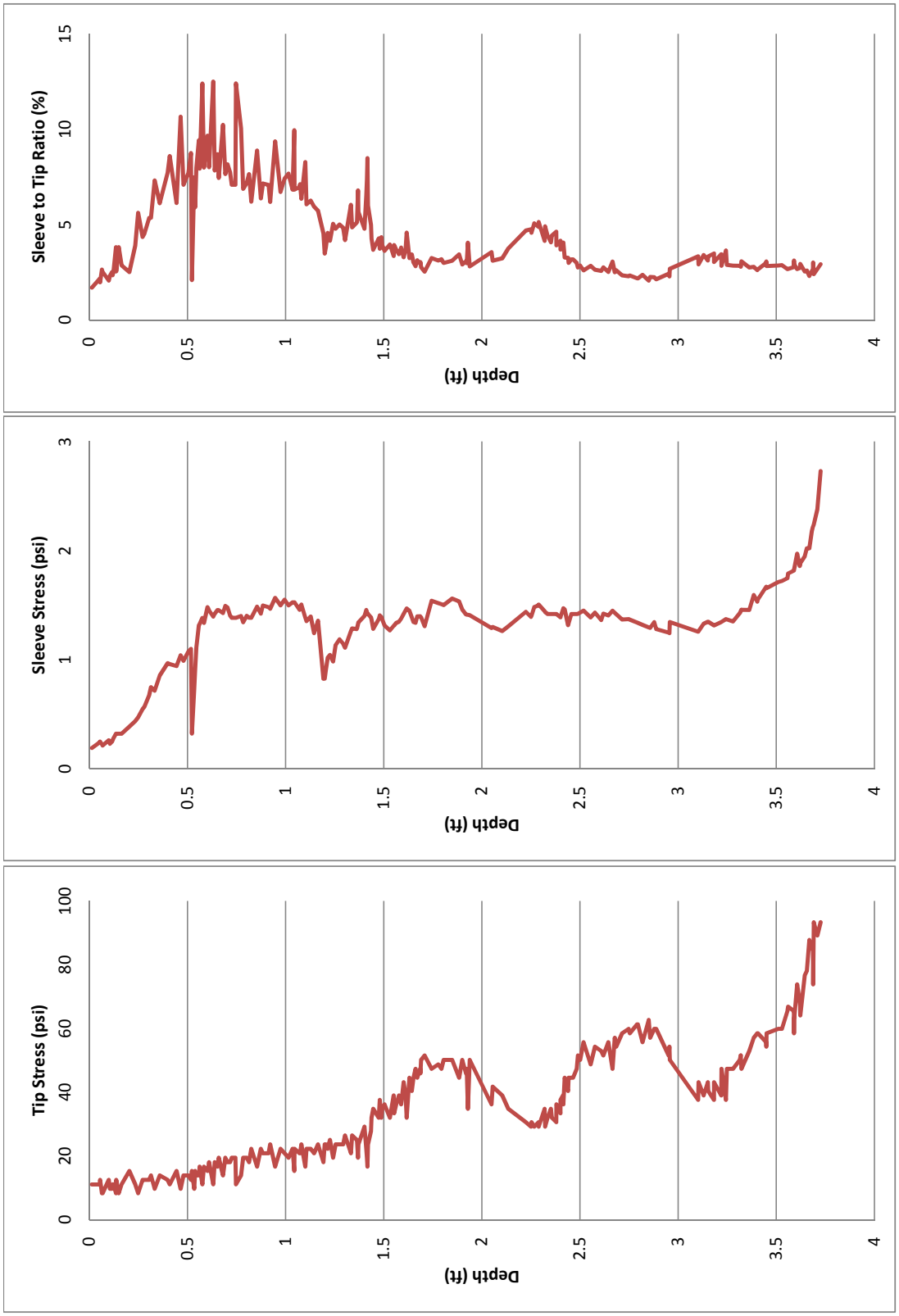

Figure 50:CPT #2 Round 2 Data

44

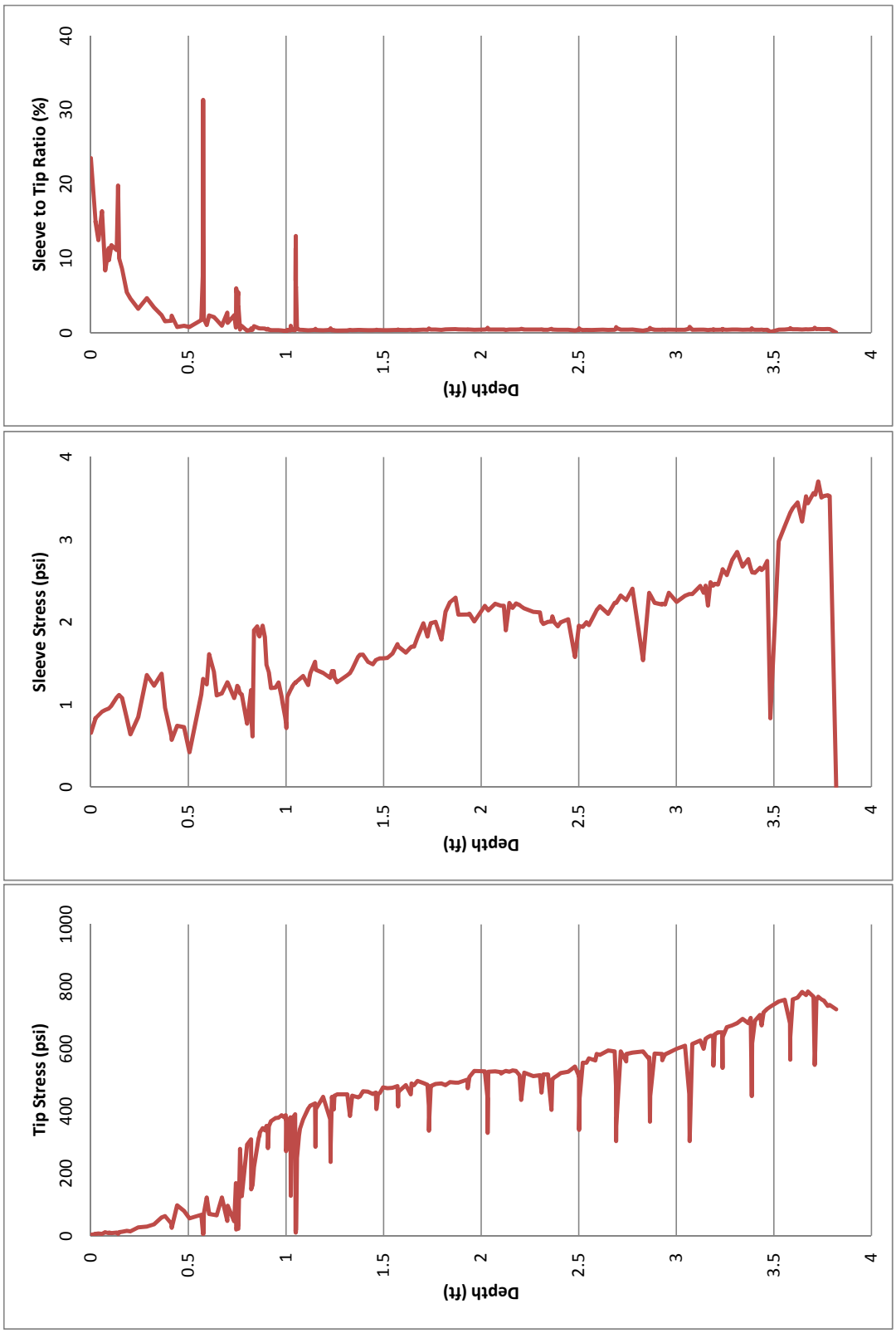

Figure 51:CPT #1 Round 3 Data

45

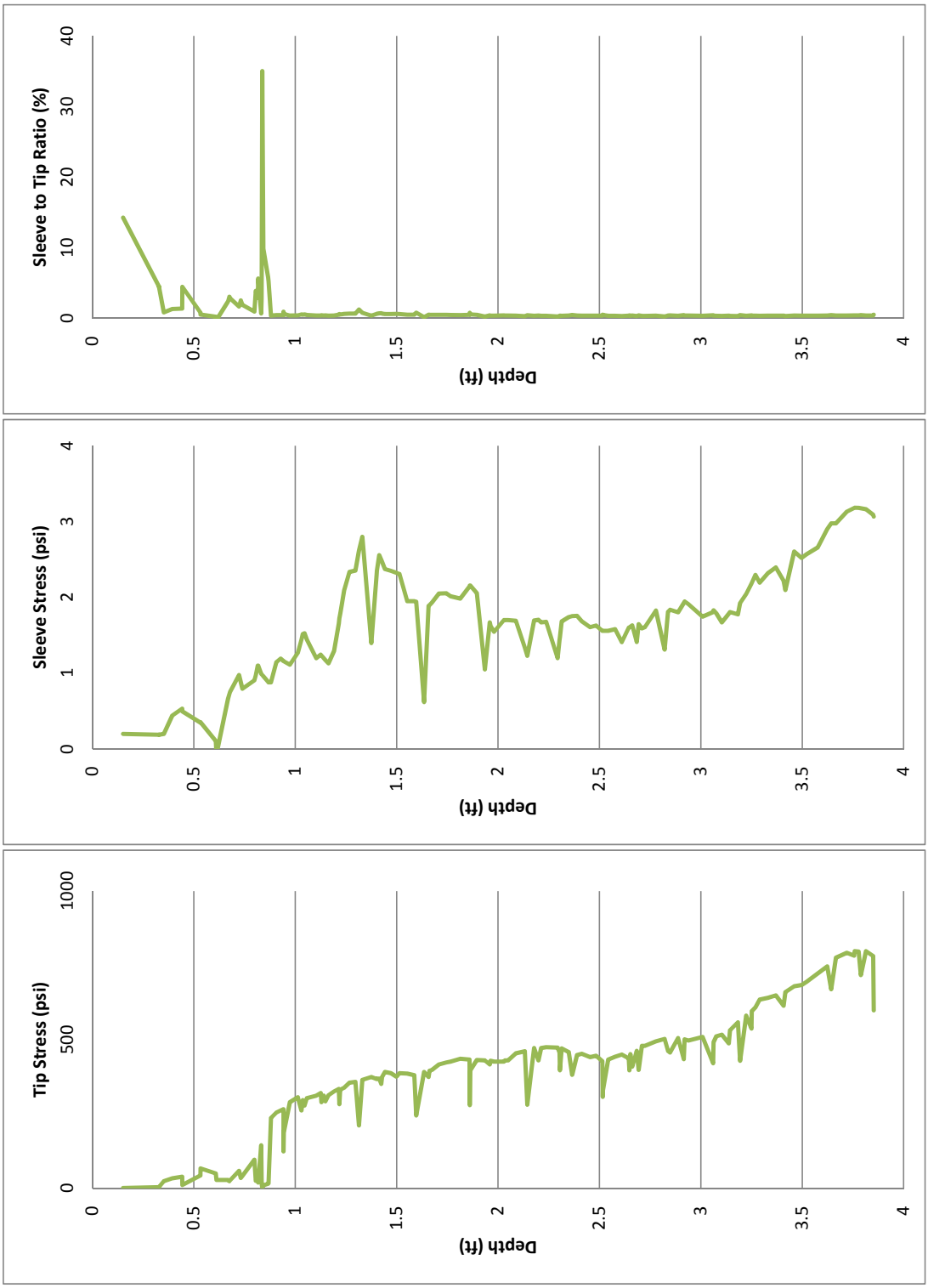

Figure 52:CPT #2 Round 3 Data

46

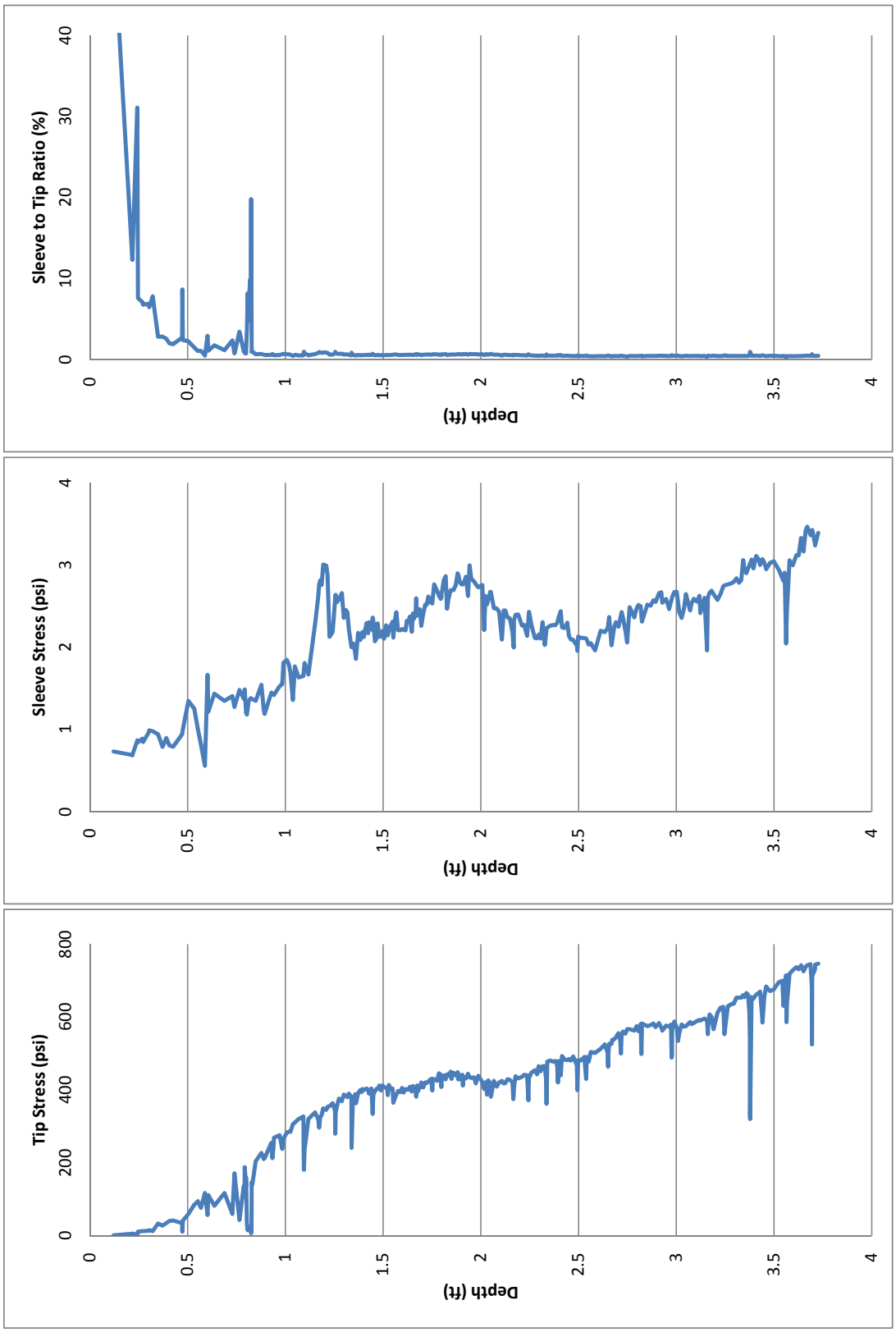

Figure 53:CPT #3 Round 3 Data

47

APPENDIX B

PHOTOGRAPHS OF EXHUMED MODEL MICROPILES

Figure B.1. Photographs of Model Micropile 1B

Figure B.2. Photographs of Model Micropile 1C

Figure B.3. Photographs of Model Micropile 1D

Figure B.4. Photographs of Model Micropile 1E

Figure B.5. Photographs of Model Micropile 1F

Figure B.6. Photographs of Model Micropile 2A

Figure B.7. Photographs of Model Micropile 2B

Figure B.8. Photographs of Model Micropile 2C

Figure B.9. Photographs of Model Micropile 2D

Figure B.10. Photographs of Model Micropile 2E

Figure B.11. Photographs of Model Micropile 2F

Figure B.12. Photographs of Model Micropile 3A

Figure B.13. Photographs of Model Micropile 3B

Figure B.14. Photographs of Model Micropile 3C

Figure B.15. Photographs of Model Micropile 3D

Figure B.16. Photographs of Model Micropile 3E

Figure B.17. Photographs of Model Micropile 3F

APPENDIX C

WARRENSBURG TEST SITE BORING LOGS

Form T-737-1RMO
Rev. 05/01

MISSOURI DEPARTMENT OF TRANSPORTATION
Construction and Materials

BORING DATA (CORE & SPT)

Sheet 1 of 9c

Job No.:	TMTIPROJ				
County:	Johnson	**Route:**	13	**Design:**	MTI-WAR-1A
Over:	Route 50 over Route 13			**Skew:**	Right Angles
Logged by:	Owens			**Operator:**	Donahoe
Equipment:	Failing 1500			**Drillers Hole No.:**	H-09-65
Hole Stab. by:	Drilling Fluids			**Date of Work:**	10/28/2009
Automatic Hammer Efficiency:	80 %			**Drill No.:**	G-7888

Bent	Station	Location		Surface Elevation, ft.
MTI-WAR-1A	210+03.4	142.9' LT.		780.2
Longitude:	-93.688318W		Latitude:	38.773746N

TEST DATA

Depth, ft.	SPT Blows/6"	N_{60}	P.P., tsf	Tv., tsf	Est. Equiv., Qu, tsf
5.0	4-4-5	12	3.25		--
10.0	4-6-6	16	3.50		12.0
15.0	12-32-38 in 5"	50 in 5"	3.50		30.0
20.0	32-88 in 2"	50 in 2"	9.00+		4.7
25.0	10-13-22	47	9.00+		--
30.0	25-38 in 2½"	50 in 2½"	9.00+		12.0
35.0	38 in 5"	50 in 5"	9.00+		60.0
40.0	38 in 1"	50 in 1"	--		20.0
45.0	38 in 3"	50 in 3"	9.00+		24.0
50.0	38 in 2½"	50 in 2½"	9.00+		15.0
55.0	38 in 4"	50 in 4"	9.00+		17.0
60.0	38 in 3½"	50 in 3½"	9.00+		120.0
65.0	38 in ½"	50 in ½"	9.00+		

LOG OF MATERIALS*

0.0-15.2'	Gray-brown mottled lean clay, very stiff, moist.
15.2-17.0'	Brown shale, soft.
17.0-28.5'	Gray shale, soft.
28.5-32.5'	Tan shale, soft.
32.5-67.0'	Gray shale, soft.

TEXAS CONE TEST DATA

Depth, ft.	Blows/6"	Blows/6"
17.5	50 in 4"	50 in 1½"
22.5	50 in 2"	50 in 1"
27.5	50 in 2"	50 in ½"
32.5	50 in 3½"	50 in 4"
37.5	50 in 1¼"	50 in ¼"
42.5	50 in 2"	50 in ½"
47.5	50 in 1½"	50 in ½"
52.5	50 in 1½"	50, no advance
57.5	50 in 1½"	50 in ½"
62.5	50 in 1½"	50 in ½"

CORING LOG (NX Double Tube Barrel)

From	To	Run	Rec	Loss	% RQD	Notes

WATER TABLE OBSERVATIONS

Date	Time Change	Depth Hole Open	Depth To Water

Coordinate System: Geographic **Coordinate Zone:**
Coordinate Datum: NAD 83 (CONUS) **Coordinate Units:** U.S. Survey Feet **Coordinate Projection Factor:**

N_{60} - Corrected N value for standard 60% SPT efficiency.
$N_{60} = (Em/60)Nm$ Em - Measured transfer efficiency in percent.
Nm - Observed N-value.

* Persons using this information are cautioned that the materials shown are determined by the equipment noted and accuracy of the "log of materials" is limited thereby and by judgment of the operator.
THIS INFORMATION IS FOR DESIGN PURPOSES ONLY.

Form T-737-1RMO
Rev. 05/01

MISSOURI DEPARTMENT OF TRANSPORTATION
Construction and Materials

BORING DATA (CORE & SPT)

Sheet 3a of 9c

Job No.:	TMTIPROJ				
County:	Johnson	**Route:**	13	**Design:**	MTI-WAR-1B
Over:	Route 50 over Route 13			**Skew:**	Right Angles
Logged by:	Stevens			**Operator:**	Mathews
Equipment:	Failing 1500			**Drillers Hole No.:**	H-09-72
Hole Stab. by:	Drilling Fluids			**Date of Work:**	11/19/2009
Automatic Hammer Efficiency:	80 %			**Drill No.:**	G-7888

Bent	Station	Location	Surface Elevation, ft.
MTI-WAR-1B	210+08.3	152.2' LT.	780.5
Longitude:	-93.688295W	Latitude:	38.773772N

TEST DATA

Depth, ft.	Sample No.	Shelby Tube	P.P., tsf	Tv., tsf	Wn%
2.5-5.0	9MSJS729	3"	2.75	0.90	21.4
5.0-7.5	9MSJS730	3"	2.25	0.50	26.1
7.5-10.0	9MSJS731	3"	2.00	0.40	33.6
10.0-12.5	9MSJS732	3"	3.50	0.35	34.6

SOIL CLASSIFICATION TEST DATA

Depth, ft.	Elev., ft.	LL	PI	ASTM Class.
21.8	758.7	32	9	CL
34.5	746.0	42	20	CL
45.0	735.5	28	8	CL
54.5	726.0	36	15	CL
62.0	718.5	33	18	CL

CORING LOG (NX Double Tube Barrel)

From	To	Run	Rec	Loss	% RQD	Notes
15.0	20.0	5.0	0.0	5.0	Shale	
20.0	25.0	5.0	4.8	0.2	Shale	
25.0	30.0	5.0	3.9	1.1	Shale	
30.0	35.0	5.0	5.0	0.0	Shale	
35.0	40.0	5.0	5.0	0.0	Shale	
40.0	45.0	5.0	5.0	0.0	Shale	
45.0	50.0	5.0	5.0	0.0	Shale	
50.0	55.0	5.0	5.0	0.0	Shale	
55.0	60.0	5.0	5.0	0.0	Shale	
60.0	65.0	5.0	5.0	0.0	Shale	
65.0	70.0	5.0	5.0	0.0	Shale	

WATER TABLE OBSERVATIONS

Date	Time Change	Depth Hole Open	Depth To Water

LOG OF MATERIALS*

0.0-0.8'	Cobbles, (access road).
0.8-8.0'	Reddish-tan and olive-gray mottled lean clay, with black iron concretions, moist, very stiff.
8.0-12.0'	Reddish-tan and olive-gray fat clay, with sand and black iron concretions, moist, very stiff.
12.0-25.9'	Yellow and gray shale, moist, soft.
25.9-33.2'	Tan and pale green-gray argillaceous sandstone to sandy shale, scattered black partings, soft.
33.2-35.2'	Medium gray poorly laminated shale, very soft.
35.2-36.1'	Dark brown-gray siltstone, medium hard.
36.1-38.1'	Brownish-gray irregularly laminated clay shale, very soft.
38.1-53.6'	Light gray siltstone to silt shale, thickly laminated, medium hard.
53.6-60.0'	Black pyritic shale to coal, soft.
60.0-62.7'	Light gray poorly laminated silt shale, very soft, (underclay).
62.7-66.8'	Light gray to pale green siltstone to silt shale, soft to medium hard, thickly laminated.
66.8-68.5'	Pale green and black shale, soft.
68.5-70.0'	Dark brownish-gray fossiliferous, calcareous siltstone, medium hard, thin bedded.

Coordinate System: Geographic **Coordinate Zone:**
Coordinate Datum: NAD 83 (CONUS) **Coordinate Units:** U.S. Survey Feet **Coordinate Projection Factor:**

N_{60} - Corrected N value for standard 60% SPT efficiency.
$N_{60} = (Em/60)Nm$ Em - Measured transfer efficiency in percent.
Nm - Observed N-value.

* Persons using this information are cautioned that the materials shown are determined by the equipment noted and accuracy of the "log of materials" is limited thereby and by judgment of the operator.
THIS INFORMATION IS FOR DESIGN PURPOSES ONLY.

Form T-737-1RMO
Rev. 05/01

MISSOURI DEPARTMENT OF TRANSPORTATION
Construction and Materials

BORING DATA (CORE & SPT)

Sheet 3b of 9c

Job No.:	TMTIPROJ				
County:	Johnson	**Route:**	13	**Design:**	MTI-WAR-1B
Over:	Route 50 over Route 13			**Skew:**	Right Angles
Logged by:	Stevens			**Operator:**	Mathews
Equipment:	Failing 1500			**Drillers Hole No.:**	H-09-72
Hole Stab. by:	Drilling Fluids			**Date of Work:**	11/19/2009
Automatic Hammer Efficiency:	80 %			**Drill No.:**	G-7888

Bent	Station	Location	Surface Elevation, ft.	LOG OF MATERIALS*
MTI-WAR-1B	210+08.3	152.2' LT.	780.5	
Longitude:	-93.688295W	Latitude:	38.773772N	

UNCONFINED COMPRESSIVE STRENGTH TEST DATA

Sample No.	Depth, ft/m	Elev., ft/m	Qu, ksf	P.P., tsf
9MSJS733	23.3	757.2	MTI	3.5
9MSJS738	27.7	752.8	MTI	7.5
9MSJS739	27.8	752.7	MTI	9.0+
9MSJS740	28.7	751.8	MTI	9.0+
9MSJS744	30.8	749.7	MTI	9.0+
9MSJS745	34.5	746.0	MTI	7.5
9MSJS750	35.8	744.7	MTI	9.0+
9MSJS751	38.4	742.1	MTI	9.0+
9MSJS752	38.9	741.6	MTI	9.0+
9MSJS753	37.5	743.0	MTI	5.0
9MSJS756	41.3	739.2	MTI	9.0+
9MSJS757	44.2	736.3	MTI	9.0+
9MSJS762	45.7	734.8	MTI	9.0+
9MSJS763	46.2	734.3	MTI	9.0+
9MSJS768	50.8	729.7	MTI	9.0+
9MSJS769	51.8	728.7	MTI	9.0+
9MSJS770	52.7	727.8	MTI	9.0+
9MSJS775	56.3	724.2	MTI	9.0+
9MSJS776	56.9	723.6	MTI	9.0+
9MSJS777	58.3	722.2	MTI	9.0+
9MSJS781	63.0	717.5	MTI	9.0+
9MSJS782	63.6	716.9	MTI	9.0+
9MSJS783	64.2	716.3	MTI	9.0+
9MSJS788	67.7	712.8	MTI	9.0+
9MSJS789	68.2	712.3	MTI	9.0+

SLAKE DURABILITY TEST

Sample No.	Depth, ft.	Elev., ft.	Slake Durability Index Id(2)	Description Type
9MSJS734	22.5	758.0	7.9	3
9MSJS741	28.0	752.5	7.9	2
9MSJS747	34.5	746.0	14.6	2
9MSJS754	37.5	743.0	0.8	3
9MSJS758	42.5	738.0	29.1	2
9MSJS764	46.8	733.7	84.0	2
9MSJS771	53.4	727.1	78.6	2
9MSJS778	56.0	724.5	72.3	2
9MSJS787	65.5	715.0	93.9	1
9MSJS790	67.0	713.5	56.8	2

INSOLUBLE RESIDUE TEST

Sample No.	Depth, ft.	Elevation, ft.	% Insoluble Residue	% Acid Soluble	% Insoluble Residue Passing #270 Sieve	Lab Classification
9MSJS734A	22.5	758.0	97.6	2.4	84.4	Shale
9MSJS749A	34.5	746.0	81.5	18.5	71.1	Shale
9MSJS759A	43.0	737.5	90.4	9.6	86.4	Shale
9MSJS772	52.1	728.4	93.4	6.6	65.6	Shale
9MSJS785	64.2	716.3	97.1	2.9	69.5	Shale

Coordinate System: Geographic **Coordinate Zone:**
Coordinate Datum: NAD 83 (CONUS) **Coordinate Units:** U.S. Survey Feet **Coordinate Projection Factor:**

N_{60} - Corrected N value for standard 60% SPT efficiency.

$N_{60} = (Em/60)Nm$ Em - Measured transfer efficiency in percent.

Nm - Observed N-value.

* Persons using this information are cautioned that the materials shown are determined by the equipment noted and accuracy of the "log of materials" is limited thereby and by judgment of the operator.
THIS INFORMATION IS FOR DESIGN PURPOSES ONLY.

Form T-737-1RMO
Rev. 05/01

MISSOURI DEPARTMENT OF TRANSPORTATION
Construction and Materials

BORING DATA (CORE & SPT)

Sheet 4 of 9c

Job No.:	TMTIPROJ				
County:	Johnson	**Route:**	13	**Design:**	MTI-WAR-1C
Over:	Route 50 over Route 13			**Skew:**	Right Angles
Logged by:	R. Todd			**Operator:**	Mathews
Equipment:	Failing 1500			**Drillers Hole No.:**	H-09-74
Hole Stab. by:	Drilling Fluids			**Date of Work:**	12/1/2009
Automatic Hammer Efficiency:	80 %			**Drill No.:**	G-7888

Bent	Station	Location	Surface Elevation, ft.
MTI-WAR-1C	210+07.1	129.6' LT.	779.8
Longitude:	-93.688312W	Latitude:	38.773697N

LOG OF MATERIALS*

0.0-11.5'	Tannish-brown, yellow mottled fat clay, moist, very stiff.
11.5-60.0'	Shale, ran pressuremeter tests.

TEST DATA

Depth, ft.	Sample No.	Shelby Tube	P.P., tsf	Tv., tsf	Wn%
2.5-5.0	9MRNT669	3"	4.0	0.8	
5.0-7.5	9MRNT670	3"	--	--	

MENARD PRESSUREMETER TESTS

Depth, ft.				
2.5-5.0				
7.5-10.0				
11.0-14.0				
27.0-30.0				
37.0-40.0				
47.0-50.0				
57.0-60.0				

CORING LOG (NX Double Tube Barrel)

From	To	Run	Rec	Loss	% RQD	Notes

WATER TABLE OBSERVATIONS

Date	Time Change	Depth Hole Open	Depth To Water

Coordinate System: Geographic **Coordinate Zone:**
Coordinate Datum: NAD 83 (CONUS) **Coordinate Units:** U.S. Survey Feet **Coordinate Projection Factor:**

N_{60} - Corrected N value for standard 60% SPT efficiency.
$N_{60} = (Em/60)Nm$ Em - Measured transfer efficiency in percent.
Nm - Observed N-value.

* Persons using this information are cautioned that the materials shown are determined by the equipment noted and accuracy of the "log of materials" is limited thereby and by judgment of the operator.
THIS INFORMATION IS FOR DESIGN PURPOSES ONLY.

Form T-737-1RMO
Rev. 05/01

MISSOURI DEPARTMENT OF TRANSPORTATION
Construction and Materials

BORING DATA (CORE & SPT)

Sheet 7 of 9c

Job No.:	TMTIPROJ				
County:	Johnson	**Route:**	13	**Design:**	MTI-WAR-8
Over:	Route 50 over Route 13			**Skew:**	Right Angles
Logged by:	R. Todd			**Operator:**	Donahoe
Equipment:	Failing 1500			**Drillers Hole No.:**	H-09-75
Hole Stab. by:	Drilling Fluids			**Date of Work:**	12/2/2009
Automatic Hammer Efficiency:	80 %			**Drill No.:**	G-7888

Bent	Station	Location	Surface Elevation, ft.
MTI-WAR-8	209+77.7	179.5' LT.	781.2
Longitude:	-93.688409W	Latitude:	38.773849N

TEST DATA

Depth, ft.	Sample No.	Shelby Tube	P.P., tsf	Tv., tsf	Wn%
3.0	9MRNT633	3"	4.0	0.85	17.8
6.0	9MRNT634	3"	2.5	--	--
13.5	9MRNT635	3"	6.0	0.9+	12.9

LOG OF MATERIALS*

0.0-10.0'	Grayish-brown mottled fat clay, scattered gravel, moist, very stiff.
10.0-14.5'	Brown mottled fat clay, trace shale, scattered gravel, moist, very stiff.
14.5-19.5'	Tan to gray thinly laminated shale, soft.
19.5-28.0'	Gray thinly laminated shale, soft.
28.0-35.0'	Gray shale, thinly laminated, soft.
35.0-35.2'	Coal.
35.2-39.5'	Gray poorly laminated clay shale, soft, (underclay).
39.5-53.3'	Gray thinly laminated shale.
53.3-54.1'	Black shale, soft.
54.1-57.5'	Coal.
57.5-60.1'	Black shale, soft.
60.1-64.5'	Gray poorly laminated clay shale, soft, (underclay).

CORING LOG (NX Double Tube Barrel)

From	To	Run	Rec	Loss	% RQD	Notes
14.5	19.5	5.0	5.0	0.0	Shale	
19.5	24.5	5.0	5.0	0.0	Shale	
24.5	29.5	5.0	4.8	0.2	Shale	
29.5	34.5	5.0	4.4	0.6	Shale	
34.5	39.5	5.0	5.0	0.0	Shale	
39.5	44.5	5.0	5.0	0.0	Shale	
44.5	49.5	5.0	4.2	0.8	Shale	
49.5	54.5	5.0	4.8	0.2	Shale	
54.5	59.5	5.0	5.0	0.0	Shale	
59.5	64.5	5.0	5.0	0.0	Shale	

WATER TABLE OBSERVATIONS

Date	Time Change	Depth Hole Open	Depth To Water

Coordinate System: Geographic **Coordinate Zone:**
Coordinate Datum: NAD 83 (CONUS) **Coordinate Units:** U.S. Survey Feet **Coordinate Projection Factor:**

N_{60} - Corrected N value for standard 60% SPT efficiency.
$N_{60} = (Em/60)Nm$ Em - Measured transfer efficiency in percent.
Nm - Observed N-value.

* Persons using this information are cautioned that the materials shown are determined by the equipment noted and accuracy of the "log of materials" is limited thereby and by judgment of the operator.
THIS INFORMATION IS FOR DESIGN PURPOSES ONLY.

Form T-737-1RMO
Rev. 05/01

MISSOURI DEPARTMENT OF TRANSPORTATION
Construction and Materials

BORING DATA (CORE & SPT)

Sheet 8 of 9c

Job No.:	TMTIPROJ				
County:	Johnson	**Route:**	13	**Design:**	MTI-WAR-8
Over:	Route 50 over Route 13			**Skew:**	Right Angles
Logged by:	R. Todd			**Operator:**	Donahoe
Equipment:	Failing 1500			**Drillers Hole No.:**	H-09-75
Hole Stab. by:	Drilling Fluids			**Date of Work:**	12/2/2009
Automatic Hammer Efficiency:	80 %			**Drill No.:**	G-7888

Bent	Station	Location	Surface Elevation, ft.	LOG OF MATERIALS*
MTI-WAR-8	209+77.7	179.5' LT.	781.2	
Longitude:	-93.688409W	Latitude:	38.773849N	

UNCONFINED COMPRESSIVE STRENGTH TEST DATA

Sample No.	Depth, ft.	Elev., ft.	Qu, ksf	P.P., tsf
9MRNT636	17.7	763.5	MTI	9.0+
9MRNT639	21.5	759.7	MTI	9.0+
9MRNT640	22.8	758.4	MTI	9.0+
9MRNT641	24.7	756.5	MTI	9.0+
9MRNT643	23.8	757.4	MTI	9.0+
9MRNT644	27.3	753.9	MTI	9.0+
9MRNT648	32.0	749.2	MTI	9.0+
9MRNT651	38.1	743.1	MTI	9.0+
9MRNT652	39.2	742.0	MTI	9.0+
9MRNT653	36.5	744.7	MTI	9.0+
9MRNT656	42.3	738.9	MTI	9.0+
9MRNT657	43.3	737.9	MTI	9.0+
9MRNT660	47.8	733.4	MTI	9.0+
9MRNT664	49.9	731.3	MTI	9.0+
9MRNT666	63.0	718.2	MTI	9.0+
9MRNT667	64.0	717.2	MTI	9.0+

INSOLUBLE RESIDUE TEST

Sample No.	Depth, ft.	Elevation, ft.	% Insoluble Residue	% Acid Soluble	% Insoluble Residue Passing #270 Sieve	Lab Classification
9MRNT659	40.5	740.7	91.1	8.9	79.5	Shale

SLAKE DURABILITY TEST

Sample No.	Depth, ft.	Elev., ft.	Slake Durability Index Id(2)	Description Type
9MRNT645	28.1	753.1	96.0	1
9MRNT649	30.8	750.4	77.6	2
9MRNT654	37.0	744.2	7.7	3
9MRNT665	50.1	731.1	81.6	2
9MRNT668	63.7	717.5	86.8	2

Coordinate System: Geographic **Coordinate Zone:**
Coordinate Datum: NAD 83 (CONUS) **Coordinate Units:** U.S. Survey Feet **Coordinate Projection Factor:**

N_{60} - Corrected N value for standard 60% SPT efficiency.

$N_{60} = (Em/60)Nm$ Em - Measured transfer efficiency in percent.

Nm - Observed N-value.

* Persons using this information are cautioned that the materials shown are determined by the equipment noted and accuracy of the "log of materials" is limited thereby and by judgment of the operator.
THIS INFORMATION IS FOR DESIGN PURPOSES ONLY.

Form T-737-1RMO
Rev. 05/01

MISSOURI DEPARTMENT OF TRANSPORTATION
Construction and Materials

BORING DATA (CORE & SPT)

Sheet 9a of 9c

Job No.:	TMTIPROJ				
County:	Johnson	**Route:**	13	**Design:**	MTI-WAR-9
Over:	Route 50 over Route 13			**Skew:**	Right Angles
Logged by:	Stevens, Todd			**Operator:**	Mathews
Equipment:	Failing 1500			**Drillers Hole No.:**	H-09-73
Hole Stab. by:	Drilling Fluids			**Date of Work:**	11/23 & 30/2009
Automatic Hammer Efficiency:	80 %			**Drill No.:**	G-7888

Bent	Station	Location	Surface Elevation, ft.
MTI-WAR-9	209+59.2	144.8' LT.	779.0
Longitude:	-93.688469W	Latitude:	38.773758N

TEST DATA

Depth, ft.	Sample No.	Shelby Tube	P.P., tsf	Tv., tsf	Wn%
2.5-5.0	9MSJS791	3"	5.50	--	22.8
5.0-7.5	9MSJS792	3"	2.25	0.4	33.0
7.5-10.0	9MSJS793	3"	3.50	0.8	27.1
10.0-12.0	9MSJS794	3"	9.00+	Sand	12.1

CORING LOG (NX Double Tube Barrel)

From	To	Run	Rec	Loss	% RQD	Notes
15.0	20.0	5.0	4.7	0.3	0	
20.0	25.0	5.0	3.5	1.5	Shale	
25.0	30.0	5.0	4.5	0.5	100**	
30.0	35.0	5.0	5.0	0.0	Shale	
35.0	40.0	5.0	5.0	0.0	Shale	
40.0	45.0	5.0	3.9	1.1	Shale	
45.0	50.0	5.0	5.0	0.0	Shale	
50.0	55.0	5.0	5.0	0.0	Shale	
55.0	60.0	5.0	3.5	1.5	Shale/Coal	
60.0	65.0	5.0	4.8	0.2	Shale	
65.0	70.0	5.0	4.4	0.6	Shale	
70.0	75.0	5.0	4.0	1.0	Shale	
75.0	80.0	5.0	5.0	0.0	Shale	
80.0	85.0	5.0	4.8	0.2	Shale	
85.0	90.0	5.0	5.0	0.0	Shale	
90.0	95.0	5.0	5.0	0.0	50**	
95.0	100.0	5.0	5.0	0.0	98	
100.0	102.5	2.5	2.4	0.1	Shale	

**RQD on sandstone or limestone portions only

WATER TABLE OBSERVATIONS

Date	Time Change	Depth Hole Open	Depth To Water

LOG OF MATERIALS*

0.0-0.6'	Gravel, (access road).
0.6-11.0'	Tan, yellow, and gray shaley fat clay, with black iron concretions, moist, hard.
11.0-14.0'	Tannish-gray, yellow, and red, fine grained, micaceous sandstone, weathered.
14.0-27.0'	Tannish-gray, yellow, and red, micaceous sandy shale, interlayered with sandstone, thickly laminated, very soft.
27.0-29.8'	Tannish-yellow and pale green irregularly bedded siltstone, medium hard.
29.8-33.1'	Pale green and dark gray shale, thinly laminated, soft.
33.1-35.0'	Light gray poorly laminated shale, very soft, (underclay).
35.0-42.0'	Pale green silt shale, thin to thickly laminated, soft to medium hard.
42.0-49.8'	Medium to dark gray silt shale to siltstone, soft to medium hard.
49.8-55.8'	Black shale, soft.
55.8-59.0'	Coal, very soft.
59.0-68.0'	Light gray poorly laminated shale to calcareous siltstone, (underclay), soft to medium hard.
68.0-70.0'	Black shale, soft.
70.0-79.0'	Grayish to pale green thinly laminated shale, soft.
79.0-80.6'	Coal, soft.
80.6-81.4'	Gray limey shale to shaley limestone, soft.
81.4-83.7'	Gray thickly laminated shale, soft.
83.7-86.3'	Gray fine grained sandstone, medium to thick bedded, moderately hard.
86.3-92.8'	Gray shale, thickly laminated, soft.
92.8-101.3'	Gray fine grained shaley limestone, medium bedded, hard.
101.3-102.5'	Dark gray thickly laminated shale, medium hard.

Coordinate System: Modified U.S. State Plane 1983 **Coordinate Zone:** Missouri
Coordinate Datum: NAD 83 (CONUS) **Coordinate Units:** U.S. Survey Feet **Coordinate Projection Factor:**

N_{60} - Corrected N value for standard 60% SPT efficiency.
$N_{60} = (Em/60)Nm$ Em - Measured transfer efficiency in percent.
Nm - Observed N-value.

* Persons using this information are cautioned that the materials shown are determined by the equipment noted and accuracy of the "log of materials" is limited thereby and by judgment of the operator.
THIS INFORMATION IS FOR DESIGN PURPOSES ONLY.

Form T-737-1RMO
Rev. 05/01

MISSOURI DEPARTMENT OF TRANSPORTATION
Construction and Materials

BORING DATA (CORE & SPT)

Sheet 9b of 9c

Job No.:	TMTIPROJ				
County:	Johnson	**Route:**	13	**Design:**	MTI-WAR-9
Over:	Route 50 over Route 13			**Skew:**	Right Angles
Logged by:	Stevens, Todd			**Operator:**	Mathews
Equipment:	Failing 1500			**Drillers Hole No.:**	H-09-73
Hole Stab. by:	Drilling Fluids			**Date of Work:**	11/23 & 30/2009
Automatic Hammer Efficiency:		80 %		**Drill No.:**	G-7888

Bent	Station	Location	Surface Elevation, ft.	LOG OF MATERIALS*
MTI-WAR-9	209+59.2	144.8' LT.	779.0	
Longitude:	-93.688469W	Latitude:	38.773758N	

UNCONFINED COMPRESSIVE STRENGTH TEST DATA

Sample No.	Depth, ft.	Elev., ft.	Qu, ksf	P.P., tsf
9MSJS795	17.7	761.3	MTI	9.0+
9MSJS796	18.2	760.8	MTI	9.0+
9MSJS799	22.7	756.3	MTI	5.5
9MSJS803	25.6	753.4	MTI	9.0+
9MSJS804	28.2	750.8	MTI	9.0+
9MSJS805	28.7	750.3	MTI	7.5
9MSJS809	31.1	747.9	MTI	9.0+
9MSJS810	31.5	747.5	MTI	9.0+
9MSJS811	31.9	747.1	MTI	9.0+
9MSJS814	36.0	743.0	MTI	5.0
9MSJS815	36.7	742.3	MTI	9.0+
9MSJS816	38.7	740.3	MTI	9.0+
9MSJS820	42.2	736.8	MTI	9.0+
9MSJS822	47.4	731.6	MTI	9.0+
9MSJS823	49.1	729.9	MTI	9.0+
9MSJS824	49.6	729.4	MTI	9.0+
9MSJS828	52.0	727.0	MTI	9.0+
9MSJS829	52.7	726.3	MTI	9.0+
9MSJS830	53.2	725.8	MTI	9.0+
9MSJS834	55.5	723.5	MTI	9.0+
9MSJS835	61.5	717.5	MTI	9.0+
9MSJS836	62.7	716.3	MTI	9.0+
9MSJS837	63.3	715.7	MTI	9.0+
9MSJS841	69.6	709.4	MTI	9.0+
9MRNT607	71.2	707.8	MTI	9.0+
9MRNT609	72.3	706.7	MTI	9.0+
9MRNT610	73.0	706.0	MTI	9.0+
9MRNT613	76.6	702.4	MTI	9.0+
9MRNT614	77.2	701.8	MTI	9.0+
9MRNT617	81.9	697.1	MTI	9.0+
9MRNT618	83.2	695.8	MTI	9.0+
9MRNT619	84.7	694.3	MTI	9.0+
9MRNT621	87.2	691.8	MTI	9.0+
9MRNT622	88.4	690.6	MTI	9.0+
9MRNT623	87.6	691.4	MTI	9.0+
9MRNT625	90.3	688.7	MTI	9.0+
9MRNT626	91.0	688.0	MTI	9.0+
9MRNT627	92.2	686.8	MTI	9.0+
9MRNT629	95.3	683.7	MTI	9.0+
9MRNT630	101.7	677.3	MTI	9.0+

Coordinate System: Geographic **Coordinate Zone:**
Coordinate Datum: NAD 83 (CONUS) **Coordinate Units:** U.S. Survey Feet **Coordinate Projection Factor:**

N_{60} - Corrected N value for standard 60% SPT efficiency.
$N_{60} = (Em/60)Nm$ Em - Measured transfer efficiency in percent.
Nm - Observed N-value.

* Persons using this information are cautioned that the materials shown are determined by the equipment noted and accuracy of the "log of materials" is limited thereby and by judgment of the operator.
THIS INFORMATION IS FOR DESIGN PURPOSES ONLY.

Form T-737-1RMO
Rev. 05/01

MISSOURI DEPARTMENT OF TRANSPORTATION
Construction and Materials

BORING DATA (CORE & SPT)

Sheet 9c of 9c

Job No.:	TMTIPROJ				
County:	Johnson	**Route:**	13	**Design:**	MTI-WAR-9
Over:	Route 50 over Route 13			**Skew:**	Right Angles
Logged by:	Stevens, Todd			**Operator:**	Mathews
Equipment:	Failing 1500			**Drillers Hole No.:**	H-09-73
Hole Stab. by:	Drilling Fluids			**Date of Work:**	11/23 & 30/2009
Automatic Hammer Efficiency:		80 %		**Drill No.:**	G-7888

Bent	Station	Location	Surface Elevation, ft.	LOG OF MATERIALS*
MTI-WAR-9	209+59.2	144.8' LT.	779.0	
Longitude:	-93.688469W	Latitude:	38.773758N	

SLAKE DURABILITY TEST

Sample No.	Depth, ft.	Elev., ft.	Slake Durability Index Id(2)	Description Type
9MSJS797	17.5	761.5	69.3	3
9MSJS800	21.5	757.5	58.8	2
9MSJS806	29.0	750.0	79.8	2
9MSJS812	32.0	747.0	2.4	3
9MSJS817	35.5	743.5	78.6	2
9MSJS821	43.0	736.0	77.7	2
9MSJS825	48.0	731.0	86.6	2
9MSJS831	51.4	727.6	55.7	3
9MSJS838	62.0	717.0	84.3	2
9MRNT608	70.7	708.3	13.5	2
9MRNT615	78.0	701.0	5.3	3
9MRNT624	86.6	692.4	30.3	3
9MRNT628	91.6	687.4	64.7	3

INSOLUBLE RESIDUE TEST

Sample No.	Depth, ft.	Elevation, ft.	% Insoluble Residue	% Acid Soluble	% Insoluble Residue Passing #270 Sieve	Lab Classification
9MSJS801	22.0	757.0	94.8	5.2	73.6	Shale
9MSJS813	32.3	746.7	92.8	7.2	24.2	Sand
9MSJS839	64.0	715.0	94.7	5.3	59.8	Shale

CORING LOG (NX Double Tube Barrel)

From	To	Run	Rec	Loss	% RQD	Notes

WATER TABLE OBSERVATIONS

Date	Time Change	Depth Hole Open	Depth To Water

Coordinate System: Geographic **Coordinate Zone:**
Coordinate Datum: NAD 83 (CONUS) **Coordinate Units:** U.S. Survey Feet **Coordinate Projection Factor:**

N_{60} - Corrected N value for standard 60% SPT efficiency.

$N_{60} = (Em/60)Nm$ Em - Measured transfer efficiency in percent.

Nm - Observed N-value.

* Persons using this information are cautioned that the materials shown are determined by the equipment noted and accuracy of the "log of materials" is limited thereby and by judgment of the operator.
THIS INFORMATION IS FOR DESIGN PURPOSES ONLY.

Form T-737-1RMO
Rev. 05/01

MISSOURI DEPARTMENT OF TRANSPORTATION
Construction and Materials

BORING DATA (CORE & SPT)

Sheet 1 of 3

Job No.:	TMTIPROJ				
County:	Johnson	**Route:**	13	**Design:**	MTI-OFF-3
Over:	Route 50 over Route 13			**Skew:**	Right Angles
Logged by:	Stevens			**Operator:**	Donahoe
Equipment:	Failing 1500			**Drillers Hole No.:**	A-10-03
Hole Stab. by:	Casing			**Date of Work:**	4/29/2010
Automatic Hammer Efficiency:	80 %			**Drill No.:**	G-7887

Bent	Station	Location	Surface Elevation, ft.
MTI-OFF-3	209+45.7	189.9' LT.	781.1
Latitude:	38.77388	Longitude:	-93.68852

TEST DATA

Depth, ft.	Sample No.	Shelby Tube	P.P., tsf	Tv., tsf	Wn%
2.5-5.0	10MSJS185	3"	5.00	--	17.3
5.0-7.5	10MSJS186	3"	2.50	0.90+	33.7
7.5-10.0	10MSJS187	3"	5.50	0.90+	22.9
10.0-12.5	10MSJS188	3"	3.50	0.70	--0
12.5-14.4	10MSJS189	3"	3.75	0.60	15.1

LOG OF MATERIALS*

0.0-5.0'	Tan and gray mottled lean clay, hard, moist.
5.0-8.0'	Tan and gray mottled fat clay, with fine gravel, moist, very stiff.
8.0-20.1'	Yellow, tan, and maroon weathered sandstone to sand shale, with black concretions, moist, very stiff to hard.
20.1-35.5'	Tan and pale green sandy shale to argillaceous sandstone, soft.
35.5-44.5'	Dark to light gray shale, soft.

CORING LOG (NX Double Tube Barrel)

From	To	Run	Rec	Loss	% RQD	Notes
14.5	19.5	5.0	4.2	0.8	Shale	
19.5	24.5	5.0	4.8	0.2	Shale	
24.5	29.5	5.0	4.6	0.4	Shale	
29.5	34.5	5.0	4.3	0.7	Shale	
34.5	39.5	5.0	5.0	0.0	Shale	
39.5	44.5	5.0	5.0	0.0	Shale	

UNCONFINED COMPRESSIVE STRENGTH TEST DATA

Sample No.	Depth, ft.	Elev.	Qu, ksf	P.P., tsf
10MSJS190	17.3	763.8	MTI	9.0+
10MSJS191	22.2	758.9	MTI	9.0+
10MSJS192	22.9	758.2	MTI	9.0+
10MSJS193	27.1	754.0	MTI	9.0+
10MSJS194	28.6	752.5	MTI	9.0+
10MSJS195	30.2	750.9	MTI	9.0+
10MSJS196	36.8	744.3	MTI	9.0+
10MSJS197	38.6	742.5	MTI	9.0+
10MSJS198	41.1	740.0	MTI	9.0+
10MSJS199	44.2	736.9	MTI	9.0+

WATER TABLE OBSERVATIONS

Date	Time Change	Depth Hole Open	Depth To Water
4/29/2010	0		43.8'
4/30/2010	1 day		29.8'

Coordinate System: Geographic **Coordinate Zone:** Missouri West 2403
Coordinate Datum: NAD 83 (CONUS) **Coordinate Units:** U.S. Survey Feet **Coordinate Projection Factor:**

N_{60} - Corrected N value for standard 60% SPT efficiency.
$N_{60} = (Em/60)Nm$ Em - Measured transfer efficiency in percent.
Nm - Observed N-value.

* Persons using this information are cautioned that the materials shown are determined by the equipment noted and accuracy of the "log of materials" is limited thereby and by judgment of the operator.
THIS INFORMATION IS FOR DESIGN PURPOSES ONLY.

Form T-737-1RMO
Rev. 05/01

MISSOURI DEPARTMENT OF TRANSPORTATION
Construction and Materials

BORING DATA (CORE & SPT)

Sheet 2 of 3

Job No.:	TMTIPROJ				
County:	Johnson	**Route:**	13	**Design:**	MTI-OFF-4
Over:	Route 50 over Route 13			**Skew:**	Right Angles
Logged by:	Stevens			**Operator:**	Donahoe
Equipment:	Failing 1500			**Drillers Hole No.:**	H-10-10
Hole Stab. by:	Drilling Fluids			**Date of Work:**	4/28/2010
Automatic Hammer Efficiency:	80 %			**Drill No.:**	G-7888

Bent	Station	Location	Surface Elevation, ft.
MTI-OFF-4	210+05.7	190.0' LT.	781.6
Latitude:	38.773875	Longitude:	-93.688309

TEST DATA

Depth, ft.	Sample No.	Shelby Tube	P.P., tsf	Tv., tsf	Wn%
2.5-5.0	10MSJS177	3"	3.75	0.45	24.7
5.0-7.5	No Recovery	--	--	--	20.0
7.5-10.0	10MSJS178	3"	3.50	0.90+	28.3
10.0-12.5	10MSJS179	3"	2.75	0.55	31.7
12.5-15.0	10MSJS180**	3"	6.00	0.90+	17.1
15.0-16.3	10MSJS181		3.25	--	19.7
Depth, ft.	**Sample No.**	**Pitcher Tube**	**P.P., tsf**	**Tv., tsf**	**Wn%**
17.5-20.0	10MSJS182	3"	9.00+	0.90+	16.3
20.0-22.5	10MSJS183	3"	9.00+	0.40	16.5
22.5-25.0	10MSJS184	3"	9.00+	--	22.8

**Sample fell out of tube; repushed

LOG OF MATERIALS*

0.0-7.0'	Tan, yellow, and gray mottled lean clay, with black concretions, very stiff to hard, moist.
7.0-10.5'	Tan and light gray shaley fat clay, moist, very stiff.
10.5-12.0'	Brown and gray mottled fat clay, moist, very stiff.
12.0-25.0'	Yellow and gray sandy shaley fat clay to silt shale, with maroon seams, hard, moist.

CORING LOG (NX Double Tube Barrel)

From	To	Run	Rec	Loss	% RQD	Notes

WATER TABLE OBSERVATIONS

Date	Time Change	Depth Hole Open	Depth To Water

Coordinate System: Geographic **Coordinate Zone:** Missouri West 2403
Coordinate Datum: NAD 83 (CONUS) **Coordinate Units:** U.S. Survey Feet **Coordinate Projection Factor:**

N_{60} - Corrected N value for standard 60% SPT efficiency.

$N_{60} = (Em/60)Nm$ Em - Measured transfer efficiency in percent.

Nm - Observed N-value.

* Persons using this information are cautioned that the materials shown are determined by the equipment noted and accuracy of the "log of materials" is limited thereby and by judgment of the operator.
THIS INFORMATION IS FOR DESIGN PURPOSES ONLY.

Form T-737-1RMO
Rev. 05/01

MISSOURI DEPARTMENT OF TRANSPORTATION
Construction and Materials

BORING DATA (CORE & SPT)

Sheet 3 of 3

Job No.:	TMTIPROJ				
County:	Johnson	**Route:**	13	**Design:**	MTI-OFF-5
Over:	Route 50 over Route 13			**Skew:**	Right Angles
Logged by:	Stevens			**Operator:**	Donahoe
Equipment:	Failing 1500			**Drillers Hole No.:**	A-10-04
Hole Stab. by:	Drilling Fluids			**Date of Work:**	5/3/2010
Automatic Hammer Efficiency:	80 %			**Drill No.:**	G-7887

Bent	Station	Location	Surface Elevation, ft.
MTI-OFF-5	209+83.3	128.2' LT.	779.7
Latitude:	38.773705	Longitude:	-93.688395

TEST DATA

Depth, ft.	Sample No.	Shelby Tube	P.P., tsf	Tv., tsf	Wn%
2.0-5.0	10MSJS200	3"	2.50	0.80	27.4
5.0-7.5	10MSJS201	3"	2.25	0.80	32.2
7.5-10.0	10MSJS202	3"	2.75	0.90	29.9
10.0-12.5	10MSJS203	3"	8.00	0.80	16.4
12.5-13.0	10MSJS204	3"	--	--	--
Depth, ft.	**Sample No.**	**Pitcher Tube**	**P.P., tsf**	**Tv., tsf**	**Wn%**
13.0-15.0	10MSJS205	3"	8.50	0.25	--
15.0-17.5	10MSJS206	3"	9.00+	0.50	--
17.5-20.0	10MSJS207	3"	9.00+	--	--
20.0-22.5	10MSJS208	3"	9.00+	--	--
22.5-25.0	10MSJS209	3"	8.50	--	--
25.0-27.5	10MSJS210	3"	9.00+	--	9.6
27.5-30.0	10MSJS211	3"	9.00+	--	--
30.0-32.5	10MSJS212	3"	9.00+	--	--
32.5-34.2	10MSJS213	3"	9.00+	--	--

CORING LOG (NX Double Tube Barrel)

From	To	Run	Rec	Loss	% RQD	Notes

WATER TABLE OBSERVATIONS

Date	Time Change	Depth Hole Open	Depth To Water

LOG OF MATERIALS*

0.0-12.0'	Reddish-tan and gray mottled lean to fat clay, with black concretions, moist, very stiff.
12.0-18.0'	Reddish-yellow and gray micaceous weathered silt shale, soft.
18.0-22.0'	Tannish-gray micaceous silt shale, soft.
22.0-34.2'	Tan and gray clay shale, soft.

Coordinate System: Geographic **Coordinate Zone:** Missouri West 2403
Coordinate Datum: NAD 83 (CONUS) **Coordinate Units:** U.S. Survey Feet **Coordinate Projection Factor:**

N_{60} - Corrected N value for standard 60% SPT efficiency.
$N_{60} = (Em/60)Nm$ Em - Measured transfer efficiency in percent.
Nm - Observed N-value.

* Persons using this information are cautioned that the materials shown are determined by the equipment noted and accuracy of the "log of materials" is limited thereby and by judgment of the operator.
THIS INFORMATION IS FOR DESIGN PURPOSES ONLY.

APPENDIX D

DESIGN CALCULATIONS FOR WARRENSBURG LOAD TESTS

WARRENSBURG TEST SITE

LOAD TEST SET-UP SKETCHES (6 PAGES)

JOB NAME WARRENSBURG JOB NO.
SUBJECT TEST SET-UP DATE
BY KAK CHK'D SHEET 1 of 6

WARRENSBURG, MO TEST MICROPILES

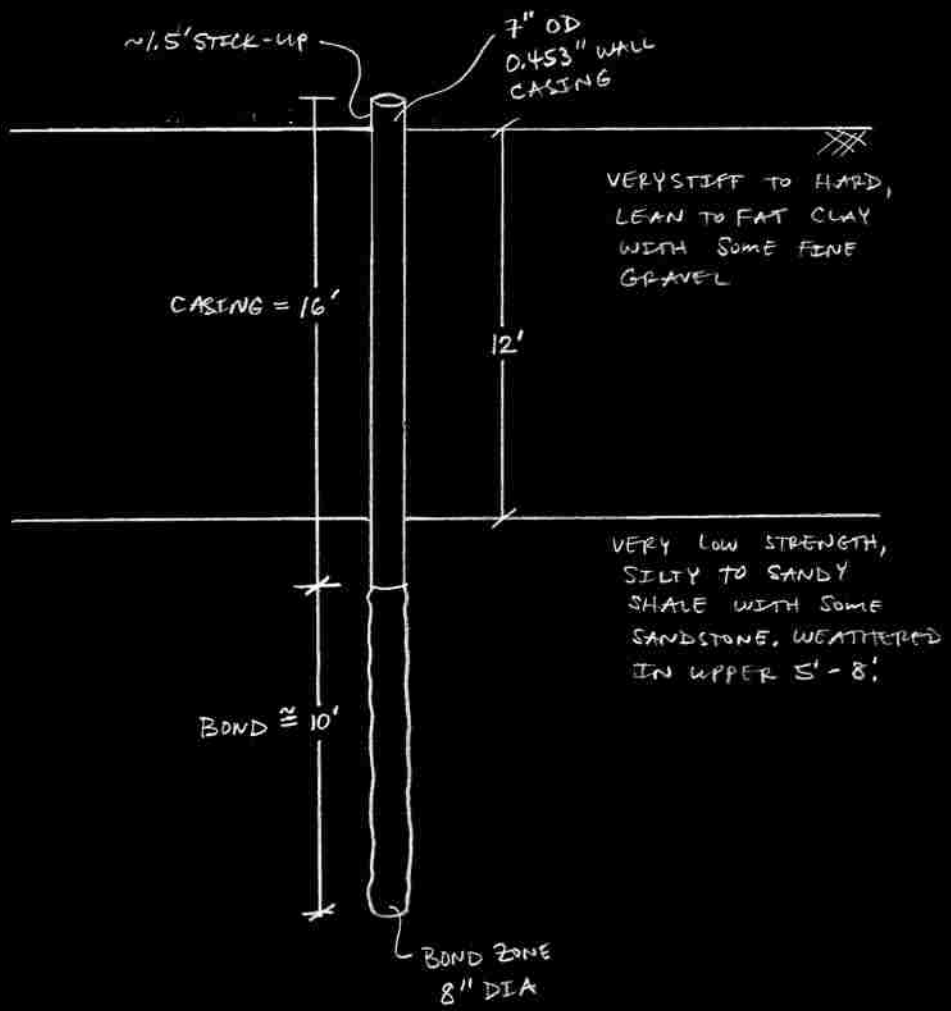

1) CENTRAL REINFORCING BAR TO BE 1 - #11 DYWIDAG BAR TO BE INSTALLED THE FULL LENGTH OF THE MICROPILE (25')

2) ESTIMATED ULTIMATE AXIAL COMPRESSIVE MICROPILE CAPACITY ≅ 120 kips. STRUCTURAL CAPACITY DESIGNED FOR 150 kip LOAD.

3) ESTIMATED ULTIMATE LATERAL CAPACITY = 20 kips (δ = 2.5")

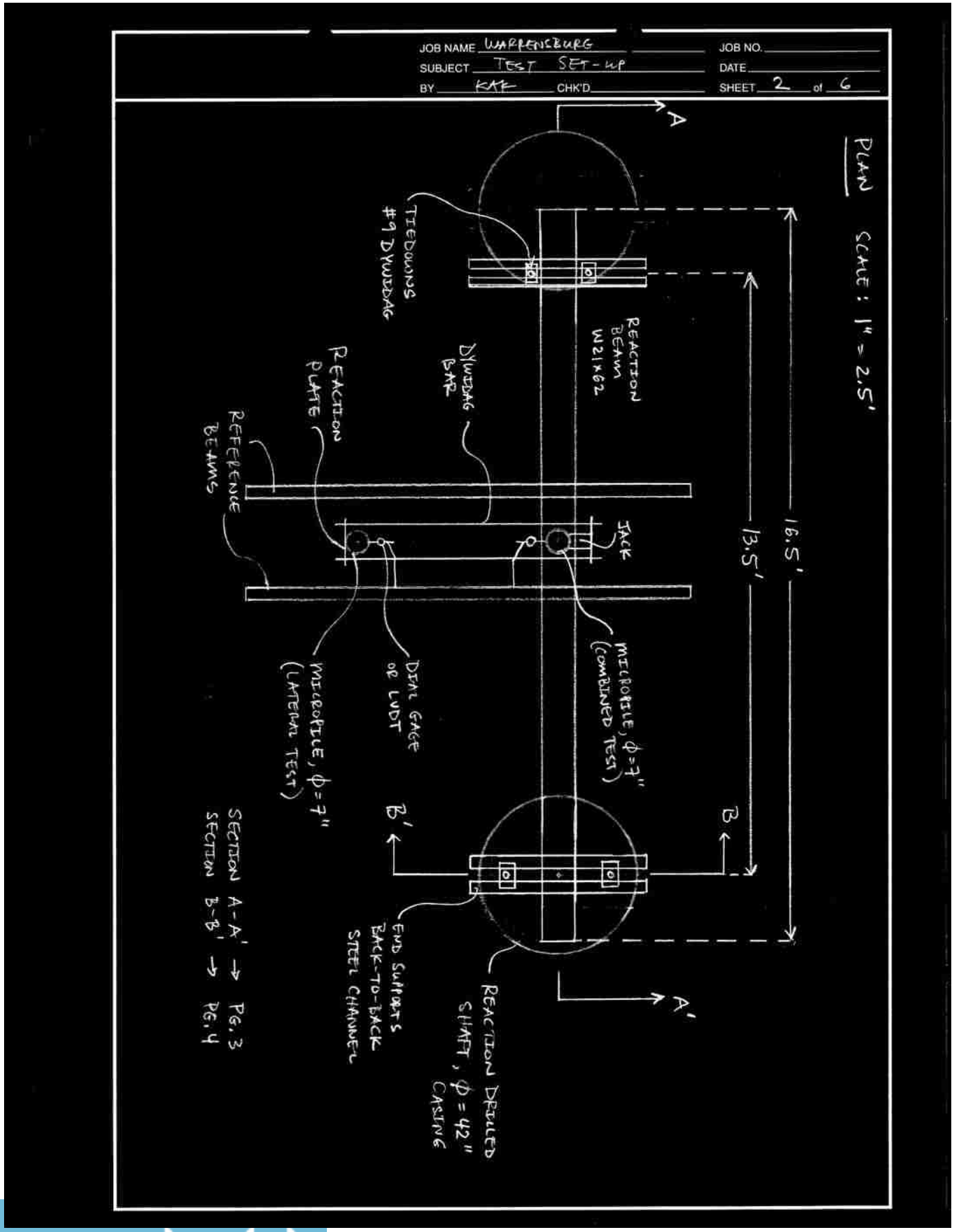

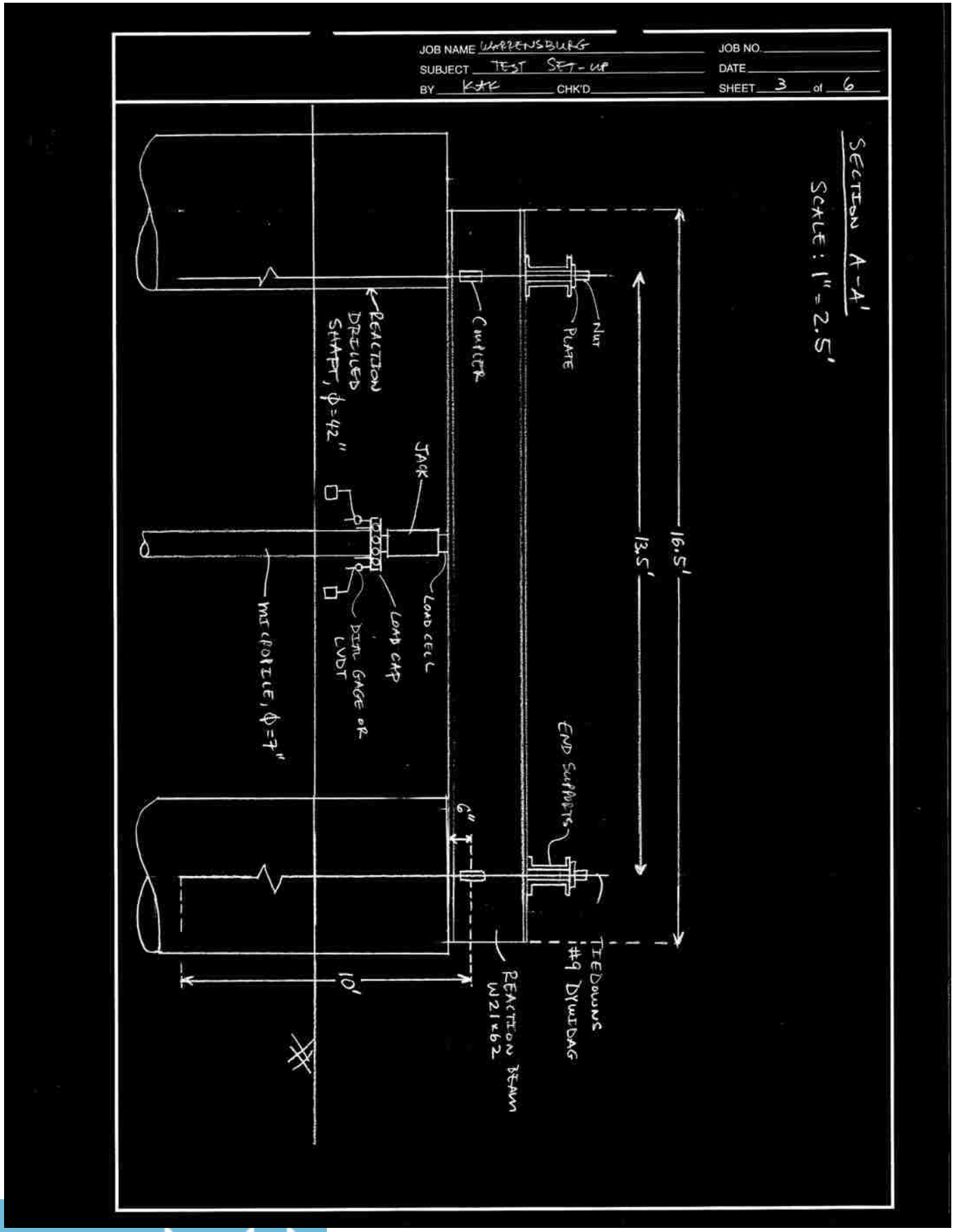

JOB NAME WARRENSBURG JOB NO.
SUBJECT TEST SET-UP DATE
BY KAK CHK'D SHEET 4 of 6

B-B'

SCALE: 1" = 2.5'

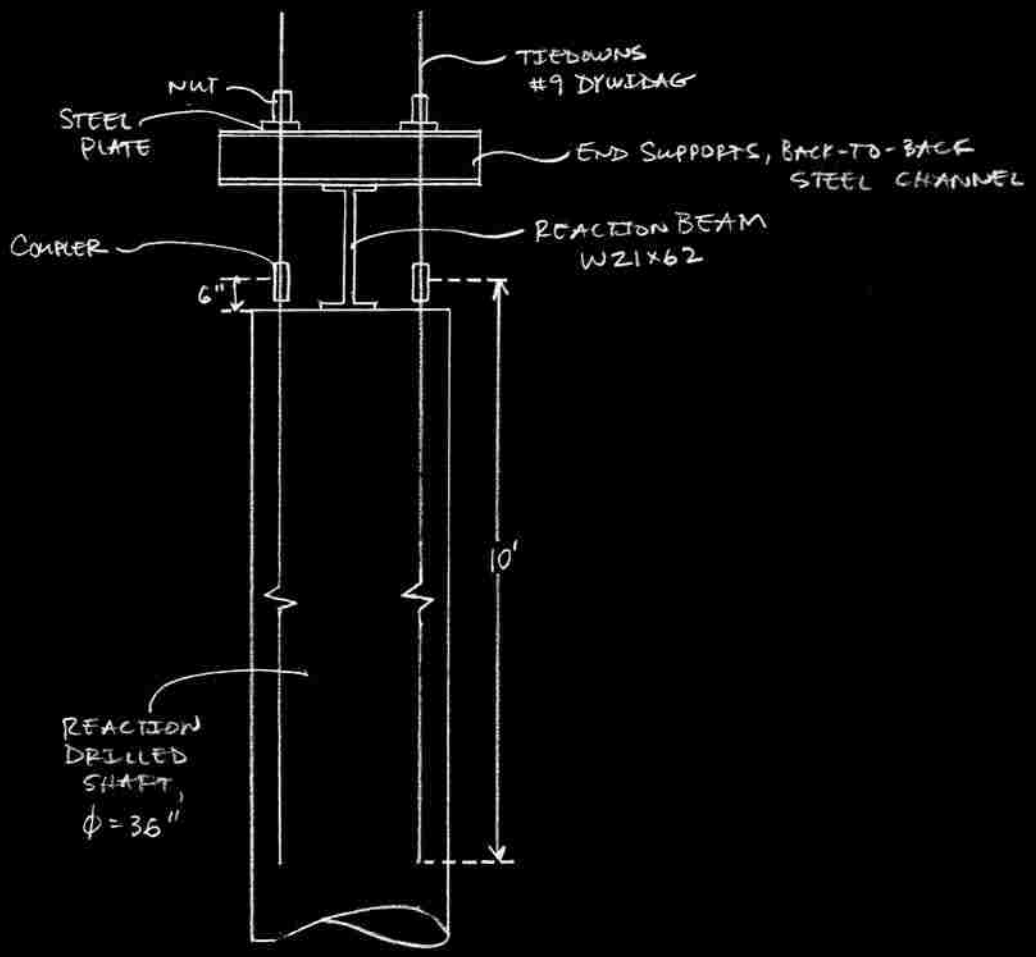

JOB NAME WARRENSBURG JOB NO.
SUBJECT TEST SET-UP DATE
BY KAF CHK'D SHEET 5 of 6

LOADING PLATFORM

(NOT TO SCALE)

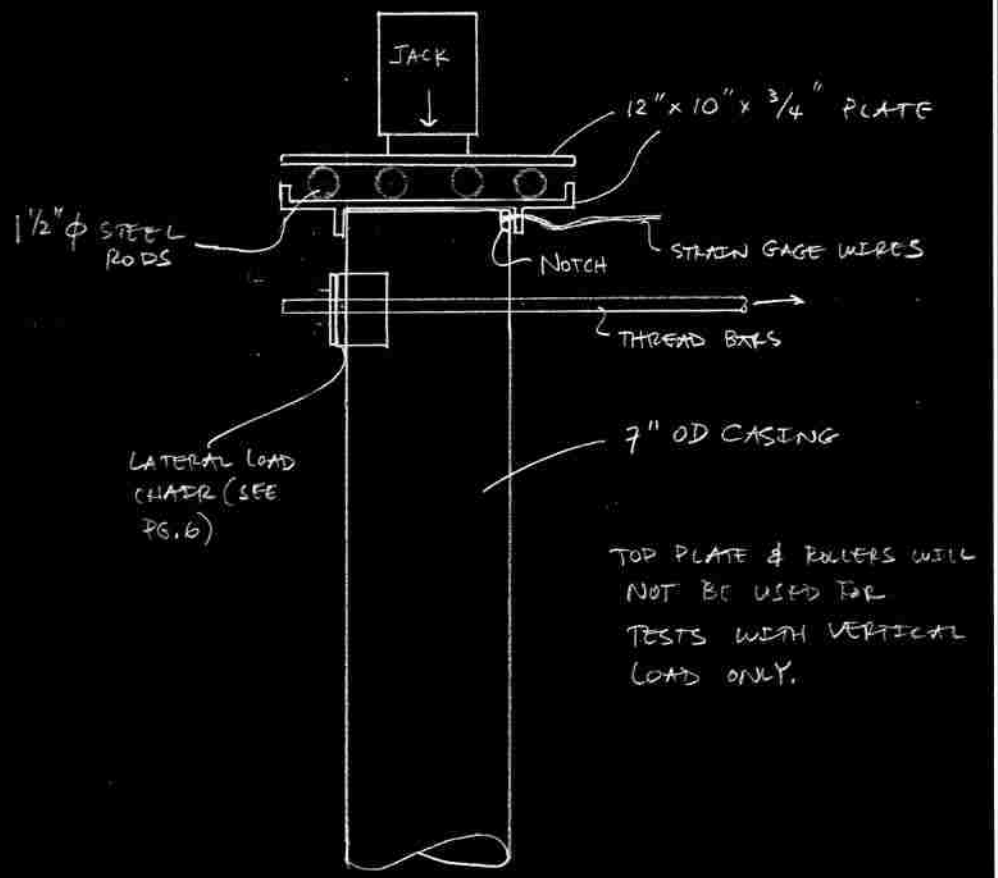

TOP PLATE & ROLLERS WILL NOT BE USED FOR TESTS WITH VERTICAL LOAD ONLY.

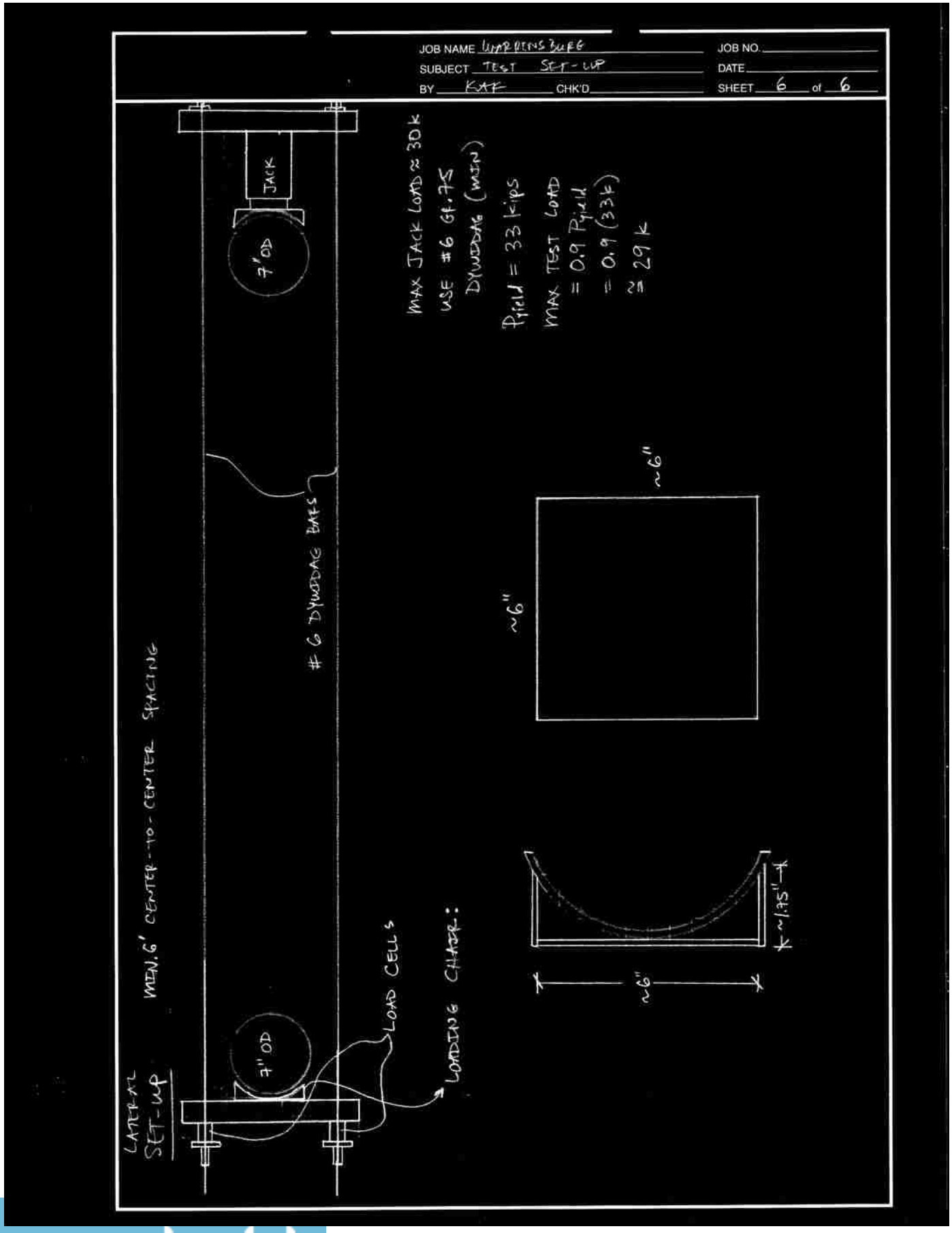

WARRENSBURG TEST SITE

MICROPILE CAPACITY CALCULATIONS (4 PAGES)

SUMMARY:

Casing OD = 7 inches

Casing Thickness = 0.453 inches

Casing Length = 15 feet

Central Reinforcing Bar = #11

Bond Zone Dia = 8 inches

Estimated Micropile Compressive Capacity = 120 kips

Estimated Micropile Lateral Capacity = 20 kips

JOB NAME WARRENSBURG JOB NO.
SUBJECT MICROPILE CAPACITY DATE
BY KAK CHK'D RL SHEET 1 of 4

CAPACITY ANALYSIS FOR FIELD TESTING @ WARRENSBURG.

- MICROPILE CASING:

$E = 29{,}000$ ksi $\quad L_c = 16' = \underbrace{14.5'}_{\text{IN GROUND}} + \underbrace{1.5'}_{\text{STICK-UP}}$

OD = 7"

ID = 6.094"

$t = 0.453"$

$A = \pi/4\,(7^2 - 6.094^2) = 9.31\ in^2$

$I = \pi/64\,(7^4 - 6.094^4) = 50.13\ in^4$

$F_y = 80$ ksi

$P_y = 744.8$ k

- CENTRAL REINFORCING BAR:

$E = 29{,}000$ ksi $\quad L = 25'$

#11 DYWIDAG BAR

Dia = 1.375"

$A = 1.56\ in^2$

$I = 0.175\ in^4$

$F_y = 75$ ksi

$P_y = 117.0$ k

- GROUT: (TREMIE GRAVITY PLACEMENT)

$f'_c = 4$ ksi

$E = 57{,}000\sqrt{f'_c} = 57{,}000\sqrt{4000} = 3{,}605$ ksi

CASED ZONE: $(L_c = 14.5')$

$A = \pi/4\,(6.094)^2 - 1.56\ in^2 = 27.6\ in^2$

UNCASED ZONE: (L_c = 10' max, & Dia = 8")

$A = \pi/4\,(8)^2 - 1.56\ in^2 = 50.2\ in^2$

$I = \pi/64\,(8)^4 = 201.0\ in^4$

JOB NAME WARRENSBURG JOB NO.
SUBJECT MICROPILE CAPACITY DATE
BY KAK CHK'D RL SHEET 2 of 4

SOIL PROFILE:

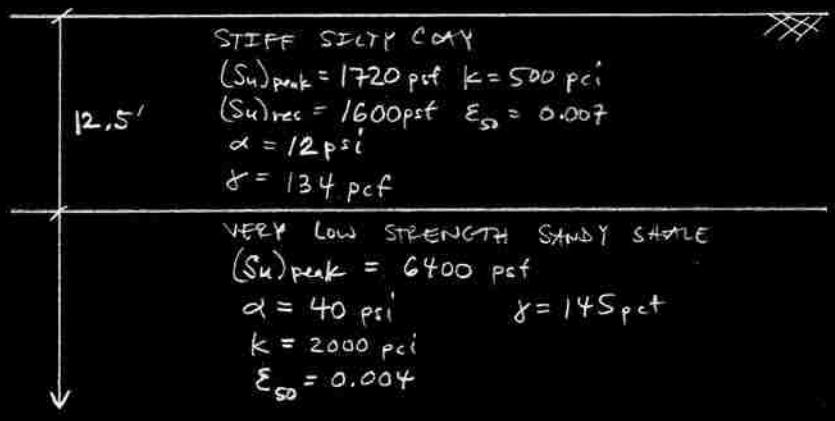

AXIAL CAPACITY:

– GEOTECHNICAL CAPACITY

$$P_{ult} = \alpha \pi D_b L_b =$$

$$= \pi (8") \ (40 psi) \ 10' \left(\frac{12"}{ft}\right)$$

$$= 120 \ k$$

$$P_{allow} = P_{ult}/2.0 = 60 \ k$$

– STRUCTURAL CAPACITY

USE $F_y = 75$ ksi FOR STRAIN COMPATIBILITY

↳ CASED ZONE:

$$P_{c\text{-}allow} = 0.4 f'_c (A_{gr}) + 0.47 F_y (A_{bar} + A_{casing})$$

$$= 0.4 (4 ksi)(27.6 in^2) + 0.47 (75 ksi)(1.56 + 9.31)$$

$$= 427.3 \ k > 120. \ k$$

JOB NAME WARRENSBURG JOB NO.
SUBJECT MICROPILE CAPACITY DATE
BY KAK CHK'D RL SHEET 3 of 4

↳ UNCASED ZONE:

$$P_{c\text{-allow}} = 0.4 f'_c (A_{gr}) + 0.47 F_y (A_{bar})$$
$$= 0.4 (4\,ksi)(50.2\,in^2) + 0.47 (75\,ksi)(1.56\,in^2)$$
$$= 135.3\,k > 120\,k$$

LATERAL CAPACITY:

– STRUCTURAL CAPACITY:

↳ CASED ZONE: (IGNORE GROUT & CENTRAL BAR)

$$M_{allow} = 0.55 F_y \frac{I}{OD/2} = 0.55 (80\,ksi) \frac{50.13\,in^4}{7in/2}$$
$$= 630.2\,k\text{-}in$$

@ THE THREADED CONNECTION USE: (DEPTH = 8.5' FROM GROUND SURFACE)

$$t = \tfrac{1}{2}(0.453") = 0.227"$$
$$ID = 6.094"$$
$$OD = 6.094" + 0.453" = 6.547"$$
$$A = \pi/4 (6.547^2 - 6.094^2) = 4.50\,in^2$$
$$I = \pi/64 (6.547^4 - 6.094^4) = 22.48\,in^4$$
$$M_{allow} = 0.55 (80\,ksi) \frac{22.48\,in^4}{7"/2}$$
$$= 282.6\,in\text{-}k$$

↳ UNCASED ZONE: (IGNORE GROUT)

$$M_{allow} = 0.55 (75\,ksi) \frac{0.175\,in^4}{1.375"/2}$$
$$= 10.5\,in\text{-}k$$

JOB NAME WATERENS BLVD. JOB NO.
SUBJECT MICROPILE CAPACITY DATE
BY EAE CHK'D RL SHEET 4 of 4

— GEOTECHNICAL CAPACITY — USING LPILE

↳ NO AXIAL LOAD, FIND LATERAL LOAD TO GET M_{allow} ALONG LENGTH OF MICROPILE.

$P_{lat} = 20.0\,k$

$\delta_{max} = 1.85" \cong 26\%$ OF OD

↳ $P_{axial} = 60.0\,k$, FIND LAT. LOAD TO GET M_{allow}.

$P_{lat} = 18.5\,k$

$\delta_{max} = 1.85" \cong 26\%$ OF OD

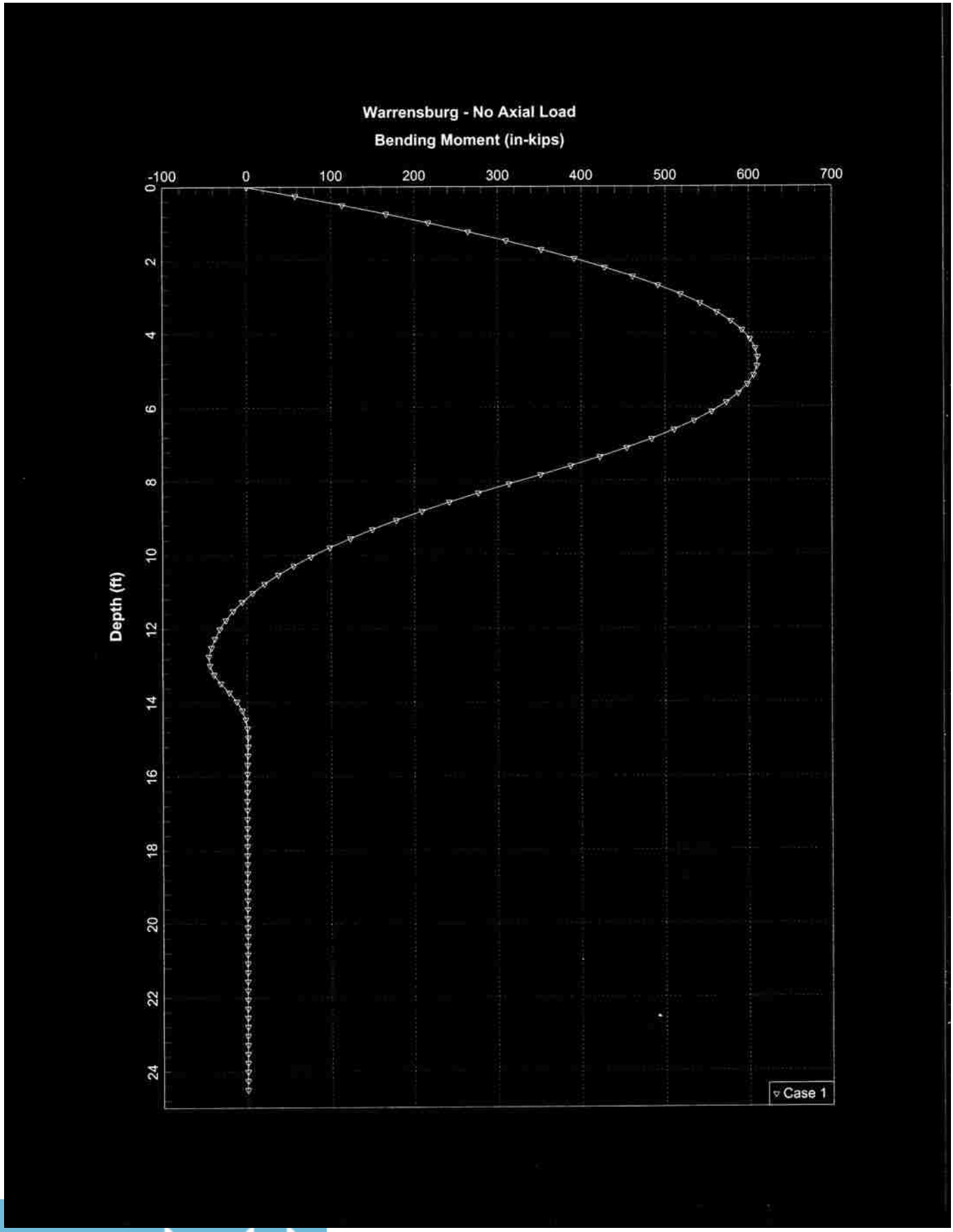

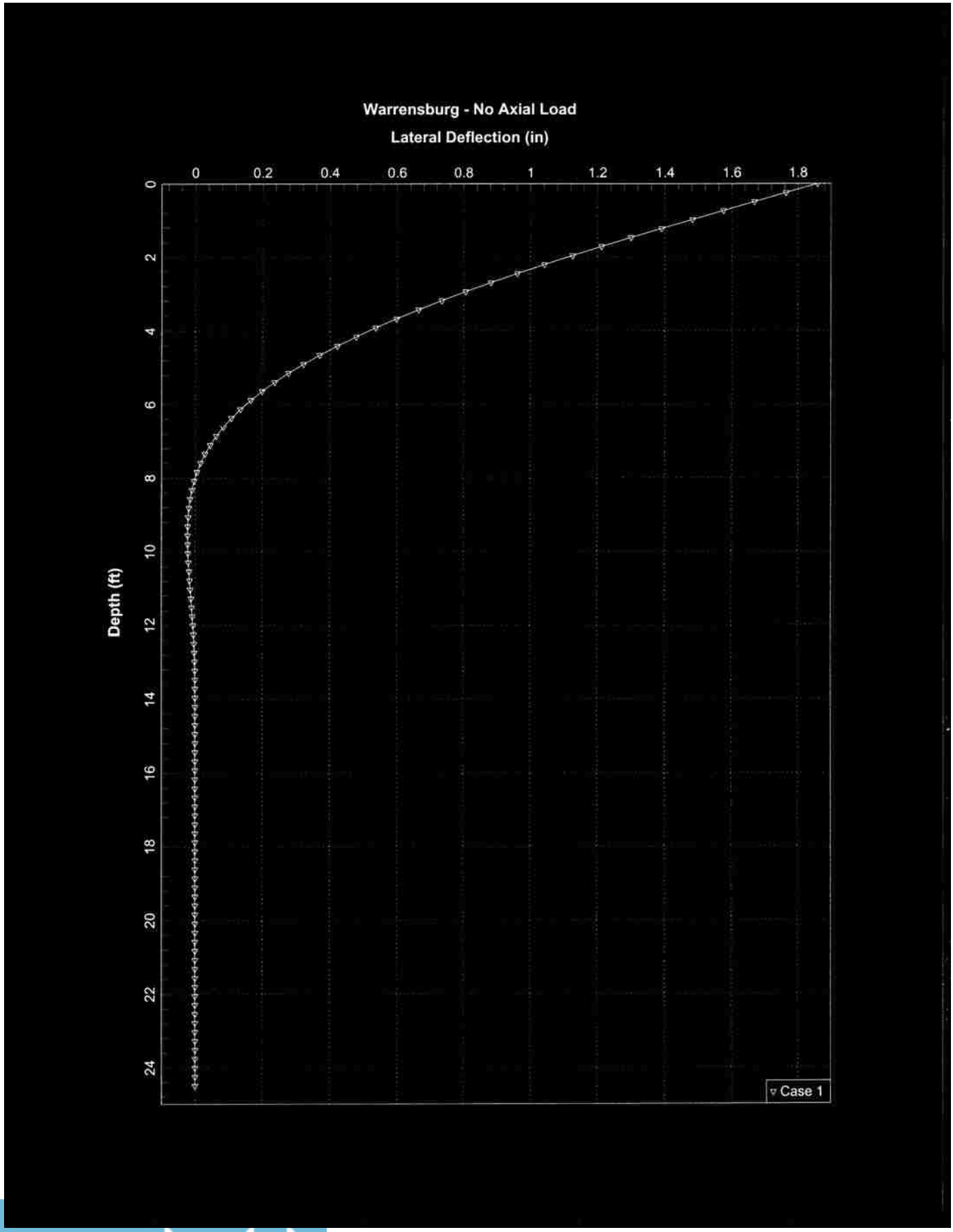

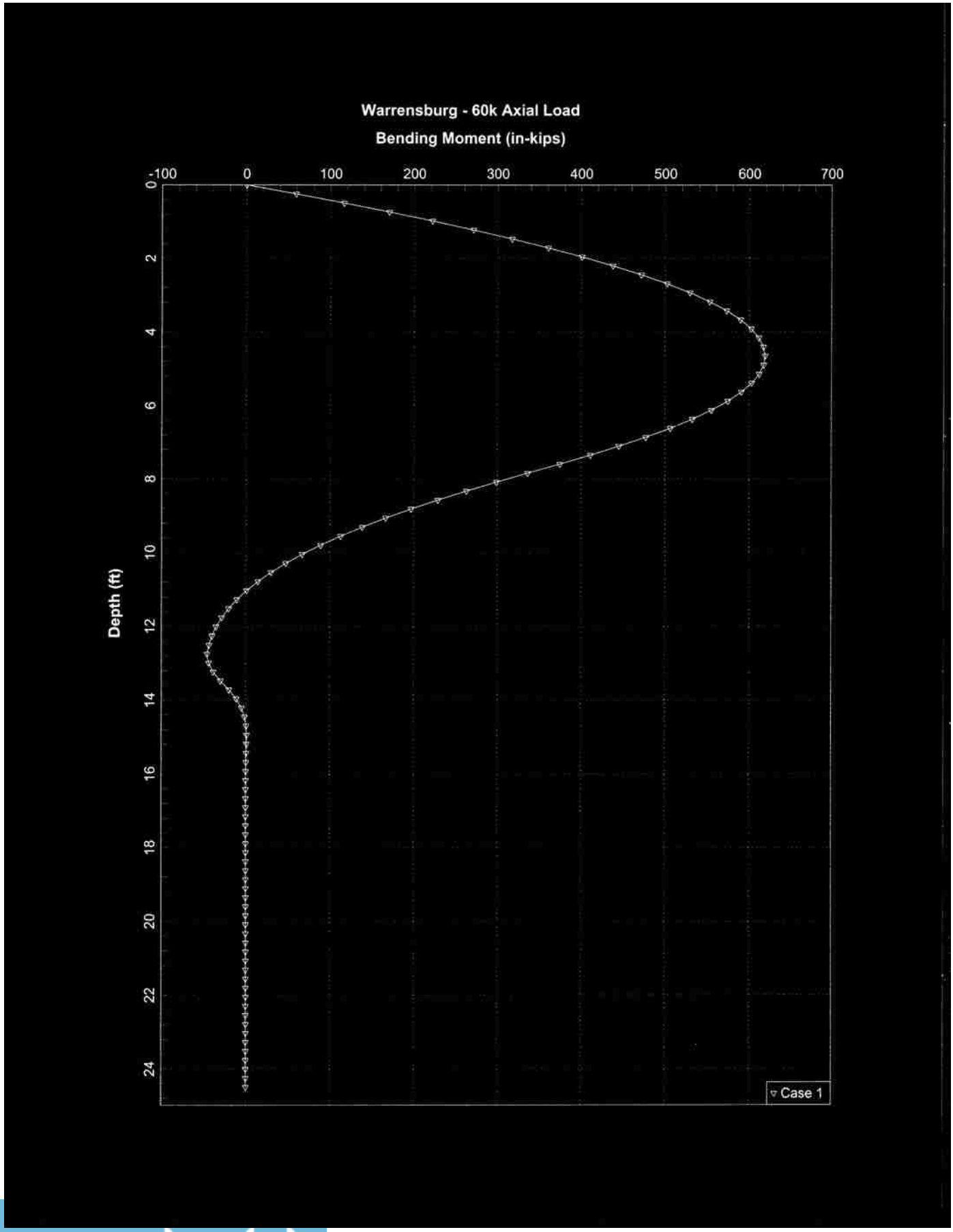

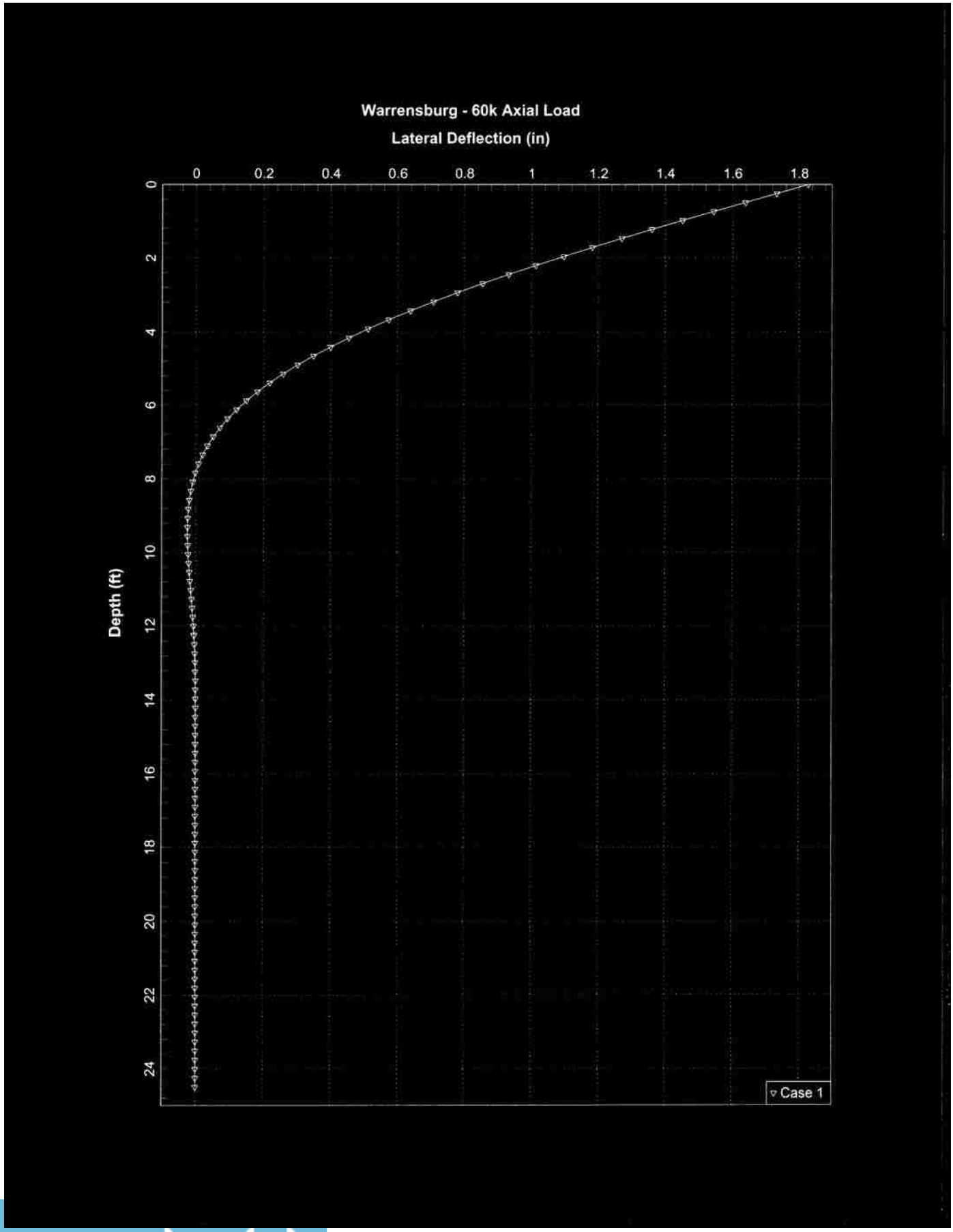

WARRENSBURG TEST SITE

LOAD FRAME CALCULATIONS (7 PAGES)

SUMMARY:

- Use 3-ft-diameter drilled shafts as reaction for loading.
- Install 2 #9 dywidag bars with 9.5 feet of embedment in each drilled shaft to act as tiedowns for the load frame beam.
- Load frame beam will consist of W21x62 beam with web stiffeners installed near the ends and at the center of the beam.

JOB NAME WARRENSBURG JOB NO.
SUBJECT REACTION FRAME DATE
BY KAF CHK'D SHEET 1 of 7

CALCULATE STRUCTURAL CAPACITY OF REACTION FRAME FOR MICROPILE TESTING

IX-S1

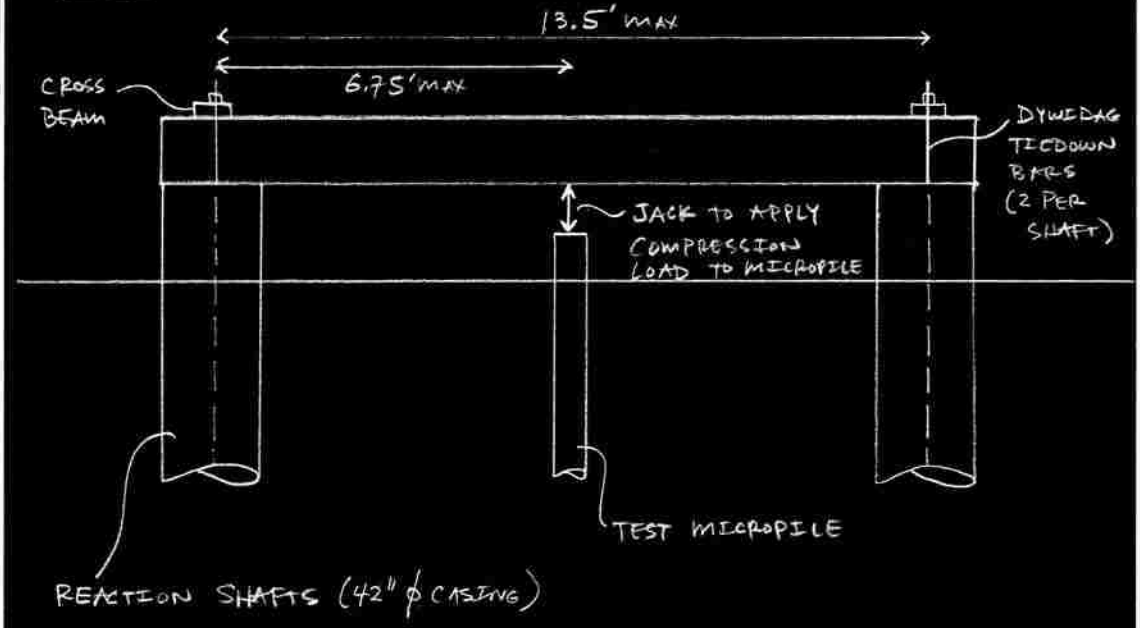

ASSUME:
- BEAM IS SIMPLY SUPPORTED
- MAX LOAD = 1.2 (120 k) = 144 k
  ↳ 20% HIGHER THAN ESTIMATED ULTIMATE CAPACITY FROM WARRENSBURG SITE

DETERMINE REACTIONS & MAX MOMENT FOR BEAM:

- END REACTIONS = $R = 144\,k/2 = 72\,k$

  IF TWO DYWIDAG BARS ARE USED ON EACH END, THE LOAD PER BAR WILL BE $72/2 = 36\,k$

- MAX MOMENT = $M_{max} = \frac{PL}{4} = \frac{144\,k\,(13.5')}{4}$

$$M_{max} = 486 \quad k\text{-ft}$$

JOB NAME WARRENSBURG | JOB NO.
SUBJECT REACTION FRAME | DATE
BY ISAE | CHK'D | SHEET 2 of 7

DETERMINE REQUIRED SIZE OF REACTION FRAME:

- DYWIDAG BARS:

MANUFACTURER SUGGESTS THAT THE MAXIMUM TEMPORARY TENSILE LOAD CAN BE 90% OF YIELD FOR $F_y = 75$ ksi BARS.

$$P_{max} = 0.90\, F_{y\text{-bar}} \times A_{bar}$$

$$A_{bar\text{-}req'd} = \frac{P_{max}}{0.90\, F_y} = \frac{36\,K}{0.90\,(75\,ksi)}$$

$$= 0.53\ in^2$$

$$A = \frac{\pi}{4}\phi_{nominal}^2$$

$$\phi_{nominal} = \sqrt{\frac{4A}{\pi}} = \sqrt{\frac{4\,(0.53\,in^2)}{\pi}}$$

$$= 0.82''$$

USE #7 BAR ($\phi = 0.875''$) OR LARGER

↳ #9 BARS INSTALLED IN SHAFTS

JOB NAME LAWRENCEBURG JOB NO.
SUBJECT REACTION FRAME DATE
BY KAK CHK'D SHEET 3 of 7

CALCULATE REQUIRED DEVELOPMENT LENGTH BASED ON ACI:

$$\frac{\ell_d}{d_b} = \frac{3 f_y \alpha \beta \lambda}{40\sqrt{f'_c}}$$

$d_b = 1.125''$ -> #9 DYWIDAG

$f_y = 75{,}000$ psi

$\alpha = 1.0$

$\beta = 1.0$

$\lambda = 1.0$

$f'_c = 4{,}000$ psi

$$\ell_d = \frac{3(75{,}000\,\text{psi})(1.0)(1.0)(1.0)(1.125'')}{40\sqrt{4000\,\text{psi}}}$$

$\ell_d = 100'' = 8.3'$

USE $\ell_d = 9.5'$

JOB NAME WARRENSBURG JOB NO.
SUBJECT REACTION FRAME DATE
BY KAE CHK'D SHEET 4 of 7

- REACTION BEAM:
  - ↳ DETERMINE REQUIRED BEAM SIZE BASED ON AISC STEEL DESIGN MANUAL
  - ↳ DYWIDAG BARS USED TO SUPPORT REACTION BEAM WILL BE SPACED AT LEAST 2' APART. SO, $(b_f)_{max} \cong 2'$.

CHECK AVAILABLE BEAM FROM ERL YARD:

$L \cong 16.5'$
$d \cong 21\ 1/16"$
$b_f \cong 8\ 1/4"$
$t_f \cong 5/8"$
$t_w \cong 5/16"$

LIKELY A W21×62 BEAM

FOR $C_b = 1.0$

$$\phi_b M_n = \phi_b \left(\frac{\pi}{L_b}\right) \sqrt{EI_y GJ + \left(\frac{\pi E}{L_b}\right)^2 I_y C_w}$$

$\phi_b = 0.9$
$L_b = 15'$
$E = 29{,}000$ ksi
$I_y = 57.5$ in^4
$G = 11{,}200$ ksi
$J = 1.83$ in^4
$C_w = 5{,}960$ in^6

JOB NAME WARRENSBURG JOB NO.
SUBJECT REACTION FRAME DATE
BY EAK CHK'D SHEET 5 of 7

$$\phi_b M_n = 0.9\left(\frac{\pi}{15' \times \frac{12''}{ft}}\right)\sqrt{(29{,}000\ ksi)(57.5\ in^4)(11{,}200\ ksi)(1.83\ in^4) + \left(\frac{\pi\,(29{,}000\ ksi)}{15' \times 12''/ft}\right)^2 (57.5\ in^4)(5960\ in^6)}$$

$$\phi_b M_n = \frac{0.0157}{in}\sqrt{3.418 \times 10^{10}\ k^2\text{-}in^4 + 8.771 \times 10^{10}\ k^2\text{-}in^4}$$

$$\phi_b M_n = 5{,}468\ k\text{-}in = 456\ k\text{-}ft$$

FOR SHORT-TERM LOADING, USE A RESISTANCE FACTOR OF $\phi_b = 0.99$ (10% INCREASE IN LOAD)

$$(M_{allow})_{temp} = 456\ k\text{-}ft\ (1.1) = 501.6\ k\text{-}ft > 486\ k\text{-}ft$$

IN ADDITION, ADD WEB STIFFENERS AT THE ENDS OF THE BEAM AND AT THE CENTER WHERE THE LOAD WILL BE APPLIED

JOB NAME WARRENSBURG JOB NO.
SUBJECT REACTION FRAME DATE
BY KAK CHK'D SHEET 6 of 7

ANALYSIS OF DRILLED SHAFTS USED FOR REACTION FOR MICROPILE TESTING AT WARRENSBURG TEST SITE

- BASED ON DESIGN OF MICROPILE TESTING, MAX LOADS ON A SINGLE DRILLED SHAFT WILL BE:

$P_{axial} = 72$ k (TENSION)

$P_{lateral} = 20$ k

- BASED ON THE 4/17/10 DRILLED SHAFT PLANS:

↳ CASING: ID = 36" , t = 1/4" , OD = 36.5" $\Rightarrow A = \frac{\pi}{4}(36.5^2 - 36^2) = 28.4\ in^2 = 0.20\ ft^2$

↳ UNCASED CONCRETE: $\phi = 36" \Rightarrow A = \frac{\pi}{4}(36^2) = 1{,}017\ in^2 = 7.07\ ft^2$

↳ FOR THE SHORTEST DRILLED SHAFT (TS-W5):

$L_{casing} = 15'$

$L_{total} = 18'$

$W = (495\ lb/ft^3)(0.20\ ft^2)(15') + (150\ lb/ft^3)(7.07\ ft^2)(18')$

$= 20.6$ k

$\Rightarrow$ 51.4 k OF LOAD WOULD NEED TO BE TAKEN IN SKIN FRICTION

↳ FOR THE MAJORITY OF DRILLED SHAFTS:

$L_{casing} = 15'$

$L_{total} = 33'$

$W = (495\ lb/ft^3)(0.20\ ft^2)(15') + (150\ lb/ft^3)(7.07\ ft^2)(33')$

$= 36.5$ k

$\Rightarrow$ 35.5 k OF LOAD TAKEN IN SKIN FRICTION

JOB NAME WARRENSBURG JOB NO.
SUBJECT REACTION FRAME DATE
BY KAK CHK'D SHEET 7 of 7

↳ LATERAL ANALYSIS OF DRILLED SHAFTS:

SOIL PROFILE: 0'-12' STIFF SILTY CLAY
12'-24' WEATHERED SANDY SHALE
>24' CLAYEY SHALE

USING ONLY THE CONCRETE FOR BENDING RESISTANCE & IGNORING CASING & REINFORCING STEEL:

$\delta \cong 0.04''$

RL
10 Aug 2010

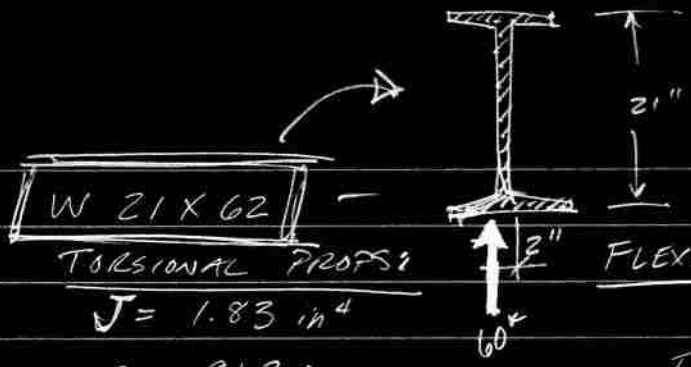

TORSIONAL PROPS:

$J = 1.83\ in^4$

$a = 91.8\ in$

$C_w = 5960\ in^6$

$W_{no} = 42\ in^2$

$S_{w1} = 53.2\ in^4$

$Q_f = 25.1\ in^3$

$Q_w = 72.2\ in^3$

FLEXURAL PROPERTIES:

$I_x = 1330\ in^4$

$S_x = 127\ in^3$

$t_f = 0.615\ in$

$t_w = 0.4\ in$

$\ell = 15\ ft = 180\ in$

$G = 11200\ ksi$

Calculate Max Rotation, θ

$T = P \cdot e = 60^k \times 2\ in = 120\ kip\text{-}in$

TORSIONAL FUNCTION $= +0.058$ from App B Case 3 $\alpha = 0.5$ $\leftarrow \ell/a = 180"/91.8" = 1.96$

$$\theta = 0.058\left(\frac{T_u \ell}{GJ}\right)$$

$$\theta = 0.058\left[\frac{(120\ k\text{-}in)(180\ in)}{(11200\ ksi)(1.83\ in^4)}\right]$$

$$\theta = 0.061\ rad. = 3.49\ degrees \checkmark$$

"TORSION9.xls" Program
Version 1.0

SIMPLIFIED TORSION ANALYSIS FOR STEEL BEAMS

Simple Span Beam with Eccentric Concentrated Load Applied at Midspan
For W, S, M, and HP Shapes and Per AISC 9th Edition (ASD) Manual

Job Name:	Warrensburg Load Test Site	Subject:	Check on Torsion of Beam		
Job Number:		Originator:	R.Luna	Checker:	K. Kershaw

Input Data:

Member Size:

Select: W21x62 ✓

Member Loading:

P =	60.000	kips
e =	2.0000	in.

Design Parameters:

Fy =	36.00	ksi
L =	15.000	ft.
Lb =	15.000	ft.
Cb =	1.00	
ASIF =	1.000	

LOAD AND SUPPORT CONDITIONS

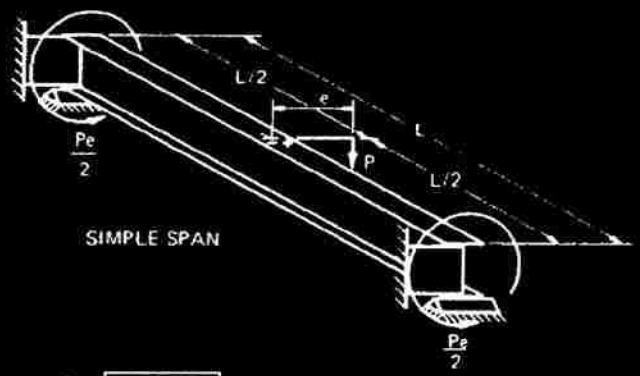

Member Properties:

A =	18.30	in.^2	Ix =	1330.00	in.^4
d =	21.000	in.	Sx =	127.00	in.^3
tw =	0.400	in.	Iy =	57.50	in.^4
bf =	8.240	in.	Sy =	14.00	in.^3
tf =	0.615	in.	J =	1.830	in.^4
rt =	2.100	in.	Cw =	5970.0	in.^6
d/Af =	4.14		wt./ft. =	62.0	plf

Reference for Torsion Analysis:
USS Steel Design Manual (1981)
Chapter 7: Torsion (Figures 7.9 & 7.10)
by: R.L. Brockenbrough & B.G. Johnston

Results:

X-axis Bending:

Mx =	226.74	ft-kips	Mx = P*L/4 + wb*L^2/8 (wb = beam self weight)
fbx =	21.42	ksi	fbx = Mx*12/Sx
Lb/rt =	85.71		Note: Lc = 8.7 ft., Lu = 11.18 ft.
Fbx =	17.78	ksi	Fbx = (2/3-Fy*(Lb*12/rt)^2/(1530000*Cb))*Fy <= 0.60*Fy

Torsion (Lateral Flange Bending):

a =	91.91	in.	a = SQRT(E*Cw/(G*J)) (where: E = 29000 ksi, G = 11200 ksi)
Mt =	16.97	ft-kips	Mt = (P*e*a/(2*df)*TANH(L*12/(2*a)))/12 (where: df = d-tf)
fby =	29.09	ksi	fby = Mt*12/(Sy/2) Note: use only 1/2 of Sy
Fby =	27.00	ksi	Fby = 0.75*Fy

Stress Ratio:

S.R. =	2.283	S.R. = fbx/(ASIF*Fbx) + fby/(ASIF*Fby) <= 1.0

Angle of Twist:

ϕ =	3.492	deg. ✓	ϕ = (P*e*a/(2*J*G)*(L*12/(2*a)-TANH(L*12/(2*a))))*180/π

8/10/2010 3:56 PM

BIBLIOGRAPHY

ACI Committee 318. (2002). *Building Code Requirements for Structural Concrete (ACI 318-02) and Commentary,* American Concrete Institute, Farmington Hills, Michigan.

AISC. (1998). *Manual of Steel Construction, Load & Resistance Factor Design*, American Institute of Steel Construction, Chicago, Illinois.

Amde, A. M., Chini, S. A., and Mafi, M. (1997). "Model study of H-Piles subjected to combined loading." *Geotechnical and Geological Engineering*, 15, 13.

American Association of State Highway and Transportation Officials (AASHTO). (2007). *AASHTO LRFD Bridge Design Specifications*, AASHTO, Washington, DC.

Anagnostopoulos, C., and Georgiadis, M. (1993). "Interaction of Axial and Lateral Pile Responses." *ASCE Journal of Geotechnical and Geoenvironmental Engineering*, 119(4), 6.

Armour, T., Gronek, P., Keeley, J., and Sharma, S. (2000). "Micropile Design and Construction Guidelines." U.S. Department of Transportation, Federal Highway Administration, Priority Technologies Program, Springfield, VA.

ASTM International. (2011). "C39/C39M-11: Standard Test Method for Compressive Strength of Cylindrical Concrete Specimens." ASTM International, West Conshohocken, PA.

Bartolomey, A. A. (1977). "Experimental Analysis of Pile Groups under Lateral Loads." *Proceedings of the Special Session 10 of the Ninth International Conference on Soil Mechanics and Foundation Engineering*, Tokyo, pp. 187-188.

Beaty, I. C. (1970). "Lateral Load Tests on Pile Groups." *Foundation Facts*, Vol. 6 (No. 1), pp. 18-21.

Boulon, M. (2001). "Modelisation en elements finis du comportement 3-D d'un pieu sous charge inclinee." Synthese de resultats et recommandations du projet national sur les micropieux, Rapport interne no FO/97/09.

Bruce, D. A., DiMillio, A. F., and Juran, I. (1995). "A Primer on Micropiles." *Civil Engineering*, 65(12), 4.

Bruce, D. A., and Juran, I. (1997). "Drilled and Grouted Micropiles: State-of-Practice." *FHWA-RD-96-016*, Nicholson Construction Company.

Bruce, D. A., Cadden, A. W., and Sabatini, P. J. (2005). "Practical Advice for Foundation Design - Micropiles for Structural Support." Geo-Frontiers, Geotechnical Special Publication 131 - Contemporary Issues in Foundation Engineering, E. M. Rathje, ed., Geoinstitute of ASCE.

Cadden, A., Gomez, J., Bruce, D. A., and Armour, T. "Micropiles: Recent Advances and Future Trends." *Current Practices and Future Trends in Deep Foundations (GSP 125)*, 140-165.

Chik, Z. H., Abbas, J. M., Taha, M. R., and Shafiqu, Q. S. M. (2009). "Lateral Behavior of Single Pile in Cohesionless Soil Subjected to Both Vertical and Horizontal Loads." *European Journal of Scientific Research*, Vol. 29(No. 2), pp. 194-205.

Coduto, D. P. (2001). *Foundation Design: Principles and Practices*, Prentice Hall, Upper Saddle River, New Jersey.

Cyna, H. (2008). "FOREVER: Synthesis of the Results and Recommendations of the French National project on Micropiles." S. Engineering, ed., ADSC: The International Association of Foundation Drilling, Dallas, TX.

Davisson, M. T. (1960). "Behavior of Flexible Vertical Piles Subjected to Moment, Shear, and Axial Load," Ph.D. Thesis, University of Illinois, Urbana, Illinois.

Dywidag-Systems-International. (2011). "DYWIDAG Micropiles." www.dsiamerica.com/products/geotechnic/dywidag-micropiles/general-information.html. Accessed October 7, 2011.

Evans, L. T. (1953). "Bearing Piles Subjected to Horizontal Loads." *ASTM Special Technical Publication*, No. 154, pp. 30-35.

el-Geneidy, A. M. (2009). "Combined load testing of piles." *17th International Conference on Soil Mechanics and Geotechnical Engineering*, Alexandria, Egypt, 1120-1123.

Geokon, Inc. (2003). "Instruction Manual, model GK-404 Vibrating Wire Readout." Lebanon, New Hampshire.

Geokon, Inc. (2008). "Instruction Manual, Model 4151 Miniature Strain Gage." Lebanon, New Hampshire.

Geokon, Inc. (2009). "Instruction Manual, Model 4999 Terminal Box." Lebanon, New Hampshire.

Geokon, Inc. (2010). "Instruction Manual, Model 4200/4202/4204/4210 Vibrating Wire Strain Gages." Lebanon, New Hampshire.

Goryunov, B. F. (1975). "Discussion on "Analysis of Piles Subjected to the Combined Action of Vertical and Horizontal Loads"." *Soil Mechanics and Foundation Engineering (Translated from Russian)*, Vol. 10(No. 1), p. 10.

Hsiung, Y.-M., Chen, S.-S., and Chou, Y.-C. (2006). "Analytical Solution for Piles Supporting Combined Lateral Loads." *ASCE Journal of Geotechnical and Geoenvironmental Engineering*, 132(10), 10.

Iai, S. (1989). "Similitude for Shaking Table Tests on Soil-Structure-Fluid Model in 1g Gravitational Field." *Soils and Foundations, Japanese Society of Soil Mechanics and Foundation Engineering*, 29(1), 14.

International Code Council (ICC) (2009). "International Building Code."

Jain, N. K., Ranjan, G., and Ramasamy, G. (1987). "Effect of Vertical Load on Flexural Behavior of Piles." *Geotechnical Engineering*, Vol. 18(No. 2), pp. 185-204.

Jamiolkowski, M., LoPresti, D. C. F., and Manassero, M. (2001). "Evaluation of Relative Density and Shear Strength of Sands from Cone Penetration Test and Flat Dilatometer Test." Geotechnical Special Publication 119 - Soil Behavior and Soft Ground Construction, American Society of Civil Engineers, pp.201-238.

Johnson, K., Lemcke, P., Karunasena, W., and Sivakugan, N. (2006). "Modelling the load-deforamtion response of deep foundations under oblique loading." *Environmental Modelling & Software*, Vol. 21, pp. 1375-1380.

Karasev, O. V. (1977). "Investigation of the Work of Single Cast Piles under Different Load Combinations." *Soil Mechanics and Foundation Engineering (Translated from Russian)*, Vol. 14(No. 3), pp. 173-177.

Karthigeyan, S., Ramakrishna, V., and Rajagopal, K. (2006). "Influence of vertical load on the lateral response of piles in sand." *Computers and Geotechnics*, 33, 11.

Karthigeyan, S., Ramakrishna, V., and Rajagopal, K. (2007). "Numerical Investigation of the Effect of Vertical Load on Lateral Response of Piles." *ASCE Journal of Geotechnical and Geoenvironmental Engineering*, 133(5), 10.

Klein, G. K., and Karavaev, V. N. (1979). "Design of Reinforced Concrete Piles for Vertical and Horizontal Loading." *Soil Mechanics and Foundation Engineering (Translated from Russian)*, No. 6, pp. 321-324.

Lee, J. (2008). "Experimental Investigation of the Load Response of Model Piles in Sand," Ph.D. Thesis, Purdue University, West Lafayette, Indiana

Lehane, B. M., Phillips, D. M., Paul, T. S., and Horkan, E. (1999). "Instrumented piles subjected to combined vertical & lateral loads." European Conference on Soil Mechanics and Foundation Engineering: Geotechnical Engineering for Transportation Infrastructure, Barends, ed., Amsterdam, Netherlands, 1145-1150.

Likos, W. J., Loehr, J. E., Maerz, N., Magner, K. A., Ge, L., and Stephenson, R. W. (2011). "MoDOT Transportation Geotechnics Research Program: Site Characterization Program Interpretation Report." Missouri Department of Transportation.

Lizzi, F. (1983). "The "Reticolo di Pali Radice" (Reticulated Root Piles) for the Improvement of Soil Resistance. Physical Aspects and Design Approaches." *The Eighth European Conference on Soil Mechanics and Foundation Engineering*, Helsinki, Finland.

Long, J., Manciani, M., and Menezes, G. (2002). "Results of Lateral Pile Load Tests: Lateral Load Tests Conducted on Micropiles, Route 57, Structure 002-001, Cairo, Illinois." SaLUT, Inc., Beltsville, Maryland.

Long, J., Manciani, M., and Menezes, G. (2004). "Results of Lateral Load Tests on Micropiles." *GeoSupport 2004: Drilled Shafts, Micropiling, Deep Mixing, Remedial Methods, and Specialty Foundation Systems (Geotechnical Special Publication No. 124)*, Orlando, FL, 122-133.

Magner, K. A., Maerz, N., Bowders, J. J., Pierce, M. D., and Loehr, J. E. (2011). "MoDOT Transportation Geotechnics Research Program: Field Site Characterization Testing Program Data Report." Missouri Department of Transportation.

Majumdar, J. P. (1980). "Fixity Effect of Axial Load on Laterally Loaded Piles," M.E. Thesis, University of Roorkee, Roorkee, India.

Mayne, P. W. (2006). "The Second james K. Mitchell Lecture - Undisturbed Sand Strength from Seismic Cone Tests." *Geomechanics and Geoengineering*, 1(4), pp.239-257.

McNulty, J. F. (1956). "Thrust Loading on Piles." *Journal of the Soil Mechanics and Foundations Division of ASCE*, Vol. 82(No. SM 2), pp. 1-25.

Missouri Department of Transportation (MoDOT). (1962). "Geology and Soils Manual." Division of Materials, Geology and Soils, Jefferson City, Missouri.

National Instruments. (2009). "LabVIEW 2009 Service Pack 1."

National Instruments. (2010). "Operating Instructions and Specifications, CompactRIO NI cRIO-9022, Intelligent Real-Time Embedded Controller for CompactRIO."

Peterson, R. W. (1988). "Laboratory Investigation of the Penetration Resistance of Fine Cohesionless Materials." *Penetraion Testing, ISOPT-1*, pp.895-901.

Pise, P. J. (1975). "Investigation on Laterally Loaded Pile Groups." *Symposium on Recent Developments in the Analysis of Soil Behavior and its Application to Geotechnical Structures*, University of New South Wales, Australia, pp. 129-144.

Ramasamy, G. (1974). "Flexural Behavior of Axially and Laterally Loaded individual Piles and Groups of Piles," Ph.D. Thesis, Indian Institute of Science, Bangalore, India.

Reese, L. C., Wang, S. T., Isenhower, W. M., and Arrellaga, J. A. (2004). *Computer Program LPILE Plus Version 5.0 Technical Manual*, Ensoft, Inc., Austin, Texas.

Richards, T. D., and Rothbauer, M. J. (2004). "Lateral Loads on Pin Piles (Micropiles)." *GeoSupport 2004: Drilled Shafts, Micropiling, Deep Mixing, Remedial Methods, and Specialty Foundation Systems (Geotechnical Special Publication No. 124)*, Orlando, Florida.

Rollins, K. M., olson, R. J., Egbert, J. J., Jensen, D. H., Olsen, K. G., and Garrett, B. H. (2006). "Pile Spacing Effects on Lateral Pile Group Behavior: Load Tests." *Journal of Geotechnical and Geoenvironmental Engineering*, 132(10), 10.

Sabatini, P. J., Tanyu, B., Armour, T., Groneck, P., and Keeley, J. (2005). "Micropile Design and Construction Reference Manual." *FHWA NHI-05-039*, Federal Highway Administration, Washington, DC.

Sarochan, E. A., and Bykov, V. I. (1976). "Performance of Groups of Cast in Place Piles Subjected to Horizontal Loading." *Soil Mechanics and Foundation Engineering (Translated from Russian)*, Vol. 13(No. 3), pp. 157-161.

Saxena, P. K. (1982). "Prediction and Performance of Lateral Load-Deflection Behavior of Piles," M.E. Thesis, University of Roorkee, Roorkee, India.

Shahrour, I., and Ata, N. (1994). "Analyse du comportement d'un pieu isole incline." Synthese de resultats et recommandations du projet national sur les micropieux, Rapport interne no FO/93/03.

Shahrour, I., and Meimon, Y. (1991). "Analyse du comportement des pieux des ouvrages en mer sous chargements inclines." Actes du colloque Fondations Profondes, organise par l'Ecole Nationale des Ponts et Chaussees, Presses de l'ENPC, Paris.

Siegel, T. C., Thompson, W. R., and Brown, D. A. (2010). "Foothills Parkway Bridge No. 2 Geotechnical Report." Dan Brown and Associates Consulting Geotechnical Engineers, Sequatchie, TN.

Textor, N. S. (2007). "Load Transfer in Reticulated and Non-Reticulated Micropiles from Large-Scale Tests," University of Missouri-Columbia, Columbia, Missouri.

Vipulanandan, C., Wong, D., Ochoa, M., and O'Neill, M. W. (1989). "Modelling of Displacement Piles in Sand Using a Pressure Chamber." Foundation Engineering Proceedings Congress, ASCE, pp.526-541.

Vishay Precision Group (2010a). "General Purpose Strain Gages - Linear Pattern, Series 250BG." Vishay Micro-Measurements, Document Number: 11294.

Vishay Pricision Group (2010b). "General Purpose Strain Gages - Linear Pattern, Series 250LW." Vishay Micro-Measurements, Document Number: 11297.

You, G.-L., Miura, K., and Ishito, M. (2003). "Behavior of Micropile Foundations Under Inclined Loads in Laboratory Tests." *Lowland Technology International*, 5(2), 11.

Zhang, L., Gong, X., Yang, Z., and Yu, J. (2011). "Elastoplastic solutions for single piles under combined vertical and lateral loads." *Journal of Central South University of Technology*, Vol. 18, pp. 216-222.

Zhukov, N. V., and Balov, I. L. (1978). "Investigation of the effect of a vertical surcharge on horizontal displacements and resistance of pile columns to horizontal loads." *Soil Mechanics and Foundation Engineering*, Vol. 15(No. 1), pp. 16-22.

VITA

Kyle Allen Kershaw was born on May 11, 1976 in Decatur, Illinois, USA to Samuel and Helen Kershaw. He earned a B.S. degree in Civil Engineering in 1999 at University Missouri-Rolla (currently Missouri University of Science & Technology). Kyle then attended University of Illinois at Urbana-Champaign where he studied geotechnical engineering and completed research regarding braced excavations under the guidance of Dr. Youssef Hashash and Dr. Edward Cording. After obtaining a M.S. degree in Civil Engineering in 2001, Kyle worked as a geotechnical engineer at Shannon & Wilson, Inc. for seven years from May 2001 to August 2008. He began his Ph.D. studies at Missouri University of Science & Technology in 2008 and received his degree in December 2011. In addition to his studies and research, Kyle served as a teaching assistant and a lecturer. Kyle has been married to Valeri for nine years and is the father of Ethan.